UNIVERSITY OF LONDON

IMPERIAL COLLEGE OF SCIENCE, TECHNOLOGY AND MEDICINE

DEPARTMENT OF ELECTRICAL AND ELECTRONIC ENGINEERING

CONTROL AND POWER SECTION

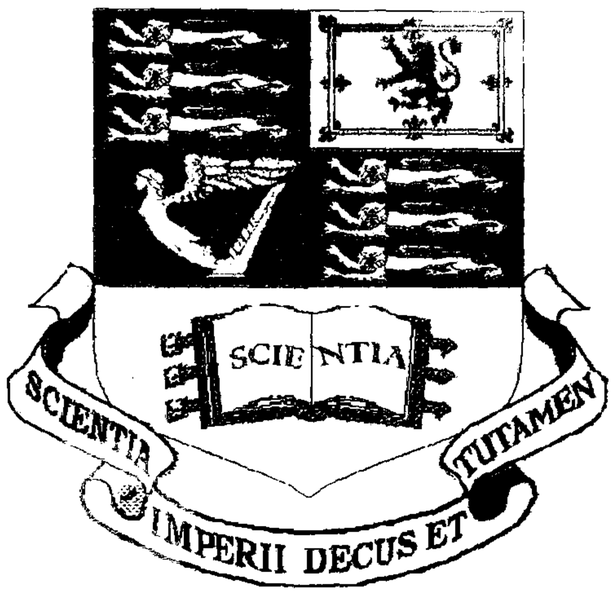

ROBUST DAMPING CONTROL OF INTER-AREA OSCILLATIONS IN POWER SYSTEMS WITH SUPERCONDUCTING MAGNETIC ENERGY STORAGE DEVICES

By

Bikash Chandra Pal

Thesis submitted for the Degree of

Doctor of Philosophy and the Diploma of

Imperial College in the Faculty of Engineering

June 1999

ABSTRACT

Poorly damped low-frequency (0.1 to 1.0 Hz) inter-area oscillations are inherent in interconnected power systems. The use of a superconducting magnetic energy storage (SMES) device to damp out these oscillations is explored further. The real power output of the SMES is modulated to damp such oscillations.

The various factors that influence the damping and frequency of the inter-area modes are thoroughly analysed. The objective of this research primarily focuses on two new approaches to robust damping control design in three sample power systems. It is aimed at enhancing the damping of the inter-area mode via real power modulation of the SMES device. The potential to stabilise the inter-area mode is only considered as the criterion for locating the SMES in the system.

A design technique based on *Weighted and Normalised Eigenvalue-distance Minimisation* (WNEDM) method is presented to design a robust low-order damping controller for a power system. The decentralised design employing several SMES devices through sequential approach is followed for a system with multiple inter-area modes.

A very recent technique of H_∞ control in the *Linear Matrix Inequalities* (LMI) framework is formulated as an H_∞ mixed-sensitivity design. The numerical nature of the solution and the multi-objective feature of the LMI formulations provide better damping to inter-area mode(s) than that by the controller designed by the Riccati approach. Effort is made to standardise the weighting functions required for mixed-sensitivity design employing SMES devices.

The large disturbance performance of the controller is verified through non-linear simulations that permit to incorporate non-linearity and saturation and operating limit associated with various devices. The performance of the controller is further verified in the face of variation in load characteristic. The performance of the controller are compared with the controller obtained by conventional approaches, such as root-locus, Riccati based H_∞ approaches.

Dedicated to

My father, wife and lovely Amartyadeep

ACKNOWLEDGEMENTS

The work reported in this thesis was carried out under the supervision of Dr. Alun H. Coonick, Ph.D, M. Sc (Eng.), B. Sc (Eng.), Lecturer in the Department of Electrical and Electronic Engineering, Imperial College. I wish to thank Dr. Coonick for his constant encouragement, discussion and guidance.

I receive plenty of assistances from Dr. Imad M. Jaimoukha, Prof. Brian J. Cory and Dr. Donald C. Macdonald through out this work. I would like to thank them very much for their supports.

The Commonwealth Scholarship Commission of the Association of Commonwealth Universities financed the programme entirely. The Jadavpur University, Calcutta, granted deputation leave to carry out the work. I am grateful to these two institutions.

Special thanks are due to Mr. Cliff Moppett for all of his help related to software and computational facilities. It is his very amicable disposition and pleasing manner that made my work very enjoyable.

My friends and colleagues in control and power section made my stay very enjoyable. I thank them very much.

Mr. Mihir Nagchowdhury helped me a lot. He took an immense share of my family duties particularly when my son was born in November 1998. Without his help and co-operation, it would have been very difficult to complete the work in time. My uncle, Dr. M. K. Guha and aunty, Dr. Mrs. P. Guha, helped and encouraged me in numerous occassions, be it academic or family matters. I am very grateful to all of them. My father, other family members and relatives in India also deserve sincere gratitude for their moral support to me.

Soma, my wonderful wife, provided all her love, care and patience to carry out the work. She sacrificed a lot to complete this work in time. Baby Amartyadeep, my son, was born in this period. His arrival undoubtedly added a new dimension to this work. To put it honestly, I do not have words to express my thanks and gratefulness to her and him.

TABLE OF CONTENTS

Abstract 2

Acknowledgements 4

Table of contents 5

Symbols and abbreviations 10

List of Tables 20

List of Figures 23

Chapter One: Introduction 25

1.1 Inter-area oscillations 25

1.1.1 A brief overview of the problem 25

1.1.2 The utility experience 27

1.1.3 Possible measures against oscillations 32

1.2 Objectives of the thesis 33

1.3 Outline of the thesis 35

1.4 Original contributions of the thesis 36

Chapter Two: Superconducting Magnetic Energy Storage: An option for effective power flow control 39

2.1 Introduction 39

2.2 SMES – the basic principle of operation 39

2.3 SMES – an effective FACTS device for power flow control 41

2.4 SMES – a brief historical perspective and the technology development worldwide 44

2.5 Benefits of SMES 48

2.6 Ratings of SMES 50
2.6.1 Power rating 51
2.6.2 Energy rating 52
2.7 Practical issues 52
2.8 Summary and conclusions 52

Chapter Three: Power System Modelling 54
3.1 Introduction 54
3.2 Speed Governor 54
3.3 Prime mover 54
3.4 Generator 55
3.4.1 Stator 55
3.4.2 Rotor 55
3.5 Excitation systems 58
3.5.1 Slow acting type (DC) 58
3.5.2 Fast acting type (ST) 60
3.6 Machine-network interface 61
3.7 Power system load 61
3.7.1 Static load 61
3.7.2 Dynamic load 63
3.8 Small signal model of the SMES 64
3.9 Overall model of a multimachine system 66
3.10 Summary and conclusions 70

Chapter Four: Analysis of low frequency electromechanical oscillations in multimachine systems 71
4.1 Introduction 71
4.2 Identification of coherent areas 71
4.2.1 Study system #1: A four-machine two-area case 73
4.2.2 Study system #2: A six-machine three-area case 76
4.2.3 Study system #3: A sixteen-machine five-area case 79

4.3 Analysing the factors affecting the damping and frequency of the inter-area modes in the study systems 82
4.3.1 Effect of machine model 82
4.3.2 Effect of excitation characteristics 84
4.3.3 Effect of tie line flows 86
4.3.4 Effect of tie line strength 87
4.3.5 Effect of load characteristics 88
4.4 Behaviour of the systems under large disturbances 89
4.5 Summary and conclusions 95
Chapter Five: Development of damping control design specifications 97
5.1 Introduction 97
5.2 Utility approaches in setting design specifications 97
5.3 Recommended guidelines to set design specifications 98
5.4 Summary and conclusions 103
Chapter Six: Identification of effective SMES locations 104
6.1 Introduction 104
6.2 Controllability, observability and residue as siting indices 104
6.3 The best location(s) and most effective stabilising signal(s) for the study systems 108
6.4 Summary and conclusions 116
Chapter Seven: Design of robust damping controller – An eigenvalue-distance minimisation approach 117
7.1 Introduction 117
7.2 The Weighted and Normalised Eigenvalue-distance Minimisation (WNEDM) technique 117
7.2.1 Modifications of the method to suit to power-system-damping-control design
7.2.2 Practical issues 121
7.2.2.1 Selections of weights 121
7.2.2.2 Model reduction 122
7.2.2.3 Solution technique 124
7.3 Damping controllers for the study systems 125

7.4 Performance evaluations 132
7.5 Evaluation of SMES ratings 139
7.6 Performance comparisons 141
7.7 Summary and conclusions 146

Chapter Eight: Design of robust damping controller- An LMI approach

8.1 Introduction 148
8.2 LMIs –A brief mathematical overview 148
8.3 LMIs and their application to control design problems 150
8.4 LMIs formulations of the mixed-sensitivity H_∞ design with additional pole-placement constraints 151
8.5 Factors influencing LMI based damping control design 156
8.5.1 Selection of weights 156
8.5.2 Model reduction 158
8.6 Damping controllers for the study systems 159
8.7 Performance evaluations 162
8.8 Evaluation of SMES ratings 166
8.9 Performance comparisons 170
8.10 Summary and conclusions 173

Chapter Nine: Conclusions and further work 175

9.1 Introduction 175
9.2 Overall conclusions 175
9.2.1 Analysing the inter-area mode damping problem 175
9.2.2 SMES as a possible solution 176
9.2.3 Robust damping control design by the WNEDM approach 177
9.2.4 Robust damping control design by LMI approach 177
9.2.5 Controller performance 178
9.3 Further work 179
9.3.1 Application of these approaches to include other FACTS devices 179
9.3.2 Application of these approaches to damp torsional oscillations 179

9.3.3 Application to mid-term and long-term stability problem 180

9.3.4 Exploring the possibilities of other decentralised control techniques 180

9.3.5 Inclusion of reactive power modulation option to minimise the ratings of the SMES 181

Appendix A: Linearisation of DAE in (3.53) to (3.77) of Chapter Three **182**

Appendix B: Parameters of the Study systems **188**

References **199**

Publications **212**

Symbols and abbreviations

$\mathbf{A}$	State matrix
$\mathbf{A_{cl}}$	Closed-loop state matrix
$A_{ex:}$	Exciter saturation constant
$\mathbf{A_j}$	General matrix
$\mathbf{A_k}$	State matrix of controller
$\hat{A}$	Intermediate control state matrix
$\mathbf{A_m}$	Modal state matrix
A(t)	Time dependant state matrix
a	Exponent in real load model
B	Bus susceptance
$\mathbf{B}$	Input Matrix
$\mathbf{B_1}$	Input Matrix
$\mathbf{B_2}$	Input matrix
$\mathbf{B_k}$	Input Control Matrix
$\hat{B}$	Intermediate input control matrix
$\mathbf{B_{ex}}$	Exciter saturation constant
$\mathbf{B_{cl}}$	Closed-loop input matrix
$\mathbf{B_m}$	Modal input matrix
$\mathbf{b}$	Input vector
b	Exponent in reactive power model
$\mathbf{C}$	Output matrix
$\mathbf{C_1}$	Output Matrix
$\mathbf{C_2}$	Output matrix
$\mathbf{C_k}$	Control output matrix
$\hat{C}$	Intermediate controller output matrix
$\mathbf{C_{cl}}$	Closed-loop output matrix
$\mathbf{C_m}$	Modal output matrix
$\mathbf{c}$	Output vector
c_i	Weighting factors
D	Damping co-efficient
$\mathbf{D}$	Input-output transmission matrix

$\mathbf{D_{11}}$	Input-output transmission matrix
$\mathbf{D_{12}}$	Input-output transmission matrix
$\mathbf{D_{21}}$	Input-output transmission matrix
$\mathbf{D_{22}}$	Input-output transmission matrix
D_k	Controller input-output Transmission Matrix
$D_k(s)$	Controller denominator polynomial
$\hat{D}$	Intermediate Controller input-output transmission matrix
$\mathbf{d}$	Input-output transmission vector
d_1	Co-efficient of numerator-polynomial
d_2	Co-efficient of numerator-polynomial
d_3	Co-efficient of numerator-polynomial
dcv	Direction cosine vector
E_{max}	Energy stored in SMES coil
E_d'	Direct axis transient voltage
E_q'	Direct axis transient voltage
E_{fd}:	Exciter voltage
$\mathbf{F(x)}$	Vector objective function
$\mathbf{F}$	Vector function operator
F	Frequency
$\mathbf{g}$	Vector function operator
$\mathbf{G(s)}$	Plant Transfer function matrix
$\mathbf{G_p(s)}$	Plant Transfer function matrix
G	Conductance
H	H-constant of machine
H_2	2-norm of a matrix or scalar function
H_∞	Infinity norm of a matrix or scalar function
$\mathbf{I}$	Identity matrix
I	Current
I_{max}	Maximum current
I_{SM}	SMES coil current
$I_{SM,\ max}$	Maximum coil current through SMES

I_d	Direct axis current
I_q	Quadrature axis current
$\bar{I}$	Current vector
$\boldsymbol{J}$	Control cost
j	Imaginary operator respectively
$K(s)$	Controller transfer function
K_a	AVR gain in excitation system
K_v	Voltage regulator gain in SMES model
K_{pv}	Co-efficient related to modified Walve type load model
K_{pw}	Co-efficient related to modified Walve type load model
K_{qv}	Co-efficient related to modified Walve type load model
K_{qv1}	Co-efficient related to modified Walve type load model
K_{qv2}	Co-efficient related to modified Walve type load model
K_{qw}	Co-efficient related to modified Walve type load model
K_{pf}	Co-efficient related to frequency dependent load model
K_{qf}	Co-efficient related to frequency dependent load model
$\boldsymbol{L}$	Function operator
L	Inductance
M	Sub-Matrix of **X**
M	Modulation index
M	Machine inertia constant
N	Sub-Matrix of **X**
n_1	Co-efficient of numerator-polynomial
n_2	Co-efficient of numerator-polynomial
n_3	Co-efficient of numerator-polynomial
n_p	Real power indices related to static exponential load model
n_q	Reactive power indices related to static exponential load model
P	Real power in general
P_L	Real power in load
P_{ZIP}	Real power of load based on ZIP model
P_{EX1}	Real power of load based on exponential model
P_{EX2}	Real power of load based on exponential model

$P_{k,m}$	Real power in the line between bus 'k' and bus 'm'
$\boldsymbol{P}$	Plant parameter matrix
$P_{SM,}$	Dynamic real power variable in the SMES model
P_{sms}	Dynamic real power variable in the SMES model
P_{smr}	Dynamic real power variable in the SMES model
p_1	Co-efficient in the real power model
p_2	Co-efficient in the real power model
p_3	Co-efficient in the real power model
p_4	Co-efficient in the real power model
p_5	Co-efficient in the real power model
Q	Reactive power in general
Q_L	Reactive power in load
Q_{ZIP}	Reactive power of load based on ZIP model
Q_{EX1}	Reactive power of load based on exponential model
Q_{EX2}	Reactive power of load based on exponential model
Q_{SM}	Dynamic reactive power variable in the SMES model
Q_{smc}	Dynamic reactive power variable in the SMES model
Q_{smt}	Dynamic reactive power variable in the SMES model
q	Number of plants
q_1	Co-efficient in the reactive power model
q_2	Co-efficient in the reactive power model
q_3	Co-efficient in the reactive power model
q_4	Co-efficient in the reactive power model
q_5	Co-efficient in the reactive power model
R	Sub-Matrix of **X**
R	Residue matrix
$\boldsymbol{R}$	Matrix function operator
R	Residue
R_s	Stator resistance
R_f	Dynamic variable in excitation system
R^N	N-dimension real Euclidean space

r	Reference
S	Sub-Matrix of **X**
S	Sensitivity Matrix
S_p	Summation of real power injected at a bus
S_q	Summation of reactive power injected at a bus
S_e	Saturation function operator
s	Laplace variable
T	Transformation matrix
T	Time constant in dynamic load
T_c	Transition temperature
T_m	Mechanical input torque
T_D	Damping torque
T_{elec}	Electrical torque
T_{d0}'	Direct axis open circuit transient time constant
T_{d0}''	Direct axis open circuit sub-transient time constant
T_{q0}'	Quadrature axis open circuit transient time constant
T_{q0}''	Quadrature axis open circuit sub-transient time constant
T_b	Lead time constant in TGR circuit in excitation system
T_c	Lag time constant in TGR circuit in excitation system
T_a	AVR time constant
T_e	Exciter time constant
T_f	Time constant in excitation stabilisation circuit
T_r	Input filter time constant in excitation system
T_{cp}	Response time constant in real power channel of SMES
T_{cq}	Response time constant in reactive power channel of SMES
T_{v1}	Lead time constant in AVR in reactive power channel of SMES
T_{v2}	Lag time constant in AVR in reactive power channel of SMES
T_{vm}	Input filter time constant in reactive power channel of SMES
T_w	Time constant of the washout filter

T_{zw}	Transfer function matrix in mixed sensitivity formulation
T_s	Settling time
U	Voltage
u	input
U	Matrix
V	Right Eigenvector matrix
V	Voltage
V_1	Voltage at bus #1
V_2	Voltage at bus #2
V_t	Terminal voltage
V_L	Load Voltage
V_0	Voltage initial operating condition
V_j	Voltage at jth bus
V_k	Voltage at kth bus
V_r	Voltage regulator output
Vq	Quadrature axis voltage in machine reference frame
V_d	Direct axis voltage in machine reference frame
V_Q	Quadrature axis voltage in network reference frame
V_D	Direct axis voltage in network reference frame
V_{ref}	Reference voltage input
V_{rmax}	Maximum output of voltage regulator
V_{rmin}	Minimum output of voltage regulator
v	Right eigenvector
W	Left eigenvector
W	Matrix of weights
$\mathbf{W_1}$	Matrix of weights
$\mathbf{W_2}$	Matrix of weights
w	Left eigenvector
w_d	Imaginary part of a complex pole
X	Symmetric positive definite matrix
$\mathbf{X_p}$	Symmetric positive definite matrix
$\mathbf{X_\infty}$	Symmetric positive definite matrix

X_l	Line reactance
X_2	Line Reactance
X_{ls}	Stator leakage reactance
X_d	Direct axis steady state reactance
$X_d^{'}$	Direct axis transient reactance
$X_d^{''}$	Direct axis sub-transient reactance
X_q	Quadrature axis steady-state reactance
$X_q^{'}$	Quadrature axis transient reactance
$X_q^{''}$	Quadrature axis sub-transient reactance
$\mathbf{X}$	Solution vector
$\mathbf{x}$	Generalised state vector
$\mathbf{x_m}$	Modal state vector
$\mathbf{y}$	Output vector
z	Complex number
z	Vector
Δ	Phase angle
Δ	Incremental operator
Φ	Intermediate matrix variable in LMI formulation
Ψ_{11}	Intermediate matrix variable in LMI formulation
Ψ_{12}	Intermediate matrix variable in LMI formulation
Ψ_{22}	Intermediate matrix variable in LMI formulation
Ψ_{1d}	Dynamic flux linkage variable
Ψ_{2q}	Dynamic flux linkage variable
Π_1	Intermediate matrix variable in LMI formulation
Π_2	Intermediate matrix variable in LMI formulation
α	Thyristor control angle
α_i	Co-efficient in convex polytope
β	Angle
γ	Optimisation variable and measure of robustness margin in LMI based design

θ	Bus voltage angle, angle in the left-half eigenplane
θ_L	Dynamic load voltage angle
ϕ	Phase angle
ς	Damping ratio
ς_{min}	Minimum required damping ratio
δ	Machine angle
$\delta(s)$	Closed-loop characteristic polynomial
λ	Eigen-value
η	Matrix in Kronecker product
μ	Eigenvalue
σ	Real part of eigenvalue
ω	Imaginary part of an eigenvalue
ω_s	Synchronous speed
$\otimes$	Kronecker product operator
*	Complex conjugate operator

AC	Alternating Current
AGC	Automatic generation control
ARE	Algebraic Riccati Equation
AVR	Automatic Voltage Regulator
BESS	Battery Energy Storage system
BFGS	Broyden Fletcher Goldfarb Shano
BPA	Bonneville Power Authority
CC	Constant Current
CP	Constant Power
CI	Constant Impedance
CICC	Cable in Conduit Conductor
CSC	Controllable Series Capacitor
DC	Direct Current
DAE	Differential algebraic equation
DE	Detroit Edison
DNA	Defence Nuclear Agency

DOE	Department of Energy
EHV	Extra High Voltage
EMF	Electro Motive Force
EPRI	Electric Power Research Institute
ETM	Engineering Test Model
FACTS	Flexible AC Transmission Systems
GTO	Gate Turn Off
GBFEL	Ground Based Free Electron Laser
HQ	Hydro Quebec
HSV	Hankel Singular Value
HTSC	High Temperature Superconducting Coil
HVDC	High Voltage Direct Current
Hz.	Hertz
IA	Inter-area
IEEE	Institute of Electrical and Electronic Engineers
ISTEC	International Superconductivity Technology Centre
kV	Kilo Volt
kWh	Kilo Watt Hour
LANL	Loss Alamos National Laboratory
LFC	Load frequency control
LHP	Left Half Plane
LMI	Linear Matrix Inequality
LSRS	Load Shedding Regional Scheme
LQG	Linear Quadratic Gaussian
MAPP	Midcontinental American Power Pool
MH	Manitoba Hydro
MIMO	Multiple input multiple output
MISO	Multiple input single output
MJ	Mega Joules
ms	milliseconds
MVAR	Mega VAR
MW	Mega Watt
MWh	Mega Watt Hour

NETS	New England Test System
NPCC	Northeast Power Co-ordinating Council
NYPS	New York Power System
OH	Ontario Hydro
PAR	Phase Angle Regulator
PWM	Pulse Width Modulation
PCS	Power Conditioning System
PSS	Power System Stabiliser
PACI	Pacific AC Inter-tie
QP	Quadratic Programming
RPV	Remotely Piloted Vehicle
RASMES	Research Association of Superconducting Magnetic Energy Storage
SDIO	Strategic Defence Initiative Organisation
SECWA	State Energy Commission of Western Australia
SI	Superconductivity Inc.
SIMO	Single input multiple output
SISO	Single input single output
SMES	Superconducting Magnetic Energy Storage
SMIB	Single Machine Infinite Bus
SSR	Sub-Synchronous Resonance
STATCOM	Static Compensator
SQP	Sequential Quadratic Programming
SVC	Static Var Compensator
TCBR	Thyristor Controlled Braking Resistor
TGB	Truck Guided Bus
TGR	Transient Gain Reduction
TRP	Technology Reinvestment Project
UPFC	Unified Power Flow Controller
USA	United States of America
WHO	Western Ontario Hydro
WNEDM	Weighted Normalised Eigenvalue Distance Minimisation
WSCC	Western System Co-ordinating Council

List of Tables

2.1 Benefits of SMES

2.2 Rating of SMES for various applications

4.1 Generator coherency matrix for Study system #1

4.2 Bus- Generator coherency matrix of Study system #1

4.3 Generator coherency matrix for Study system #2

4.4 Bus- Generator coherency matrix of Study system #2

4.5 Electromechanical modes (in Hz) of Study system #3

4.6 Generator coherency in Study system #3

4.7 Damping ratio and frequency for different models (Study system #1)

4.8 Damping ratio and frequency for different models (Study system #2)

4.9 Damping ratio and frequency for different models (Study system #3)

4.10 Effect of excitation characteristics on damping ratio and frequency (Study system #1)

4.11

4.11 Effect of excitation characteristics on damping ratio and frequency (Study system #2)

4.12 Effect of excitation characteristics on damping ratio and frequency (Study system #3)

4.13 Effect of tie line power flow on damping ratio and frequency (Study system #1)

4.14 Effect of tie line power flow on damping ratio and frequency (Study system #2)

4.15 Effect of tie line power flow on damping ratio and frequency (Study system #3)

4.16 Effect of tie line strength on damping ratio and frequency (Study system #1)

4.17 Effect of tie line strength on damping ratio and frequency (Study system #2)

4.18 Effect of tie line strength on damping ratio and frequency (Study system #3)

4.19 Effect of different load characteristics on damping ratio and frequency (Study system #1)

4.20 Effect of different load characteristics on damping ratio and frequency (Study system #2)

4.21 Effect of different load characteristics on damping ratio and frequency (Study system #3)
5.1 Desired damping ratio at different values of frequencies and at different desired settling time (oscillations settle with in 2% of initial value)
5.2 Desired damping ratio at different values of frequencies and at different desired settling time (oscillations settle with in 5% of initial value)
6.1 Residues at different potential bus locations (Study system #1)
6.2 Residues at different potential bus locations (Study system #2)
6.3 Residues at different potential bus locations (Study system #3)
7.1 Hankel Singular Values (HSV) of the plant
7.2 Poles of the reduced plant (Study system #1)
7.3 Damping ratios in both operating cases (Study system #1)
7.4 Damping ratios at various values of power flow (Study system #1)
7.5 Damping ratios at different load characteristics (Study system #1)
7.6 Damping ratios in both operating cases with $K_1(s)$ only (Study system #2)
7.7 Damping ratios in both operating cases with $K_1(s)$ & $K_2(s)$ (Study system#2)
7.8 Damping ratios at various values of power flow (Study system #2)
7.9 Damping ratios at different load characteristics (Study system #2)
7.10 Damping ratios in both operating cases with $K_1(s)$ only (Study system #3)
7.11 Damping ratios in both operating cases with $K_1(s)$ & $K_2(s)$ only (Study system #3)
7.12 Damping ratios in both operating cases with $K_1(s)$, $K_2(s)$ & $K_3(s)$ (Study system #3)
7.13 Damping ratios at various values of power flow (Study system #3)
7.14 Damping ratios at different load characteristics (Study system #3)
7.15 Comparison of damping ratios obtained by two control-design techniques
8.1 Damping ratios in both operating cases (Study system #1)
8.2 Damping ratios at various values of power flow (Study system #1)
8.3 Damping ratios at different load characteristics (Study system #1)
8.4 Damping ratios in both operating cases with $K_1(s)$ only (Study system #2)
8.5 Damping ratios in both operating cases with $K_1(s)$ & $K_2(s)$ (Study system #2)
8.6 Damping ratios at various values of power flow (Study system #2)
8.7 Damping ratios at different load characteristics (Study system #2)

8.8 Damping ratios in both operating cases with $K_1(s)$ only (Study system #3)

8.9 Damping ratios in both operating cases with $K_1(s)$ & $K_2(s)$ only (Study system #3)

8.10 Damping ratios in both operating cases with $K_1(s)$, $K_2(s)$ & $K_3(s)$ (Study system #3)

8.11 Damping ratios at various values of power flow (Study system #3)

8.12 Damping ratios at different load characteristics (Study system #3)

8.13 Poles and zeros of the 14^{th} order controllers

8.14 Closed-loop damping by two control approaches

8.15 Comparison of damping ratios obtained by two control-design techniques

List of Figures

2.1 Component Block Diagram of a SMES system

2.2 A single machine infinite bus system with shunt current device

2.3 Control of power flow in the line through shunt injection

3.1 Block Diagram of a DC1A-type Excitation System

3.2 Block Diagram of a ST1A-type Excitation System

3.3 Functional Block Diagram of a SMES System

3.4 Small Signal Model of a SMES

4.1 A 4-machine-11-bus system

4.2 A 6-machine-16-bus system

4.3 A 16-machine-five-area study system

4.4 Response of Study system #1 under large disturbances

4.5 Response of Study system #2 under large disturbances

4.6 Response of Study system #3 under large disturbances

5.1 Desired damping ratios at different frequencies and settling times

5.2 Desired damping ratios at different frequencies and settling times

6.1 Open-loop frequency response of the SMES at bus #10 (Study system #1)

6.2 Open-loop frequency response of the SMES at bus #15 (Study system #2)

6.3 Open-loop frequency response of the SMES at bus #08 (Study system #2)

6.4 Open-loop frequency response of the SMES at bus #54 (Study system #3)

6.5 Open-loop frequency response of the SMES at bus #14 (Study system #3)

6.6 Open-loop frequency response of the SMES at bus #13 (Study system #3)

6.7 Open-loop frequency response of the SMES at bus #15 (Study system #3)

7.1 Closed-loop control system

7.2 Singular value response of plant

7.3 Frequency response of $K(s)$

7.4 Frequency response of the original and the reduced system (Study system #2)

7.5 Frequency response of the original and the reduced system (Study system #2)

7.6 Frequency response of the original and the reduced system (Study system #3)

7.7 Response of Study system #1 under large disturbances

7.8 Response of SMES under large disturbances in Study system #1
7.9 Response of Study system #2 under large disturbances
7.10 Response of SMES under large disturbances in Study system #2
7.11 Response of Study system #3 under large disturbances
7.12 Response of SMES under large disturbances in Study system #3
7.13 Controller response in Study system #2 under small disturbances
7.14 Dynamic response of Study system #2 under large disturbances

8.1 Standard mixed-sensitivity design set up
8.2 Region for the closed-loop poles with minimum damping ratio $cos\theta$
8.3 Frequency response of $W_1$and W_2
8.4 Modified frequency response of $W_1$and W_2
8.5 Response of Study system #1 under large disturbances
8.6 Response of SMES under large disturbances in Study system #1
8.7 Response of Study system #2 under large disturbances
8.8 Response of SMES under large disturbances in Study system #2
8.9 Response of Study system #3 under large disturbances
8.10 Response of SMES under large disturbances in Study system #3
8.11 Controller response in Study system #2 under small disturbances
8.12 Dynamic response of Study system #2 under large disturbances

CHAPTER ONE

INTRODUCTION

1.1 INTER-AREA OSCILLATIONS

The inter-area oscillations are inherent in large interconnected power systems. The phenomenon is very complex as it involves several electromechanical oscillatory subsystems often comprising several groups of machines distributed over neighbouring utilities. These oscillations are poorly damped and hence pose a threat to the economic and reliable means of power exchange through tie lines connecting neighbouring utilities. In this chapter, a brief overview of the problem will be given. The inter-area oscillations faced by several utilities will be discussed in an attempt to develop an understanding of the basic nature and source of these oscillations.

1.1.1 A BRIEF OVERVIEW OF THE PROBLEM

Power system stability is a complex subject that has challenged power system engineers for many years. As power systems evolved, interconnections between independent systems were found to be economically attractive. While interconnections result in operating economy and increased reliability through mutual assistance, they also contribute to increased complexity of stability problems and increase the consequences of instability. Much of the industry effort and interest related to system stability since 1960s have been concentrated on transient stability. Improvements to transient stability came about by way of faster fault clearing and continuous-acting voltage regulators with no dead band, series capacitors and special stability aids. Accompanying these aids has been an increased tendency of power systems to exhibit oscillatory instability. Higher-response exciters, whilst improving transient stability, adversely affect small-signal stability by introducing negative damping.

With the growth of extensive power systems and particularly with the interconnection of these systems by tie lines of limited capacity, the power transfer between systems becomes a serious problem as low-frequency oscillations in the range of 0.1 Hz to 1.0 Hz became apparent. Under these conditions, synchronous machine rotors of one area oscillate with the rotors of other areas. The oscillations are very prolonged,

i.e. poorly damped, imposing the threat to the inter-tie power transfer. This is the historical *inter-area oscillation* problem that has been faced by many power utilities across the world for several decades. Inadequate damping restricts the maximum power transfer across the tie lines. The very general nature of the problem experienced by several interconnected power utilities can be described very briefly as follows:

- Inter-area oscillations are associated with weak transmission links and heavy power transfers.
- They are due to a natural mode of the system and therefore, cannot be eliminated. However, their damping and frequency can be modified.
- As power systems evolve, the frequency and damping of existing modes change and new ones may emerge.
- Inter-area oscillations often involve more than one utility and may require the co-operation of all to arrive at the most effective and economical solution.
- The generator amortisseur winding is no longer effective as the damping produced at very low-frequency is reduced in approximately inverse proportion to the square of the effective external impedance plus the stator impedance. Therefore, the damping torque practically disappears.
- The proliferation of automatic controls has increased the probability of adverse interactions among them. Even without such interactions, the two basic controls, i.e. the speed governor and the generator voltage regulator practically always produce negative damping for frequencies in the power system oscillation range: the governor effect is small, the AVR effect is large. As the generator initial angle increases with high tie line loading, the terminal voltage becomes very sensitive to angular swings. As a result, the voltage regulator acts and produces negative damping as an unwanted side effect.
- Even though automatic controls are practically the only devices that can produce negative damping, the damping of the uncontrolled system is itself very small and can easily allow the continually changing load and generation response to result in unsatisfactory tie line power oscillations.

1.1.2 THE UTILITY EXPERIENCES

To illustrate some of the various ways in which low damping of system oscillations has contributed to stability problems in power system; a few examples are cited of instances that have occurred:

Detroit Edison (DE) – Ontario-Hydro (OH) – Hydro Quebec (HQ) [1]: In the early 1960s, connections were tried between these three power systems. Oscillations were observed in the OH system when the power flow was in either of DE→OH→HQ or HQ→OH→DE. The role of OH in both cases was of an equivalent synchronous condenser. The bus voltage in the OH system was sensitive to the tie line loading in both sides and angular differences between the OH-DE and OH-HQ. The fast-acting-voltage-regulation systems in OH were subjected to act on. This resulted in poor inter-area mode damping. The simple solution was to reduce the regulator gains.

Saskatchewan (Ask)-Manitoba Hydro (MH) – Western Ontario Hydro (WHO) [2]: The situation was similar to that of the previous one. The MH system suffered significant oscillations.

Finland – Sweden (and Norway) – Denmark [3]: In the later half of the 1960s, oscillations were observed at various operating conditions. The situation is fundamentally similar to that of two previous systems. At this time (1969), the power system stabiliser (PSS) was available and its application was recommended.

Italy-Yugoslavia-Austria [3]: During the period 1971-1974, several attempts were made to interconnect the Yugoslavian power system with the Italian and Austrian networks. Undamped inter-area oscillations caused tripping of the tie lines. In the oscillations, the Yugoslavian generating units were swinging against the rest of the system at a frequency of 0.17 to 0.22 Hz. depending on the configuration of the interconnected system. Installing PSS in some of the Yugoslavian units cured the instability.

Western system co-ordinating council (WSCC) [4,5,6,7]: Power transfer capability in the WSCC system has been stability limited in several instances due to the long distance between load centres and power sources. Limitations were experienced due to insufficient damping torque, as well as insufficient synchronising torque. This system has a rich history of inter-area oscillations beginning in 1964. Both simulated and actual oscillations have been significant in the development of the WSCC.

In 1964, the Northwest United States and Southwest United States were interconnected through the Colorado River Storage Project 230 kV and 345 kV systems. It was immediately apparent that the damping torque was a factor that the interconnected western utility must consider. During the nine-month period of interconnected operation, there were at least 100 tie separations due to system oscillations of power, frequency and voltage. In 1965, the problem was solved by modifications made to one of the hydro-unit governors [4].

Fortunately, at about this time, work was initiated to develop time domain stability programs which allowed for more detailed analysis of interconnected systems. This was very timely since it coincided with the planning of many 345 kV and 500 kV transmission projects, including the Northwest-Southwest Inter-tie which consisted of two 500 kV ac lines and ± 400 kV dc circuit to be in-service in 1968. The system was planned initially for 2000 MW on the ac circuits and 1440 MW on the dc line. Studies conducted to assess stability performances showed that there was insufficient damping torque for ac power flows greater than 1300 MW. The study showed undamped oscillations of power, frequency and voltage at about 0.33 Hz [5].

It was determined that many of the generator automatic voltage regulators (AVR) produced negative damping at the inter-tie frequency of 0.33 Hz. This led to the development and application of PSS. It was found from time domain simulations that sufficient damping would exist for the most severe disturbance with 1800 MW through the ac lines if PSS were applied to all generators of the WSCC. After all the units were retrofitted with PSS, there were no cases of oscillations and the stability limit was based upon the synchronising torque only. To relieve the synchronising torque limitation, the Bonneville Power Authority (BPA) implemented a 1400 MW braking resistor at Chief Joseph Dam in 1974. This had the effect of increasing the synchronising torque such that loading on the ac inter-tie lines could be increased to at least 2500 MW without the concern of insufficient synchronising torque following the most severe single disturbance. With increased loading, slowly growing oscillations were observed, thus indicating that insufficient damping torque was again a problem at the higher loading level. This problem was relieved by the development of a scheme [6] to modulate the northern terminal of the Northwest-Southwest dc line in such a manner as to provide positive damping to the ac system at the inter-tie frequency.

From the above case descriptions, it is interesting to note that the transmission capacity was increased from 1300 MW to 2500 MW without adding any transmission circuits. The only system additions were PSS, braking resistors and HVDC modulation.

Many other interfaces in western USA are limited by insufficient damping torque and are highly dependent on PSS and other devices to provide positive damping. Currently there is a 0.7 Hz lightly damped inter-area mode identified from system models and various analytical techniques. In one interface, nearly 750 Mvar of static var compensators are being installed to add damping so that the planned transmission capacity will be available [7].

On August 10, 1996, the Pacific AC inter-tie (PACI) emerged from the dormancy that had lasted since 1974. The mechanism of failure (not the cause) was a transient oscillation, under conditions of high power transfer on long paths that had been progressively weakened through a series of fairly routine resource losses.

Mid-Continent Area Power Pool (MAPP): In 1971 and 1972, over seventy unstable inter-area oscillations occurred in the MAPP system in North America [8]. The oscillations were triggered by minor disturbances and had frequencies of 0.12 to 0.25 Hz. About ten of these incidents resulted in the complete isolation of the North Dakota system. The major corrective actions that were taken to the undamped oscillations were the reduction of scheduled interchanges between utilities, installation of a relay system to detect impending oscillations, the installation of PSS in some of the units, raising the system voltage by adding fixed capacitors, boosting transformer taps etc.

Southeast Australia: In 1975, unstable oscillations of 0.6 Hz appeared in the interconnected system of the states of New South Wales and Victoria [9]. Simulations of the conditions of the incident confirmed the existence of an oscillatory mode at a frequency around 0.6 Hz. The major factors those were found to contribute to low damping were high levels of transfers between the two states coupled with high average generator loading on the Latrobe valley unit. Interim operating limits, which avoided unstable conditions, were imposed to allow time to search for permanent solution. A long-term solution to the problem was found by installing PSS in several units and adopting a load modulation strategy.

Scotland-England: Spontaneous low-frequency power oscillations were first experienced on the Scotland-England interconnection in 1979 and were initially ascribed to high transfers (1400 MW+), high gain Scottish exciters and load characteristics [10].

Imposing restriction on the transfer levels apparently contained the oscillations. The problem recurred intermittently between 1979-82 at lower export (down to 400 MW) and under various system operating conditions, eventually reaching unacceptably high levels. A more permanent cure was to retrofit PSS to all of the existing excitation system [11] and to fit PSS as standard on all new exciters [12]. This allowed the export capability to increase to 1600 MW.

Western Australia: In 1982 and 1983, the State Energy Commission of Western Australia (SECWA) experienced, on a number of occasions, lightly damped system oscillations having a frequency of about 0.2 Hz [3]. A comprehensive study of the SECWA system confirmed the existence of a low-frequency, 0.2 to 0.3 Hz., inter-area mode. The damping of this mode was found to be sensitive to load characteristics, governor droop and transmission system strength. As recommended in the study, PSS were installed on selected generating units to enhance the damping of the inter-area mode.

Taiwan: In February and March of 1984, unstable inter-area oscillations of 1.0 to 1.1 Hz occurred several times on the Taiwanese power system [13]. These incidents occurred during off-peak periods when the flow on the EHV transmission lines was heavy. Studies showed that the unstable oscillations could be eliminated by restricting the flow on the EHV lines and by placing PSS in selected plants.

Ghana-Ivory Coast: In September 1985, unstable oscillations were observed on the interconnected systems of Ghana (VRA) and Ivory Coast (EECI) [3]. A full small signal analysis of the VRA-EECI system revealed the presence of a poorly damped inter-area mode in the frequency range of 0.6 to 0.7 Hz. All generating units took part in this mode, with the VRA machines oscillating against those of EECI across the 225 kV tie line between the two systems. The study demonstrated that the stability of the mode depended on the load level, generation pattern and magnitude and direction of the tie line flow. The installation of a PSS at a specific plant was recommended.

Ontario Hydro (OH): Beginning in 1985, low-frequency inter-area oscillations involving the entire Northeast Power Co-ordinating Council (NPCC) system were observed in the planning and operation studies. On-line measured system responses also indicated the presence of a low-frequency mode of oscillation. The frequency of the oscillations varied between 0.25 and 0.4 Hz depending on the operating conditions, load levels and other factors. Based on the extensive investigations, a number of remedial

measures were taken by OH to improve the damping of these oscillations. They include, the installation of PSS in major existing generating units, recommendations to equip all future generating units with PSS, installation of special monitors for capturing oscillations, etc. Since the above measures were implemented, monitoring on-line system responses show significant improvement in the damping of the low-frequency oscillation [14].

Southern Brazil: During the period between 1975 and 1980, the power flow was consistently running from the South-eastern to the Southern Region of Brazil and the system operated very near its steady-state stability limit. The situation became worse in 1978, when the power had to be rationed due to a drought throughout the Southern Region of the country. Due to these factors, the Southern system at times oscillated relative to the South-eastern system, resulting in the opening of the interconnections and operation of the Load Shedding Regional Scheme (LSRS), upon under-frequency.

At the time, considering that the proper tools for evaluation of this phenomenon were not available, a provisional solution was adopted. From the analysis performed, it was determined that whenever oscillations occurred, the internal angle difference between South and Southeast system generators, associated with the same load centre would reach beyond 75^0. A maximum angle of 70^0 was then adopted for the determination of the new operating conditions. With this procedure, a substantial reduction of the swings between the two systems was achieved.

Later, in 1981, the first 750 kV transmission line interconnecting the Southeast and the South was commissioned. A new type of oscillation now appeared, involving the Itaipu 60 Hz plant versus the interconnected system. With the commissioning of Itaipu, Salto Santiago (4x333 MW), and GB Munhoz (4x418 MW) the direction of flow most of the time was now running from the South to the Southeast.

In 1984, the critical hydro conditions in the Southern region, delays in the erection schedule of Itaipu machines, in addition to an increase of the load, requiring full utilisation of the Paranaiba plants, led to new electromechanical oscillation problem. During this time, several specific measures were adopted in order to improve the damping of these oscillations. They included the activation of additional stabilisers on those units in which the PSS had been disconnected, using generator output power as a stabilising signal etc. Later, work was also carried out in order to obtain an overall optimisation of the excitation systems at the main plants, which allowed a substantial

increase in some transmission and/or generation limits. Eigenvalue techniques [15,16] proved highly effective in this stabilisation study.

Although the results described above were quite satisfactory, with the commissioning of the second 750 kV line in 1989, the possibility of changing the stabiliser structures at the main interconnected system plants was investigated. The intent of this was to obtain further improvements of the system dynamics in terms of damping inter-area oscillation. This was done in an attempt to minimise/eliminate LSRS. The investigation process suggested some control strategies and operating procedures. Some of them were scheduling of generation so that the damping of the oscillation is improved, operating the tie lines at the highest possible voltage, restricting the power flows in the tie lines, operating some generating units as synchronous condensers to achieve better operating conditions as a consequence of improved voltage control etc.

1.1.3 POSSIBLE MEASURES AGAINST OSCILLATIONS

From the detail of the oscillation problem faced by several utilities, it is clear that PSS is the most economic solution to the problem of inter-area oscillations. Almost all of the power utilities in the world are currently equipped with PSS. Besides PSS, other strategies to damp oscillations are as follows:

- Reduce voltage regulator gain
- Switching some of the units to manual control
- Tuning Governor setting
- HVDC modulation
- Reduction of schedule interchange between utilities
- Raising system voltage by increasing excitation of generators, boosting transformer taps, and fixed capacitors
- Using some of the system generators as synchronous condensers
- Increasing transmission system voltage
- Adopting load modulation scheme
- Rescheduling generations
- Restricting the maximum angular difference between two utilities to a limiting value
- Under frequency load shedding schemes

Some of the strategies are clearly uneconomical. But they were adopted by the utilities either before the concept of PSS was known or the development on small signal analysis of the large system was inadequate to evaluate the effectiveness of PSS.

In the last two decades, the applications of several other devices for damping inter-area oscillations have been suggested. Some of them are static var compensator (SVC) [17,18,19], controllable series compensation (CSC) [20,21,22], static synchronous compensator (STATCOM) [23,24,25], thyristor controlled braking resistor (TCBR) [26,27,28], HVDC link modulation [6,27,30], phase angle regulator (PAR) [31,32,33], battery energy storage systems (BESS) [34,35], superconducting magnetic energy storage (SMES) [36-43] system and more recently the unified power flow controller (UPFC) [44,45,46]. These high power electronic devices have been considered to be on the heart of the Flexible AC Transmission Systems (FACTS), an emerging concept [47] in controlling bulk power flow in power systems.

It is generally understood that the devices installed in series with the lines are more effective in damping power oscillation. The shunt devices such as SVC, STATCOM etc. are connected to the bus and control the voltage. The damping improvement is thus through reactive power modulation. However, it will be shown in the next chapter that the energy storage option overrides the superiority of the series connected devices in damping power oscillations. The motivation comes from the fact that: real power oscillation is of concern so real power modulation will prove more effective. The superconducting magnetic energy storage (SMES) device has the potential of both voltage control and a storage option. The ability of a SMES to damp power system oscillations through independent real modulation is very promising. This exceptional feature of a SMES will be explored further in this proposed research to design damping control strategies. A controlled sequence of charging and discharging of the SMES will be shown to damp out oscillations very effectively.

1.2 OBJECTIVE OF THE THESIS

The objectives of this research are:

- To analyse the factors influencing the damping and frequency of inter-area mode of oscillations. The effects of power flow in the tie line, damping characteristics

of machines, excitation systems and nature of loads will be analysed in detail to develop an understanding of the problem in respect of several study systems.

- To investigate the potential of the SMES device(s) to damp out oscillations. Two issues will be further investigated:

  (a) Location: Emphasis will be to select a site which will provide the best location so far as the damping of inter-area oscillation is concerned. The very special feature of the SMES in terms of its real power will be exploited via a real power modulation option. Much attention will be given to the identification of the most effective stabilising signals and suitable control location.

  (b) Controller design: The design aspect of the damping controller will be the major part of the thesis. Two methods will be followed. The Weighted and Normalised Eigenvalue-distance Minimisation (WNEDM) method for low-order robust damping control design will be applied for three study systems. The application of the Linear Matrix Inequalities (LMIs) concept to H_∞ design will also be explored to design robust damping controller(s). Various practical issues such as weight selection; model reduction etc. will be discussed in detail. The robustness aspect of the controller will be the primary focus. Every effort will be made to make the design process very methodical. Care will be given to minimise interactions amongst inter-area, local and control modes. The performance of the controller(s) will be tested both in the frequency and time domains. The robustness of the controller will be tested for a wide range of operating conditions through non-linear simulation under small as well as large disturbances. It will be also shown that variation in load characteristics will not affect the controller performance.

- To investigate the sizing of the SMES device(s) mainly based on its capability to damp out inter-area mode oscillations.

1.3 OUTLINE OF THE THESIS

The thesis mainly describes the damping control design strategies employing SMES device(s) for three study power systems. A brief description of the contents of each chapter is as follows.

Chapter Two: The role of the SMES device as a power flow control option is discussed. It is explained through a proper illustration that the injection or absorption of shunt real power provides a wider range of generator real power modulation than that by injection or absorption of shunt reactive power through a SMES. The basic principle of operation and structure of a SMES unit in a power system is detailed. The various application options of SMES in a power system is described. Several benefits that have been and can be achieved by SMES devices of various sizes are discussed in detail. The technology development across the world is also elaborated. Some practical issues such as costing, sizing etc. are addressed.

Chapter Three: The modelling of various components of power systems such as synchronous machines, excitation systems, transmission networks and load for small signal stability studies is discussed. The small signal model for the SMES system is also discussed in detail in this chapter.

Chapter Four: Three study power systems are described. The effects of various factors such as machine model, excitation model, load model, tie line strength, power flow through tie lines etc. on the damping and frequencies of inter-area modes are examined. Non-linear simulations, following a large disturbance are also performed to see how inadequately damped inter-area modes govern the system dynamics.

Chapter Five: The damping design criteria followed by various utilities are discussed. The advantages and disadvantages of these criteria are detailed to stress the need for developing more general guidelines. An analytical approach is introduced based on the simple concept of settling time in a linear second order system. A discussion is made about the allowance of a safety factor in the damping ratio because of the saturation limit imposed on the output of the controller.

Chapter Six. The methods of controllability, observability and residue are discussed to identify the effective locations and stabilising signals. The possible location and signals for the study systems are suggested.

Chapter Seven: The description of WNEDM technique for low-order robust damping control is discussed. The modification of the method to suit to power system damping control design is suggested. Some practical issues related to the weight selection and model reduction for better controller design are addressed. The damping controller(s) is designed for three study systems. The performance of the controller(s) is evaluated by eigenvalue techniques. The effect of system non-linearity, saturation etc. on the controller performance has been examined further through non-linear simulation following a large disturbance. The effect of various load characteristics is also examined to further verify the performance of the controller(s). The required rating of the SMES device(s) to damp out inter-area mode(s) for the study systems is evaluated.

The performance comparison of the controller based on this method is made with that of the controller obtained by the root-locus technique.

Chapter Eight: A brief discussion of LMI is made. The solution technique to the LMI problem is discussed. The H_∞ mixed sensitivity control design in the LMI framework is described. The controller(s) is designed for the study systems. The selection of weights for the successful design and relevant controller order reduction is discussed. The recommendation on standardising weights is made. The performance of the controller(s) is evaluated in the frequency and time domains. The robustness of the controller is also verified in the face of the uncertainty of the load characteristics. The power and energy ratings of the SMES devices are evaluated. A discussion is also provided on the availability of the required size of the devices.

Chapter Nine: This chapter provides an overall conclusion of the thesis. The scope of further work is also discussed.

1.4 ORIGINAL CONTRIBUTIONS OF THE THESIS

It is thought that the following matters reported in the thesis are original.

- The problem of inter-area oscillations has been analysed in great detail. The possible factors such as; excitation characteristic, tie line strength, power flow patterns, load characteristic etc. help to understand the nature and the source of the oscillations thoroughly. The relationship of the inter-area mode damping with the number of damper windings, representing damping due to eddy current effect, is discussed. The analysis provides a comprehensive understanding of the inter-area oscillations in

power systems. Such a comprehensive analysis is not available in a single reference in the opinion of the author.

- The effectiveness of the SMES in the damping control exercise has been analysed clearly. The SMES is modelled as a controllable shunt current source. Within the range of the output current, real power modulation of SMES provides larger variation in generator power transfer limit than that by the reactive power modulation. It is shown that real modulation is more effective in damping real power oscillations.

- A very useful discussion is provided on the damping design requirement. An analytical approach is introduced to decide adequate damping considering various practical factors of power system operations. The requirements and specifications of damping control design are not unique and standardised in power systems. These are set by different utilities in different ways. It is believed that the analytical approach introduced in this thesis for an adequate damping ratio at various modal frequencies is very general and standard.

- The concept of robust stabilisation through an approximate pole-placement approach is introduced first in the power system damping control. A robust low-order controller design problem (WNEDM) is formulated as a non-linear optimisation problem. A modified algorithm is proposed to design an internally stabilising controller. The performance robustness of the controller(s) has been verified through eigenvalue analysis and non-linear simulations. A successful attempt is made to develop the standard weighting factors that are independent of any specific system. The recommended weights are shown to work with three study systems having varying degree of complexities.

- The very recent concept of H_∞ control via an LMI approach is introduced in power-system-damping-control design. The multi-objective nature of the LMI formulation has been exploited to design the damping controller(s). It is shown that the numerical nature of the solution of the LMIs is more relevant to power system damping design practice. The drawbacks associated with the conventional Riccati

approach is shown to be absent in the proposed approach. The success of the H_∞ control hinges on the choice of suitable weights. The damping control requirement in power system cannot be translated to weights analytically. In the proposed approach the recommendation on the standardisation of the weight selection procedure is discussed. This is done based on the experiences gathered from the damping control design for three study systems. These recommendations make the application of the H_∞ approach in power-system-damping-control design simple and appealing.

- Some of the practical issues, such as model reduction, controller performance comparison, SMES sizing etc. in both of the approaches provide more insight and understanding to develop new damping control strategies for future researchers. The choice of a specific model reduction technique in robust damping control design in power systems is very much dependent on the input-output characteristics of the system. No single technique is best. The approach adopted for the comparison of the performance of the controller in the thesis is believed to be more realistic than other approaches reported in the literature.

CHAPTER TWO

SUPERCONDUCTING MAGNETIC ENERGY STORAGE: AN OPTION FOR EFFECTIVE POWER FLOW CONTROL

2.1 INTRODUCTION

In this chapter, the basic principle of the operation of the SMES device along with its associated control, protection, refrigeration subsystem is discussed. The SMES is considered as a shunt device that can control power flow through the injection of real and reactive power. The effectiveness of the real power injection over reactive power is illustrated in a simple power system. The worldwide efforts in the technology developments, demonstrations and commercial productions are discussed in detail. The application of SMES in power systems to realise several operating benefits is discussed. The evaluation of the ratings of a SMES device is outlined. Some of the practical issues are discussed.

2.2 SMES – THE BASIC PRINCIPLE OF OPERATION

Since the discovery of superconductivity, people have expected a revolution to occur in the field of electrical engineering. However, the conditions of the low transition temperature (T_c), critical magnetic field and critical current density have limited the applications of the superconductor. Several new superconducting materials of high transition temperature have been announced since 1987. The high temperature superconductor has been considered helpful to reduce the cost of the superconducting equipment and expand the applications of the superconductors. The basic principle of operation of a SMES device is rather simple. The component block diagram of a SMES connected to power system is shown in Fig 2.1. The transmission level voltage (several hundred kV) is stepped down to several hundred volts by a step-down transformer. The low voltage side of this step-down transformer provides the input to the power converter. The output of the power converter is a DC voltage. The converter feeds the superconducting coil. When power flows from the system towards the coil, the DC voltage charges the coil. The energy is stored in the coil. The maximum amount of energy that can be stored in the coil is specified by design considerations. This can be

sensed through the coil current to control the firing circuit. Whenever the AC network demands power, the coil is allowed to discharge. The direction of power flow at that time will be from the SMES system to the AC network. The coil acts as the source of energy. The power conversion is from the DC to the AC side i.e. in the inverter mode. The amount of time of charging /discharging depends on the energy and power rating of the device. The converter system is accordingly designed.

The coil maintains its superconducting nature at very low temperature (typically 4.5 Kelvin). So the coil is normally immersed in liquid helium or nitrogen depending on the material used to fabricate the coil. The coil protection system is also necessary to disconnect the coil when the current through or voltage across the coil exceeds the permissible limit. The protection system also works when the refrigeration

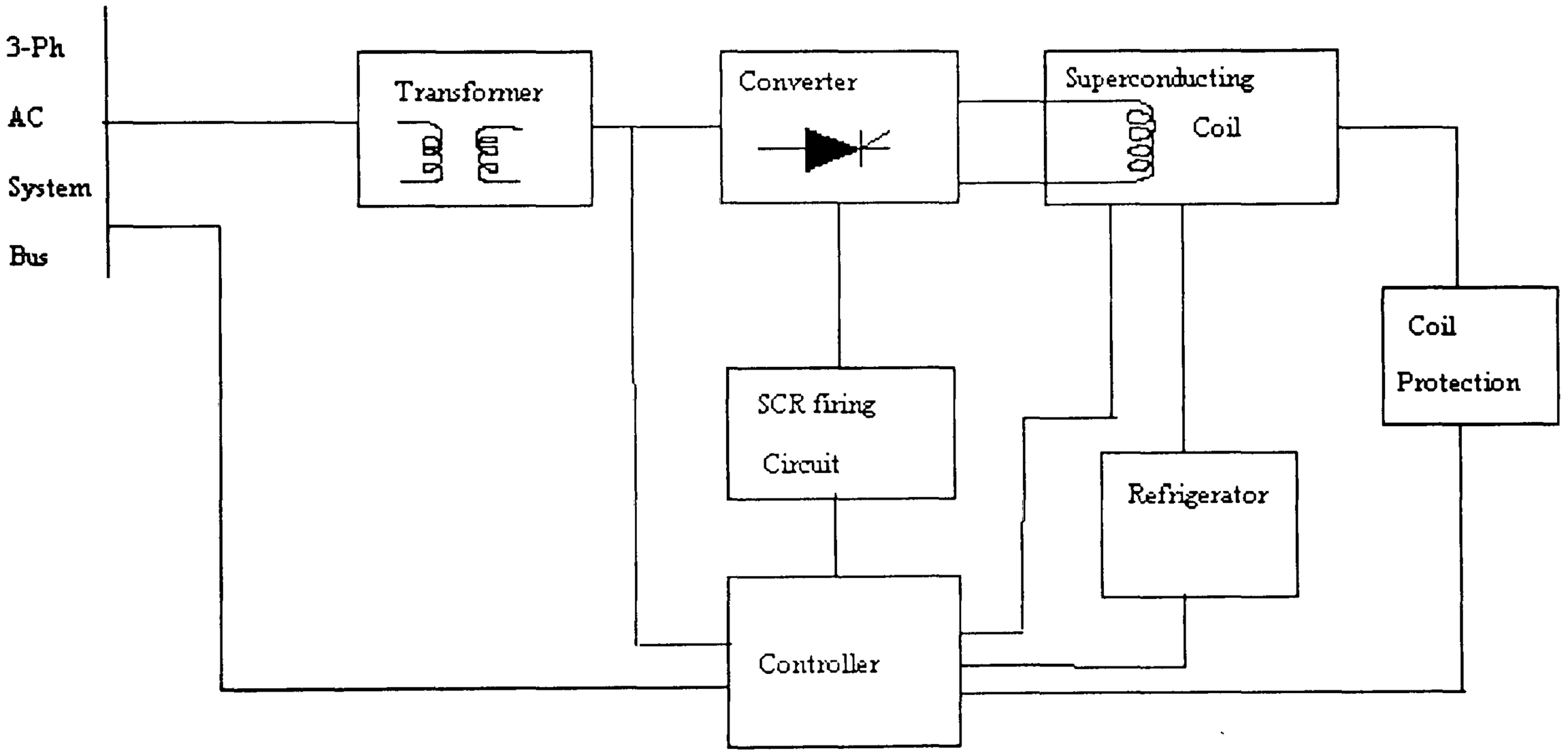

Fig. 2.1 Component Block Diagram of a SMES system

system fails. Once the coil is charged to its rated capacity, the converter no longer feeds the coil and the voltage across the coil is zero. This is maintained by a short-circuit by-pass switch across the coil. The switch remains closed as long as the coil is not required to charge or discharge. This is the free wheeling mode of the coil. The current remains constant, as the coil resistance is virtually nil. When the power is demanded by the AC

system, an interlock mechanism connects the converter across the coil and opens the by-pass switch. The firing angle is generated accordingly to steer the flow of the power to the AC systems. It is possible to control the real and reactive power simultaneously. This provides an option for the control of the bus voltage and angle. The bus voltage, frequency, SMES coil current etc. are sensed and fed back to the control circuit to generate firing pulses. The rating of the SMES can range from several kWh to several thousands MWh, depending on the application. In the next section, the various application options of SMES in power system will be discussed.

2.2 SMES – AN EFFECTIVE FACTS DEVICE IN POWER FLOW CONTROL

The idea of shunt current injection into the power system was traditionally for reactive compensation in power system. For example, the STATCOM in its early stage of development was usually referred to as an advanced version of the SVC. Though a major function, the capability of the shunt current injection device is not limited to the reactive power compensation. For example, by the inclusion of an energy-storage option as in the SMES, a STATCOM can inject the real as well as reactive power into the power system. This is an attractive feature to damp out power system oscillations, as the real power stability is of concern. This present work focuses on the active and reactive power modulation via the SMES. In this configuration, the SMES can be simply treated as a controllable shunt current device with an energy storage option.

Consider a single-machine-infinite-bus power system with a SMES treated as a shunt current injection device, as shown in the Fig. 2.2. The variables and parameters are also defined as in the Fig. 2.2. For the ease of explanation, the SMES is assumed installed in the middle of the transmission line. The current injection has a magnitude 'I' and phase angle $\angle\phi+\Delta$, where ϕ is the phase angle of the bus voltage to which the SMES is connected.

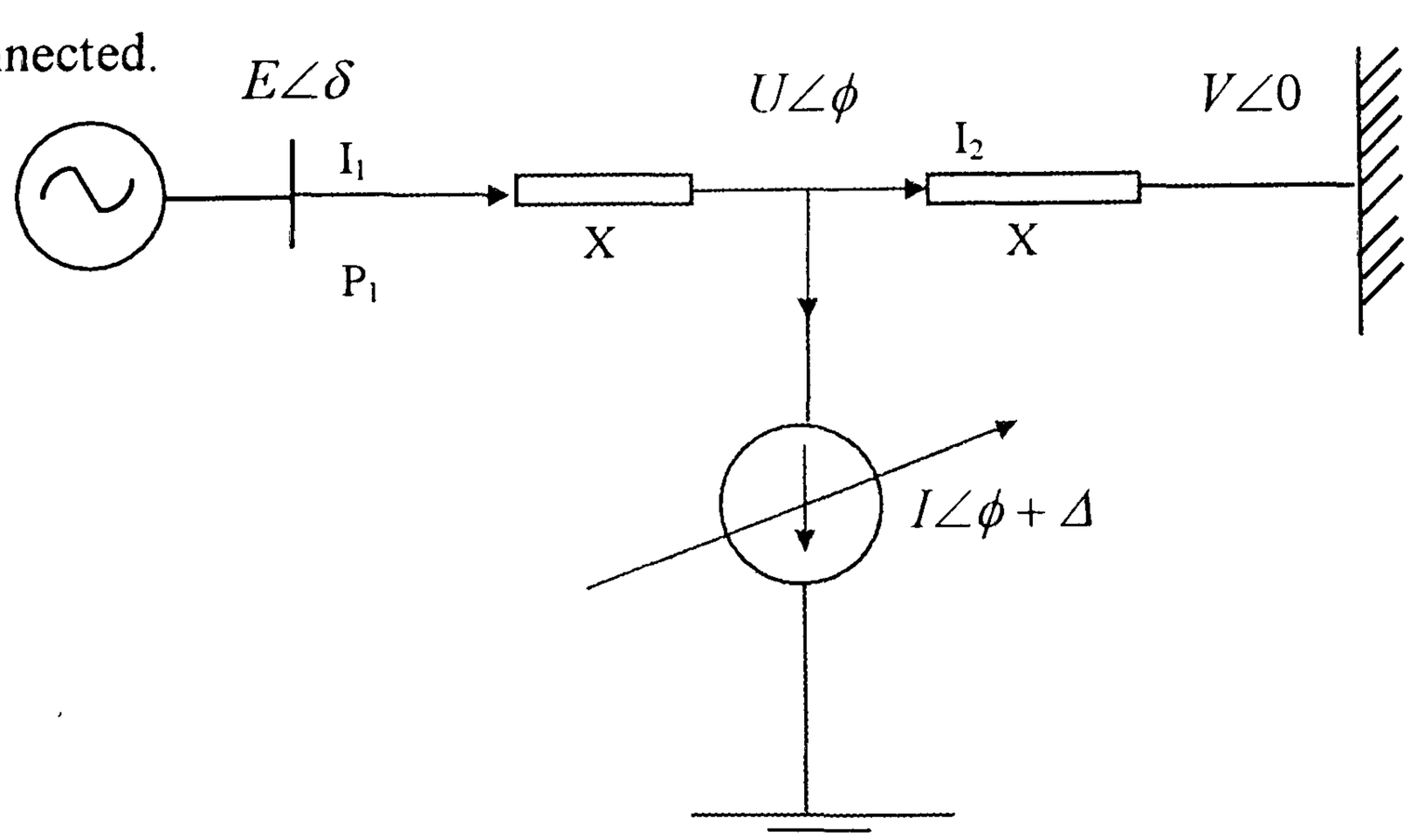

Fig: 2.2 A single machine infinite bus system with shunt current device

The real power output from the generator can be obtained as:

$$P_1 = \frac{EU}{X} sin(\delta - \phi) \tag{2.1}$$

$$\bar{I}_1 = \bar{I}_2 + \bar{I} \tag{2.2}$$

$$\bar{I}_1 = \frac{\bar{E} - \bar{U}}{jX} \tag{2.3}$$

$$\bar{I}_2 = \frac{\bar{U} - \bar{V}}{jX} \tag{2.4}$$

From (2.3) through (2.5) we obtain:

$$\bar{U} = \frac{1}{2}\left(\bar{E} + \bar{V} - jX\bar{I}\right) \tag{2.5}$$

which is equivalent to:

$$U\cos\phi = \frac{1}{2}\left[E\cos\delta + V + xI\sin(\phi + \Delta)\right] \tag{2.6}$$

$$U\sin\phi = \frac{1}{2}\left[E\sin\delta - XI\cos(\phi + \Delta)\right] \tag{2.7}$$

$$P_1 = \frac{EV}{2X}\sin\delta + \frac{1}{2}EI\cos(\delta - \phi - \Delta) \tag{2.8}$$

From (2.7) and (2.8), there can also be obtained:

$$E\sin(\delta - \phi) - V\sin\phi - XI\cos\Delta = 0 \tag{2.9}$$

The equations in (2.8) through (2.9) describe the classical power angle relationship of the system. It is to be noted that the first term in (2.9) describes the power output of the generator without the shunt injection. The second term is the addition due to the shunt compensation. Since both the shunt current magnitude, I, and the phase angle relative to the bus voltage, Δ, can be modulated, it can be seen that the generator power output can be modulated using the SMES, and thus the system dynamic stability performance can be modified.

Let us assume that Δ is a constant in the range of 0 to $\pi/2$, and the magnitude can be modulated for control purposes in the range $-I_{max}$ to $+ I_{max}$. It is important to note that, when $\Delta = 0$, the SMES device provides the real power injection (or absorption depending on the sign of the current). When $\Delta = \pi/2$, it provides the reactive power injection (capacitive or inductive depending on the sign of the current) and whilst Δ is

between 0 and $\pi/2$, the SMES provides both of the real and reactive power injection. Two extreme cases, $\Delta = 0$ and $\Delta = \pi/2$ are discussed in the following sections.

When $\Delta = 0$, the SMES injects (or absorbs) the real power and the modulation of the injected current magnitude results in the modulation of the injected real power. Fig. 2.3 shows the generator power angle curves for this case. A small region (shaded area) around the steady state power output is considered. When this modulation is guided by some feedback, it can control the power oscillations between P1 and P2 as shown in Fig. 2.3

When $\Delta = \pi/2$, the device provides reactive power injection that can be modulated. Fig. 2.3 shows the generator power-angle curves for this case. As in the case of modulation of the real power, the modulation of the reactive power can also be used to control real power oscillations.

It should be noted that the current limits are the same in both cases. By comparing the shaded areas in both cases, it is clear that modulating the shunt real power injection provides a larger range of the generator power output modulation than modulating the shunt reactive power injection, assuming the current magnitudes are the same. This indicates that the modulation of the shunt real power injection may be more effective for the control of the real power oscillations than the modulation of the shunt reactive power injection. This is as expected.

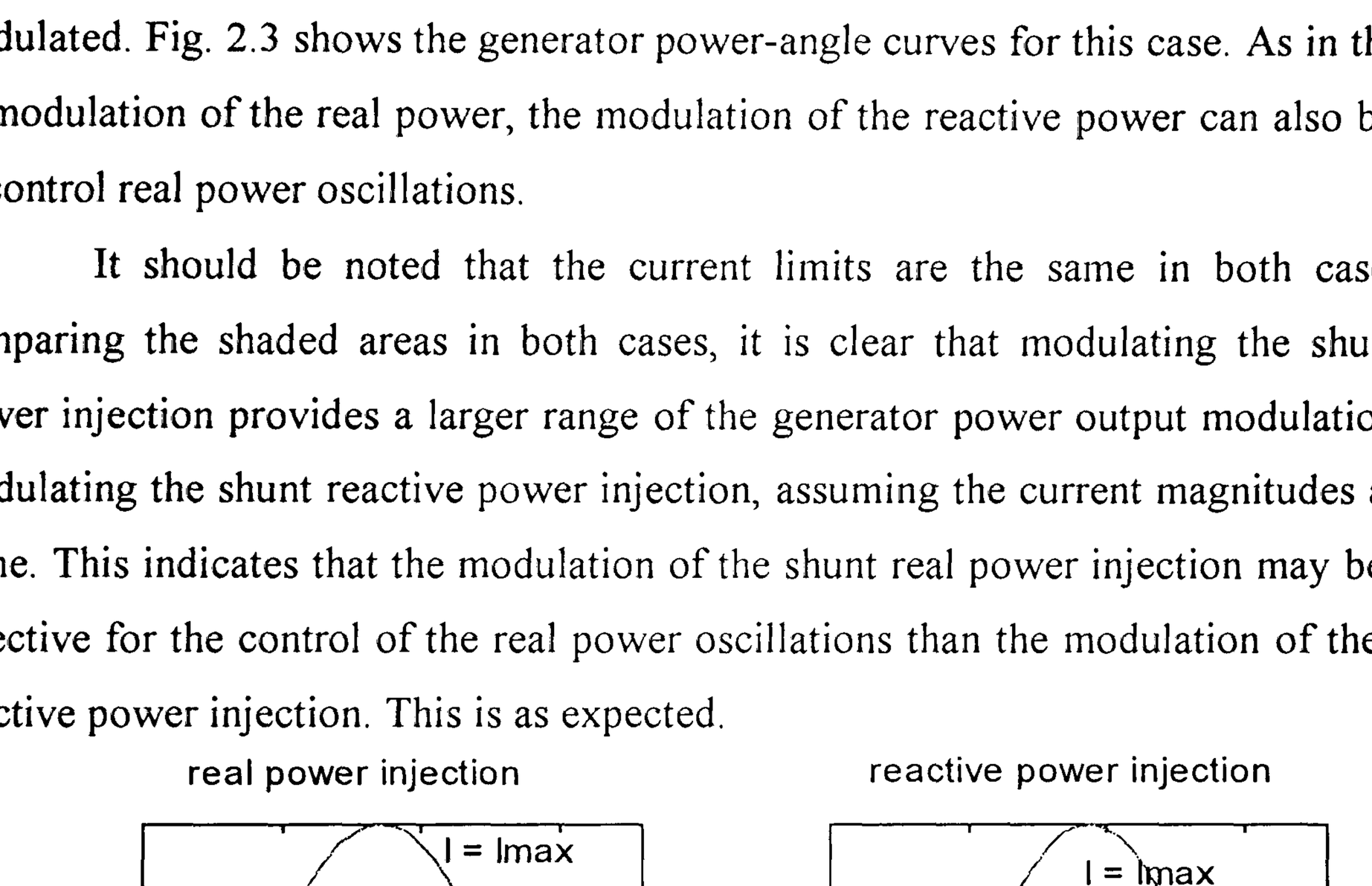

Fig. 2.3 Control of power flow in the line through shunt injection.

2.4 SMES – A BRIEF HISTORICAL PERSPECTIVE AND THE TECHNOLOGY DEVELOPMENT WORLDWIDE

The initial proposal of a superconducting coil for the utility applications was by Ferrier who, in 1969 [48], considered a large toroidal coil capable of supplying diurnal storage of electrical energy for all of France. The idea was not pursued because costs appeared to be high, based on the prevailing cost and performance of available superconductors. Studies in the US began at the University of Wisconsin in 1971 under the direction of Drs Boom and Peterson [49]. They studied the fundamental interaction between an energy storage unit and an electric utility system through a multiphase bridge, including the evaluation of the stabilising effect [50] of the rapid response of the converter on electric utility variations.

In a sense, SMES is the child of the nuclear era and the oil crisis in the U.S.A. Back in the early seventies, when SMES was conceived, the perception world-wide was that most of the electricity was going to be produced in nuclear power plants serving as base load generation. The fossil power plants were thought to provide only peaking duty. Utilities would try to smooth the daily differences between the peaks and valleys in demand by all means, via the addition of energy storage to the mix of facilities, in order to minimise the use of the fossil-powered peaking units.

Because of the perceived need for the large-scale load levelling and to exploit economies of scale, early SMES designs concentrated on coils storing 5000 MWH or more [51,52,53]. These conceptual designs called for solenoids of 1 km in diameter and built in deep tunnels or in surface trenches dug in bedrock or competent soil. These SMES coils were orders of magnitude larger than any superconducting device built, designed, or envisaged at the time. Only the feasibility, conceptual design and cost studies were undertaken during those early SMES years.

Beginning in 1976, Los Alamos National Laboratory (LANL) spearheaded a programme that led to the design and construction of a 30 MJ SMES device to provide stability support to Bonneville Power Authority's Pacific Inter-tie [40-43, 54]. The motivation behind this was the instability at a frequency of about 0.3 Hz that limited the maximum north-to-south power flow under certain conditions. The project was carried through to completion, including tests of the unit on the power grid. The unit was located at BPA's Tacoma-Washington substation and operated for about a year. The need for the unit that existed in 1976 was later reduced with the addition of power control to an existing dc transmission line to provide the necessary damping. Had there

not been this latter alternative, the 30 MJ SMES unit might still be operating. The cost estimates have suggested that economic payoff would have been reached in about two years. This BPA-LANL program represents the only instance of a SMES coil fully connected to a utility grid. In a sense, this 30 MJ SMES was a forerunner of some of the units being considered today for the transmission stability duty.

In 1987, the Defence Nuclear Agency (DNA) of the USA was tasked by the Strategic Defence Initiative Organisation (SDIO) to undertake management of a dual-use (military-electric utilities) programme to design, construct and demonstrate a 20-MWh SMES Engineering Test Model (ETM). This SMES-ETM was to demonstrate a dual-use technology that could be scaled to full-size SMES plants storing 1000 to 5000 MWh. At this capacity, the SMES plants were to provide power for the military ground-based, free-electron laser (GBFEL) directed-energy weapon under development by the SDIO. For electric utilities, these large SMES plants were to provide diurnal storage of electric energy to level the day night cycle of electricity usage. The ETM programme was initially structured as a competition between two teams (Bechtel, EBASCO) in two phases (Phase I for the design and selection of a winner, Phase II for the construction).

The Phase I competition spanned the 1988-1990 period, at the end of which two radically different designs emerged. Even though both teams worked from the same specifications and started from similar conceptual design, the design at the end of Phase I had few similarities. At the beginning of the ETM programme, the SMES standard design was based on the concept of high-purity aluminium-stabilised superconductor in a bath of super-fluid helium. The solenoid coil was built inside a surface trench and used the earth to withstand the radial Lorenz force. Such large SMES magnets were designed to be self-protected and use the thermal mass of the structure to absorb the stored energy during a quench. At the end of Phase I, the two proposed designs shared only a few features: earth support, operation in helium and the self-protection scheme. Otherwise, the designs were structurally and functionally different. One design was based on a 60-kA aluminium-stabilised superconductor that relied on helium bath cooling [55,56,57], with the other design based on a 200-kA cable-in-conduit conductor (CICC) [58,59,60]. The difference added variety, not to mention interest, to future SMES development.

The unexpected divergence in philosophy by the design teams coupled with the demise of the GBFEL programme within SDIO led to a "de facto" cancellation of the SMES-ETM programme in 1990. A design selection was never made and funds for the

construction were never approved. There was little activity on large-scale SMES between 1990 and 1992. That year, the original funding agency revived the ETM programme with what was supposed to be an interim "Risk Reduction" phase intended to add design detail, reduce risk and cost and test critical components. At the end of this phase in late 1993, the designs had been modified and new concepts were introduced [61].

The most important outcome from the Risk Reduction Phase was the realisation that the support for the Lorenz force is not the most cost-effective approach. Contrary to two decades of SMES "dogma", it is better to balance the magnetic forces internally to the magnet in a self-supported design built above ground [62]. Depending on the specific design, the self-supported option is cheaper than the earth-supported equivalent for stored energy up to at least 1000 MWh. The Risk Reduction programme also saw the development and testing of the full-scale conductors, as well as other critical components and subsystems [63,64].

Today nuclear generation is all but disappearing in the U.S.A. The oil crises have come and gone and the current prices of the natural gas are at the record lows. The conditions that spawned the need for large-scale energy storage and SMES no longer exist. The future has never arrived. The conditions in the US electric utility industry today are different from what was envisioned 25 years ago. However, the SMES has remained viable, thanks to the merit of the concept, as well as advances in the superconducting technologies that keep bringing the concept closer to reality.

The SMES is not now seen as an energy storage technology but as a new tool to help utilities manage their systems in light of rapid market deregulation. To effectively manage highly interconnected transmission/distribution systems, and to do so reliably, utilities will need a mechanism to absorb and dispatch power on demand. The SMES is called to fill a very unique market niche in this new environment.

The SMES will ultimately serve the commercial sector that requires heavy industrial participation in its development. The lack of strong national programmes has conspired against similar international collaboration on the SMES. In light of the scattering of efforts, this section presents a picture of the different SMES programmes around the world, without attempting to be exhaustive. The U.S. SMES programme is presently fragmented and without a clearly defined objective. Any government-sponsored programme is likely to eventually be abandoned, and long term development and commercialisation of SMES is going to depend on private industry initiatives. The

original funding agency steering the ETM programme has transferred the responsibility to the Air Force, which is concentrating, on developing a micro-SMES industrial base through power quality applications. Micro-SMES is a vaguely defined term, but it generally applies to units in the 1 to 10 MJ range of storage energy. In addition to 1 to 3 MJ units already being marketed by Superconductivity Inc. (SI) [65], the Air Force programme aims at developing 10 MJ units, as well as encouraging the introduction of new players to that market. Intermagnetics under the direction of the US Air Force is developing a SMES aimed at improving the power quality by mitigating momentary (0 –100 cycles) voltage interruptions [66]. The effort continues in developing a cost model of a 1–10 MWh toroidal coil structure design [67].

The second initiative in the U.S. involves, in a sense, the continuation of the ETM programme under Navy sponsorship. The programme was intended to further pursue the two concepts developed during the ETM programme: cable-in-conduit and aluminium-based conductor. The Navy programme involves the design, fabrication and both types of conductors in a test coil configuration, as well as application studies and conceptual designs. The design and demonstration experiences are reported [68,69] for the testing of the superconducting coil samples.

The third U.S. effort is being sponsored by the Technology Reinvestment Project (TRP) and managed by the Department of Energy (DOE). This programme is structured as a cost-shared effort between the government and private industry. The lead contractor is Babcock and Wilcox which is engaged in designing and building a 0.5 MWh/50 MW unit for the Anchorage Municipal Light and Power Co., Alaska. The quench-protection system in cryostat design is reported [70] and the project is yet to be commissioned.

Some development in Europe is being pursued at the national level and in many instances with local utility sponsorship. Unlike other applied superconductivity technologies, it appears that SMES is not being pursued or funded as a joint European effort. A 25-kJ SMES coil has been designed and manufactured [71] to test its performance against voltage dips and frequency variation in Spain. The experimental and simulation results closely agree [72]. There are relatively active SMES programmes in Finland, Germany, France, Italy, Switzerland and Russia [73–77]. As in the U.S.A., these programmes have involved industrial participation and not all information stemming from them is easily available.

The concept of SMES is being pursued further in Japan for last two decades [37,39]. The Japanese SMES activities receives sponsorship mainly from the International Superconductivity Technology Centre (ISTEC) and Research Association for SMES (RASMES). The ISTEC programme is geared towards the design and construction of a 100-kWh/40-MW toroidal SMES [79]. The unit with a very progressive power/energy ratio would serve, as demonstration of those required for power grid stability/reliability enhancement (in the 10 MWh class). The ISTEC programme is heavily phased. The technology evaluation phase was successful. The design and construction of the pilot plant (1kWh/1 MW) [80] was complete by 1998. The test results in the utility are expected by the beginning of 1999. The SMES programme in Japan has received relatively modest funding, however, it appears to be making steady progress towards hardware production and testing.

In the light of the above assessment of the SMES activities around the world, it appears that an international collaboration is unlikely at this point. Just as the technology development is going to follow an evolutionary path, fielding of the technology around the world is going to depend on specific applications and circumstances that are local in nature.

2.5 BENEFITS OF SMES

Technology developments are important, however the SMES will not succeed until an economically viable application is found. It has already been stated in the previous section that large-scale load levelling is not an application that will drive investment into a SMES demonstration unit. Other applications in the utility market need to be studied. Most of the applications where SMES appears attractive fall into the category that the utility industry calls 'ancillary services'. A new exhaustive list of what utilities mean by ancillary services include: load regulation, transmission stability, spinning reserve, frequency control, voltage control, SSR damping, low-frequency power oscillation damping, black start etc. Unlike diurnal load levelling, the economic benefits of these factors tend to be indirect and harder to quantify which does not mean that they are not real. The perspective on SMES is that the technology offers a wide range of strategic and dynamic benefits. Some of the benefits are listed in Table 2.1. Most of these benefits have been mentioned in the technology-development section.

Table 2.1: Benefits of SMES

	Generation	**T&D**	**Corporate**	**Customer**
Strategic benefits	Reduced/shifted emissions	Fewer outages	Lower fuel shock risks	Fewer blackouts
Dynamic benefits	Improved frequency control	Improved power quality	Less reliance on purchase power	Improved power quality
Load levelling benefits	Increased utilisation of base load plants	Improved grid utilisation	Potential wheeling revenue	Improved customer retention

They are explained in detail here to emphasise the role of SMES in reliable and economic system operation and management.

Generation benefits: Daily storage and the utilisation of off-peak generation to provide peak load requirements results in both reduced capital and operational expenses which are generation benefits of SMES. In the BPA service area, future load is projected to be met through a balanced mix of new resources, including the addition of the natural gas fired combustion turbines with an equal amount of capacity limited by the availability of the off-peak generation.

Automatic Generation Control (AGC) and Load frequency Control (LFC): The SMES system with a large amount of storage can be used as part of the AGC control strategy [81,82]. The rapid peaks and power swings on the system is managed by the SMES whilst the generators with AGC respond to the slower variations of load. In 1983, the BPA has estimated that this strategy could save about $1 million per year in turbine maintenance costs [83].

Voltage support benefits: With the appropriate design, the SMES power-conditioning system would be capable of providing four-quadrant power control [83,84,85]. The reactive power capacity is relatively independent of the real power capacity and, hence, is not constrained by the other functions of the SMES dispatch scenario. Dispatching reactive power can be used for the voltage support or for the substitution of otherwise needed control equipment, such as the static VAR controller.

Many industrial supplies suffer from voltage sags ranging from several milliseconds to a few seconds. Sophisticated process control systems require a continuous high quality power supply at the distribution level. It is explained in [66] that, even a momentary drop in the supply voltage of half a cycle causes the malfunctioning of many manufacturing systems. The SMES, therefore, has to have

sufficient storage capacity to maintain the supply for a few cycles (1- 100 cycles) before other sources can return the supply. The thrust is, therefore, towards the development of SMES [71,72,73] units that can improve the power quality.

Transmission Loss and loading management benefits: Because of their high efficiencies and fast dynamic responses, a major application of SMES in power systems is diurnal load levelling. At night, when the load demand is low, the electric power produced by generators operated at relatively low costs is used to charge up a SMES unit. During the day when the load demand is high, the energy stored in the SMES system is discharged to supply the load. Using load flow program, transmission losses for a test system with and without SMES were computed [86]. Losses are high when load demand is more and low during off-peaks hours. The losses are brought down by SMES and hence the line loading is controlled. With the introduction of the SMES, most of the overloaded lines are relieved partially by the reduction of the losses. In large interconnected system, the reduction in the line loading saves enormous amount of energy. The SMES when placed near to the load centres saves maximum energy losses.

Stability enhancement benefits: Both the real and reactive power of the SMES unit can be modulated to improve the stability performance of power system. It is shown in Section 2.3 that real power modulation is very effective. Since the early seventies, it has been known that SMES has the potential to improve the transient stability performance of power systems [36,37,38]. It has already been outlined in Chapter One that the SMES is very effective [36, 38-43] in damping out low-frequency oscillations in the frequency range of 0.2-2.0 Hz. The SMES can be effective in damping turbo-generator shaft oscillations, commonly termed sub-synchronous resonance (SSR) [87]. It is also reported that [88,89] SMES, when connected to a turbo-generator unit, SSR can be prevented.

2.6 RATINGS OF SMES

The design of SMES differs depending on the applications, sizes and charge discharge duration. Table 2.2 lists several applications of SMES along with their power ratings. It can be seen from the table that a SMES of very low power and energy rating is adequate in safeguarding against momentary power interruption in industrial premises. A 10-50 MW SMES delivering rated power for about 1.0–5.0 s is necessary for dynamic stabilisation. This means the energy rating will be 10–250 MJ. In a generation system, a large SMES 100–500 MWh is necessary to realise frequency

control, spinning reserve, load levelling and other options. The Sizing of a SMES device requires the determination of both power and energy ratings. The power rating helps determine the nominal voltage and current of the energy source and the nominal current of the converter. The energy rating allows the sizing of the energy source. The nominal energy can be computed from the inductance and rated current ($\frac{1}{2}LI^2$).

2.6.1 POWER RATING

It is known that a high power rating has the effect of damping oscillations first but at the cost of large nominal current. If the power rating is too low, the output of SMES will be limited during disturbances. It will also take several tens of seconds to regain linearity. This means that the SMES will not be very effective in controlling these oscillations quickly. So a compromise is necessary between the two extremes. Normally, the utility requirement for a damping control strategy is to ensure that the oscillations settle in 10 to 20 s following the most credible contingency. A real power rating of 10 to 50 MW is, therefore, found to be satisfactory.

Table 2.2: Rating of SMES for various applications

Types of Application	**Power**	**Duration**
Customer level		
Power interruptions	0.2-5.0 MW	0.1-5.0 s
Carryover	0.2-5.0 MW	0.1-5.0 s
Distribution feeder		
Power interruptions	1.0-5.0 MW	0.1-5.0 s
Voltage/VAR support	1.0-5.0 MW	0.1-5.0 s
Load levelling/peak shaving	1.0-5.0 MW	1 minute-2 hours
Transmission substation		
Power flow control	10-500 MW	1.0 -30 s
Dynamic stabilisation	10-50MW	1.0-5.0 s
Voltage/VAR support	10-500 MW	0.1-0.5 s
Generation system		
Frequency control	100-1000 MW	10-60 s
Spinning reserve	100-1000 MW	15-30 s
Dynamic response	100-1000 MW	1-2 hours
Load levelling	100-1000 MW	1-5 hours

2.6.2 ENERGY RATING

The EPRI practice [90] on the energy requirements of a SMES is evaluated by integrating the power output trace. The energy stored in the coil can be made fully available assuming that the loss in the coil is zero. This means 100% turnaround efficiency i.e. MW-s stored during charging is MW-s available during discharging. The positive output trace indicates the discharging of the coil whilst the negative output indicates charging. The area under each individual charging and discharging cycle can be evaluated to estimate the energy involved with the charging and discharging cycle. The absolute value of the largest individual area (charging or discharging) can be decided as the energy rating in MJ when power is expressed in MW.

2.7 PRACTICAL ISSUES

Since the early seventies, there has been an enormous amount of research activity on the application aspects of SMES in power systems. The SMES is a very costly option unless a very large-size is realised for diurnal load levelling, spinning reserve, load frequency control etc. The cost-effective technology is not yet available to design, construct and commission such large SMES. The SMES technology for the application in the customer level, and distribution system is available. This means that safeguards against momentary power interruptions, voltage sag mitigation etc. can be realised with a commercially available SMES of energy rating 1.0 to 3.0 MJ. Some of the benefits for transmission system (Dynamic voltage support and low-frequency oscillation control) operation require a low rated SMES (10 MW for few seconds). Clearly a SMES of this size is under development and at the demonstration stage. It is expected that a 10 to 20 MJ SMES will be commercially available in the near future so that these functions can be realised in a practical utility.

Considering these practical issues related to SMES technology developments, this research concentrates on the power system damping control strategy under various power flow scenarios. Smaller SMES devices of the order of 10 MJ or less can control the poorly damped inter-area oscillations (0.1-2.0 Hz) very effectively.

2.8 SUMMARY AND CONCLUSIONS

The basic principle of the operation of a SMES device is discussed with the help of a functional block diagram. The associated auxiliaries such as the coil

protection, refrigeration etc. are described. The option of real power modulation for controlling power flow is explained with the help of a single-machine-infinite-bus system (SMIB). The SMES device is modelled as a controllable shunt current injection device. It is shown that the device when located on the transmission path has positive influence on generator power output through the modulation of injected real and reactive power. It is also shown that the real power has much greater leverage on power modulation and damping power oscillations thereby improving the steady state as well as the dynamic stability margin of the system. A brief historical review on the technology development throughout the world is presented. The application benefits of the SMES in power system are discussed. The evaluation of the power and energy rating of the SMES device is discussed.

CHAPTER THREE

POWER SYSTEM MODELLING

3.1 INTRODUCTION

It is clear that the problem of inter-area oscillations is one of insufficient damping. The available damping comes from the connected components. These are the speed governor, prime mover, generator, excitation systems, interconnected network, system loads, and other FACTS controllers added for other specific purposes. To understand how these devices produce damping, it is necessary that they are modelled.

3.2 SPEED GOVERNOR

Although the effects of the prime-mover control should not be neglected in the analysis of power system oscillations, it is understood [3] that faster excitation control is better suited for the damping of system oscillations than the relatively slow mechanical control. On the other hand, the prime mover has a dominant role in the system-wide Load-Frequency-Control (LFC) which is part of the Automatic-Generation-Control (AGC). It should be noted that the relatively slow mechanical control is sufficient to maintain the system frequency whilst faster controllers are needed to improve the damping of system oscillations [3], which are characterised by low frequencies (0.1 to 2.0 Hz). In all further analysis, it will be assumed that the speed governors in the system are properly tuned and the power input to all of the generators is constant.

3.3 PRIME MOVER

In a power plant, the generator is driven either by a steam-turbine or a hydraulic turbine. Depending on the size, construction and principle of operation, different small signal models can be derived. For a steam turbine with tandem compound structure, various stages should be modelled adequately to represent the torsional dynamics [87]. Normally, for the electromechanical modes in the frequency range of 0.2 to 2.0 Hz, the dynamic interaction of these turbine masses can be of important consideration if the associated governor is not properly tuned. Generally, the damping of inter-area mode is decreased slightly if the governor is not tuned properly. All present day speed-governing systems are properly tuned making the turbine less interactive. Inclusion of a small signal

model of the turbine can increase the frequency of the inter-area mode very slightly. In view of this discussion, in this research, the input torque of the generator is assumed constant.

3.4 GENERATOR

The generator is the electromechanical energy conversion device which when driven by a turbine, produces electrical power. The generator has mainly two parts: the stator and rotor.

3.4.1 STATOR

The stator is a laminated steel structure accommodating a 3-phase balanced winding system. As the rotor rotates, it produces a rotating magnetic field with the help of the rotor excitation. The rotating flux induces an EMF on the stator winding. The stator voltage is connected to the electrical grid through a transformer and circuit breaker arrangement. Whenever the stator winding faces any electrical disturbances (short circuit, load changes etc.) a very high-frequency current flows very momentarily. These transients, commonly known as stator transients, settle down very quickly. In low-frequency electromechanical stability analysis, stator transients are ignored. This means that the stator voltage equations in the network or machine-d-q frame of reference are simply treated as algebraic equations.

3.4.2 ROTOR

The rotor is a solid cylindrical structure embraced by a coil system that provides excitation. In a hydro-alternator, damper windings are placed in the rotor surface. The rotor rotates at constant speed (synchronous speed). Any imbalance in the input (prime mover torque) and output (electrical torque) results in the following equations:

$$\frac{d\delta}{dt} = \omega - \omega_s \tag{3.1}$$

$$\frac{2H}{\omega_s}\frac{d\omega}{dt} = T_m - T_{elec} - T_D \tag{3.2}$$

where H, ω_s are the machine inertia constant and synchronous speed respectively. T_m, T_{elec}, T_D are the mechanical torque input to the machine, the electrical torque developed in the machine and the mechanical damping torque respectively.

The expression for the electrical torque (T_{elec}) in terms of machine internal voltage, rotor winding flux linkage and current is dependent on the modelling details of the machine and will be given at the end of each rotor circuit model.

The damping torque is directly proportional to the oscillation frequency and can be represented as follows:

$$T_D = D(\omega_s - \omega) \tag{3.3}$$

It should also be noted that the damping between the rotors of different machines, known as asynchronous damping, is neglected. The only contribution to T_D is due to the speed deviation of each individual mass with respect to the synchronous speed ω_s. The degree of modelling is dependent on the number of rotor circuits representing the damping action of the rotor body. Two damper windings on the quadrature axis are commonly considered [91,92]. One winding represents damping due to surface eddy current effects and the other represents damping due to deeper flowing eddy current effects. Normally, one coil is enough to represent the damping action due to eddy currents in the direct axis of the rotor. With these aspects of the modelling, four windings (one field and three other hypothetical coils one in the direct axis and two in the quadrature axis) are considered to represent flux dynamics in the rotor. It will be shown in Chapter Four that in a sample power system, the increase in the number of damper windings on each axis does not influence the inter-area mode damping significantly but has a significant effect on local modes. The equations to represent the rotor electrical dynamics are as follows:

$$\frac{dE_q'}{dt} = \frac{1}{T_{do}'}\left[-E_q' - (X_d - X_d')\left[-I_d - \frac{(X_d' - X_d'')}{(X_d' - X_{ls})^2}(\Psi_{1d} - (X_d' - X_{ls})I_d - E_q')\right] + E_{fd}\right] \tag{3.4}$$

$$\frac{d\Psi_{1d}}{dt} = \frac{1}{T_{do}''}\left[-\Psi_{1d} + E_q' + (X_d' - X_{ls})I_d\right] \tag{3.5}$$

$$\frac{dE_d'}{dt} = -\frac{1}{T_{qo}'}\left[+E_d' + (X_q - X_q')\left[I_q - \frac{(X_q' - X_q'')}{(X_q' - X_{ls})^2}(-\Psi_{2q} + (X_q' - X_{ls})I_q - E_d')\right]\right] \tag{3.6}$$

$$\frac{d\Psi_{2q}}{dt} = -\frac{1}{T_{qo}''}\left[\Psi_{2q} + E_d' - \left(X_q' - X_{ls}\right)I_q\right] \tag{3.7}$$

$$T_{elec} = \frac{(X_d'' - X_{ls})}{(X_d' - X_{ls})}E_q' I_q + \frac{(X_d' - X_d'')}{(X_d' - X_{ls})}\Psi_{1d} I_q + \frac{(X_q'' - X_{ls})}{(X_q' - X_{ls})}E_d' I_d$$
$$-\frac{(X_q' - X_q'')}{(X_q' - X_{ls})}\Psi_{2q} I_d - (X_q'' - X_d'')I_q I_d \tag{3.8}$$

where,

E_{fd} : Exciter input voltage on stator base (p.u)

$E_q'(E_d')$: Quadrature (direct) axis transient voltage (p.u.).

$\Psi_{1d}(\Psi_{2q})$: Flux linkage in the direct (inner quadrature) axis damper (p.u.)

X_{ls}: Stator leakage reactance (p.u.).

X_d, X_d', X_d'': Direct axis synchronous, transient and sub-transient reactance (p.u.) respectively.

X_q, X_q', X_q'': Quadrature axis synchronous, transient and sub-transient reactance (p.u.) respectively.

T_{do}', T_{do}'': Direct axis open circuit transient and sub-transient time constants (seconds) respectively.

T_{qo}', T_{qo}'': Quadrature axis open circuit transient and sub-transient time constants (seconds) respectively.

Normally, T_{do}'' and T_{qo}'' are very small compared to T_{do}' and T_{qo}'. In view of this, it is possible to further simplify the above model by substituting the following expressions for flux linkages in the damper circuits as function of E_q', E_d', I_q, I_d and machine constants.

$$\Psi_{1d} = E_q' + (X_d' - X_{ls})I_d \tag{3.9}$$

$$\Psi_{2q} = -E_d' + (X_q' - X_{ls})I_q \tag{3.10}$$

Substituting the above into the equations (3.4) and (3.6) and into the expression for the electrical torque developed, the following equations can be obtained.

$$\frac{dE_q'}{dt} = -\frac{1}{T_{do}'}\left[E_q' - (X_d - X_d')I_d - E_{fd}\right] \tag{3.11}$$

$$\frac{dE_d'}{dt} = -\frac{1}{T_{qo}'}\left[E_q' + (X_q - X_q')I_q\right] \tag{3.12}$$

$$T_{elec} = (E_q' + I_d X_d')I_q + (E_d' - I_q X_q')I_d \tag{3.13}$$

3.5 EXCITATION SYSTEMS

The excitation system provides the necessary rotor flux to induce a voltage in the stator. E_{fd} is never manipulated directly but is changed through the actuation of the exciter. Excitation systems are broadly classified into two types:

3.5.1 SLOW ACTING TYPE (DC)

A typical slow excitation system (termed DC1A exciter) [93] consists of four basic blocks as shown in Fig. 3.1. They are the exciter, amplifier, excitation-stabiliser and terminal voltage sensor.

A basic model for an exciter is:

$$T_e \frac{dE_{fd}}{dt} = -\left[K_e E_{fd} + S_e(E_{fd})E_{fd}\right] + V_r \tag{3.14}$$

$S_e(E_{fd})$ is the saturation in the exciter. It is approximated as $A_{ex}(exp)^{B_{ex}E_{fd}}$. The constants K_e and T_e relate to exciter gain and time constant respectively. The K_e is normally not fixed [92] but varies with the operating conditions. For each operating condition, it is assumed that K_e is such as to make the voltage regulator output zero in the steady state.

The exciter provides the mechanism for the control of the synchronous machine terminal voltage magnitude. In order to automatically control the terminal voltage a

sensed voltage signal must be compared to a reference voltage and amplified to produce the exciter input V_r. The amplifier can be a pilot exciter or a solid state amplifier. In either case, the amplifier is modelled as:

$$T_a \frac{dV_r}{dt} = -V_r + K_a V_i \tag{3.15}$$

$$V_{r\,min} \le V_r \le V_{r\,max}$$

The above regulator, when equipped with the necessary stabilising transformer gives rise to the following set of equations:

$$T_a \frac{dV_r}{dt} = -V_r + K_a V_i \tag{3.16}$$

$$V_{r\,min} \le V_r \le V_{r\,max}$$

$$T_f \frac{dV_f}{dt} = -V_f + K_f \left(-\frac{K_e + S_e(E_{fd})}{T_e} E_{fd} + \frac{V_r}{T_e} \right) \tag{3.17}$$

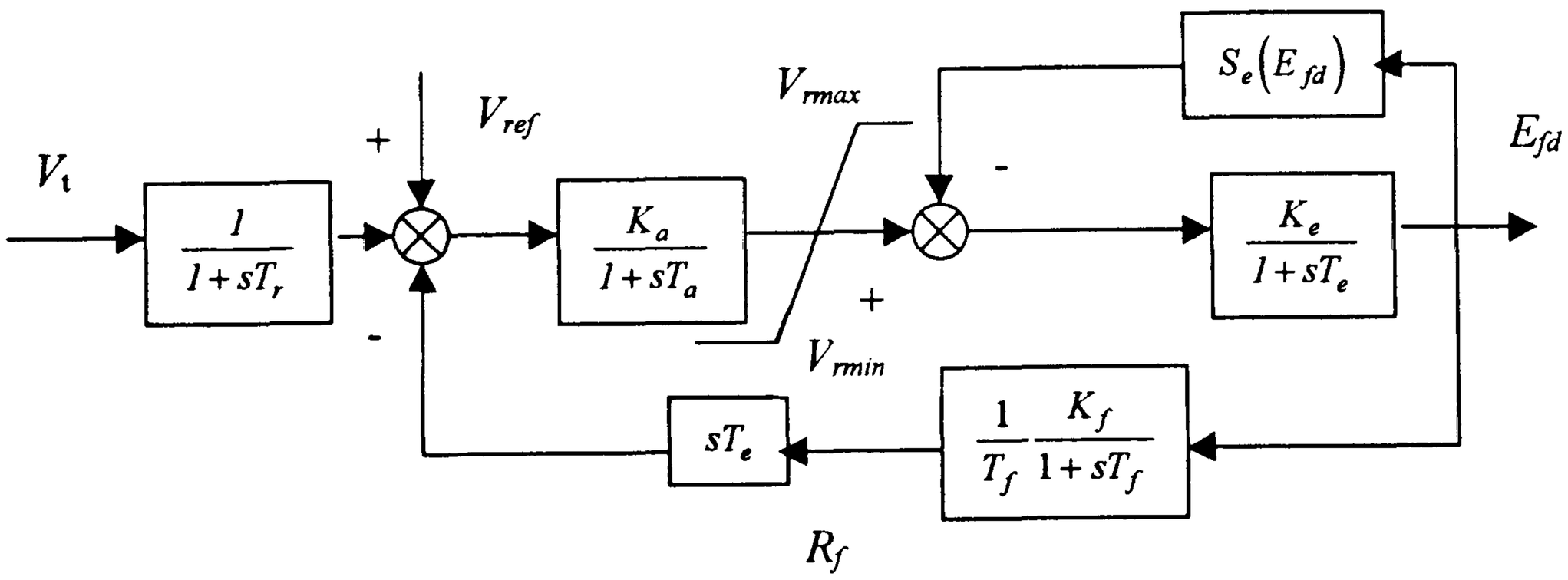

Fig. 3.1: Block Diagram of a DC1A-type Excitation System

where, K_a, T_a and K_f, T_f are the gain and time constant of the amplifier and stabiliser circuit respectively. Another form of this model is often used; i.e. $R_f = \frac{K_f}{T_f} E_{fd} - V_f$:

where, R_f (called rate feed back) as the dynamic state.

$$T_f \frac{dR_f}{dt} = -R_f + \frac{K_f}{T_f} E_{fd} \tag{3.18}$$

This form will be used throughout. The terminal voltage sensor is modelled as a first order block with a filter time constant T_r and is given by the following equation:

$$\frac{dV_{tr}}{dt} = -\frac{1}{Tr}\left[V_{tr} - V_t\right] \tag{3.19}$$

When put together, a summary of a fundamental model of an excitation system results:

$$T_e \frac{dE_{fd}}{dt} = -\left[K_e + S_e(E_{fd})\right]E_{fd} + V_r \tag{3.20}$$

$$T_a \frac{dV_r}{dt} = -V_r + K_a R_f - \frac{K_a K_f}{T_f} E_{fd} + K_a(V_{ref} - V_{tr}) \tag{3.21}$$

$$T_f \frac{dR_f}{dt} = -R_f + \frac{K_f}{T_f} E_{fd} \tag{3.22}$$

$$\frac{dV_{tr}}{dt} = -\frac{1}{Tr}\left[V_{tr} - V_t\right] \tag{3.23}$$

3.5.2 FAST ACTING TYPE (ST)

Modern large machines are equipped with thyristor based excitation systems. The exciter power is drawn from the generator bus through an exciter transformer. Such a type of excitation system (ST1A) is often modelled as a single time-constant block [93]. The error signal is used as input and E_{fd} as output. Fig 3.2 of this section shows a small signal representation for a high gain (of the order 200 to 400) and fast (of the order of a few milliseconds) exciter. Normally, T_a is neglected. When T_a is ignored, the dynamic behaviour is described by

$$\frac{dV_{tr}}{dt} = -\frac{1}{Tr}\left[V_{tr} - V_t\right] \tag{3.24}$$

$$E_{fd} = K_A(V_{ref} - V_{tr}) \tag{3.25}$$

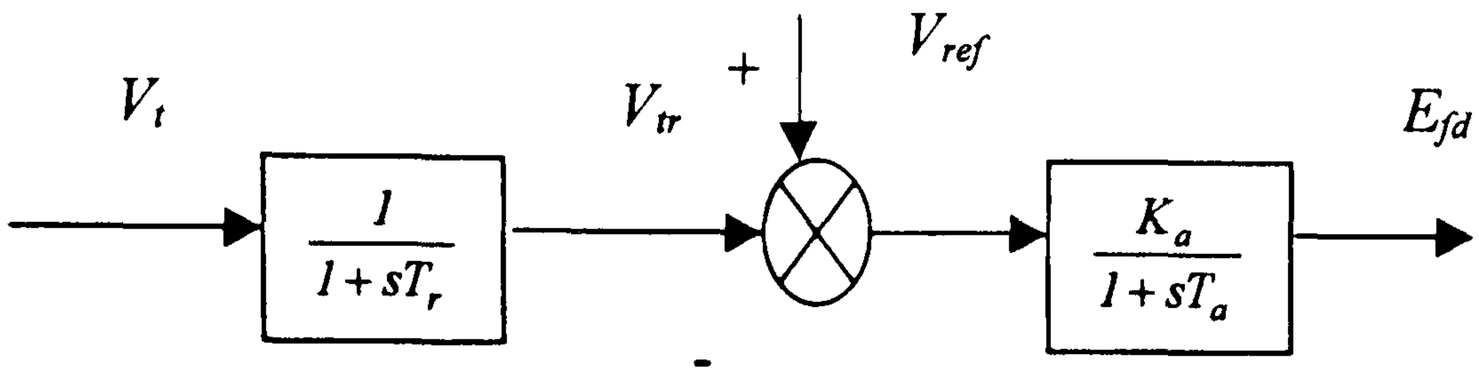

Fig 3.2: Block Diagram of a fast ST1A-type Excitation System

In the case where the voltage regulator gain (K_a) is too large for better transient stability performance, the damping torque introduced by the exciter becomes negative. In order to ensure a well-damped post-fault response of the system, the regulator block is preceded by a transient gain reduction (TGR) block. The widely used transfer function of TGR is $\frac{1+sT_b}{1+sT_c}$. Typically, the ratio $\frac{T_c}{T_b}$ is 10.

3.6 MACHINE-NETWORK INTERFACE

It is convenient to transform all synchronous machine stator and network variables into the synchronously rotating reference frame. Variables within the synchronously rotating reference frame are denoted with $DQ0$ subscripts and those within the individual machine with $dq0$ subscripts. With these notations, the voltages and currents of the ith machine in the system can be expressed as:

$$V_{qi} + jV_{di} = \left(V_{Qi} + jV_{Di}\right)e^{-j\delta_i} \tag{3.26}$$

$$I_{qi} + jI_{di} = \left(I_{Qi} + jI_{Di}\right)e^{-j\delta_i} \tag{3.27}$$

3.7 POWER SYSTEM LOAD

In power system stability and power flow studies, the common practice is to represent the composite load characteristics as seen from bulk power delivery points. The load models are traditionally classified into two broad categories.

3.7.1 STATIC LOAD

A static load model expresses the characteristics of the load at any instant of time as algebraic functions of the bus voltage magnitude and frequency at that instant. The active power component, P, and reactive power component, Q, are considered separately. Traditionally, the voltage dependency of the load characteristics has been represented by the exponential model [92].

$$P = P_0\left(\overline{V}\right)^a \tag{3.28}$$

$$Q = Q_0\left(\overline{V}\right)^b \tag{3.29}$$

where, $$\overline{V} = \left(\frac{V}{V_0}\right) \tag{3.30}$$

when P_0, Q_0 and V_0 are the values at the initial operating condition. The parameters of this model are the exponents 'a' and 'b'. With these exponents equal to 0,1,2, the model represents load of a constant power (CP), constant current (CC) or constant impedance (CI) type respectively. The exponent 'a' (or 'b') is approximately equal to the slope dp/dv (or dq/dv) at $V = V_0$. For composite system loads, the exponent 'a' usually lies in the range between 0.5 and 1.8. Exponent 'b' varies as a non-linear function of the voltage. For Q at higher voltages, 'b' tends to be significantly higher than 'a'.

An alternative model that has been widely used to represent the voltage dependency of loads is the polynomial model.

$$P = P_0\left[p_1\left(\overline{V}\right)^2 + p_2\overline{V} + p_3\right] \tag{3.31}$$

$$Q = Q_0\left[q_1\left(\overline{V}\right)^2 + q_2\overline{V} + q_3\right] \tag{3.32}$$

This model is commonly referred to as the *ZIP* model as it is composed of constant impedance (Z), constant current (I) and constant power (P) components. The parameters of the model are the coefficient 'p_1' to 'p_3' and 'q_1' to 'q_3' that denote the proportion of each component. The frequency dependency of the load characteristic is usually represented as the exponential and polynomial model by a factor as follows:

$$P = P_0\left(\overline{V}\right)^a\left[1 + K_{pf}\Delta f\right] \tag{3.33}$$

$$Q = Q_0\left(\overline{V}\right)^b\left[1 + K_{qf}\Delta f\right] \tag{3.34}$$

and,

$$P = P_0\left[p_1(\overline{V})^2 + p_2\overline{V} + p_3\right]\left(1 + K_{pf}\Delta f\right) \tag{3.35}$$

$$Q = Q_0\left[q_1(\overline{V})^2 + q_2\overline{V} + q_3\right]\left(1 + K_{qf}\Delta f\right) \tag{3.36}$$

Typically, K_{pf}, ranges from 0 to 3.0 and K_{qf} ranges from -2.0 to 0.0.

A comprehensive static model that offers the flexibility of accommodating several forms of load representation is as follows:

$$P = P_0\left[P_{ZIP} + P_{EX1} + P_{EX2}\right] \tag{3.37}$$

$$Q = Q_0\left[Q_{ZIP} + Q_{EX1} + Q_{EX2}\right] \tag{3.38}$$

when,

$$P_{ZIP} = p_1\overline{V}^2 + p_2\overline{V} + p_3 \tag{3.39}$$

$$P_{EX1} = p_4(\overline{V})^{a1}\left[1 + K_{pf1}\Delta f\right] \tag{3.40}$$

$$P_{EX2} = p_5(\overline{V})^{a2}\left[1 + K_{pf2}\Delta f\right] \tag{3.41}$$

A similar expression for Q_{ZIP} Q_{EX1} and Q_{EX2} can be written.

3.7.2 DYNAMIC LOAD

The response of most of the composite loads to voltage and frequency changes is fast and the steady state condition for the response is reached very quickly. This is true at least for the modest amplitudes of the voltage/frequency change. The use of the static models described in the previous sections is justified in such cases.

There are, however, many cases where it is necessary to account for the dynamics of the load components. Studies of inter-area oscillations, voltage instability and long term stability often require load dynamics to be modelled. A study of systems with large concentrations of motors also requires the representation of load dynamics. Reference [92] discusses various models in use for stability studies and proposes a general model that encompasses a large variety of models with suitable modification of the coefficients. A CIGRE task force, formed to investigate the causes of the Swedish system blackouts in 1983, produced the following recommendations [94] on the effect of load models in stability studies in stressed power systems.

$$P_L = P_0 + P + K_{pw}\frac{d\theta_L}{dt} + K_{pv}\left(V_L + T\frac{dV_L}{dt}\right) \tag{3.42}$$

$$Q_L = Q_0 + Q + K_{qw}\frac{d\theta_L}{dt} + K_{qv1}V_L + K_{qv2}V_L^{\,2} \tag{3.43}$$

where, P and Q are static power loads, P_0 and Q_0 are the constant power portion of the induction motor load and the rest depends on bus voltage and frequency deviation. V_L and θ_L are the bus voltage magnitude and phase angle respectively. A more simplified load model [95] incorporating static and dynamic behaviour is applied in this work by the following equations:

$$P_L = P_{L0}\left(\frac{V_L}{V_{L0}}\right)^{np} + K_{pw}\frac{d\theta_L}{dt} + K_{pv}T\frac{dV_L}{dt} \tag{3.44}$$

$$Q_L = Q_{L0}\left(\frac{V_L}{V_{L0}}\right)^{nq} + K_{qw}\frac{d\theta_L}{dt} \tag{3.45}$$

with P_{L0} and Q_{L0} and V_{L0} are nominal values of real power, reactive power and voltage.

3.8 SMALL SIGNAL MODEL OF THE SMES

Chapter Two described the technological and economic benefits of a SMES connected to a power system. It was mentioned that the real power of a SMES unit could be modulated to effectively improve the stability performance of a power system. The SMES have been put into use for the enhancement of transient, dynamic and torsional stability performance. Independent active and reactive power control over four quadrants can be achieved for a converter bridge operating under an appropriate switching strategy. The current in the superconducting coil and hence, the stored energy is controlled by the output voltage of the power conditioning system (PCS). The PCS is an ac/dc converter bridge which connects the superconducting coil to the power system. Power transfer into or out of the coil is by a positive or negative voltage across the coil and changes in the coil current. If the pulse width modulation (PWM) switching strategy with GTO switches is applied to the control of the PCS, the simultaneous control of the active and reactive power flow can be achieved in both directions. The power flows into the SMES are given by:

$$P_{SM} = V_t I_{SM\,max} M \cos\alpha \tag{3.46}$$

$$Q_{SM} = V_t I_{SM\,max} M \sin\alpha \tag{3.47}$$

where, P_{SM}, Q_{SM} are the active and reactive power flows to the SMES, V_t is the network voltage and I_{SM} is the coil current. M and α are the modulation index and delay angle of the switching strategy. The energy capacity of the coil is given by

$$E_{max} = \frac{1}{2} L I_{SM\,max}^{\ 2} \tag{3.48}$$

where, $I_{SM_{max}}$ is the maximum permitted coil current.

The main objective of the SMES controller is to regulate both the real and reactive power. For this purpose, the real power output of the SMES is measured and compared with the reference power input. The only function of the reactive power controller in a SMES is to provide dynamic reactive power support. The bus voltage is compared with a reference voltage and the error voltage is fed back to the voltage regulator.

Fig. 3.3 represents a SMES system in block diagram form. The response of the SMES to the real and reactive power commands can be represented by a first order block [96]. The voltage regulator, shown in Fig.3.4, generates the reactive power demand. The gain of the voltage controller block can be set from the Q-V characteristics of the bus to which the SMES is connected. The parameters of the lead-lag block can be selected so that the voltage regulator enhances the transient stability (high initial response). In view of the above discussion and Fig. 3.3–3.4, the dynamic behaviour of the SMES system is given by the following equations:

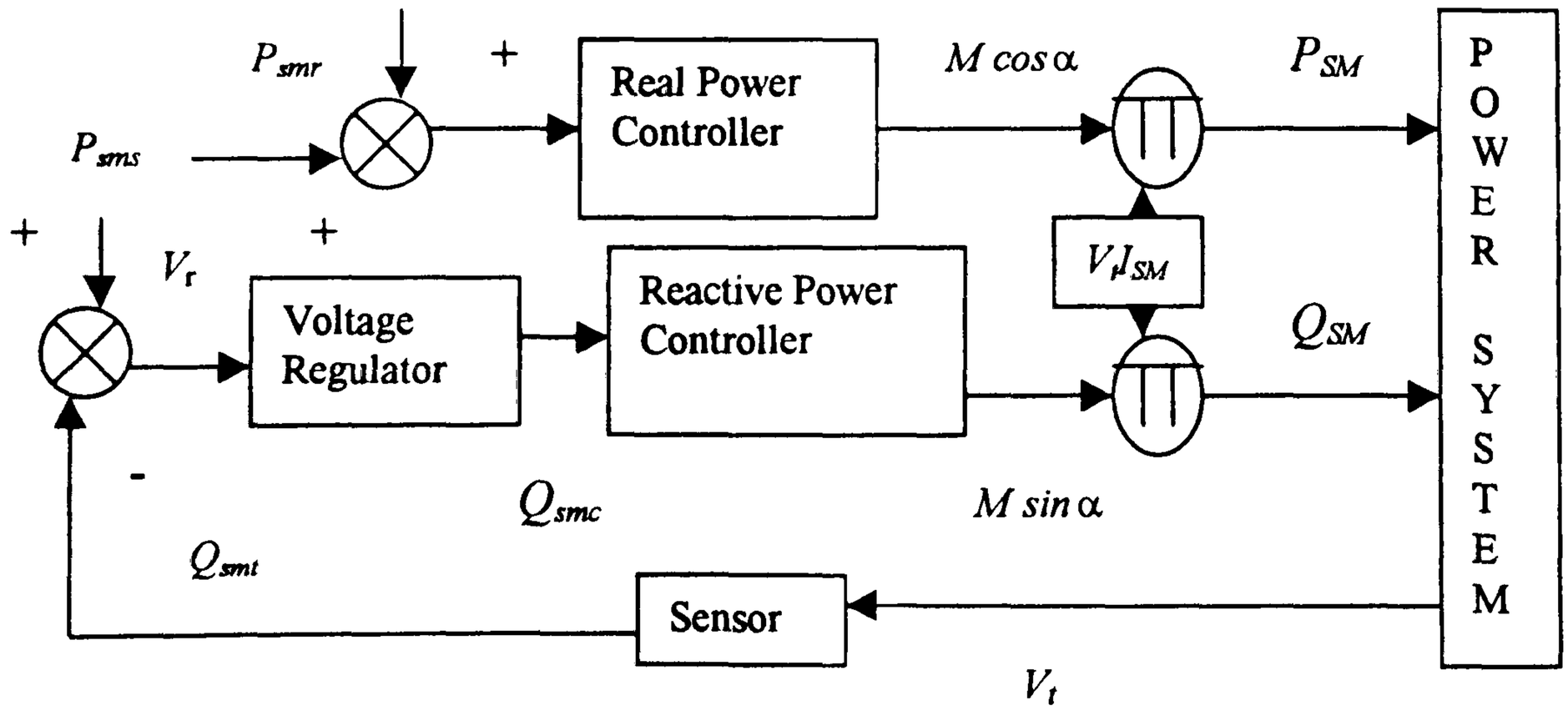

Fig. 3.3 Functional Block Diagram of a SMES System

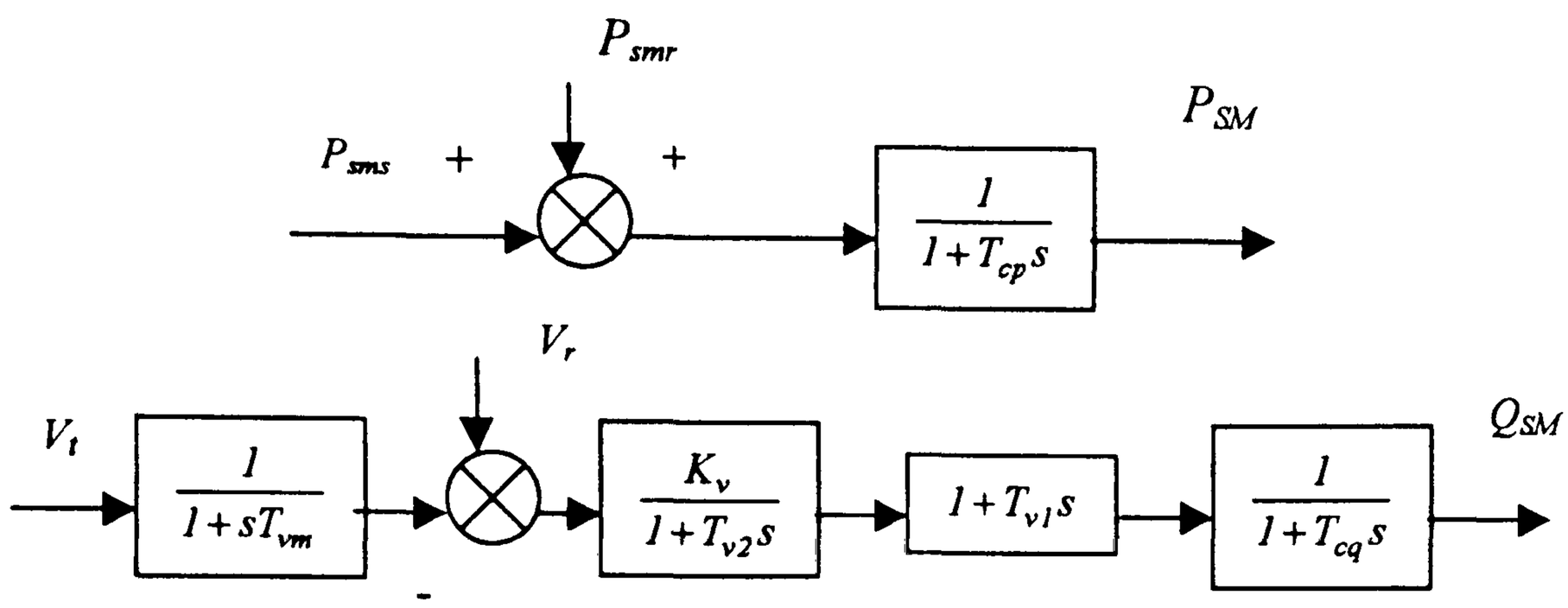

Fig 3.4: Small Signal Model of a SMES

$$\frac{dP_{SM}}{dt} = +\frac{1}{T_{cp}}\left(-P_{SM} + P_{smr} + P_{sms}\right) \tag{3.49}$$

$$\frac{dQ_{smc}}{dt} = \frac{1}{T_{v2}}\left[-Q_{smc} - K_v Q_{smt} + K_v V_r\right] \tag{3.50}$$

$$\frac{dQ_{SM}}{dt} = \frac{1}{T_{cq}}\left[-Q_{SM} + \left(1 - \frac{T_{v1}}{T_{v2}}\right)Q_{smc} - K_v \frac{T_{v1}}{T_{v2}} Q_{smt} + K_v \frac{T_{v1}}{T_{v2}} V_r\right] \tag{3.51}$$

$$\frac{dQ_{smt}}{dt} = \frac{1}{T_{vm}}\left(-Q_{smt} + V_t\right) \tag{3.52}$$

where, P_{sms} is the supplementary control signal to be generated by the damping controller. The other variables are same as shown in Fig.3.3.

3.9 OVERALL MODEL OF A MULTIMACHINE SYSTEM

The dynamic behaviour of a practical power system with 'm' generators, 'n' buses and 'k' SMES devices connected to one of the load buses can now be presented in a systematic manner. Three damper winding model and DC Type excitation is considered for the machines. For i = 1 to m

$$\frac{d\delta_i}{dt} = \omega_i - \omega_s \tag{3.53}$$

$$\frac{d\omega_i}{dt} = \frac{\omega_i}{2H_i}\left[T_{mi} - T_{eleci} - T_{Di}\right] \tag{3.54}$$

$$\frac{dE_{qi}'}{dt} = \frac{1}{T_{doi}'}\left[-E_{qi}' - \left(X_{di} - X_{di}'\right)\left[-I_{di} - \frac{\left(X_{di}' - X_{di}''\right)}{\left(X_{di}' - X_{lsi}\right)^2}\left(\Psi_{1di}\right.\right.\right.$$

$$\left.\left.\left.-\left(X_{di}' - X_{lsi}\right)I_{di} - E_{qi}'\right)\right] + E_{fdi}\right]$$

(3.55)

$$\frac{dE_{di}'}{dt} = -\frac{1}{T_{qoi}'}\left[+E_{di}' + \left(X_{qi} - X_{qi}'\right)\left[I_{qi} - \frac{\left(X_{qi}' - X_{qi}''\right)}{\left(X_{qi}' - X_{lsi}\right)^2}\left(-\Psi_{2qi}\right.\right.\right.$$

$$\left.\left.\left.+\left(X_{qi}' - X_{lsi}\right)I_{qi} - E_{di}'\right)\right]\right]$$

(3.56)

$$\frac{d\Psi_{1di}}{dt} = \frac{1}{T_{doi}''}\left[-\Psi_{1di} + E_{qi}' + \left(X_{di}' - X_{lsi}\right)I_{di}\right] \tag{3.57}$$

$$\frac{d\Psi_{2qi}}{dt} = -\frac{1}{T_{qoi}''}\left[\Psi_{2qi} + E_{di}' - \left(X_{qi}' - X_{lsi}\right)I_{qi}\right] \tag{3.58}$$

$$T_{eleci} = \frac{\left(X_{di}'' - X_{lsi}\right)}{\left(X_{di}' - X_{lsi}\right)}E_{qi}'I_{qi} + \frac{\left(X_{di}' - X_{di}''\right)}{\left(X_{di}' - X_{lsi}\right)}\Psi_{1di}I_{qi} + \frac{\left(X_{qi}'' - X_{lsi}\right)}{\left(X_{qi}' - X_{lsi}\right)}E_{di}'I_{di}$$

$$-\frac{\left(X_{qi}' - X_{qi}''\right)}{\left(X_{qi}' - X_{lsi}\right)}\Psi_{2qi}I_{di} - \left(X_{qi}'' - X_{di}''\right)I_{qi}I_{di}$$

(3.59)

$$\frac{dV_{tri}}{dt} = -\frac{1}{Tri}\left[V_{tri} - V_{ti}\right] \tag{3.60}$$

$$\frac{dE_{fdi}}{dt} = -\frac{1}{T_{ei}}\left[K_{ei} + S_{ei}(E_{fdi})\right]E_{fdi} + \frac{V_{ri}}{T_{ei}} \tag{3.61}$$

$$\frac{dV_{ri}}{dt} = \frac{1}{T_{ai}}\left[-V_{ri} + K_{ai}R_{fi} - \frac{K_{ai}K_{fi}}{T_{fi}}E_{fdi} + K_{ai}\left(V_{refi} - V_{ti}\right)\right] \tag{3.62}$$

$$V_{r\min i} \le V_{ri} \le V_{r\max i}$$

$$\frac{dR_{fi}}{dt} = \frac{1}{T_{fi}}\left[-R_{fi} + \frac{K_{fi}}{T_{fi}}E_{fdi}\right] \tag{3.63}$$

Stator algebraic equations:

$$V_i Cos(\delta_i - \theta_i) - \frac{\left(X_{di}'' - X_{lsi}\right)}{\left(X_{di}' - X_{lsi}\right)}E_{qi}' - \frac{\left(X_{di}' - X_{di}''\right)}{\left(X_{di}' - X_{lsi}\right)}\Psi_{1di} + R_{si}I_{qi} - X_d''I_{di} = 0 \tag{3.64}$$

$$V_i Sin(\delta_i - \theta_i) + \frac{\left(X_{qi}'' - X_{lsi}\right)}{\left(X_{qi}' - X_{lsi}\right)}E_{di}' - \frac{\left(X_{qi}' - X_{qi}''\right)}{\left(X_{qi}' - X_{lsi}\right)}\Psi_{2qi} - X_{qi}''I_{qi} - R_{si}I_{di} = 0 \tag{3.65}$$

Network algebraic equations pertaining to generator busses:

$$V_i Cos(\delta_i - \theta_i)I_{qi} - V_i Sin(\delta_i - \theta_i)I_{di} - S_{pi} = 0 \tag{3.66}$$

$$-V_i Sin(\delta_i - \theta_i)I_{qi} - V_i Cos(\delta_i - \theta_i)I_{di} - S_{qi} = 0 \tag{3.67}$$

Power balance equations for dynamic load busses:

$$\frac{d\theta_{Li}}{dt} = -\frac{1}{K_{qwi}}\left[-Q_{SMj} + S_{qi} + Q_L(V_{Li})\right] \tag{3.68}$$

$$\frac{dV_{Li}}{dt} = -\frac{1}{K_{pvi}T_i}\left[-P_{SMj} + S_{pi} + P_L(V_{Li}) - \frac{K_{pwi}}{K_{qwi}}\left(-Q_{SMj} + S_{qi} + Q_L(V_{Li})\right)\right] \tag{3.69}$$

where,

$$P_{Li}(V_{Li}) = P_{Li0}\left(\frac{V_{Li}}{V_{Li0}}\right)^{n_{pi}} \tag{3.70}$$

$$Q_{Li}(V_{Li}) = Q_{Li0}\left(\frac{V_{Li}}{V_{Li0}}\right)^{n_{qi}} \tag{3.71}$$

$$S_{pi} = \sum_{k=1}^{k=n} V_i V_k \left[G_{ik} Cos(\theta_i - \theta_k) + B_{ik} Sin(\theta_i - \theta_k)\right] \tag{3.72}$$

$$S_{qi} = \sum_{k=1}^{k=n} V_i V_k \left[G_{ik} Sin(\theta_i - \theta_k) - B_{ik} Cos(\theta_i - \theta_k)\right] \tag{3.73}$$

for j = 1to k

$$\frac{dP_{SMj}}{dt} = +\frac{1}{T_{cpj}}\left(-P_{SMj} + P_{smrj} + P_{smsj}\right) \tag{3.74}$$

$$\frac{dQ_{smcj}}{dt} = \frac{1}{T_{v2j}}\left[-Q_{smcj} - K_{vj}Q_{smtj} + K_{vj}V_{rj}\right] \tag{3.75}$$

$$\frac{dQ_{SMj}}{dt} = \frac{1}{T_{cq}j}\left[-Q_{SMj} + \left(1 - \frac{T_{v1j}}{T_{v2j}}\right)Q_{smcj} - K_{vj}\frac{T_{v1j}}{T_{v2j}}Q_{smtj} + K_{vj}\frac{T_{v1j}}{T_{v2j}}V_{rj}\right] \tag{3.76}$$

$$\frac{dQ_{smtj}}{dt} = \frac{1}{T_{vmj}}\left(-Q_{smtj} + V_{ti}\right) \tag{3.77}$$

The j^{th} SMES is assumed connected to the i^{th} load bus.

Equation (3.53) to (3.77) can be written in compact form:

$$\frac{\mathbf{dx}}{\mathbf{dt}} = \mathbf{f}(\mathbf{x}, \mathbf{y}, \mathbf{u}) \tag{3.78}$$

$$\mathbf{0} = \mathbf{g}(\mathbf{x}, \mathbf{y}) \tag{3.79}$$

where $[\ \delta, \omega, E_q', E_d', E_{fd}, V_r, R_f, \theta_L, V_L\ ]$ form **x** known as state variables, θ, V, I_q, I_d for all busses except for the dynamic load bus, comprise **y,** known as algebraic variables. Linearising (3.78) and (3.79) around a nominal operating point, the following is obtained:

$$\Delta\dot{\mathbf{x}} = \frac{\mathbf{df}}{\mathbf{dx}}\Delta\mathbf{x} + \frac{\mathbf{df}}{\mathbf{dy}}\Delta\mathbf{y} + \frac{\mathbf{df}}{\mathbf{du}}\Delta\mathbf{u} \tag{3.80}$$

$$\mathbf{0} = \frac{\mathbf{dg}}{\mathbf{dx}}\Delta\mathbf{x} + \frac{\mathbf{dg}}{\mathbf{dy}}\Delta\mathbf{y} \tag{3.81}$$

Vector equations (3.80) and (3.81) are in a suitable form to carry out the eigenvalue analysis described in the next section. The detail of the linearization of the vector differential and algebraic equations (DAE) given in (3.78) and (3.79) is provided in Appendix A.

3.10 SUMMARY AND CONCLUSIONS

In this chapter, the small signal models of various power system dynamic devices have been described. Various simplifications have been made with regards to the generator stator, prime mover and the transmission network. These simplifications are widely adopted in small signal stability analysis, specifically in the studies of very low-frequency electromechanical oscillations. The overall description of the dynamic behaviour of a multimachine system with SMES devices is provided by a set of differential and algebraic equations. This lays the foundation stone for the small signal analysis and control design that will be the topic of the next few chapters.

CHAPTER FOUR

ANALYSIS OF LOW-FREQUENCY ELECTROMECHANICAL OSCILLATIONS IN MULTIMACHINE POWER SYSTEMS

4.1 INTRODUCTION

It was noted that low-frequency oscillations, especially the inter-area modes are associated with the weak transmission links and heavy power transfers. The problem is made more critical with the automatic voltage control of the generating units adversely interacting in the low-frequency range. In this chapter, the analysis will be carried out first to identify coherent groups of machines in the selected inter-area modes. The generator coherency is extended to busses in an attempt to identify coherent areas and tie lines. The analysis of the study systems under several power flow scenarios, variable transmission strength and different excitation characteristics with a variety of loads will provide a quantitative assessment of the role of each individual component and their contribution to damping. Three study systems will be considered. The SMES will be assumed disconnected so that the small signal behaviour of the original system at different operating conditions can be understood. Both eigenvalue analysis and time domain simulations are performed in order to have a better understanding of the dynamic stability problem.

4.2 IDENTIFICATION OF COHERENT AREAS

In a power system formed by interconnecting two or more closely coupled generation/load areas through relatively weak ties, the generators in each area are close to being coherent in the inter-area mode of oscillations. In systems having a number of low-frequency inter-area modes, one can use the coherency property to identify relatively closely coupled generators from the angle components of eigenvectors of the inter-area modes. In addition, one can also identify the busses whose angles oscillate coherently with the generator angles. This divides the system into sets of coherent busses and generators. The number of coherent areas is one more than the number of inter-area modes. The tie lines between one coherent group and another are the weak connections. These are the root cause of the inter-area oscillations.

It is not easy to determine coherent groups by visual inspection of the eigenvectors. What is required is to find the generator rotor angles and bus voltage phase angle changes which have the most consistently similar pattern over all the inter-area modes. This is done by calculating the direction cosines of the rows of the eigenvectors corresponding to the generator angles. The use of direction cosines to identify coherent group of machines and areas is made by Yusof et. al. [97]. This is briefly described here.

The power system dynamic behaviour is described by the following set of DAE equations.

$$\dot{\mathbf{x}} = \mathbf{f}(\mathbf{x}, \mathbf{y}) \tag{4.1}$$

$$\mathbf{0} = \mathbf{g}(\mathbf{x}, \mathbf{y}) \tag{4.2}$$

x is the state variables (machine angle and speed) and **y** is the algebraic variables (bus voltage magnitude, bus angle). Linearising the above set of equations around an initial operating condition and eliminating the algebraic variables, the following state-space form is arrived at:

$$\Delta\dot{\mathbf{x}} = \mathbf{A}\Delta\mathbf{x} \tag{4.3}$$

where $\mathbf{A} = \dfrac{\partial \mathbf{f}}{\partial \mathbf{x}} - \dfrac{\partial \mathbf{f}}{\partial \mathbf{y}}\left(\dfrac{\partial \mathbf{g}}{\partial \mathbf{y}}\right)^{-1}\left(\dfrac{\partial \mathbf{g}}{\partial \mathbf{x}}\right)$

For any eigenvalue λ_i of **A:**

$$\mathbf{A}\mathbf{v} = \lambda_i \mathbf{v} \tag{4.4}$$

where **v** is the eigenvector. For '*r*' number of eigenvalues corresponding to '*r*' number of inter-area modes, '*r*' number of eigenvectors can be found. Normally for coherency identification a classical generator model with no mechanical damping is often enough since the electromechanical modes can be visualised by the use of the classical model itself. But there is no harm in considering a detailed model except for adding complexities. With this assumption, in a p-machine and n-bus system, the system state matrix will be of (*2p x 2p*). If '*r*' number of modes are considered (including modes corresponding to zero eigenvalue), the dimension of **v** will be (*2p x r*). A new vector **w** *(p x r)* is constructed by considering the rows corresponding to machine angle. For two vectors w_1, w_2, the direction cosine is defined as:

$$dcv = \frac{\sum_{i=1}^{p} w_{1i} w_{2i}}{\sqrt{\sum_{i=1}^{p} w_{1i}^{\,2} \sum_{i=1}^{p} w_{2i}^{\,2}}} \tag{4.5}$$

If the vectors are identical, the direction cosine is unity. If two generators are in a coherent group, the direction cosine will be very close to unity. If two generators belong to two different coherent groups, the direction cosine will be less. Whilst it is possible to examine the coherency properties of all the generators in the chosen eigenvectors, a number of compromises arise. There is the problem of the choice of direction cosine level at which to consider two generators to be coherent. This can be resolved by examining the values of the direction cosines. The differences between the direction cosine of any one generator and all other generators in a coherent group are very small. These differences are quite noticeable when two generators belong to two different coherent groups. It is possible to associate each of the generators with a group. The number of coherent group will be equal to one more than the number of inter-area modes selected. The approach is extended to include network busses for coherency identification. This is done as follows.

The eigenvector **v** in (4.3) can be appended to include the bus voltage magnitude and angle term. The appended vector, say **u**, can be computed from the relation:

$$\mathbf{u} = -\frac{\partial \mathbf{g}}{\partial \mathbf{x}} \left(\frac{\partial \mathbf{g}}{\partial \mathbf{y}} \right)^{-1} \mathbf{v} \tag{4.6}$$

The rows of **u** corresponding to bus angle can be extracted and appended with **w.** The direction cosines between the bus angle and machine angles are computed. The values can be examined to associate a particular bus with a particular generator group already identified. Eventually, each of the busses can be associated with its most appropriate coherent generator group. Once the busses are identified as part of a coherent generator group, several coherent areas are identified. The connections between coherent areas are the tie lines. This will be illustrated with three study systems in the next section.

4.2.1 STUDY SYSTEM #1: A FOUR-MACHINE-TWO-AREA CASE

A simple 4-machine-11-bus system is shown in Fig. 4.1. Several researchers [98,92,96] have considered this system for low-frequency oscillation studies. The

machines are modelled with four windings (one field and three dampers) on the rotor. The excitation systems are of ST1A type [93]. In the normal operating condition, 400 MW flows through the tie lines. Operation of the system with fewer ties will also be considered later in the analysis. Loads are connected to busses #5 and #6. The system data and load flow solution is provided in Appendix B.

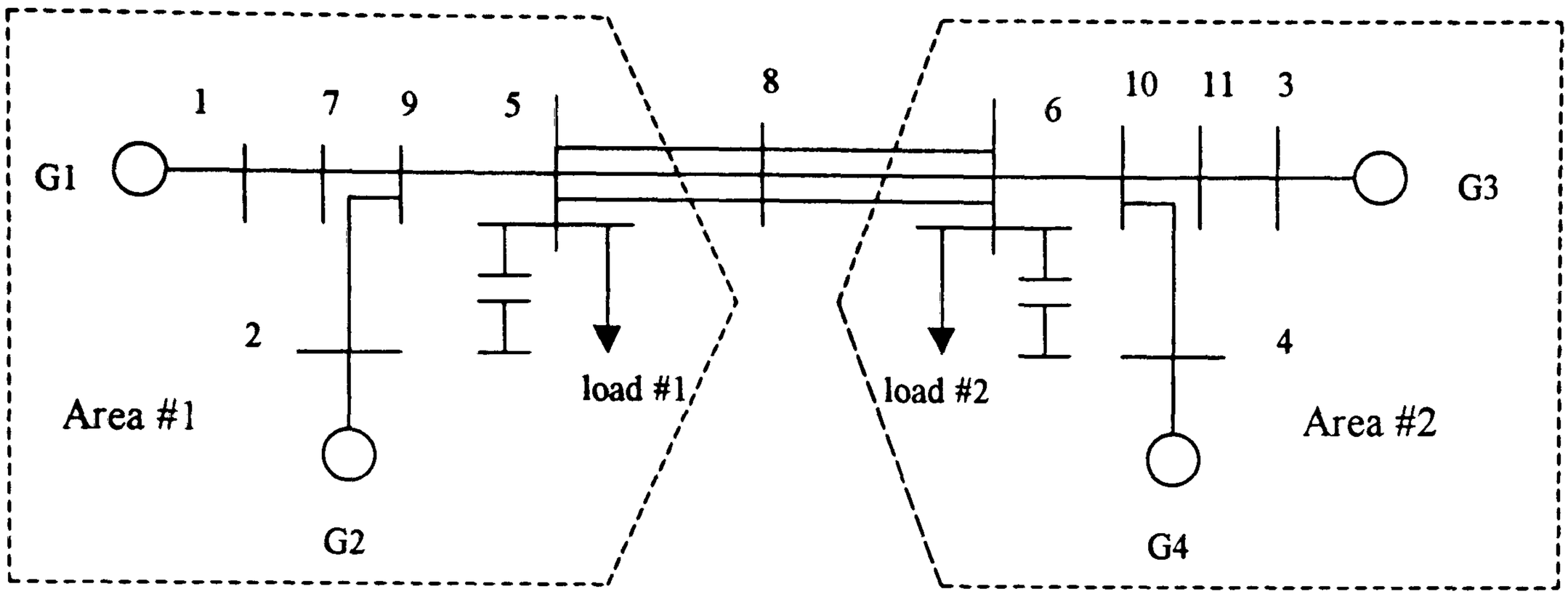

Fig 4.1: A 4-machine-11-bus system

The direction cosine approach, described above, is applied to this system. The generator model is simplified to a classical one leaving only the swing equations. The loads are treated as of the constant impedance type. It is found from the eigenvalue analysis that the system has three electromechanical modes. The frequencies of these modes are 0.62, 1.08, 1.0444 Hz. respectively. The slowest mode (0.62 Hz) is selected for obvious reasons as the frequency is in the inter-area mode range. There are two zero eigenvalues because of expressing the machine angle deviations in absolute terms i.e. no machine is selected as reference machine and mechanical damping effect being ignored. The eigenvectors corresponding to these two zero eigenvalues and that due to 0.62 Hz form the eigenvectors matrix. The direction cosines corresponding to the machine angles of this eigenvectors matrix provides a generator coherency matrix that is displayed in Table 4.1.

Table 4.1: Generator coherency matrix for Study system #1

	G#1	G#2	G#3	G#4
G#1	**1.0000**	**0.9979**	0.8660	0.8822
G#2	**0.9979**	**1.0000**	0.8966	0.9109
G#3	0.8660	0.8966	**1.0000**	**0.9994**
G#4	0.8822	0.9109	**0.9994**	**1.0000**

It is clear from the entries in Table 4.1 that the direction cosines of the angles between machines #1 and #2 and that between machines #3 and #4 are close to unity. They are highlighted as two block diagonal small matrices inside the original matrix. This suggests that machines #1 and #2 form one coherent group and machines #3 and #4 another coherent group in the inter-area mode. This is independently verified by mode shape analysis [92].

The direction cosine approach is extended to identify bus coherency after coherent machine groups are identified. The rows corresponding to the angle components of all bus voltages are selected for the computation of the direction cosines with machine angle rows as described in the last section. The direction cosine matrix is displayed in Table 4.2. Bus #5 is abbreviated as B#5, generator #3 is as G#3 and so on. The direction cosines, those are very close or equal to unity, are highlighted once again. It is very straightforward to say that busses #2, #5, #7, #9 are coherent with generators #1 and #2. Busses #3, #4, #6, #10, #11 are coherent with generators #3 and #4. It is very interesting to note the entries corresponding to bus #8. All of the four entries are very high. This suggests that bus #8 is under the influence of all four machines. In the single line diagram of Fig. 4.1, bus #8 is the mid-point of the lines between bus #5 and #6. This

Table 4.2 Bus-Generator coherency matrix of study system #1

	G#1	G#2	G#3	G#4
B#1	**0.9992**	**0.9997**	0.8853	0.9003
B#2	**0.9955**	**0.9995**	0.9095	0.9229
B#3	0.8905	0.9181	**0.9987**	**0.9998**
B#4	0.9039	0.9297	**0.9967**	**0.9988**
B#5	**0.9845**	**0.9938**	0.9402	0.9511
B#6	0.9168	0.9407	**0.9937**	**0.9969**
B#7	**0.9974**	**1.0000**	0.8996	0.9137
B#8	0.9556	**0.9727**	**0.9749**	**0.9818**
B#9	**0.9919**	**0.9980**	0.9227	0.9350
B#10	0.9099	0.9348	**0.9954**	**0.9981**
B#11	0.8985	0.9251	**0.9976**	**0.9994**

means busses #1, #2, #5, #7, #9 and machines #1, #2 form one coherent area (say Area #1) and busses #3, #4, #6, #10, #11 and machines #3, #4 form another coherent area (say Area #2). The lines between bus #5 and #6 are the tie lines. This inference is very interesting as it analytically identifies the coherent areas. The two coherent areas are identical to the areas identified by inspecting the network configuration blended with a basic sense of power system structure. Bus #8 is the middle of tie lines but because of tie lines flow from Area #1 to Area #2, it is coherent with Area #2. If the direction of the flow is reversed it will be coherent with Area #1. In the original configuration [98] bus #8 is not shown. It is introduced in this study to evaluate the potential of mid-point as a possible SMES location.

The system with three tie lines transferring 400 MW power from Area #1 to Area #2 is defined pre-fault steady state. The steady state operation of the system with two tie lines is defined post-fault operating case.

4.2.2 STUDY SYSTEM #2: A SIX-MACHINE-THREE-AREA CASE

The 6-machine-16-bus system shown in Fig. 4.2 is used in [22,99,100] to explore the possibility of damping out more than one inter-area mode with more than one FACTS device. Machine parameters are identical to those used in Study system #1. Excitation systems are type ST1A [93]. The loads are of constant impedance (CI) type. The details of the machine parameters, generations and loads levels are provided in Appendix B. Eigenvalue analysis on the classical machine model with no mechanical damping provides five electromechanical modes. The frequencies of these modes are 0.82, 1.14, 1.65, 1.67 and 1.68 Hz respectively. In addition to this, there are two zero eigenvalues present for the reason already discussed in Study system #1. The first two modes i.e. modes of 0.82 and 1.14 Hz. are considered for the identification of the coherent generator groups and coherent bus groups. The direction cosines are computed and displayed in Table 4.3 for generator coherency and in Table 4.4 for bus-generator coherency.

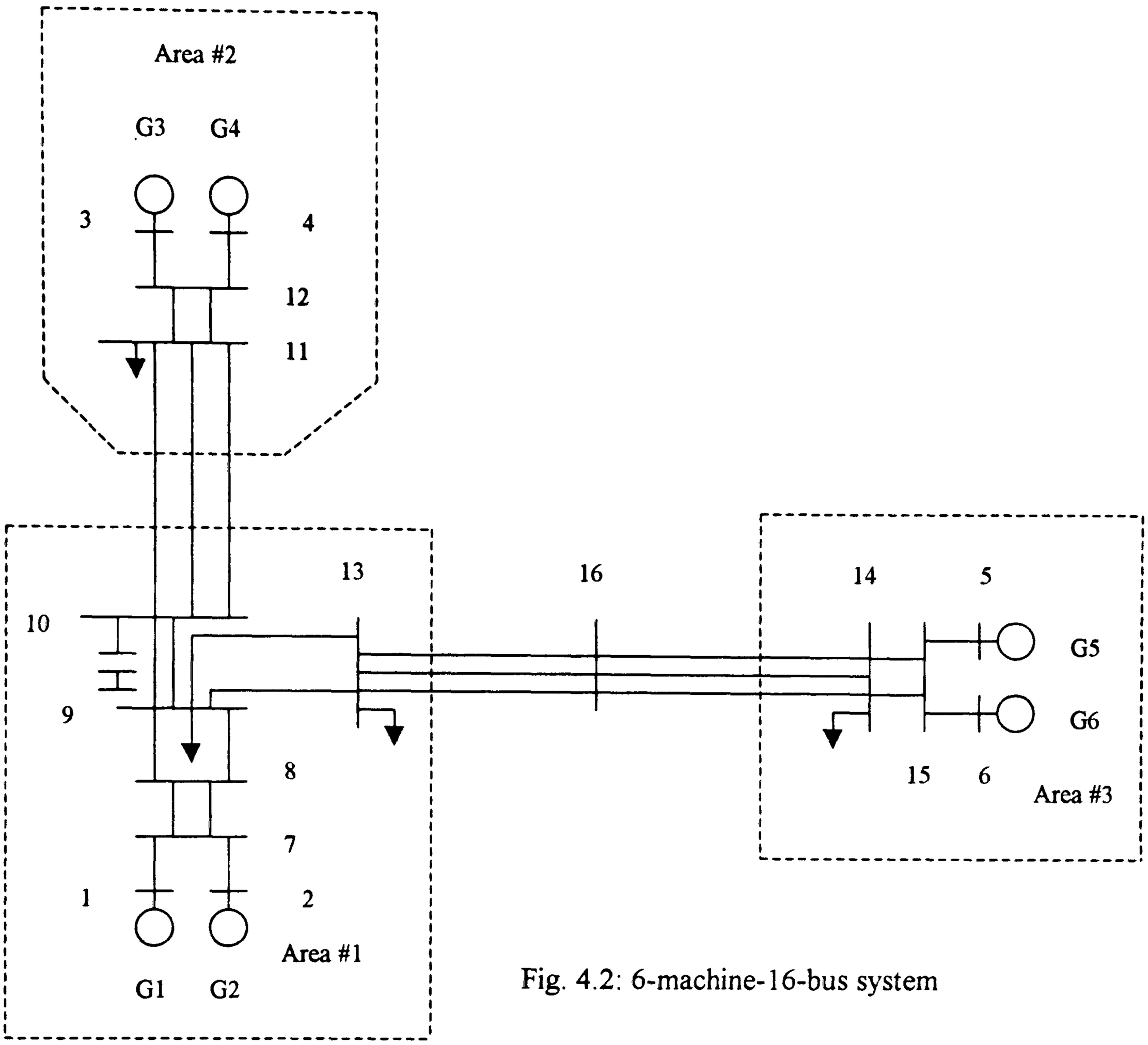

Fig. 4.2: 6-machine-16-bus system

Table 4.3: Generator coherency matrix for Study system #2

	G #1	G #2	G #3	G #4	G #5	G #6
G #1	**1.0000**	**1.0000**	0.9486	0.9486	0.9174	0.9183
G #2	**1.0000**	**1.0000**	0.9486	0.9486	0.9174	0.9183
G #3	0.9486	0.9486	**1.0000**	**1.0000**	0.9047	0.9049
G #4	0.9486	0.9486	**1.0000**	**1.0000**	0.9047	0.9049
G #5	0.9174	0.9174	0.9047	0.9047	**1.0000**	**1.0000**
G #6	0.9183	0.9183	0.9049	0.9049	**1.0000**	**1.0000**

Table 4.4: Bus-Generator coherency matrix of Study system #2

	G #1	G #2	G #3	G #4	G #5	G #6
B #1	**0.9977**	**0.9977**	0.9647	0.9647	0.9352	0.9360
B #2	**0.9977**	**0.9977**	0.9647	0.9647	0.9352	0.9360
B #3	0.9598	0.9598	**0.9990**	**0.9990**	0.9193	0.9196
B #4	0.9598	0.9598	**0.9990**	**0.9990**	0.9193	0.9196
B #5	0.9308	0.9308	0.9197	0.9197	**0.9992**	**0.9993**
B #6	0.9319	0.9319	0.9205	0.9205	**0.9991**	**0.9992**
B #7	**0.9930**	**0.9930**	0.9736	0.9736	0.9458	0.9464
B #8	**0.9952**	**0.9952**	0.9704	0.9704	0.9419	0.9426
B #9	**0.9877**	**0.9877**	0.9788	0.9788	0.9524	0.9529
B #10	**0.9859**	**0.9859**	0.9822	0.9822	0.9502	0.9507
B #11	0.9699	0.9699	**0.9961**	**0.9961**	0.9312	0.9316
B #12	0.9661	0.9661	**0.9975**	**0.9975**	0.9269	0.9272
B #13	**0.9845**	**0.9845**	0.9756	0.9756	0.9619	0.9623
B #14	0.9441	0.9441	0.9337	0.9337	**0.9967**	**0.9968**
B #15	0.9392	0.9392	0.9285	0.9285	**0.9979**	**0.9980**
B #16	0.9688	0.9688	0.9595	0.9595	**0.9839**	**0.9842**

From the entries in Table 4.3, it is clear that generators #1 and #2 form the first coherent group, generators #3 and #4, the second coherent group and generators #5 and #6, the third coherent group respectively. It is interesting to see that the direction cosines are unity in each coherent group. This means that the angle rows of eigenvectors are identical. It is obvious when the same angle row vector of a particular machine is considered to compute the direction cosine of machine with itself. The generators in each coherent group are identical to each other. They are loaded almost identically. That also gives rise to the identical angle row of the eigenvectors for the machines in each coherent group. The system state matrix is singular because of two zero eigenvalues. The eigenvector computation of a singular matrix is an ill-conditioned problem. Even the most efficient routine available with *Matlab* [101] will provide inaccurate eigenvectors matrix. As a result of this, two eigenvectors will be almost linearly dependent. These eigenvectors, when normalised, are basically the same to produce to a unity direction cosine.

The entries in Table 4.4 reveals that busses #1, #2, #7, #8, #9, #10 and #13 have high direction cosines with the coherent generators #1 and #2. This suggests that

they can form the first coherent area (say Area #1). The busses #3, #4, #11 and #12 belong to second coherent group. The generators #3, #4 and busses #3, #4, #11 and #12 form another coherent area (say Area #2). From the results in Table 4.4, it is very clear that generators #5 and #6 and busses #5, #6, #14, #15 and #16 form the third coherent area (say Area #3). These areas are shaded and labelled in Fig. 4.2. Bus #16 is the mid-point of the lines running between busses #13 and #14. In reference [22,99,100], bus #16 is not shown but it is introduced here to explore the potential of locating a SMES to damp out oscillations.

A 550 MW power flow from Area #3 to Area #1 with three tie lines in operation is termed the pre-fault steady state. The operation of the system with one tie line between Area #1 and Area #2 disconnected is assumed to be the post-fault steady state.

4.2.3 STUDY SYSTEM #3: A SIXTEEN-MACHINE-FIVE-AREA CASE

This system, shown in Fig 4.3, has 16 machines and 68 busses. This is a reduced order model [102] of the New England and New York interconnected system. The first nine machines are the simple representation of the New England Test System (NETS) generation. Machines #10 to #13 represent the New York Power System (NYPS). The last three machines are the dynamic equivalent of three large neighbouring areas interconnected to the NYPS. Loads and generations correspond to a typical late 70's operating scenario. The first eight machines have slow excitation (IEEE type DC1A) whilst machine #9 is equipped with a fast acting static excitation system (IEEE ST1A). This machine is also assumed to have a speed input power system stabiliser (PSS) to ensure adequate damping of the electromechanical mode of this machine. The rest of the machines are under manual excitation control. The eigenvalue analysis of the system considering classical machine model without mechanical damping provides fifteen electromechanical modes in addition to two zero eigenvalues as expected. These are displayed in Table 4.5. From the results in Table 4.5, it is interesting to note that there can be several inter-area modes. The system is highly interconnected and it is very difficult to identify coherent generators by inspection. The direction cosine approach is applied to identify coherent generators and coherent areas.

Table 4.5:Electromechanical modes (in Hz) of Study system #3

0.0000	0.7934	1.2330	1.5573
0.3716	0.9965	1.2673	1.5608
0.5140	1.0677	1.2892	1.5691
0.5571	1.1325	1.3434	1.8253

The first step is to determine the modes of oscillation in which the coherency groupings are to be determined. We select the lowest frequency oscillations, including the zero eigenvalues, and look for a gap in frequency between the highest mode and the next. The modes in the first column are those chosen to be inter-area modes. The criterion for the choice is that there is a significant gap in frequency between the highest in the chosen group and the next highest mode. The choice is somewhat arbitrary in many systems, but in this system it is a satisfactory choice.

The direction cosine approach provides the following generator coherency matrix displayed in Table 4.6. It is clear from the entries in Table 4.6 that generators #1 - #9 form one coherent group. Generators #10 - #13 form another coherent group. In real life, these two coherent groups are the generators of NETS and NYPS respectively. The generators #14, #15 and #16 form three separate coherent groups respectively. In practice these three generators are the dynamic equivalents of large external systems. The bus-generator coherency studies reveal further interesting facts. The system has 68 busses. It is neither necessary nor practical to show the bus-generator coherency groupings for all of these busses in tabular form. It is found from the bus-generator coherency matrix that the busses #1 - #9, #19 - #29, #37, #52, #54 - #60 and #62-#68 belong to the coherent group formed by generators #1 - #9. This is the NETS system. The busses #10 - #13, #17, #30 - #36, #38 - #40, #42 - #51, #53 and #61 are coherent with the generator coherent group comprising of generators #10 - #13. Very interestingly, this is the NYPS system. Generator #14 and bus #14 form third coherent area. The generator #15 and bus #41 form the fourth coherent area. The generator #16, bus #16 and #18 form the fifth coherent area. The last three areas are termed Area #3, Area #4 and Area #5 respectively. The boundaries of these coherent areas are shown in Fig 4.3 by the dashed lines. The interconnections between these areas are the critical tie lines.

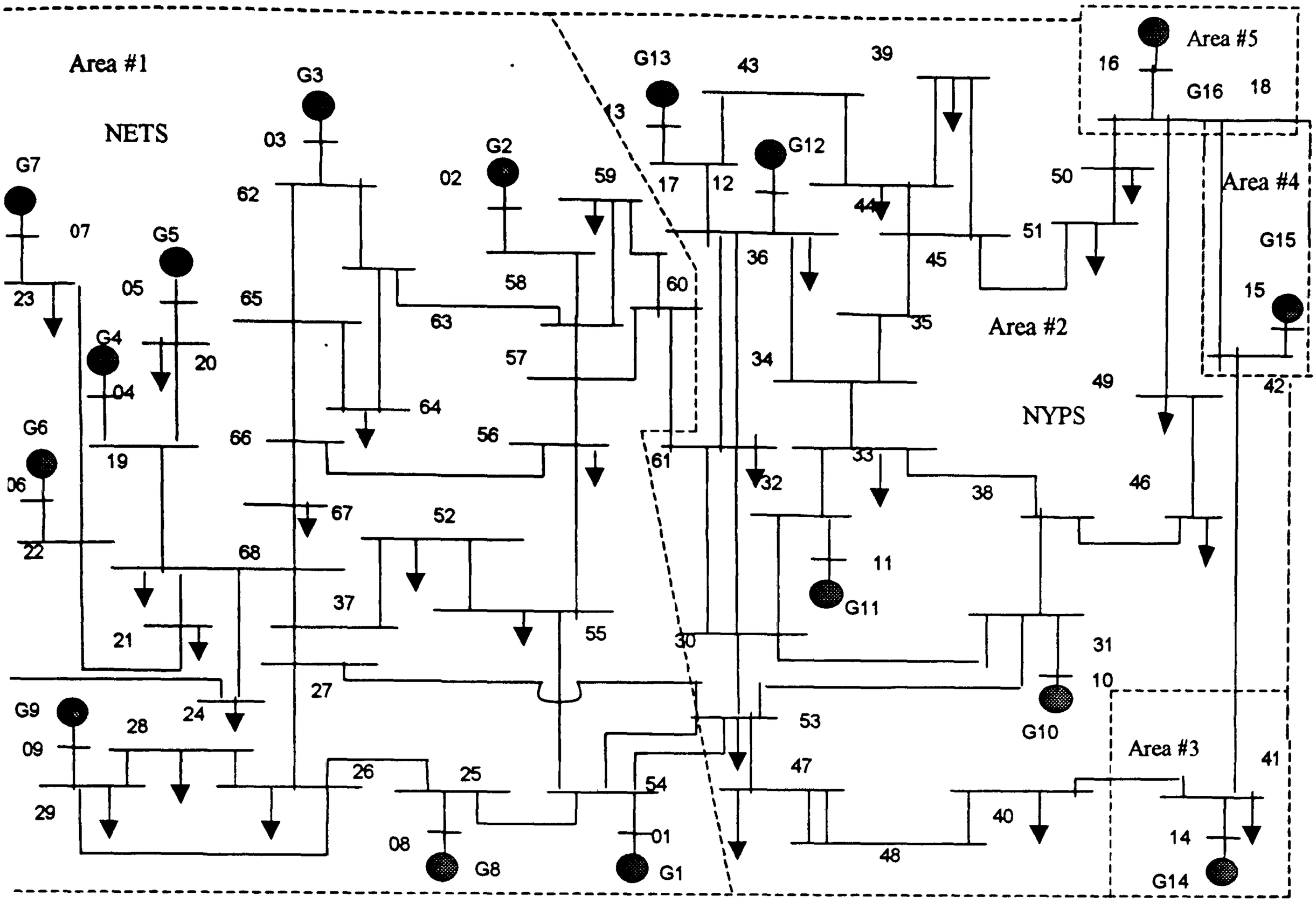

Fig. 4.3: Sixteen -machine-five -area study system

Table 4.6: Generator coherency in study system #3

	G#1	G#2	G#3	G#4	G#5	G#6	G#7	G#8	G#9	G#10	G#11	G#12	G#13	G#14	G#15	G#16
G#1	**1.000**	**0.982**	**0.982**	**0.984**	**0.980**	**0.981**	**0.982**	**0.999**	**0.989**	0.935	0.915	0.869	0.848	0.700	0.648	0.709
G#2	**0.982**	**1.000**	**1.000**	**1.000**	**0.999**	**1.000**	**1.000**	**0.987**	**0.999**	0.852	0.824	0.764	0.738	0.633	0.590	0.613
G#3	**0.982**	**1.000**	**1.000**	**1.000**	**0.999**	**1.000**	**1.000**	**0.987**	**0.999**	0.852	0.824	0.764	0.738	0.633	0.590	0.613
G#4	**0.984**	**1.000**	**1.000**	**1.000**	**0.999**	**1.000**	**1.000**	**0.989**	**0.999**	0.857	0.824	0.764	0.738	0.635	0.593	0.618
G#5	**0.980**	**0.999**	**0.999**	**0.999**	**1.000**	**1.000**	**0.999**	**0.985**	**0.998**	0.846	0.818	0.757	0.731	0.626	0.586	0.605
G#6	**0.981**	**1.000**	**1.000**	**0.999**	**1.000**	**1.000**	**1.000**	**0.987**	**0.999**	0.850	0.822	0.762	0.736	0.631	0.589	0.611
G#7	**0.982**	**1.000**	**1.000**	**1.000**	**0.999**	**1.000**	**1.000**	**0.987**	**0.999**	0.853	0.825	0.764	0.739	0.632	0.590	0.613
G#8	**0.999**	**0.987**	**0.987**	**0.989**	**0.985**	**0.987**	**0.987**	**1.000**	**0.993**	0.923	0.902	0.853	0.831	0.694	0.639	0.696
G#9	**0.989**	**0.999**	**0.999**	**0.999**	**0.998**	**0.999**	**0.999**	**0.993**	**1.000**	0.873	0.846	0.788	0.763	0.653	0.601	0.637
G#10	0.935	0.852	0.852	0.857	0.846	0.850	0.853	0.923	0.873	**1.000**	**0.998**	**0.981**	**0.968**	0.766	0.701	0.836
G#11	0.915	0.824	0.824	0.830	0.818	0.822	0.825	0.902	0.846	**0.998**	**1.000**	**0.990**	**0.980**	0.747	0.707	0.840
G#12	0.869	0.764	0.764	0.770	0.757	0.762	0.764	0.853	0.788	**0.981**	**0.990**	**1.000**	**0.998**	0.685	0.678	0.797
G#13	0.848	0.738	0.738	0.745	0.731	0.736	0.739	0.831	0.763	**0.968**	**0.980**	**0.998**	**1.000**	0.653	0.668	0.771
G#14	0.700	0.633	0.633	0.635	0.626	0.631	0.632	0.694	0.653	0.766	0.747	0.685	0.653	**1.000**	0.594	0.742
G#15	0.648	0.590	0.590	0.593	0.586	0.589	0.590	0.639	0.601	0.701	0.707	0.678	0.668	0.594	**1.000**	0.668
G#16	0.709	0.613	0.613	0.618	0.605	0.611	0.613	0.696	0.637	0.836	0.840	0.797	0.771	0.742	0.668	**1.000**

It is clear in Fig 4.3 that the lines between bus #53 and #54, bus #53 and #27, bus #60 and #61 are the three important interconnections between NETS and NYPS. The other interconnections are lines between bus #18 and #50, bus #18 and #49, bus #18 and #42, bus #41 and #42, bus #41 and #40 between NYPS and Area #3, Area #4 and Area #5.

A 100 MW of export from NETS to NYPS with two tie lines between bus #53 and #54 is regarded as a pre-fault operating system. A fault, when developed in one of these lines, makes it unavailable and the steady state operation of the system with one line out of operation is considered post-fault operating system.

4.3 ANALYSING THE FACTORS AFFECTING THE DAMPING AND FREQUENCY OF THE INTER-AREA MODES IN THE STUDY SYSTEMS

In Chapter one, it was mentioned that the inter-area mode damping is affected by various factors, such as number of damper windings, power flow in the tie lines, strength of the tie lines, dynamic characteristics of the excitation systems, characteristics of loads etc. In this section, these factors will be analysed further for the study systems already described.

4.3.1 EFFECT OF MACHINE MODEL

The damping ratios [92] and frequencies of various electromechanical modes for different machine models are computed in the pre-fault cases. In the classical model, mechanical damping is considered. In one-damper winding model, the damper winding is considered on the q-axis. In the two-damper winding model, two damper windings are considered on the q-axis apart from one on the d-axis. The load is of constant impedance type throughout. The excitation system is not included so as to make the damping contribution of damper circuits very clear.

Table 4.7: Damping ratio and frequency for different machine models (Study system #1)

Machine Model	Mode #1		Mode #2		Mode #3	
	ς	f (Hz)	ς	f (Hz)	ς	f (Hz)
Classical	0.000	0.62	0.000	1.08	0.000	1.11
1-damper	0.030	0.62	0.058	1.05	0.069	1.06
2-damper	0.032	0.62	0.081	1.08	0.097	1.10

Table 4.8: Damping ratio and frequency for different machine models (Study system #2)

Machine Model	Mode #1		Mode #2		Mode #3		Mode #4		Mode #5	
	ς	*f* (Hz)	ς	*f* (Hz)	ς	*f* (Hz)	ς	*f* (Hz)	ς	*f* (Hz)
Classical	0.000	0.82	0.000	1.14	0.000	1.65	0.000	1.67	0.000	1.68
1-damper	0.020	0.82	0.027	1.13	0.067	1.60	0.058	1.63	0.051	1.65
2-damper	0.022	0.82	0.035	1.14	0.105	1.68	0.094	1.70	0.083	1.70

Table 4.9: Damping ratio and frequency for different machine models (Study system #3)

Machine Model	Mode #1		Mode #2		Mode #3		Mode #4	
	ς	*f* (Hz)	ς	*f* (Hz)	ς	*f* (Hz)	ς	*f* (Hz)
Classical	0.029	0.37	0.022	0.50	0.014	0.54	0.016	0.79
1-damper	0.051	0.38	0.041	0.50	0.038	0.54	0.051	0.79
2-damper	0.052	0.38	0.042	0.50	0.041	0.55	0.049	0.79

In Table 4.7, the damping ratios and frequencies of three electromechanical modes are shown. Mode #1 is inter-area whilst modes #2 and #3 are local modes [92]. It is not the objective of this research to analyse or damp out local modes. The damping ratios of these local modes are displayed to show some interesting fact that will be clear from the next paragraph.

In the classical model, the damping ratios are zeros in the absence of any mechanical damping. When one damper winding is added to the q-axis (1-damper winding model), the damping of the inter-area mode is increased to 0.03 and that of the local modes to 0.058 and 0.069 respectively. This damper on the q-axis represents eddy currents in the deeper section of the rotor. When an additional damper winding is added to the q-axis and another to the d-axis, the damping ratios of modes #1, #2 and #3 increase to 0.032, 0.081 and 0.097 respectively. It is interesting to note that the damping of the inter-area mode is not increased much whilst the damping ratios of the local modes are increased noticeably with the addition of two more dampers. These two additional windings represent the surface eddy current effect in the rotor body. At higher frequencies (local modes), these hypothetical coils are effective, as current crowding takes place towards the surface. Sustained low-frequency (inter-area mode) currents penetrate deeper into the rotor and the coil to represent this becomes effective to provide damping action. Secondly, since the inter-area mode involves two groups of machines

connected through long lines, the magnitude of the induced eddy currents that flow through the lines are limited by the high transfer impedance of the lines. Such low values of current contribute virtually negligible amounts of damping torque. The same observation holds good for the results in Table 4.8 where the first two modes are inter-area modes and the last three modes (mode #3, #4 and #5 in Table 4.8) are local modes. The results displayed in Table 4.9 relate to the damping ratios of four inter-area modes in Study system#3. The other eleven local modes in Study system #3 are not listed. The observations in this system are similar to that in study systems #1 and #2.

From the results and discussions, it can be said that a machine model with two damper windings on the q-axis and one damper winding on the d-axis is more than adequate to study inter-area oscillations. A further increase in the number of damper winding does not improve the damping of the inter-area modes. The damping control based on machine model with one or two damper windings will, therefore, provide more damping in practice than the designed level.

4.3.2 EFFECT OF EXCITATION CHARACTERISTICS

Three basic types of excitation control; manual, slow excitation (DC1A) and fast (ST1A) [93] are considered. Tables 4.10, 4.11 and 4.12 display the variation of damping ratios and frequency of the inter-area mode(s) for various exciter models for the study systems #1, #2 and #3 respectively.

Table 4.10: Effect of excitation characteristics on damping ratio and frequency (Study system #1).

Excitation type	Mode #1	
	ς	f (Hz)
Manual	0.032	0.62
Slow	0.018	0.61
Fast	0.009	0.69

Table 4.11: Effect of excitation characteristics on damping ratio and frequency (Study system #2).

Excitation type	Mode #1		Mode #2	
	ς	f (Hz)	ς	f (Hz)
Manual	0.022	0.82	0.035	1.14
Slow	0.020	0.80	0.036	1.13
Fast	0.000	0.82	0.027	1.14

Table 4.12: Effect of excitation characteristics on damping ratio and frequency (Study system #3).

Excitation Type	Mode #1		Mode #2		Mode #3		Mode #4	
	ς	*f* (Hz)	ς	*f* (Hz)	ς	*f* (Hz)	ς	*f* (Hz)
Manual	0.052	0.37	0.042	0.49	0.041	0.55	0.049	0.79
Slow	-0.013	0.37	0.032	0.49	0.027	0.53	0.049	0.79
Fast	0.030	0.39	0.043	0.50	0.017	0.59	0.049	0.79

In manual control mode, the demagnetising effect of the armature reaction reduces the field flux linkage. The reduction in field flux introduces a positive damping torque in the range of frequencies of oscillation. Demagnetisation also reduces the synchronising torque. With slow exciter in operation, the reduction in the field flux linkage due to armature reaction is prevented because of the AVR action. Whether the damping improves or not, is dependent on the gain and response time of the excitation and on the frequency of oscillation. Normally damping is only slightly affected. Damping is found to be very poor with a fast exciter but the frequency can be higher than that in manual and slow exciters as the synchronising torque is much improved with high exciter gain. The effect of the mismatch in excitation characteristics is also very important. In Study system #3, the machines on NETS are physical in nature, whilst machines on NYPS and other areas are equivalent. It is very difficult to get an equivalent excitation system for these machines. In the absence of any suitable excitation system they are considered as manual excitation systems. The excitation characteristics of machines in NETS are varied. It is found that when all of the NETS machines are of the slow type excitation, the damping is negative. If all of the excitations are changed to the fast type, the damping is less than in the manual mode. A straightforward relationship of damping with excitation type is very difficult to establish here. The reason is that the rest of the machines (machines #10-#16) do not have any excitation control. This is termed excitation mismatch that is detrimental to reliable system operation as it is clear from the results of Study system #3. From the results and discussion, one point is established: the damping of the inter-area mode is significantly reduced in a system equipped with fast excitation system or mismatched excitation characteristics. This was described in Chapter One whilst discussing the causes of inter-area oscillations.

4.3.3 EFFECT OF TIE LINE FLOWS

For different levels of power flow through tie lines in the study systems #1, #2 and #3, the damping of the inter-area mode(s) is computed and displayed in Table 4.13, 4.14, 4.15 respectively. The various levels of power flow are created by adjustment of the loads and generation units.

Table 4.13: Effect of tie line power flows on damping ratio and frequency (Study system #1).

Power flow (Area #1→Area #2)	Mode #1	
	ς	f (Hz)
0 MW	0.026	0.72
200 MW	0.010	0.72
400 MW	0.009	0.69
-400 MW	0.008	0.69

Table 4.14: Effect of tie line power flow on damping ratio and frequency (Study system #2).

Power Flow (Area #3 → Area #1)	Mode #1		Mode #2	
	ς	f (Hz)	ς	f (Hz)
0 MW	0.047	0.87	0.027	1.16
550 MW	0.003	0.82	0.027	1.14
750 MW	-0.009	0.73	0.027	1.13

Table 4.15: Effect of tie line power flow on damping ratio and frequency (Study system #3).

Power flow (NETS →NYPS)	Mode #1		Mode #2		Mode #3		Mode #4	
	ς	f (Hz)	ς	f (Hz)	ς	f (Hz)	ς	f (Hz)
100 MW	0.051	0.37	0.040	0.50	0.042	0.54	0.050	0.79
500 MW	0.020	0.36	0.022	0.48	0.041	0.53	0.050	0.79
700 MW	-0.001	0.35	0.009	0.47	0.042	0.52	0.050	0.79

It can be seen from the results of these tables that the damping ratio is decreased as the power flow through the tie lines is increased. A greater power flow demands a greater phase angle difference between the bus voltages at the two ends of the tie lines. As this angle is increased, the relevant machine internal angles δ's are also increased. This causes armature reaction, which in turn demagnetises the field circuit. This demagnetising effect reduces the terminal voltage. The reduction in the terminal

voltage forces the AVR to act. It has already been established that if the AVR is of high gain and fast response type, the damping of inter-area mode is reduced.

4.3.4 EFFECT OF TIE LINE STRENGTH

The damping ratios and frequency of the inter-area modes in the three study systems are computed with different number of tie circuits. The number of tie circuits are varied by opening /connecting lines between bus #5 and #6, between bus#13 and #15 and between bus #53 and #54 in Study system #1, #2 and #3 respectively. The results are displayed in Table 4.16, 4.17 and 4.18. A tie line with more tie circuits is termed a strong tie because the transfer impedance is low. The transfer impedance is higher with fewer tie circuits. From the results of Table 4.16 – 4.17, it is clear that the damping is reduced when the strength of the tie line is reduced. The high transfer impedance of the tie line demands increased angular separation between areas for scheduled power flow. As already explained, the greater angular separation increases the sensitivity of the machine terminal voltage to load angle and compels the AVR to respond, resulting in a reduction in damping. The loss of a line results in higher transfer impedance and less line charging leading to less synchronising power. The reduction in synchronising power reduces the frequency of oscillations.

Table 4.16: Effect of tie line strength
on damping ratio and frequency (Study system #1).

No of Tie circuits (Area #1 → Area #2)	Mode #1	
	ς	f (Hz)
3	0.009	0.69
2	0.003	0.59

Table 4.17: Effect of tie line strength
on damping ratio and frequency (Study system #2).

No of Tie circuits (Area #3 → Area #1)	Mode #1		Mode #2	
	ς	f (Hz)	ς	f (Hz)
3	0.003	0.82	0.027	1.14
2	-0.010	0.69	0.022	1.06

Table 4.18: Effect of tie line strength on damping ratio and frequency (Study system #3).

No of Tie circuits (NETS →NYPS)	Mode #1		Mode #2		Mode #3		Mode #4	
	ς	*f* (Hz)	ς	*f* (Hz)	ς	*f* (Hz)	ς	*f* (Hz)
2	0.061	0.36	0.039	0.49	0.037	0.54	0.050	0.79
1	0.044	0.32	0.025	0.48	0.040	0.51	0.050	0.79

4.3.5 EFFECT OF LOAD CHARACTERISTICS

The effect of the following load models on the inter-area mode were investigated:

- Constant current
- Constant impedance
- Constant power
- Dynamic (modified Walve type)

The first three types are applied to all of the loads in each of the study systems. In the dynamic load category, the loads on busses #5 and #6, loads on bus #7 and loads on bus #17 are considered dynamic respectively in study systems #1, #2 and #3. The rest of system load in this dynamic category is treated as of a constant impedance (CI) type. This means a mix of static (CI) and dynamic loads is considered whilst computing the damping ratio for the dynamic (modified Walve type) type of load. The results are summarised in Table 4.19, 4.20 and 4.21.

Table 4.19: Effect of different load characteristics on damping ratio and frequency (Study system #1).

Characteristic of load	Mode #1	
	ς	*f* (Hz)
CI	0.009	0.69
CC	0.009	0.70
CP	0.007	0.70
Dynamic	0.017	0.69

Table 4.20: Effect of different load characteristics on damping ratio and frequency (Study system #2).

Characteristic of load	Mode #1		Mode #2	
	ς	*f* (Hz)	ς	*f* (Hz)
CI	0.003	0.82	0.027	1.14
CC	0.004	0.84	0.031	1.13
CP	0.010	0.86	0.044	1.08
Dynamic	0.028	0.82	0.046	1.08

Table 4.21: Effect of different load characteristics on damping ratio and frequency (Study system #3).

Power flow (NETS →NYPS)	Mode #1		Mode #2		Mode #3		Mode #4	
	ς	f (Hz)	ς	f (Hz)	ς	f (Hz)	ς	f (Hz)
CI	0.051	0.37	0.040	0.50	0.042	0.54	0.050	0.79
CC	0.051	0.36	0.040	0.50	0.042	0.54	0.050	0.79
CP	0.054	0.36	0.040	0.52	0.043	0.55	0.050	0.79
Dynamic	0.065	0.36	0.041	0.50	0.047	0.54	0.050	0.79

It is difficult to establish a straightforward relationship between the damping ratios of the inter-area mode(s) and the nature of the non-linear static loads. It is important how these types of loads are distributed with respect to tie line location and generations. One important observation is made from the results linked to the dynamic nature of the load that it generally improves the damping of the inter-area mode(s). The behaviour of the dynamic load on the damping of the inter-area mode is in agreement with the results reported in [98]. When a significant amount of induction motor load is present in the system, the modal power exchange associated with the inter-area mode partly takes place with the load and relieves the tie circuit. This means that the damping will be larger than would be experienced with a static load if the other conditions remain the same. In a recent [3] survey on the South Australian interconnected system, the effect of the load model on the damping of the inter-area mode was reported. It was demonstrated that the damping of two inter-area modes of oscillations on the interconnected system is sensitive to the index 'n_p' of real power. Varying the time constants of a dynamic model improved the damping to one inter-area mode and worsened the other.

4.4 BEHAVIOUR OF THE SYSTEMS UNDER LARGE DISTURBANCES

The systems have been analysed thus far in the frequency domain. Eigenvalue analysis is the tool used to identify the electromechanical modes including the inter-area modes. All of these analyses are based on the linear behaviour of the system around the operating point. Unfortunately, disturbances in power systems are mostly large in nature. Most of the time, the impact of the disturbance is so great that the actions of some of dynamic components in the system become highly non-linear. These devices can even

saturate or reach their limits. Among these devices, excitation systems and machines are very common. The characterisation of the dynamic behaviour of the system based on an eigenvalue approach will be inaccurate. In order to visualise what goes on in the system during large disturbances, non-linear time domain simulations are necessary with saturation and limiting action properly modelled.

The disturbance is initiated commonly by a fault on the lines or on the busses. In Study system #1, a three-phase fault is applied in one of the tie circuits at bus #8. The fault persists for 70.0 ms; following this, the faulted circuit is disconnected by the appropriate circuit breaker. The system operates with two tie circuits connecting busses #5 and #6 and transfers the same amount of power it transferred before the fault appeared. The operation of the system after the clearance of the fault is termed "post-fault operation". The three-phase fault at bus #16 in Study system #2 for 70 ms is considered to be the disturbance. The system operates with two tie circuits in the post-fault case. A similar type of fault at bus #53 in Study system #3 for the same duration is treated to be the disturbance. The faulted line between busses #53 and #54 is disconnected by circuit breaker after 70 ms. The operation of the system with only one tie circuits between busses #53 and #54 is defined post fault-system. The pre-fault operating cases are already described earlier in this section. The transition from the pre-fault to post-fault is through the large disturbances. The nature and the location of the disturbances in each of the study systems affect the inter-area mode damping significantly. The disturbance also forces the exciter outputs to hit their limits. The dynamic behaviours of the systems are evaluated for 20 s. The machine angle 'δ's with respect to a particular machine, real power flow in the tie line, faulted bus voltage and exciter outputs are computed over the simulation period. In Study system #1, machine #3 is considered as the reference generator whilst machine #6 and machine #15 are reference generators in Study system #2 and Study system #3 respectively. These dynamic variables in Study system #1 are plotted in Fig 4.4. Fig. 4.5 and 4.6 display the dynamic responses of study systems #2 and #3 respectively.

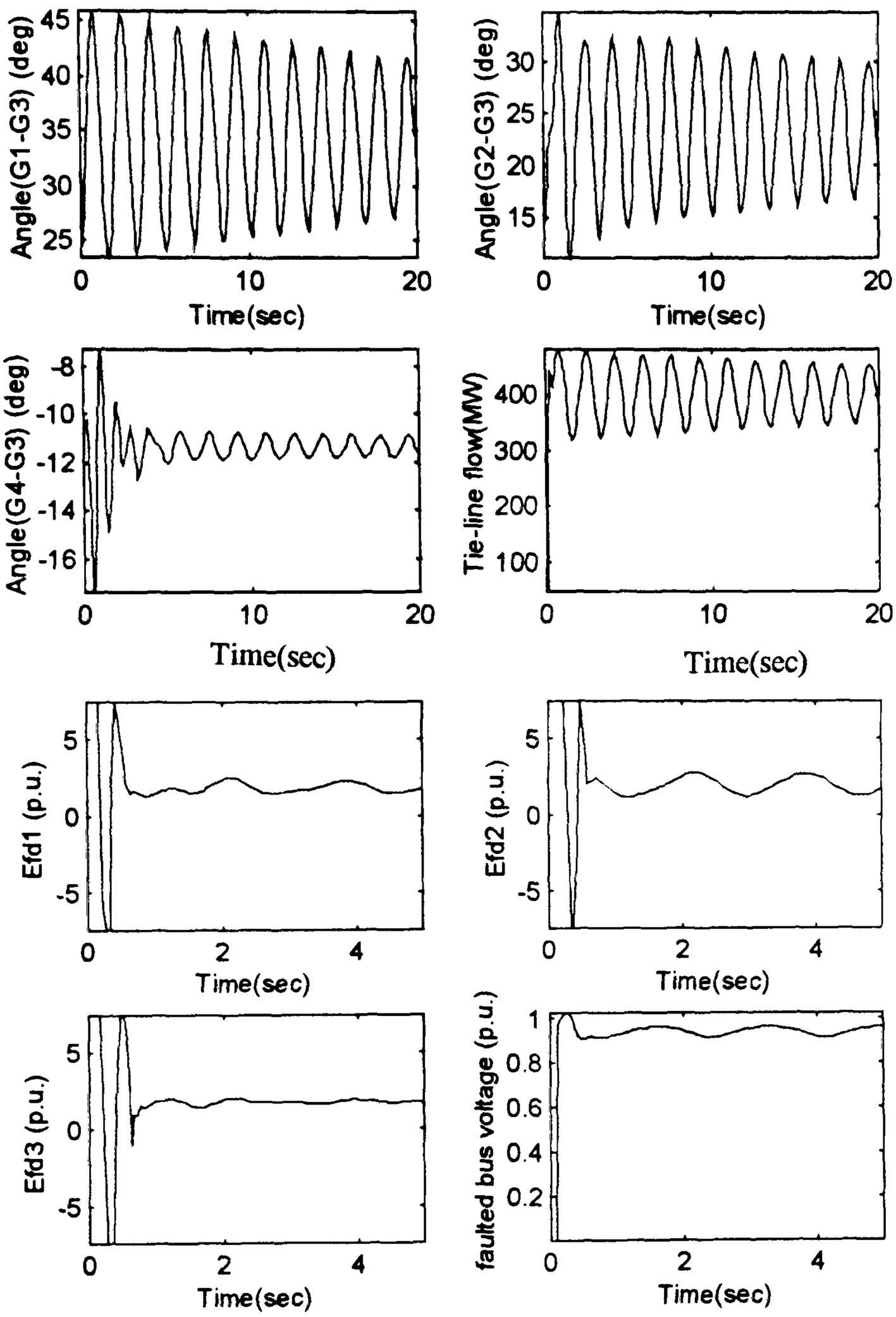

Fig. 4.4: Response of Study system #1 under large disturbances

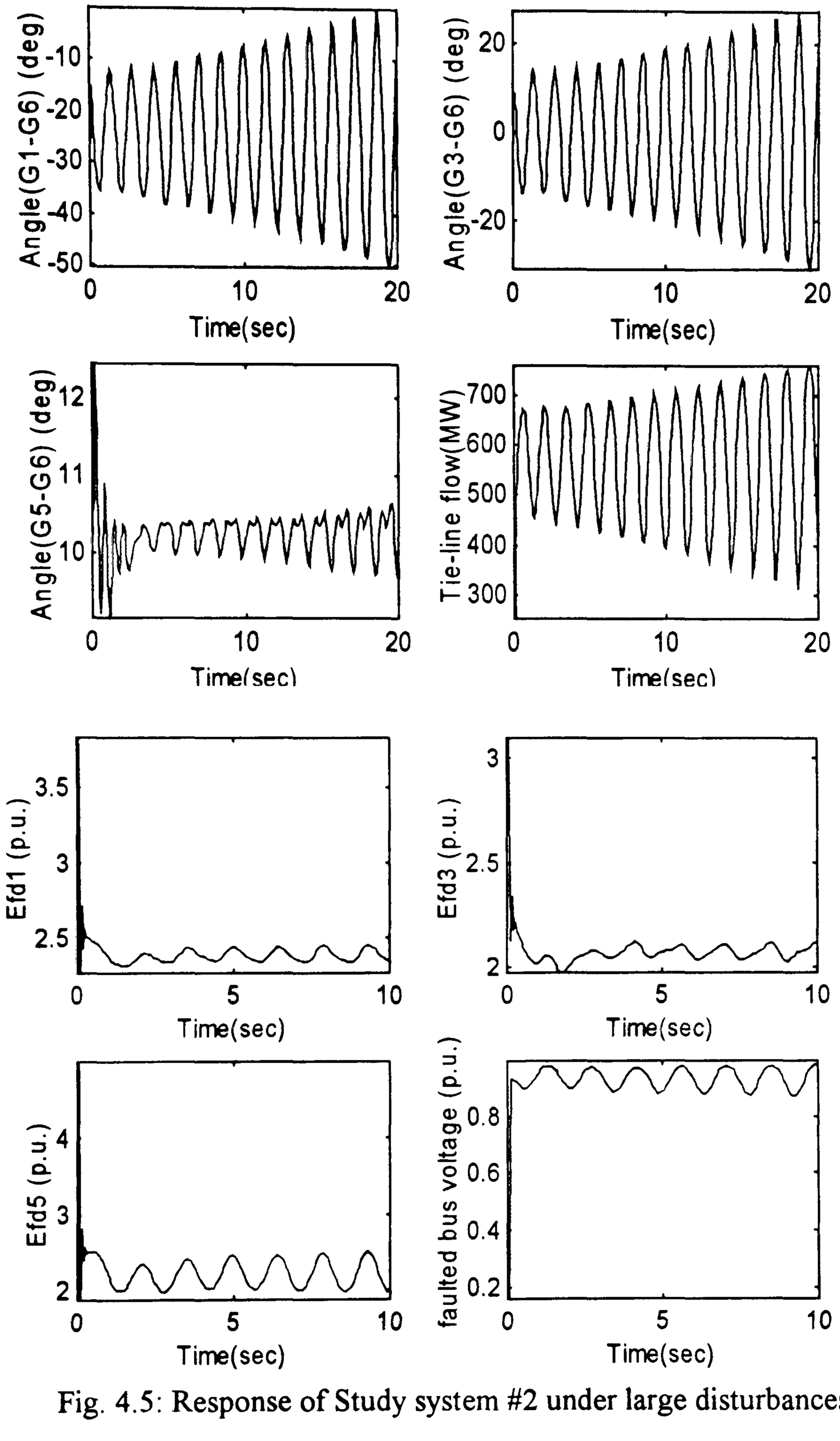

Fig. 4.5: Response of Study system #2 under large disturbances

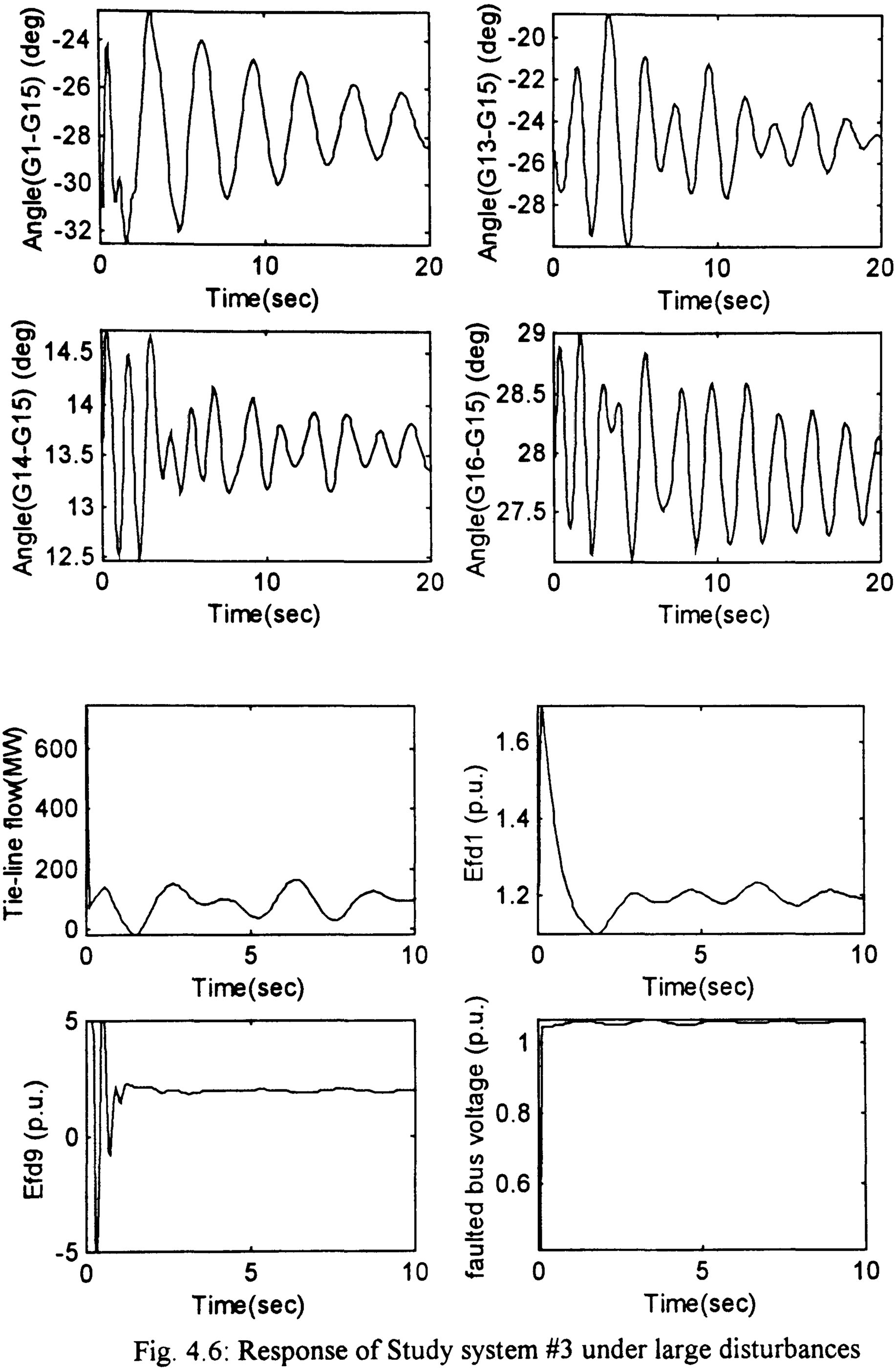

Fig. 4.6: Response of Study system #3 under large disturbances

The dynamic response of Study system #1 in Fig 4.4 shows oscillatory behaviour. The angular swings between G#1-G#3 and G#2-G#3 clearly displays a poorly damped inter-area mode. The frequency of this mode is similar to that obtained from eigenvalue analysis (Table 4.16). The swing between G#4-G#3 is initially dominated by a high-frequency inter-machine mode. This mode is in fact one of the local modes already

estimated from eigenvalue analysis. The frequency of oscillation is higher initially because of the dominance of this mode. After approximately 5 s of fault inception, this mode is damped out because of the better damping ratio. For the rest of the time, the inter-area mode governs the dynamics. In the response of the line power, it is very clear that the inter-area mode dominates the dynamics from the very beginning. The exciter outputs are also displayed in Fig. 4.4. These exciters are high gain fast acting type (ST1A) [93]. Because of the fault, generator voltage drops significantly forcing the AVR to work. The exciter hits the limits in both directions in order to restore the voltage in an attempt to improve the transient performance of the system. The exciter outputs finally settle to new values as dictated by the post-fault system. The voltage at bus #8 drops to zero during the fault as seen from the response. Following the removal of the fault, the voltage is restored to an acceptable value. It also oscillates as a result of power oscillations. The oscillation frequency is once again the inter-area mode frequency.

The argument about the same set of variables in the Study system #2 is similar to that in Study system #1 with few new features. The behaviour of the system is displayed in Fig. 4.6. Unlike Study system #1, this system is unstable in the post-fault case. This is very clear from the growing oscillations of the generator angles, tie line power flows, exciter outputs and faulted bus voltage. In this system, the exciter output limits are reached. The instability in time response is already confirmed in eigenvalue analysis by a negative damping ratio (Table 4.17). The oscillation frequency estimated from simulation is very close to the value computed by the eigenvalue approach. Also the inter-area mode governs the dynamics mostly after the fault is cleared.

In Study system #3, it is found that the nature of the swings involving all of the generators in the NETS area was similar. In view of this, the swing of G#1 is displayed. In the NYPS area, the swing of generator #13 is displayed in Fig. 4.6. The swings between G #14 - #15 and G#16 - #15 are also shown in Fig. 4.6. It is very clear from these plots that the generators in the NETS area oscillate with respect to the rest of the system and the oscillations are very largely governed by mode #1 (Table 4.18). The nature of the swings involving G #10 to G #16 conveys a different message: all of the four inter-area modes (mode #1 to mode #4 in Table 4.18) govern the dynamics. The response is very complex and an estimation of the frequency from the response by measurement is not simple. The response of the power flow in the tie line is also oscillatory. As expected, the exciter output of generator #9 hits the limit because it is of

type ST1A. The exciter outputs of the other generators in the NETS area do not hit the limit because they are sluggish (DC1A type) in action. It is very clear from these output response that the inter-area oscillations dominate the dynamic post-fault system behaviour.

From the non-linear time domain analysis of the three study systems, it is clear that these systems survive first swing stability; i.e. the systems are transiently stable but suffer from oscillatory instability (Study system #2) or poorly damped oscillatory stability (Study system #1 and Study system #3). This leads to the need for a damping control device that can effectively damp out these oscillations.

4.5 SUMMARY AND CONCLUSIONS

In this chapter, an analytical approach to identify coherent areas in an interconnected power system is discussed. The direction cosine approach of coherency identification is explained in greater detail. Three study systems are described with various degrees of complexity. The direction cosine approach is applied to these study systems to determine the coherent areas. The results are very revealing. The coherent areas are exactly similar to what they should be when determined from the physical nature of the system network. The effect of various factors such as the number of damper windings, excitation system characteristics, power flow in the tie lines, the strength of the tie lines and nature of loads are discussed in detail in these study systems. The observations are pointed out briefly here:

(i) One damper winding in the d-axis and two in the q-axis are adequate to study inter-area oscillations. As the frequency of oscillations become lower, the damper winding becomes ineffective. They do not produce a considerable amount damping torque for the inter-area mode.

(ii) The damping of the inter-area mode is very much affected by the excitation system characteristics. Fast excitation, in general, reduces damping and increases frequency. Damping is better in manual excitation mode and decreases when equipped with slow excitation (DC1A type). The mismatch of the excitation characteristics is also very important for an oscillatory instability. Normally, fast excitation in the receiving area and slow or no excitation in the sending area ensure better damping than vice-versa. Systems with manual excitation or slow excitation have less severe operational problems when compared to other systems with fast excitation.

(iii) Normally, an increase in power flow in the line results in reduced damping.

(iv) Tie line strength has a dominant role to play in inter-area mode damping and frequency. As the strength of the tie is decreased (by tripping one or more tie circuits), the damping as well as frequency drops.

(v) A straightforward relationship between the static non-linear load and the inter-area mode damping is difficult to establish. The effect of load on the damping of the oscillations is dependent on the topology of the network, power flow pattern, relative location of the loads in the system and, most importantly, the sensitivity of the active component of the loads with respect to voltage. In general, an induction motor load has a beneficial effect on the damping of inter-area mode.

(vi) The frequency domain approach is not adequate to predict the dynamic behaviour of the system when subjected to large disturbances. Non-linear simulation in addition to eigenvalue analysis is therefore required fully to analyse the oscillatory behaviour of the power system under large disturbances.

(vii) It is clear from the non-linear simulations that the post-fault dynamics of the systems are largely governed by the poorly damped inter-area modes. This suggests the installation of damping controllers that can damp out these oscillations in the pre-fault and post-fault operating cases.

The observations made from the results and analyses are in agreement with the results reported in the literature. Naturally, they do not contribute much that is new to the understanding of the inter-area oscillations but this chapter provides clear and comprehensive explanations of the factors affecting inter-area mode damping. The software developed to perform the analysis is also validated through these results. This validation is very important because it will be used in the control design and system simulations in the rest of the work.

CHAPTER FIVE

DEVELOPMENT OF DAMPING CONTROL DESIGN SPECIFICATIONS

5.1 INTRODUCTION

In this chapter, the various approaches of the utilities in formulating damping control design specification will be discussed. The factors that largely influence the design requirements will also be discussed. An analytical approach will be discussed to help suggest the desired damping ratio for different frequencies. Finally, guidelines will be set to specify acceptable damping ratios.

5.2 UTILITY APPROACHES IN SETTING DESIGN SPECIFICATIONS

Damping control in power systems is largely viewed as a supplementary functior in the voltage and power control loops. The most economic solution is the use of PSSs to modulate the voltage reference point of an AVR control loop [92]. Modulation ensures the damped behaviour of the system. The action of the damping controller is not required during the fault. It is however required to damp the post-fault oscillations. With this objective in mind, every individual utility sets its own design specification. In this section, the approaches adopted by several utilities will be discussed. This will help in the development of the general guidelines for the design specifications.

The Northeast Power Co-ordinating Council (NPCC) includes the power systems in Ontario Hydro, Quebec, New Brunswick, Nova Scotia, New York and New England. The Ontario Hydro system uses the damping ratio as a design criterion. The damping ratio (ς) of an oscillatory mode represented by a complex eigenvalue $\sigma \pm j\omega$ is given by:

$$\varsigma = \frac{-\sigma}{\sqrt{\sigma^2 + \omega^2}} \tag{5.1}$$

The damping ratio determines the rate of decay of the amplitude of the oscillation. The time constant of amplitude decay is $\frac{1}{|\sigma|}$. This means, the amplitude of oscillation decays to 37% of initial amplitude in $\frac{1}{|\sigma|}$ s. or $\frac{1}{2\pi\varsigma}$ cycles of oscillations. The minimum

acceptable level of damping below which the power system cannot be operated satisfactorily is not clearly known. In Ontario Hydro's operating experience, situations with a damping ratio of less than 0.03 are not acceptable. In addition to the value of the damping ratio, its sensitivity to variations in operating conditions is also very important. A damping ratio of 0.02 has in a few cases been adequate for the units on manual excitation control but unacceptable with the unit on automatic voltage regulation. In the design of a PSS, a minimum damping ratio of 0.1 is targeted.

The Australian small-signal-control-design practice states that [3]: "System damping is considered adequate if, at any credible operating point, after the most critical single contingency, simulations indicate that the halving time of the least damped electromechanical mode of oscillation is not more than 5 s (the 5 s halving time corresponds to a damping constant of 0.14 Nepers/s)". On the Queensland power system, there are no specific damping criteria. Damping is generally considered adequate if all of the electromechanical modes have a predicted damping ratio of at least 0.05.

In the Danish and Norwegian power systems, damping performance is considered satisfactory if system oscillations settle down within 10 to 20 s [3].

The design practice adopted by the utilities in the United Kingdom and New Zealand power systems [3] allow only 12 s for the oscillations to settle down. In the Irish system [3], small signal design is considered adequate if the damping ratio is 0.05 or greater.

5.3 RECOMMENDED GUIDELINES TO SET DESIGN SPECIFICATIONS

The system design and operating criteria described in the previous section indicate that significant differences exist amongst utilities in the way in which the damping of the power system oscillations are considered. Many utilities specify the maximum time within which the amplitude of the least-damped oscillatory mode decays to a specific level. Such specifications are time constant of amplitude decay, halving time and time for the damping down of the oscillations. Some utilities specify the minimum level of damping in terms of the damping ratio. The advantage of the time constant of amplitude decay is that it can be measured easily from the time domain simulations used for transient stability analysis. It also has the disadvantages. For example, a 5 s time constant represents an amplitude decay to 37% of its initial value in

110 cycles of oscillation for a 22 Hz SSR mode, in 5 cycles for a 1 Hz local mode and in one-half cycle for a 0.1 Hz inter-area mode of oscillation. The use of the damping ratio is more appropriate than the time constant of decay since oscillatory modes having a wide range of frequencies are involved. This is a more appropriate measure of the degree of damping. The disadvantage with the damping ratio approach is that, the same degree of damping for different frequencies results in a different time constant of decay. From the operator's viewpoint, the settling down of oscillation in 10 cycles does not make much sense as the frequency of oscillations can change with a change in operating conditions. This gives rise to different value of the absolute settling time. But a fixed time for the damping down of the oscillations is a good measure. A fixed time for the damping down of oscillations provides a very clear margin to other protection devices and the control logic of the system. For a given time for the damping down of oscillations (henceforth called settling time), it is possible to evaluate suitable damping ratios at different frequencies of oscillations. This is detailed in an attempt to further develop the design guidelines.

It is assumed that the oscillation is required to settle down in T_s s and the eigenvalue ($\sigma \pm j\omega$) of the mode is given. The undamped natural frequency of the mode is given by:

$$\omega_n = \frac{\omega}{\sqrt{1-\varsigma^2}} \tag{5.2}$$

where ς is as defined in equation (5.1) The time constant (T_c) is $\frac{1}{\varsigma\omega_n}$ s. From standard results of a linear second order system [103] the settling time $\left(T_s\right)$ is related to T_c by the following:

$$T_s = kT_c \tag{5.3}$$

The factor k is 4 to ensure that the oscillation is reached within 2% of its initial value. If k is 3, the oscillation will settle with in 5% of its initial value. Substituting for T_c in (5.3)

$$\frac{\sqrt{1-\varsigma^2}}{\varsigma\omega} = \frac{T_s}{k} \tag{5.4}$$

Rearranging (5.4) and substituting $\omega = 2\pi f$ equation (5.5) is obtained as:

$$\varsigma = \frac{k}{\sqrt{k^2 + 4\pi^2 T_s^2 f^2}} \tag{5.5}$$

f is the oscillation frequency in hertz.

The damping ratio at different frequencies for fixed T_s and k can be computed. It was shown in an earlier section that some of the utilities specify their design criteria as a time of damping down oscillation in 10 to 20 s. Three sample values of T_s are considered here. The results are displayed in Table 5.1 and 5.2.

Table 5.1 Desired damping ratio at different values of frequencies and at different desired settling time (oscillations settle with in 2% of initial value)

Frequency (Hz)	Settling Time (Ts) 10 s	Settling Time (Ts) 15 s	Settling Time (Ts) 20 s
0.1000	0.5372	0.3909	0.3035
0.2000	0.3035	0.2077	0.1573
0.3000	0.2077	0.1401	0.1056
0.4000	0.1573	0.1056	0.0794
0.5000	0.1264	0.0846	0.0636
0.6000	0.1056	0.0706	0.0530
0.7000	0.0906	0.0605	0.0454
0.8000	0.0794	0.0530	0.0398
0.9000	0.0706	0.0471	0.0354
1.0000	0.0636	0.0424	0.0318
1.1000	0.0578	0.0386	0.0289
1.2000	0.0530	0.0354	0.0265
1.3000	0.0489	0.0326	0.0245
1.4000	0.0454	0.0303	0.0227
1.5000	0.0424	0.0283	0.0212
1.6000	0.0398	0.0265	0.0199
1.7000	0.0374	0.0250	0.0187
1.8000	0.0354	0.0236	0.0177
1.9000	0.0335	0.0223	0.0168
2.0000	0.0318	0.0212	0.0159

It can be seen from Table 5.1 that the required damping ratio is 0.53 for an oscillatory mode with 0.1 Hz when settling time is specified to be 10 s. If the settling time is allowed to be 15 s, the required damping ratio is 0.39. The required damping ratio is 0.30 if the settling time is allowed to be 20 s. The required damping ratio is less for a particular settling time if the frequency of oscillations increases. A damping ratio of as low as 0.0159 is acceptable for a 2.0 Hz oscillation if the settling time is fixed at 20 s. The observation from Table 5.2 is similar to that in Table 5.1. In Table 5.2 it can be seen that the required damping ratio is lesser than its Table 5.1 counterpart for the same settling time and frequency of oscillations. This is expected, as in this case the

oscillation is said to be settled, if the magnitude of the final response is 5% of its initial response. In this case, the accuracy band is less stringent than the first case.

Table 5.2 Desired damping ratio at different values of frequencies and at different settling time (oscillations settle with in 5% of initial value)

Frequency (Hz)	Settling Time (Ts) 10 s	Settling Time (Ts) 15 s	Settling Time (Ts) 20 s
0.1000	0.4310	0.3035	0.2323
0.2000	0.2323	0.1573	0.1186
0.3000	0.1573	0.1056	0.0794
0.4000	0.1186	0.0794	0.0596
0.5000	0.0951	0.0636	0.0477
0.6000	0.0794	0.0530	0.0398
0.7000	0.0681	0.0454	0.0341
0.8000	0.0596	0.0398	0.0298
0.9000	0.0530	0.0354	0.0265
1.0000	0.0477	0.0318	0.0239
1.1000	0.0434	0.0289	0.0217
1.2000	0.0398	0.0265	0.0199
1.3000	0.0367	0.0245	0.0184
1.4000	0.0341	0.0227	0.0171
1.5000	0.0318	0.0212	0.0159
1.6000	0.0298	0.0199	0.0149
1.7000	0.0281	0.0187	0.0140
1.8000	0.0265	0.0177	0.0133
1.9000	0.0251	0.0168	0.0126
2.0000	0.0239	0.0159	0.0119

In order to have a better understanding, these results are plotted in Figs. 5.1 and 5.2.

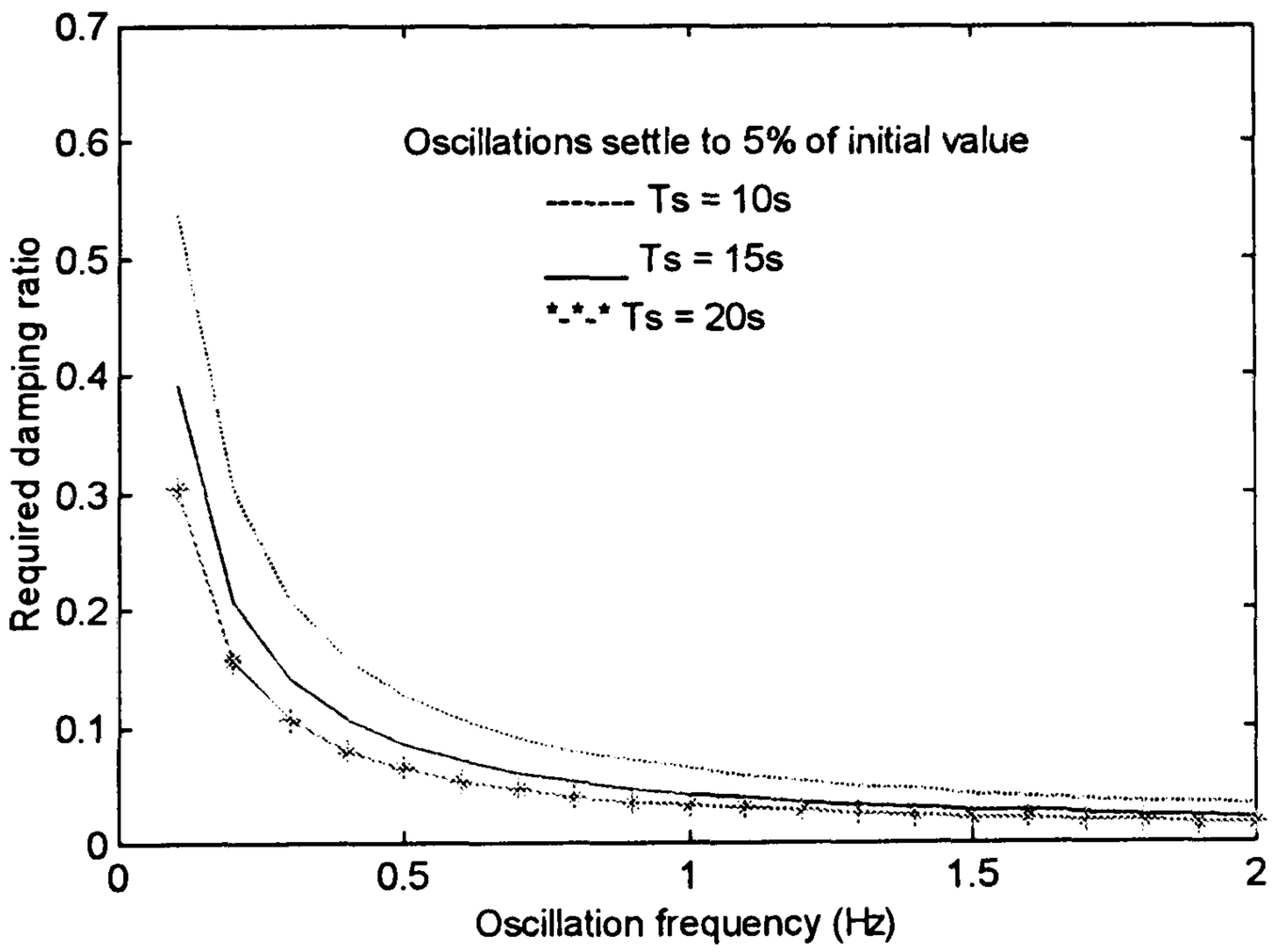

Fig. 5.1: Desired damping ratios at different frequencies and settling times

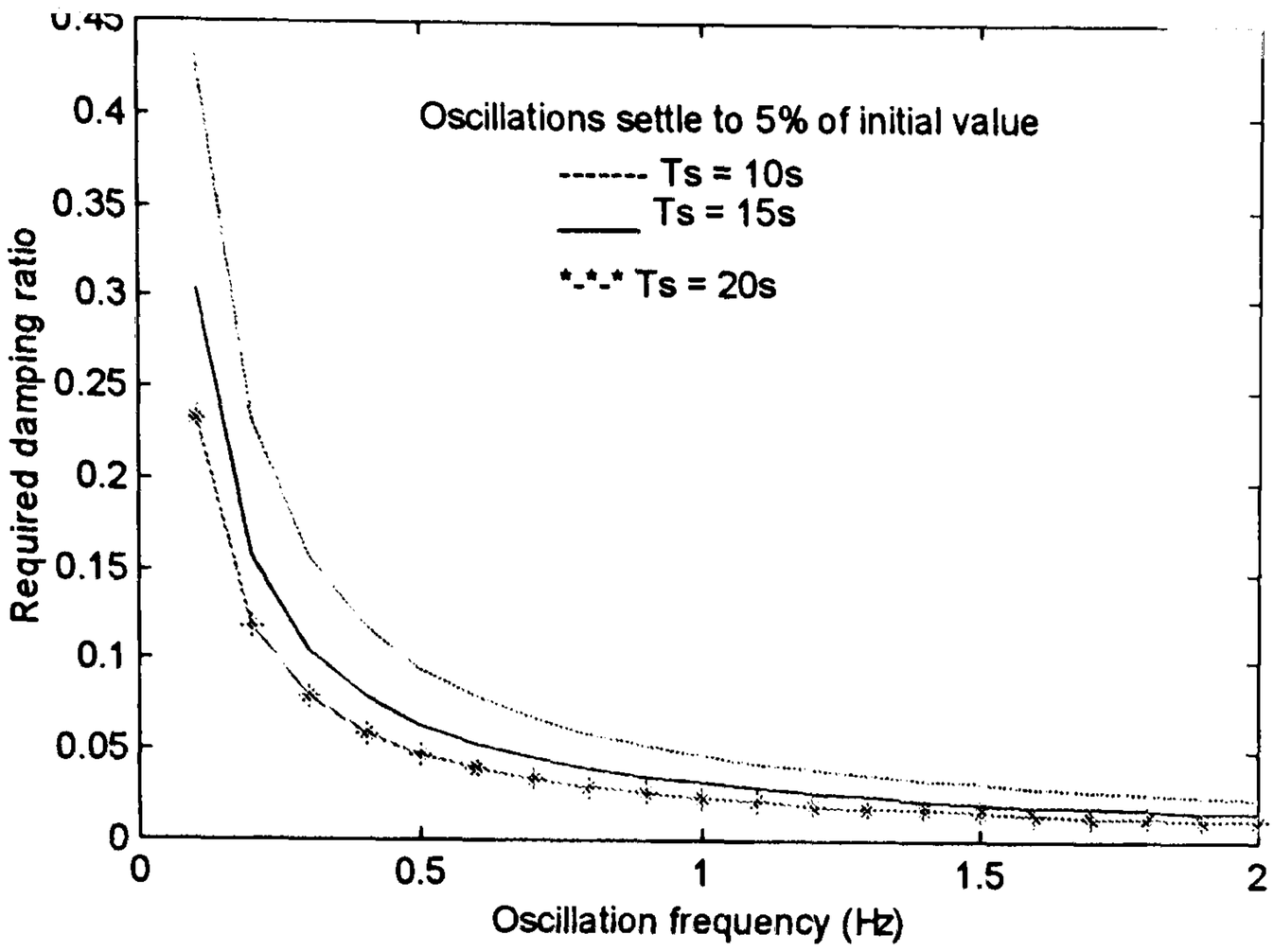

Fig. 5.2: Desired damping ratios at different frequencies and settling times

From the plots in Fig 5.1 and 5.2, it is clear that as the specified settling time and frequency of oscillation increase, the required damping ratio is decreased.

From the results and plots one point is very clear: the use of a fixed value of the damping ratio as a design specification does not have much relevance. For example, a damping ratio of 0.1 may be more than adequate for an inter-area mode having a frequency of 0.80 Hz but is very poor for an inter-area mode of 0.2 Hz. It is already known that the frequency of an inter-area mode ranges between 0.2 to 1.0 Hz. The design criteria of the utilities based on the damping ratio do not consider this aspect. It is a serious drawback in the design specifications.

As the frequency of the inter-area mode is decreased, a higher damping ratio is required to damp down the oscillation within the specified settling time. A lesser damping ratio always means a reduced cost for controller action. The relationship between the settling time and damping ratio is the relationship between the performance (settling time) and the cost of the control effort (damping ratio).

In power systems, a 10-15 s settling time and 5% settling accuracy is acceptable. In view of this, a damping ratio of 0.05 to 0.10 may be considered acceptable for a 0.6 Hz inter-area mode. One final point must be made clear here: all of these conclusions are based on the linear dynamics of the system. In a power system, a disturbance is large and the dynamics are highly non-linear. The limits will be imposed on the damping controller output that cannot be easily incorporated in to the linear model. Once the controller output hits the limits, the control action is restricted and damping of the oscillations will be delayed. In view of this, the specified damping ratio at a given frequency has to be scaled up to compensate for this delay. There is no straightforward way to do this. Using the recommended damping ratio for a 10-second

settling time can be a good starting point. This can ensure that the oscillations settle down in an actual system within 15 s.

The damping design techniques in the subsequent chapters will follow the design specifications based on these guidelines.

5.4 SUMMARY AND CONCLUSSIONS

The damping design criteria followed by various utilities are summarised. The advantages and disadvantages of these criteria are discussed to stress the need for development of more general guidelines. An analytical approach is adopted based on the simple concept of settling time in a linear second order system. The settling time and acceptable band of accuracy in settling are suggested based on the general understanding of the requirements for power system operation. A suggestion is also made to incorporate the effect of the controller limits in the design specifications.

CHAPTER SIX

IDENTIFICATION OF EFFECTIVE SMES LOCATIONS

6.1 INTRODUCTION

Identification of a suitable location for the SMES in the system plays an important role in the design of damping control. The siting of many controllable power system devices are based on issues unrelated to damping the oscillations in the system (e.g. HVDC transmission and generators), and the only question is whether they can be utilised effectively as a stability aid. In other situation, FACTS devices are installed primarily to help support the transmission system. For example, an SVC improves transmission system voltage, thereby enhancing the maximum power transfer limit; TCSC control reduces the transfer impedance of a long line, enhancing the maximum power transfer limit. In addition to these primary functions, the supplementary damping control is also added. The location is dictated by the primary function of the device. The SMES, in this research, will be located solely on the basis of its potential to damp inter-area oscillations. It has already been discussed in Chapter Two that the application of small SMES (micro SMES) for the improvement of power quality and system damping is receiving significant attention.

The costs of SMES represent an important driving force in the selection of a location that makes the optimum use of its controllability. If it is located at a different location, a larger-sized device will be needed to achieve the desired damping control objective. In this chapter, methods of controllability, observability and residue will be discussed in detail. The most effective location(s) and suitable output signal(s) will be suggested for the three study systems.

6.2 CONTROLLABILITY, OBSERVABILITY AND RESIDUE AS SITING INDICES

Chapter Three shows that the linearised dynamic behaviour of a power system can be expressed in state space form as:

$$\dot{\mathbf{x}} = \mathbf{A}\mathbf{x} + \mathbf{B}\mathbf{u} \tag{6.1}$$

$$\mathbf{y} = \mathbf{C}\mathbf{x} + \mathbf{D}\mathbf{u} \tag{6.2}$$

where, $\mathbf{A} \in \Re^{nxn}$, $\mathbf{B} \in \Re^{nxp}$, $\mathbf{C} \in \Re^{mxp}$, $\mathbf{D} \in \Re^{mxp}$

Let us consider a similarity transformation **T** ($\in \Re^{nxn}$) characterised by the diagonalising

$$\mathbf{x} = \mathbf{T}\mathbf{x}_{\mathbf{m}} \tag{6.3}$$

Equation (6.3), when applied to equation (6.1) and (6.2) produces the following:

$$\dot{\mathbf{x}}_{\mathbf{m}} = \mathbf{A}_{\mathbf{m}}\mathbf{x}_{\mathbf{m}} + \mathbf{B}_{\mathbf{m}}\mathbf{u} \tag{6.4}$$

$$\mathbf{y} = \mathbf{C}_{\mathbf{m}}\mathbf{x}_{\mathbf{m}} + \mathbf{D}\mathbf{u} \tag{6.5}$$

where, $\mathbf{A}_{\mathbf{m}} = \mathbf{T}^{-1}\mathbf{A}\mathbf{T}$, $\mathbf{B}_{\mathbf{m}} = \mathbf{T}^{-1}\mathbf{B}$ and $\mathbf{C}_{\mathbf{m}} = \mathbf{C}\mathbf{T}$; $\mathbf{x}_{\mathbf{m}}, \mathbf{A}_{\mathbf{m}}, \mathbf{B}_{\mathbf{m}}, \mathbf{C}_{\mathbf{m}}$ are modal state vector, modal state matrix, modal input matrix and modal output matrix respectively. The transfer characteristic in terms of the new variable becomes

$$\mathbf{G}_{\mathbf{p}}(\mathbf{s}) = \mathbf{C}\mathbf{T}(\mathbf{s}\mathbf{I} - \mathbf{A}_{\mathbf{m}})^{-1}\mathbf{T}^{-1}\mathbf{B} + \mathbf{D} \tag{6.6}$$

Equation (6.6) can be written in partial fraction expansion as follows:

$$\mathbf{G}_{\mathbf{p}}(\mathbf{s}) = \mathbf{C}\mathbf{T}(s\mathbf{I} - \mathbf{A}_{\mathbf{m}})^{-1}\mathbf{T}^{-1}\mathbf{B} = \sum_{i=1}^{i=n} \frac{\mathbf{R}_{\mathbf{i}}}{s - \lambda_i} + \mathbf{D} \tag{6.7}$$

$$\mathbf{V} = \left[\mathbf{v}_1, \mathbf{v}_2, \ldots \mathbf{v}_n\right] = \mathbf{T}^{-1}\mathbf{B}; \tag{6.8}$$

$$\mathbf{W} = \left[\mathbf{w}_1, \mathbf{w}_2, \ldots, \mathbf{w}_n\right] = \mathbf{C}\mathbf{T} \tag{6.9}$$

The matrix **V** and **W** are modal controllability and modal observability matrices respectively. $\mathbf{R}_i$ is the residue matrix for the i^{th} mode and can be expressed as:

$$\mathbf{R}_{\mathbf{i}} = \mathbf{w}_{\mathbf{i}}\mathbf{v}_{\mathbf{i}}^{\mathbf{t}} \tag{6.10}$$

In equation (6.10), $\mathbf{v}_i$ is the i^{th} modal controllability vector and $\mathbf{w}_i$ is the i^{th} modal observability vector. It is necessary to examine the effect of j^{th} input ($\mathbf{b}_j$) and k^{th} output ($\mathbf{c}_k$) on the i^{th} mode. The modal controllability is an implicit function of the state matrix (**A**) and the input vector ($\mathbf{b}_j$). Modal observability is an implicit function of the state matrix (**A**) and the output vector ($\mathbf{c}_k$). They are independent and so can be computed separately.

The higher the magnitude of the modal controllability, the more effective is the input to influence that mode. This provides an indication on the most effective location for the SMES. As '**A**' matrix changes with the location of the SMES, the modal

controllability changes at various bus locations. This means that the bus with the largest magnitude of modal controllability is apparently the most effective bus.

The modal controllability alone does not guarantee an effective location. The strength of the feedback signal is also important. The modal observability addresses this issue. The modal observability indicates the degree to which this mode can be observed in a particular signal. The higher the magnitude of the modal observability, the better is the feedback signal. The choice of the feedback signal can be many, local or global, it can be bus voltage magnitude, line power, line current magnitude etc.

Local signals are those signals that are local to the proposed SMES location. Local signals are more reliable and easily available. They do not suffer from communication delays but may not have the largest observability when compared with the global signal. The global signal can be a remote signal that is not very reliable and corrupted with noise during transmission. In this research, the choice is restricted to local signals only.

A comparison of modal observabilities should be done with care. The modal observability of bus voltage must not be compared with the modal observability of the line power. Although bus voltage and line power are expressed in p.u., a 10% change in bus voltage does not mean a 10% change in line power. In view of this argument, the signals compared will be of the same type; i.e. power with power, voltage with voltage, system frequency with generator speed etc. The feedback signal should have a very low sensitivity to the SMES output. The signal should be more sensitive to the swing mode than to itself. Once the issues related to the choice of signal are resolved, the residue can be computed. The residue (R_i) for single-input-single-output case is a scalar quantity.

It was found that, in all of the three test systems, the line real power is the most sensitive signal to the inter-area mode. The line current magnitude does have a high observability but does not have a self-limiting action during the fault. During the fault, the line current magnitude in the vicinity of the fault is very high. This signal, if used for damping control with SMES real power modulation, always forces the controller to act and hit the limits. This is not desirable. The whole objective of damping control is that controller action, during the fault, is not required. During the fault, the system passes through a transient stage and it is a transient stability problem. The transient stability problem are solved by the use of a high-gain and fast-acting AVR. After the fault is cleared, the low frequency oscillations start to grow. It is during this time that the feed

back signal should be strong. The line active power is very small during a fault and hence the damping controller does not affect the transient stability problem. This is the reason that the choice of signal is restricted to the line active power for the SMES. This choice may not be applicable for other FACTS devices with different inputs (e.g. shunt susceptance for an SVC).

The residue approach was first suggested in [104] to determine the most effective location. The residue, as already pointed out, is the product of the modal controllability and observability and can be used to identify the most effective location. If in a particular location and for a particular feedback signal, the modal controllability and observability are both high, the residue will be large. A larger residue always means that the mode is highly controllable and observable at that location for that particular feedback signal. The large residue also means that a reduced control effort will be required to influence that particular mode. This results in a smaller gain for the controller. The residue is a complex number so it has a phase in addition to magnitude. The magnitude decides the controller gain requirement and the phase decides the required phase compensation.

The identification is carried using the following procedure. The SMES is located first at bus #1 and the line power in all the adjacent lines are considered one at a time. The modal controllability is fixed for a particular bus and does not change. The modal observability will change depending on the particular line considered. The residue will change accordingly. If there are '*l*' lines emanating from this bus, there will be '*l*' residues. The highest of these '*l*' residues is selected. This corresponds to the active power of a particular line as the feedback signal. The SMES is moved to bus #2 and line powers adjacent to this bus are considered. The best signal is chosen to be the one that provides the highest residue. The process is repeated for all of the bus locations. In an N-bus system, 'N' such residues are obtained with 'N' feedback signals. The highest of these residues is selected. This will correspond to a particular bus location and a feedback signal. This bus location is the best location and the feedback signal is the most effective signal. This completes the task of identifying the best location and the most effective signal for the system with one operating condition. For other operating conditions, the process can be repeated. Different operating conditions may provide different locations and feedback signals. Engineering judgement must be used based on the greatest likelihood for the system operating condition.

6.3 THE BEST LOCATION(S) AND MOST EFFECTIVE STABILIZING SIGNAL(S) FOR THE STUDY SYSTEMS

The residue approach has been applied to identify the most effective location of the SMES in the study systems. The active power in the adjacent line is chosen as the feedback signal. Each bus location is assigned a rank depending on the relative magnitude of the residue. The bus with the largest magnitude of the residue is the most effective location and hence ranks one. The rank-two bus has the second largest magnitude of the residue and so on. Screening is performed here to eliminate the least effective busses with regards to their stabilising potential to the inter-area mode. The busses with residues less than 70% of the largest residue have been discarded. With this cut-off criterion, the less effective busses are eliminated and the number of potential locations for the SMES is restricted to a select few. The screening process is extended to incorporate multiple inter-area modes. The residue computations are considered based on one mode at a time to select the potential locations. Table 6.1 displays the residue magnitude and phase at the selected locations, for the inter-area mode, in Study system #1. The residues are computed for both pre-fault and the post-fault conditions as described earlier. Results in Table 6.2 and Table 6.3 correspond to Study system #2 and Study system #3 respectively. The feedback signal used is also indicated as power in the adjacent line of the SMES bus location. When power is used in the line between the bus 'k' and bus 'm', it is denoted by $P_{k,m}$.

Table 6.1: Residues at different potential bus locations (Study system #1).

SMES Bus Number	Mode No.	Residue (pre-fault)		Residue (post-fault)		Signal used
		Magnitude	Phase (deg.)	Magnitude	Phase (deg.)	
3	1	0.6060	-83.1364	0.5694	-83.9759	$P_{3,11}$
6	1	0.6190	86.9901	0.7027	86.7305	$P_{6,10}$
10	**1**	**0.8131**	**-90.3647**	**0.8736**	**-90.2772**	$P_{10,6}$

From Table 6.1, it is clear that bus #10 is the one with the largest residue when $P_{10,6}$ is used as the feedback signal. It is highlighted in Table 6.1. It is, therefore, recommended that the SMES be sited at bus #10. From Table 6.2, it can be seen that, in Study system #2, mode #1 has the largest residue at bus #15 and mode #2 has the largest residue at bus #8. It can also be seen that bus #11 and bus #12 have good residue magnitudes for both of the modes. The phase difference between them is also much less. So, any control

action to improve the damping of one mode is expected to improve the damping of other mode. It can be seen from Table 6.3 that mode #1 has the largest residue at bus #54 both in the pre-fault and post-fault operating cases. Mode #2 has fairly large residues at busses #14, #16, #18, #41. Bus #14 is the best location to effectively damp this mode. A closer look at the relative magnitudes of the residues for mode #3 reveals that busses #13, #17, #16, #18, #41 are potentially the most effective locations. Bus #13 has the highest residue for this mode. Mode #4 can be damped out very effectively at bus #15 although bus #42 is potentially another effective location. Whilst trying to damp one mode at a particular location, one has to ensure that the damping of other modes are not worsened if not at least improved. This requires a systematic procedure to be applied to damp out all of these modes by the least number of SMES devices. This will be elaborated in the next few paragraphs. Nothing will be considered as absolute in concrete regarding the final locations of SMES in the study systems # 2 and #3 in this chapter. The selection of the location process will be integrated into the controller design. In the sequential controller design, the potential locations might change as one mode is damped at a time.

Table 6.2: Residues at different potential bus locations (Study system #2).

SMES Bus Number	Mode No.	Residue (pre-fault)		Residue (post-fault)		Signal used
		Magnitude	Phase (deg.)	Magnitude	Phase (deg.)	
1	1	0.0608	-99.7748	0.1407	-98.7544	$P_{1,7}$
	2	0.9204	-96.8135	0.8859	-96.8175	
2	1	0.0608	-99.7748	0.1407	-98.7544	$P_{2,7}$
	2	0.9204	-96.8135	0.8859	-96.8175	
7	1	0.0645	79.7091	0.1604	80.1650	$P_{7,8}$
	2	0.9044	81.6491	0.8774	81.6572	
8	1	0.0892	-100.0754	0.2134	-99.2947	$\boldsymbol{P_{8,7}}$
	2	**1.2780**	**-97.6149**	**1.2364**	**-97.6032**	
11	1	0.5366	82.5407	0.5838	82.4211	$P_{11,12}$
	2	0.3089	84.8441	0.3806	86.1156	
12	1	0.6512	-97.2215	0.6811	-97.3705	$P_{12,11}$
	2	0.4261	-94.2469	0.5034	-94.1269	
14	1	0.8805	83.6891	0.6310	84.3365	$P_{14,15}$
	2	0.0212	97.5364	0.0021	157.4906	
15	**1**	**1.0332**	**-96.9301**	**0.7227**	**-96.2470**	$\boldsymbol{P_{15,14}}$
	2	0.0291	-81.9908	0.0030	-23.5175	

It is general practice in power systems to damp out one mode by one device. In the case of multiple inter-area modes, more than one device is employed. In this research, the guidelines for the selection of sites for multiple inter-area modes are discussed as follows.

In the open-loop system, the inter-area modes are identified. The modes are organised and numbered in ascending order of the value of natural frequency of oscillation. This ranks the lowest frequency inter-area mode as the first mode and the highest frequency inter-area mode as the last mode. For each inter-area mode, a range for the acceptable damping ratios is selected, based on the rule developed in the previous chapter. This is done to ensure that the modal oscillations settle down in 10 to 15 ss following a large disturbance with controller limits in action.

The allowable range of variation of modal frequencies is restricted to 10 to 20% around the open-loop value. If this restriction is not imposed, the controller may adversely affect the synchronising power of the system by changing the modal frequencies in the closed-loop. Each SMES is intended to improve the damping of one particular mode. This mode is termed as the primary mode and the rest of the inter-area modes are defined the secondary modes. It is expected that a damping controller, besides improving the damping to the primary mode, should also contribute to the damping of the secondary modes although this may not be possible for all of the potential locations. The damping controller can be designed to achieve a desirable damping ratio for the primary mode with positive damping influences on the secondary modes. The procedure will be repeated to exhaust all of the potential locations. After this, the most effective location will be selected based on an examination of the performance of the controllers in these locations. The influence of each of the controllers on the damping ratios and the frequencies of the secondary inter-area modes will be examined. The most favourable influence is considered to be that with the closest proximity of the damping ratios and frequencies of the secondary modes to their respective specified ranges. The controller modes, if they exist, must be well damped. Normally, the increase of the gain of the controller increases the damping of the inter-area modes. However, as the gain increases, the damping of the controller modes may worsen. This will manifest itself as an oscillatory response in the controller output. This is normally undesirable. The controller at a particular location with the most favourable influence on the secondary modes is the best location to damp out a primary inter-area mode with maximum beneficial effects on other inter-area modes. Once the best location and the controller are decided, they can be treated as part of the system. An eigenvalue analysis will be carried out in the closed-loop to identify other inter-area modes whose damping ratios are to be improved. The insufficiently damped modes will be reorganised and numbered. The primary mode will

again be defined and secondary modes are grouped. The entire process is repeated to get the best location to damp out the newly defined primary mode.

Table 6.3: Residues at different potential bus locations (Study system #3).

SMES Bus Number	Mode No.	Residue (pre-fault)		Residue (post-fault)		Signal used
		Magnitude	Phase (deg.)	Magnitude	Phase (deg.)	
13	1	0.1081	-92.4313	0.0354	-116.4848	$P_{13,17}$
	2	0.1281	-71.0419	0.5675	-74.8052	
	3	**0.8004**	**-99.4730**	**0.4561**	**-117.6615**	
	4	0.0100	-96.9689	0.0117	-96.0326	
14	1	0.0666	-84.0616	0.0499	-87.1640	$P_{14,41}$
	2	**0.6645**	**-96.0778**	**0.4457**	**-110.2002**	
	3	0.0722	-61.8900	0.3437	-68.7736	
	4	0.5979	-93.3488	0.5950	-93.3359	
15	1	0.1141	-83.7749	0.0789	-86.3764	$P_{15,42}$
	2	0.0850	-90.2018	0.1228	-92.3653	
	3	0.0032	169.6810	0.0122	43.3456	
	4	**1.4525**	**-93.4714**	**1.4543**	**-93.4712**	
16	1	0.1056	-82.8135	0.0851	-83.1107	$P_{16,18}$
	2	0.5103	-99.6732	0.1654	-139.7467	
	3	0.2049	-77.3532	0.6158	-81.9267	
	4	0.1551	-94.0559	0.1548	-94.0154	
17	1	0.0912	87.7545	0.0307	63.4331	$P_{17,13}$
	2	0.1026	111.1753	0.4629	106.7591	
	3	0.6496	81.3143	0.3767	63.2363	
	4	0.0075	82.8938	0.0088	82.8358	
18	1	0.0938	98.0870	0.0761	98.0166	$P_{18,16}$
	2	0.4326	80.9698	0.1415	41.3209	
	3	0.1707	102.7967	0.5173	98.5694	
	4	0.1075	86.9913	0.1074	86.0343	
41	1	0.0655	96.0776	0.0491	93.0188	$P_{41,14}$
	2	0.6449	84.0170	0.4327	69.9393	
	3	0.0698	118.2273	0.3330	111.2965	
	4	0.5551	86.6842	0.5523	86.6972	
42	1	0.1123	96.2732	0.0779	93.7080	$P_{42,15}$
	2	0.0828	89.8429	0.1196	87.7182	
	3	0.0031	-10.4866	0.0119	-136.6618	
	4	1.3541	86.5513	1.3558	86.5513	
54	**1**	**0.3718**	**-97.1273**	**0.4027**	**-92.7137**	$P_{54,53}$
	2	0.0356	-43.2285	0.0615	-56.0063	
	3	0.1663	-79.6423	0.0470	-104.2471	
	4	0.0001	96.3264	0.0000	100.5327	

In sequential design, the maximum number of SMES required will be the number of poorly damped inter-area modes. Hence the number of times this exercise has to be repeated is the number of poorly damped inter-area modes. At this stage, without the controller design exercise, nothing can be said as to the minimum number of SMES

to damp system with multiple inter-area modes. It is possible that 'm' number of inter-area modes may be damped by less than 'm' number of SMES. Damping to one particular inter-area mode can be improved through the collective maximum favourable influences on the secondary modes by the other controllers designed to damp the other modes.

In order to demonstrate the effectiveness of these potential SMES locations to control the inter-area mode damping, an open-loop frequency response is shown in Fig. 6.1 for Study system #1. The input-output characteristic considers the SMES location at bus #10. Fig 6.2 and 6.3 show the frequency response of the system for two potential SMES locations in Study system #2. Fig.6.4 to 6.7 display the same characteristics for four potential SMES locations in Study system #3. It is very interesting to see in Fig. 6.1 that the inter-area mode is very dominant in the frequency response. The input-output pair is very selective for the inter-area mode. The presence of local modes is not seen in this input-output characteristic. This is necessary in order to avoid interactions amongst the modes. The selection of the location and choice of feedback signal, therefore, ensure minimum interaction.

In Fig 6.2, it can be seen that only mode #1 is very dominant. If a SMES is located at this location, the associated damping controller should not interfere with any other modes. The damping of mode #2 can not be controlled from this location. If a SMES is located at bus #8, the damping of mode #2 can be influenced mostly. Mode #1 is also seen to be present (Fig. 6.3) in the selected input-output combination at this location although its dominance is relatively small.

From the responses in Fig.6.4 to Fig. 6.6, it can be seen that any one of the potential locations (busses #54, #14, #13 and #15) is effective at least for one particular mode. Mode #1 is very dominant at the input-output characteristic of the system when located at bus #54. The sensitivities of the output signal for the other three modes (mode #2 to #4) are not as good as for mode #1. The location at bus #14 and the associated feedback signal are most sensitive to mode #2. The SMES locations at bus #13 and bus #15 are very good in order to influence mode #3 and mode #4 respectively. This means, in Study system #3, it is possible to influence the damping of more than one mode from a single bus location. It is always economic to have fewer SMES to damp multiple inter-area modes but interaction amongst the modes must be avoided. The control of damping of multiple modes by a single SMES and a minimum interactions amongst modes are

conflicting requirements. The non-linear interaction following a fault is a very serious issue in damping control. This is given preference over the cost of damping control in utility control practice.

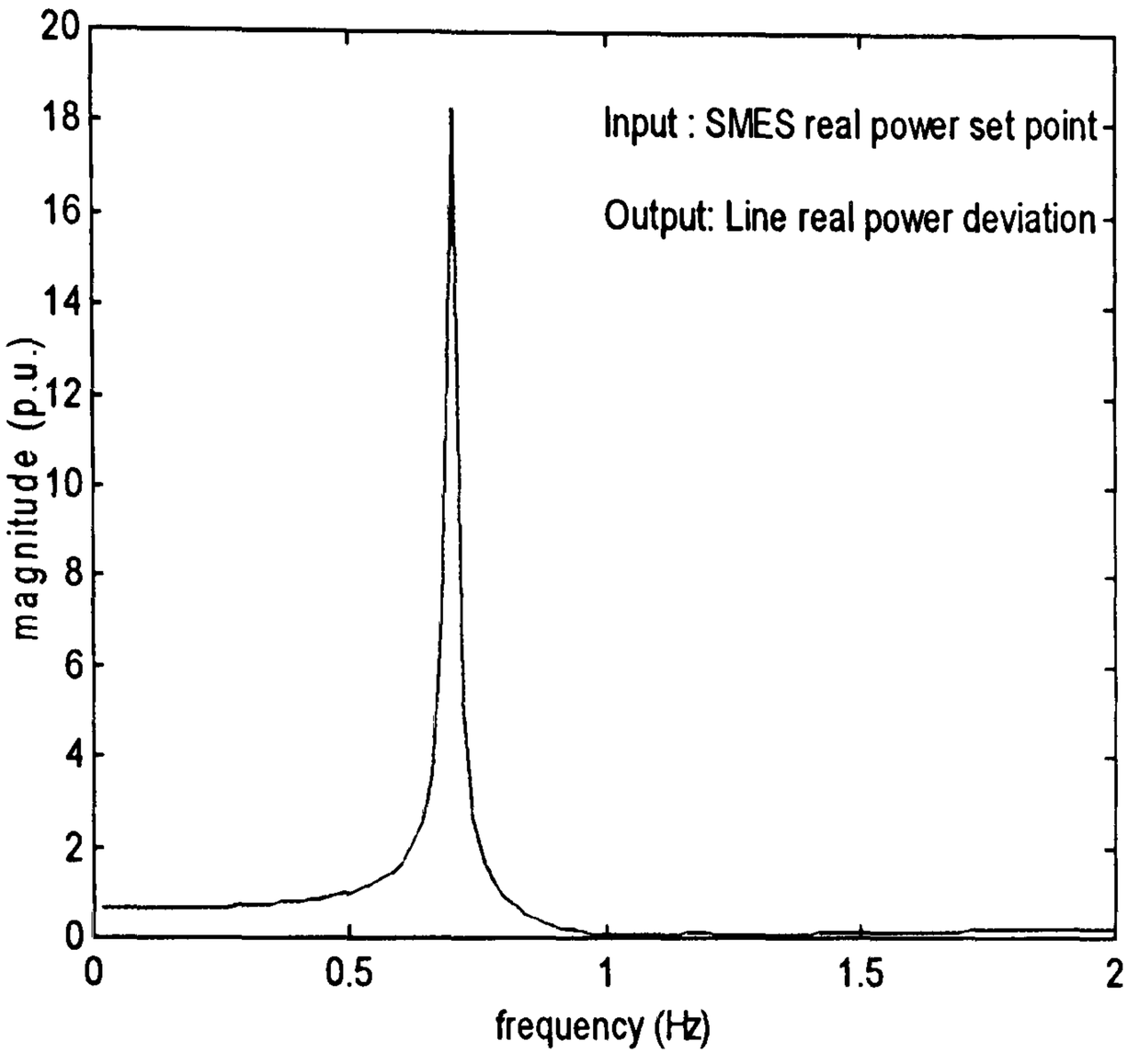

Fig. 6.1 Open-loop frequency response of the SMES at bus #10 (Study system #1)

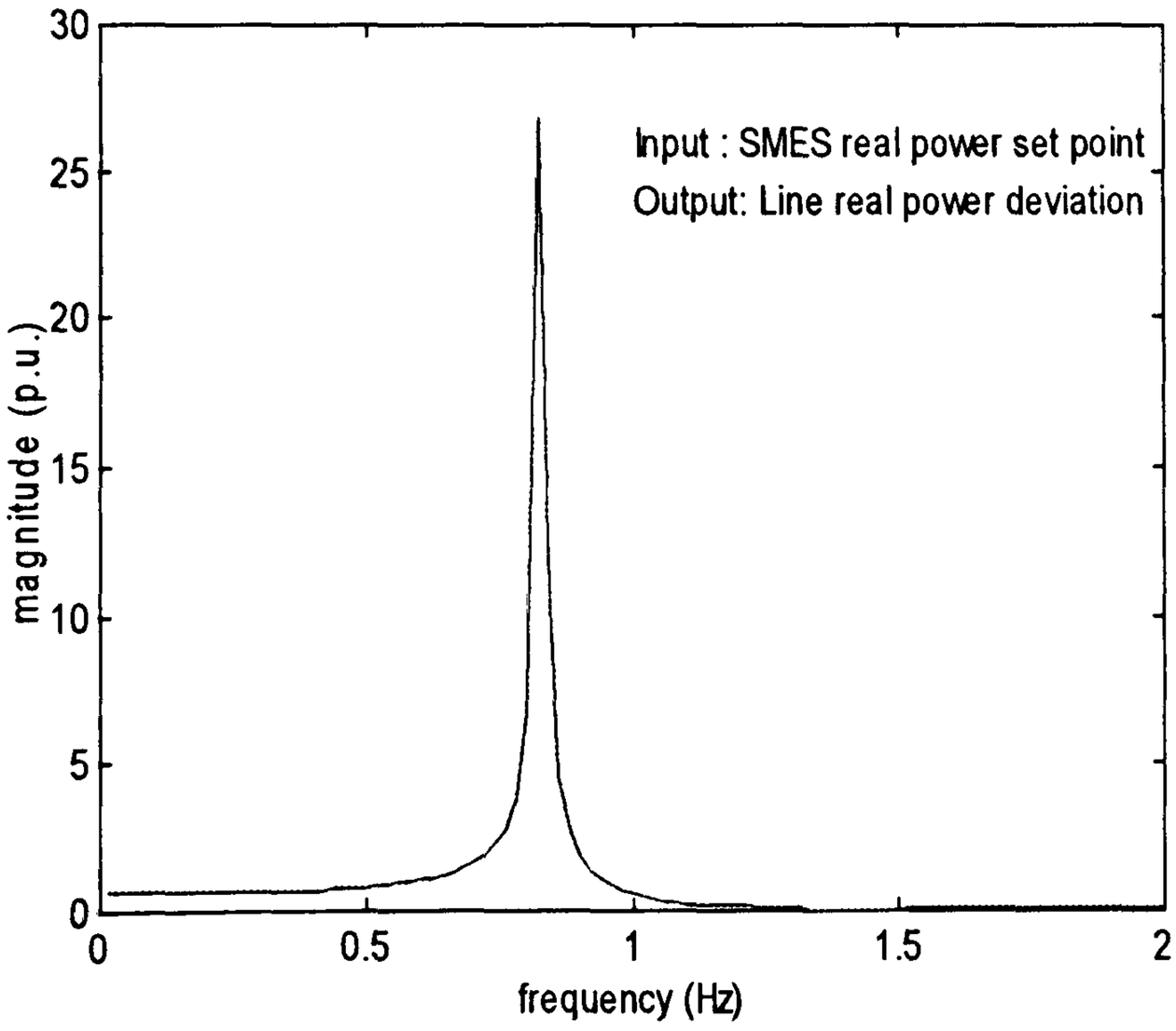

Fig. 6.2 Open-loop frequency response of the SMES at bus #15 (Study system #2)

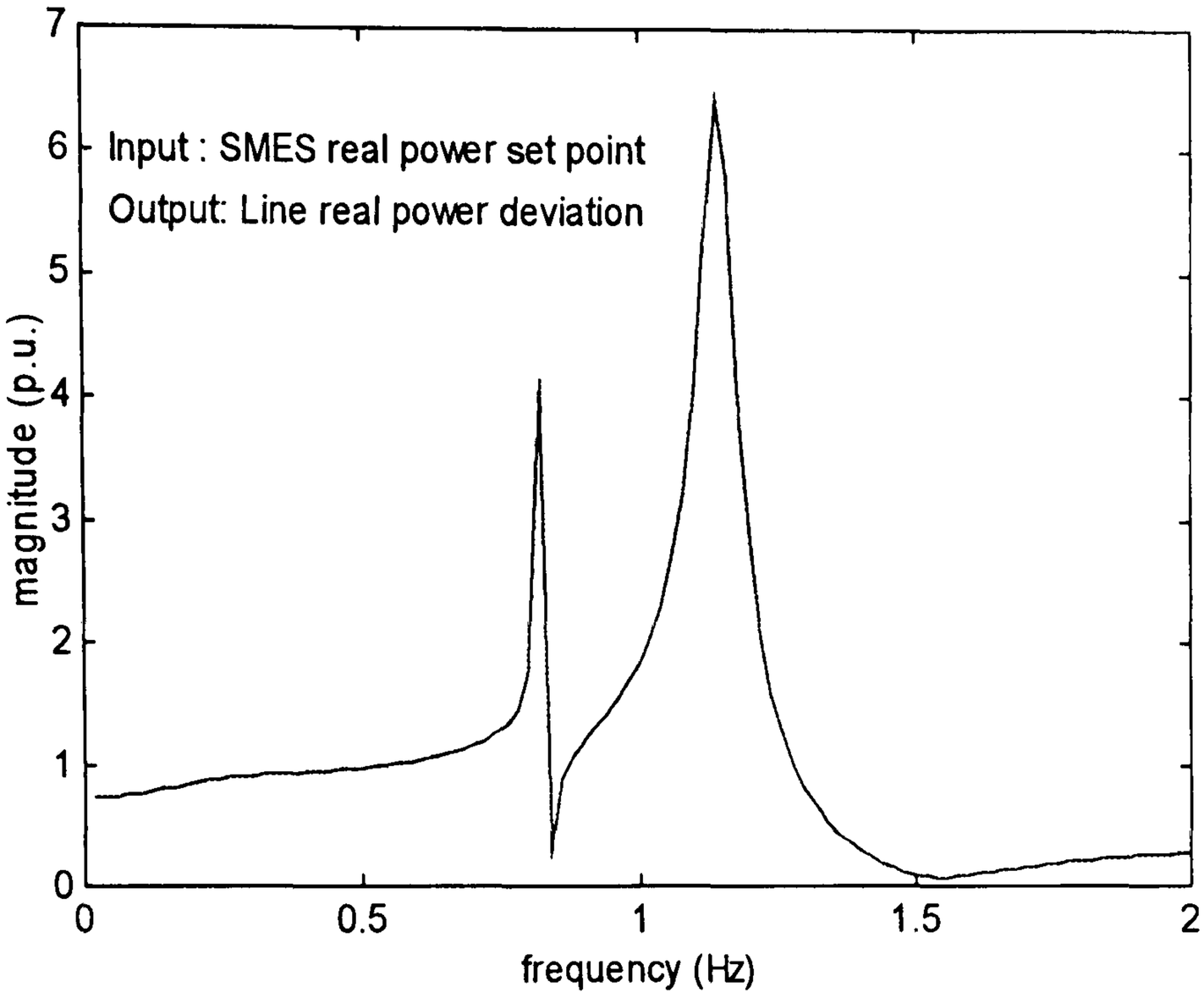

Fig. 6.3 Open-loop frequency response of the SMES at bus #08 (Study system #2)

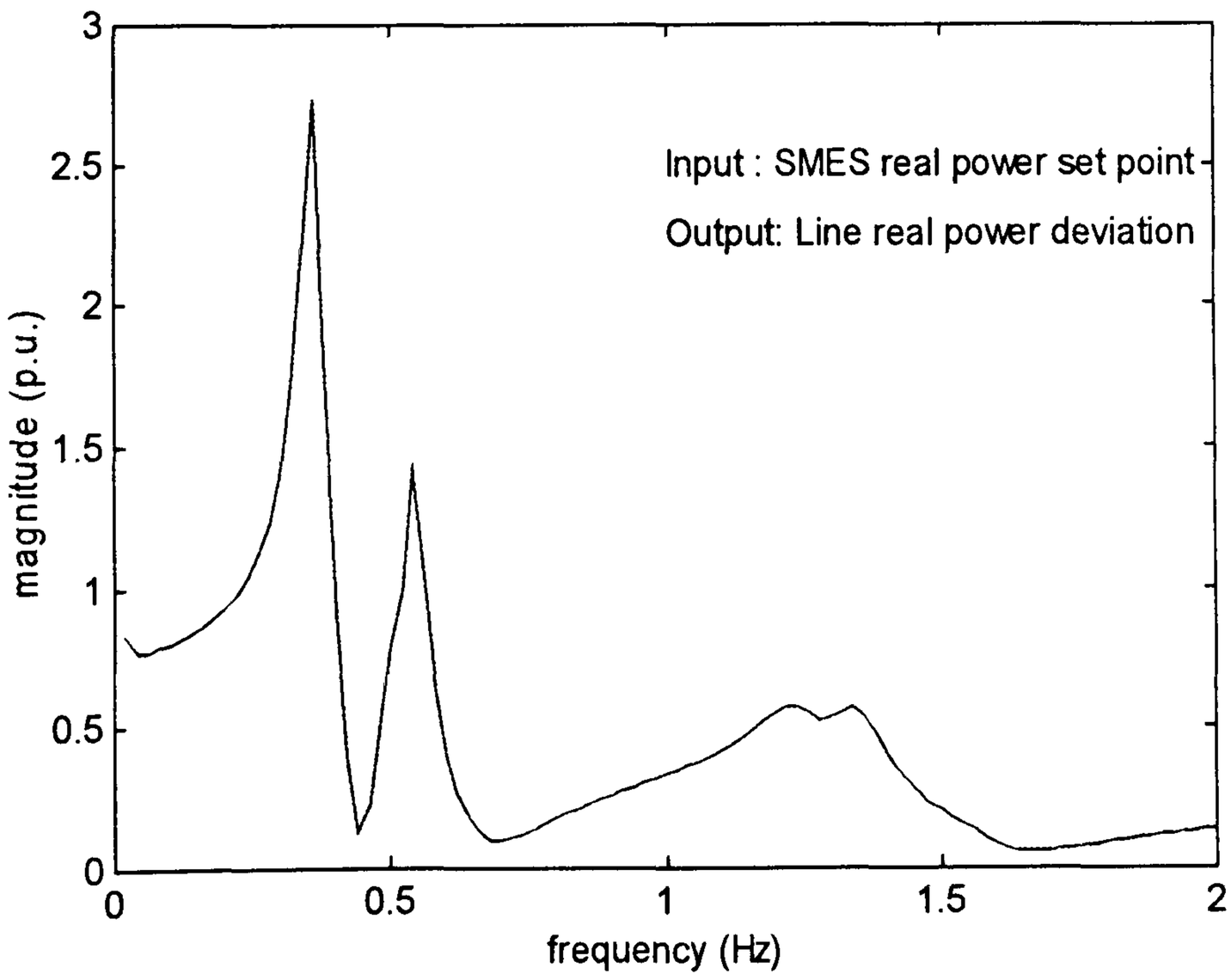

Fig. 6.4 Open-loop frequency response of the SMES at bus #54 (Study system #3)

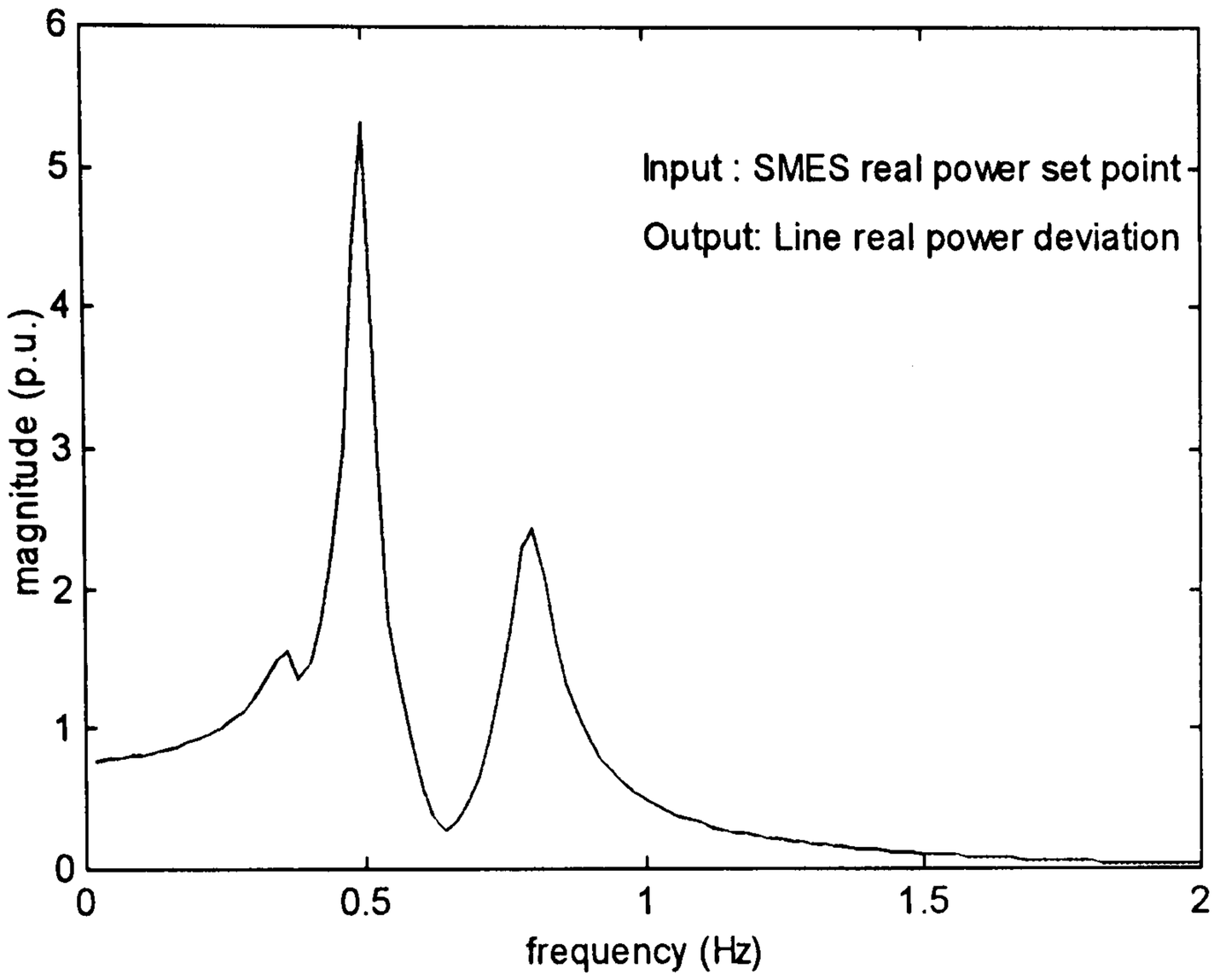

Fig. 6.5 Open-loop frequency response of the SMES at bus #14 (Study system #3)

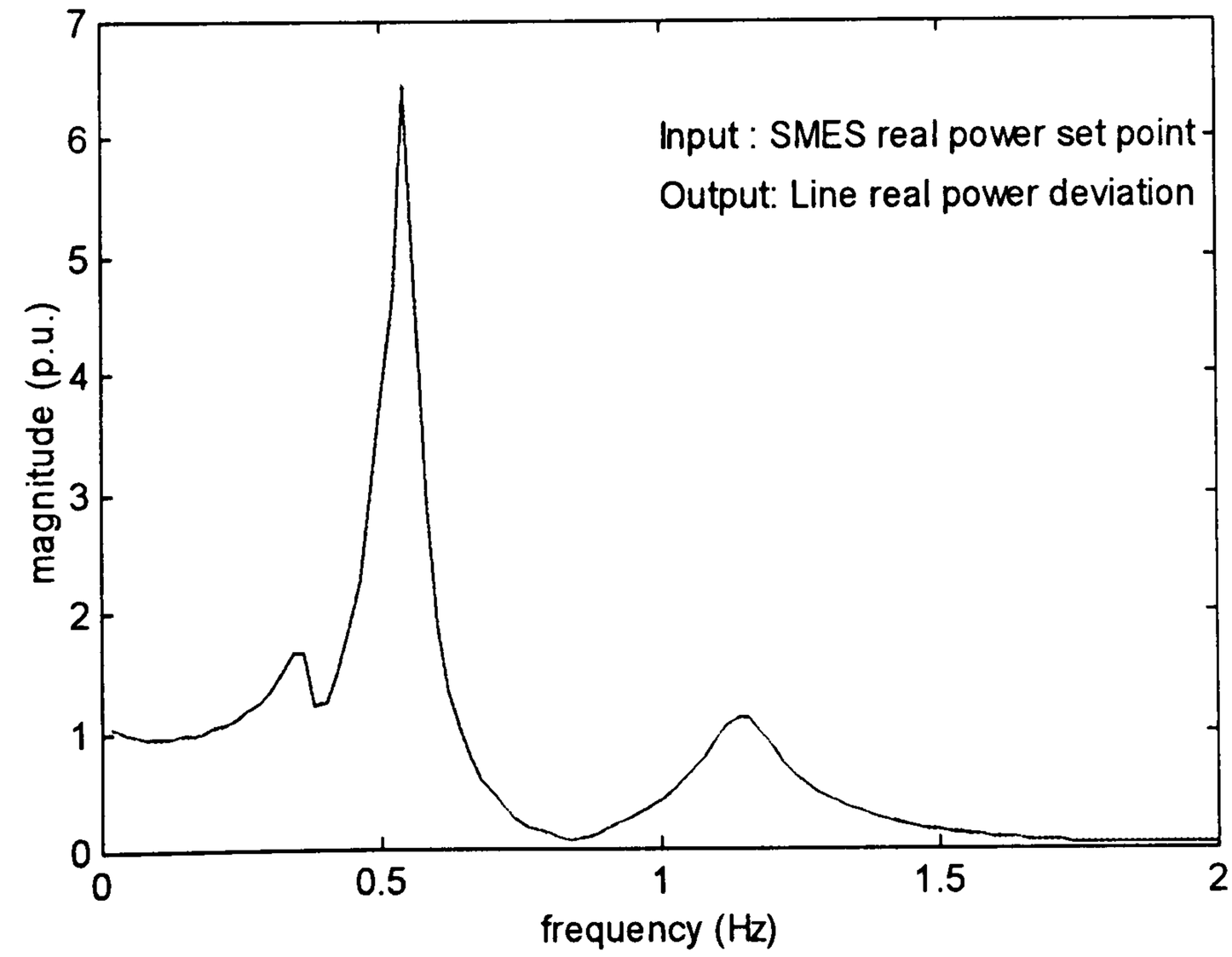

Fig. 6.6 Open-loop frequency response of the SMES at bus #13 (Study system #3)

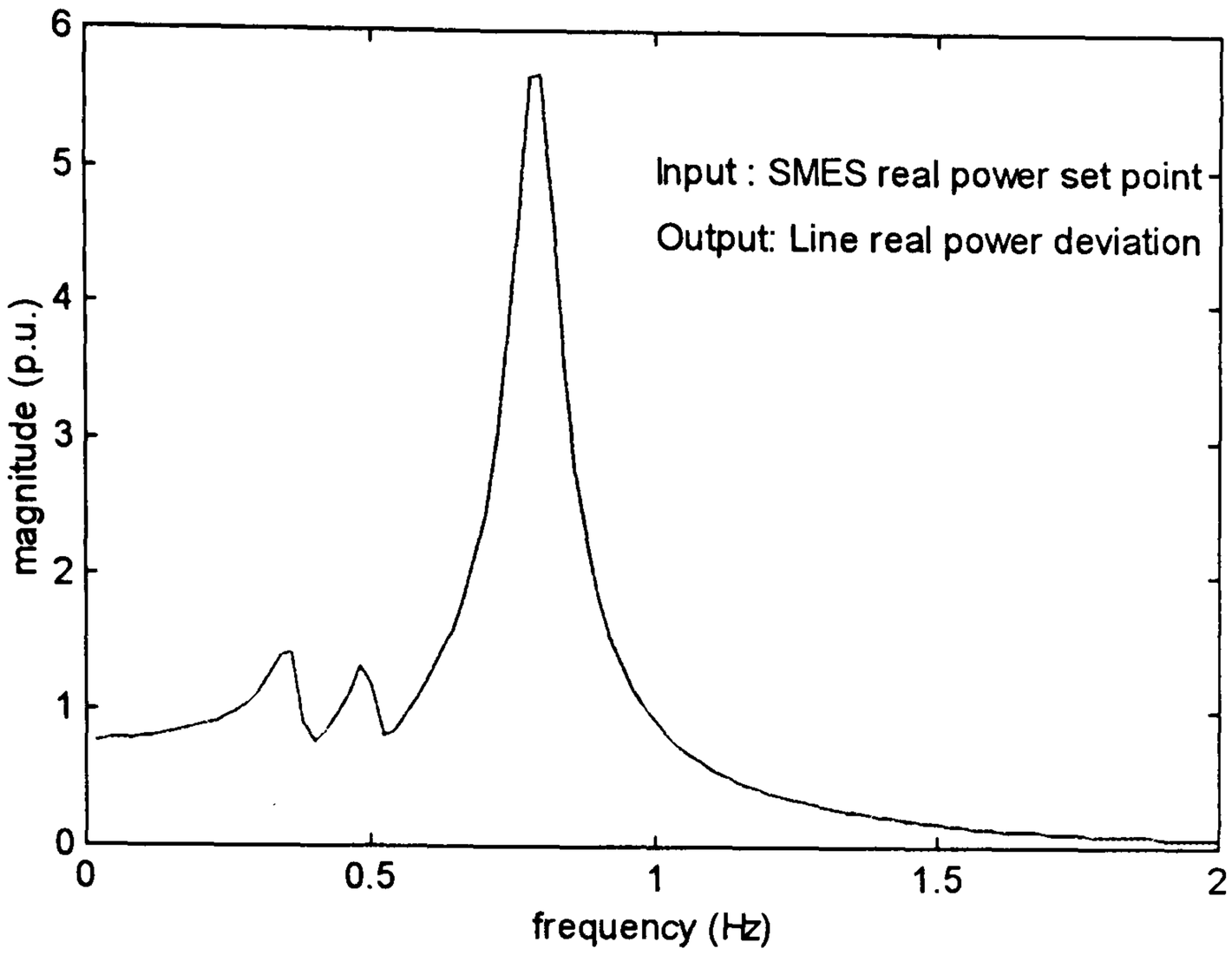

Fig. 6.7 Open-loop frequency response of the SMES at bus #15 (Study system #3)

6.4 SUMMARY AND CONCLUSIONS

In this chapter, the importance of identifying the effective location of the SMES in the system is highlighted. The selection of the best location is based exclusively on the inter-area mode damping potential of the SMES. The methods of controllability, observability and residue as analytical tools to identify the best location and the most effective feedback signals are discussed in detail. The practical basis of feedback signal selection is discussed in greater detail. An insightful discussion is also provided to highlight the preference for line active power as the feedback signal as opposed to the line current magnitude.

Residue computation is performed for three study systems. The pre-fault and post-fault operating conditions are considered. The potential SMES locations are shown. Comprehensive guidelines are provided for a system with multiple inter-area modes, as in the study systems #2 and #3. The guidelines suggest the integration of the location and controller design problems into a single problem. A sequential design is suggested. The open-loop frequency response of the system at some potential SMES locations are also shown to examine the sensitivity of a particular input-output characteristic to specific inter-area modes.

CHAPTER SEVEN

DESIGN OF ROBUST DAMPING CONTROLLER- AN EIGENVALUE-DISTANCE MINIMIZATION APPROACH

7.1 INTRODUCTION

Chapter Five illustrated that the damping ratio and frequency of an inter-area mode varies with the operating conditions of the system. A damping controller, designed for one operating condition by a conventional pole placement technique [92], may fail to maintain adequate damping at other system operating conditions. This suggests that the controller must be designed with sufficient robustness. Robustness being defined such that the damping ratio does not vary much with the operating conditions. If it varies, it must not be below an acceptable level, as described in Chapter Five, at any of the operating conditions.

In this chapter, a robust and low-order controller will be designed based on a weighted and normalised eigenvalue-distance minimisation (WNEDM) technique. The damping control design problem will be formulated as a non-linear optimisation technique. The technique will be described in detail. It will be modified to suit the power system damping design requirement. Some of the practical issues related to model reduction for ease of solution to the problem will also be discussed. Damping controller(s) will be designed for the study systems. For systems with more than one critical inter-area mode, the design will be performed sequentially. The performance of the controllers will be tested in the frequency and time domains. The performance of the controller(s) will be compared with that of the controller(s) obtained by a conventional root-locus technique. The energy and power ratings of the SMES(s) will be evaluated.

7.2 THE WEIGHTED AND NORMALISED EIGENVALUE-DISTANCE MINIMIZATION TECHNIQUE

The concept of this low-order robust controller design was developed by Schmitendorf et.al. [105] for the robust stabilisation of a remotely piloted vehicle (RPV) and a track guided bus (TGB) system. The method is discussed briefly here.

Consider the single variable feedback configuration of Fig.7.1 with $G(s)$ and $K(s)$ as the transfer function of the plant and the controller respectively. $G(s)$ and

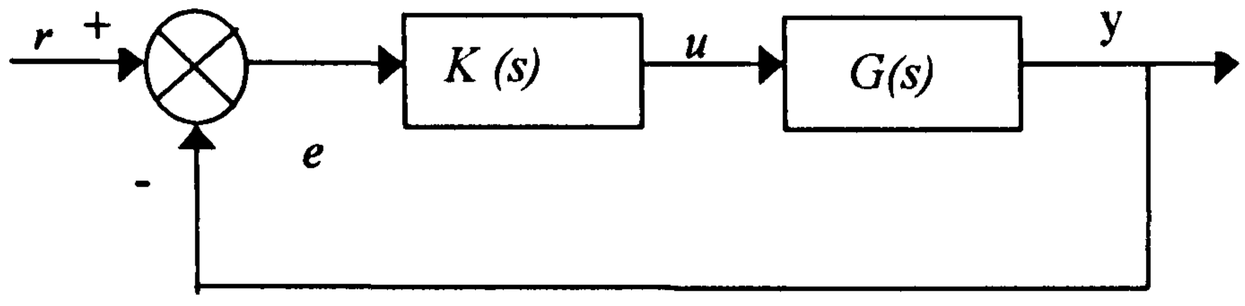

Fig. 7.1: Closed-loop control system

$K(s)$ can be expressed by a proper and rational polynomial as:

$$G(s) = \frac{N(s)}{D(s)} = \frac{n_n s^n + n_{n-1} s^{n-1} + \ldots + n_0}{d_n s^n + d_{n-1} s^{n-1} + \ldots + d_0} \tag{7.1}$$

$$K(s) = \frac{N_k(s)}{D_k(s)} = \frac{\tilde{n}_k s^k + \tilde{n}_{k-1} s^{k-1} + \ldots + \tilde{n}_0}{\tilde{d}_k s^k + \tilde{d}_{k-1} s^{k-1} + \ldots + \tilde{d}_0} \tag{7.2}$$

where, n is the order of the plant, k is that of the controller and $d_n \neq 0$. A non-zero d_n means that $G(s)$ is proper. The transfer function $T(s)$ of the closed-loop is given by:

$$T(s) = \frac{G(s)K(s)}{1 + G(s)K(s)} = \frac{N(s)N_k(s)}{N(s)N_k(s) + D(s)D_k(s)} \tag{7.3}$$

The characteristic polynomial of (7.3) can be written as:

$$\delta(s) = N(s)N_k(s) + D(s)D_k(s) \equiv \delta_{n+k} s^{n+k} + \ldots + \delta_0 \tag{7.4}$$

where, $\delta = \left[\delta_{n+k} \;\; \delta_{n+k-1} \ldots \delta_1 \;\; \delta_0\right]^T$ is termed the closed-loop characteristic vector. The roots of the polynomial of (7.4) are the closed-loop poles of the system. Hence, any arbitrary pole-placement can be achieved by suitably selecting δ. A similar vector for controller coefficients is defined as:

$$\mathbf{x} = \left[\tilde{n}_k \; \tilde{d}_k \; \tilde{n}_{k-1} \; \tilde{d}_{k-1} \ldots \tilde{n}_0 \; d_0\right]^T \tag{7.5}$$

The polynomial expression in (7.4) can be expressed as a set of algebraic equations when the coefficients of equal power of 's' on both sides of (7.4) are compared. This is given in [106] by

$$P\mathbf{x} = \delta \tag{7.6}$$

where, P is a $(n+k+1)$ x $(2k+2)$ matrix with the following structure:

$$P = \begin{bmatrix} n_n & d_n & 0 & 0 & \cdots & 0 & 0 \\ n_{n-1} & d_{n-1} & n_n & d_n & \cdots & 0 & 0 \\ \vdots & \vdots & \vdots & \vdots & \cdots & \vdots & \vdots \\ n_0 & d_0 & n_1 & d_1 & \cdots & n_k & d_k \\ \vdots & \vdots & n_0 & d_0 & \cdots & \vdots & \vdots \\ \vdots & \vdots & \vdots & \vdots & \cdots & n_1 & d_1 \\ \vdots & \vdots & \vdots & \vdots & \cdots & n_0 & d_0 \end{bmatrix} \tag{7.7}$$

P is called the plant parameter matrix as its elements are obtained from the coefficients of the plant polynomial in (7.1). Any δ, hence an arbitrary pole-placement, can be achieved through the proper choice of $\mathbf{x}$ if δ is in the range space or column space of P. This is only possible when P is of full row-rank. P satisfies full row-rank conditions if $k \geq n\text{-}1$, therefore, for arbitrary pole-placement, the minimum order of the controller is $n\text{-}1$. For a plant with a large number of open-loop poles, such as a power system, the order of the controller is very large. The order of the controller can be reduced if the aim of the arbitrary pole-placement for all of the closed-loop poles is relaxed to closed-loop stability with special treatment of a select few critical poles. This is exactly what is required in power-system-damping-controller design where improved damping ratios of the critical electromechanical modes are of paramount importance and other poles can be ignored so long as they are sufficiently damped. If the desired characteristic vector is specified as δ^* and a reduced order ($k < n\text{-}1$) controller is sought to achieve this, no $\mathbf{x}$ will be found to satisfy (7.6). The best that can be done is to choose $\mathbf{x}$ such that $\left\| P\mathbf{x} - \delta^* \right\|$ is minimised.

A solution to this optimisation problem approximates the desired characteristic polynomial but the closed-loop poles may not be close to the desired ones. Thus it is preferable to minimise the distance between the desired eigenvalues and the actual eigenvalues although straightforward distance minimisation has some drawbacks. For example, given that two of the desired real poles are –15.0 and –2.0 and if the optimisation algorithm provides a solution of –12.5 and –0.5, the absolute error of 1.5 is the same for both poles. But the pole at –0.5 causes a larger change in the dynamics of the system. In view of this, it is necessary to minimise the normalised eigenvalue-

distance instead of minimising absolute eigenvalue-distance. Furthermore, the objective of the absolute eigenvalue-distance minimisation provides equal treatment of all of the closed-loop eigenvalues. In order to attach more importance to the critical eigenvalues, the objective of eigenvalue-distance minimisation must be weighted in addition to normalisation. The modified objective function becomes:

$$F(\mathbf{x}) = \sum_{i=1}^{n+k} c_i \frac{\left\|\mu_i - \lambda_i(\mathbf{x})\right\|}{\left\|\mu_i\right\|} = \sum_{i=1}^{n+k} c_i \sqrt{\left(\left[Re(\mu_i) - Re(\lambda_i(\mathbf{x}))\right]^2 + \left[Im(\mu_i) - Im(\lambda_i(\mathbf{x}))\right]^2\right)} \tag{7.8}$$

where, $\{\mu_i\}$ and $\{\lambda_i\}$ are the desired and the actual closed-loop poles respectively and c_i is the weight associated with the *'i'th* pole. The prerequisite for the distance evaluation is that both the actual poles and the desired poles are in an order representing the magnitude of their real parts,

$$Re(\lambda_1) \le Re(\lambda_2) \le .... \le Re(\lambda_{n+k}).$$

Poles with identical real parts are ordered so that the pole with the smaller index corresponds to the pole with the smaller imaginary part.

The controller parameter vector **x** is optimised based on the plant parameter matrix P. As the operating condition varies, so does P. In order to maintain an acceptable performance at other operating conditions, the robustness property has to be built into the controller. This will be achieved by extending the technique already described to incorporate other plant parameter matrices corresponding to several (say q) operating conditions. For a specific choice of δ and an initial choice of **x**, q weighted and normalised eigenvalue-distances are evaluated. The objective of the optimisation procedure is to find **x** such that the maximum of all of the objectives $\{F_j(\mathbf{x})\}$ is minimised. The controller design task reduces to a non-linear optimisation problem as:

$$\underset{\mathbf{x}}{Minimise} \ \underset{j}{maximise} \ F_j(\mathbf{x}) \tag{7.9}$$

This is a typical unconstrained *min-max* problem. It can be solved by a non-linear optimisation technique. The optimisation procedure requires an initial value of the

controller parameter vector **x**. A *least-squares* solution of (7.6) provides the initial value of **x**. In addition to this, the algorithm requires a set of specified eigenvalues (μ_i). For a second order controller, this can be obtained by appending the open-loop poles with two fast decaying real poles in the left-half of the eigen-plane and increasing the real part of the critical complex eigenvalues. Alternatively, a second order controller can be designed for the reduced order plant by a conventional method such as the root-locus technique. The closed-loop poles can then be set as the desired poles.

7.2.1 MODIFICATIONS OF THE METHOD TO SUIT TO POWER-SYSTEM-DAMPING-CONTROL-DESIGN

The controller design formulation in (7.9) is a typical unconstrained optimisation problem as there is no bound on **x**. It may produce an **x** to provide the desired closed-loop damping. However, the controller can have unstable poles. In the case of controller design for RPV and TGB problems [105] stable controllers were found. In power system it may not be the case. In fact, in a model power system, it is experienced. This drawback is overcome by the introduction of an implicit constraint to ensure a stable controller. The controller design task reduces to a constrained non-linear optimisation problem as:

$$\begin{aligned} &Minimise \quad maximise \; F_j(\mathbf{x}) \\ &\quad \mathbf{x} \qquad\quad j \\ &subject\ to: \\ &Real\left(roots\left(D_k(s)\right)\right) < 0 \end{aligned} \tag{7.10}$$

7.2.2 PRACTICAL ISSUES

Two practical issues, one related to the weighting of the open-loop plant and the other related to the model reduction are very important here. The success of the WNEDM method hinges on these two aspects. They are briefly discussed next.

7.2.2.1 SELECTION OF WEIGHTS

The problem formulation is straightforward. The proper selection of weights $\left(c_i\right)$ is very important for the optimisation algorithm to produce desired results. For unstable poles, real poles with a small absolute magnitude and poorly damped complex poles, the weights must be very high. For other poles, the weights can be much smaller.

For any unstable open-loop pole, $c_i = 1000$ is a good choice. For real poles with a small absolute magnitude, the weighting factor can be chosen between 10 to 100. All poorly damped poles can be weighted by $m_c \frac{\varsigma_{min}}{\varsigma}$; where, ς_{min} is the minimum required damping ratio of the pole and ς is the damping ratio as the iteration proceeds. 'm_c' is a suitable constant. These choices of weights are suggested in [105].

7.2.2.2 MODEL REDUCTION

The length of the desired closed-loop characteristic vector δ^* in (7.4) is dependent on the number of open-loop poles and the order of the controller. For example, a plant with 150 open-loop poles and a second order controller, the length of the desired δ is 152. The number of closed-loop poles to be specified will be 151. Specifying such a large number of poles is neither practical nor necessary. In order to ease the controller design, the order of the plant can be reduced to a much lower order by model reduction. The Hankel singular value (HSV) [107] associated with each state is a measure of the degree to which that state contributes to the input-output behaviour of the plant. In a power system, it can be found from HSV analysis that about 90% to 95 % of these HSV will be very close to zero. This means only 5% of the HSV govern the dynamics of the system. This suggests reduction of the order of the model drastically.

There are various methods of model reduction. Each method has its advantages and disadvantages. In this research, four standard methods such as balanced truncation, balanced residualisation, Schur's balanced truncation and Hankel norm approximation were considered. Ref [107,108] provides a theoretical treatment of this subject in great detail.

Four model reduction techniques were applied to Study system #1. The input-output characteristic was obtained in the pre-fault operating condition with the SMES located at bus #10. The original plant was of 32^{nd} order. The HSV were computed and displayed in Table 7.1. It can be seen from Table 7.1 that the first three HSV are large. As many as 29 HSV are very small. This indicates the system dynamics is governed by four equivalent states. The system is, therefore, reduced to fourth order by each of the methods. The *Robust Control Toolbox* available with Matlab [109] was used to perform the necessary computations. Such a drastic reduction of the order of the plant is not

unusual as is reported in [110], where a large system with 13000 states was reduced to 8 states before the damping controller was designed by the H_∞ approach. The order of the reduced plant is immaterial as long as the input-output characteristic in the desired frequency range is very close to that of the full system. In order to justify this, the singular value [107] response of the full plant and the reduced plant is shown in Fig.7.2 .

Table 7.1: Hankel singular values (HSV) of the plant.

HSV No	HSV	HSV No	HSV	HSV No	HSV	HSV No	HSV
01	9.72	09	8.71e-04	17	6.99e-08	25	6.38e-09
02	9.54	10	1.12e-04	18	2.62e-08	26	6.38e-09
03	1.58e-01	11	9.15e-05	19	1.73e-08	27	0.00
04	4.60e-02	12	8.44e-05	20	1.73e-08	28	0.00
05	4.18e-02	13	1.05e-05	21	1.38e-08	29	0.00
06	2.99e-02	14	9.66e-07	22	1.38e-08	30	0.00
07	5.73e-03	15	1.41e-07	23	7.06e-09	31	0.00
08	1.50e-03	16	6.99e-08	24	7.06e-09	32	0.00

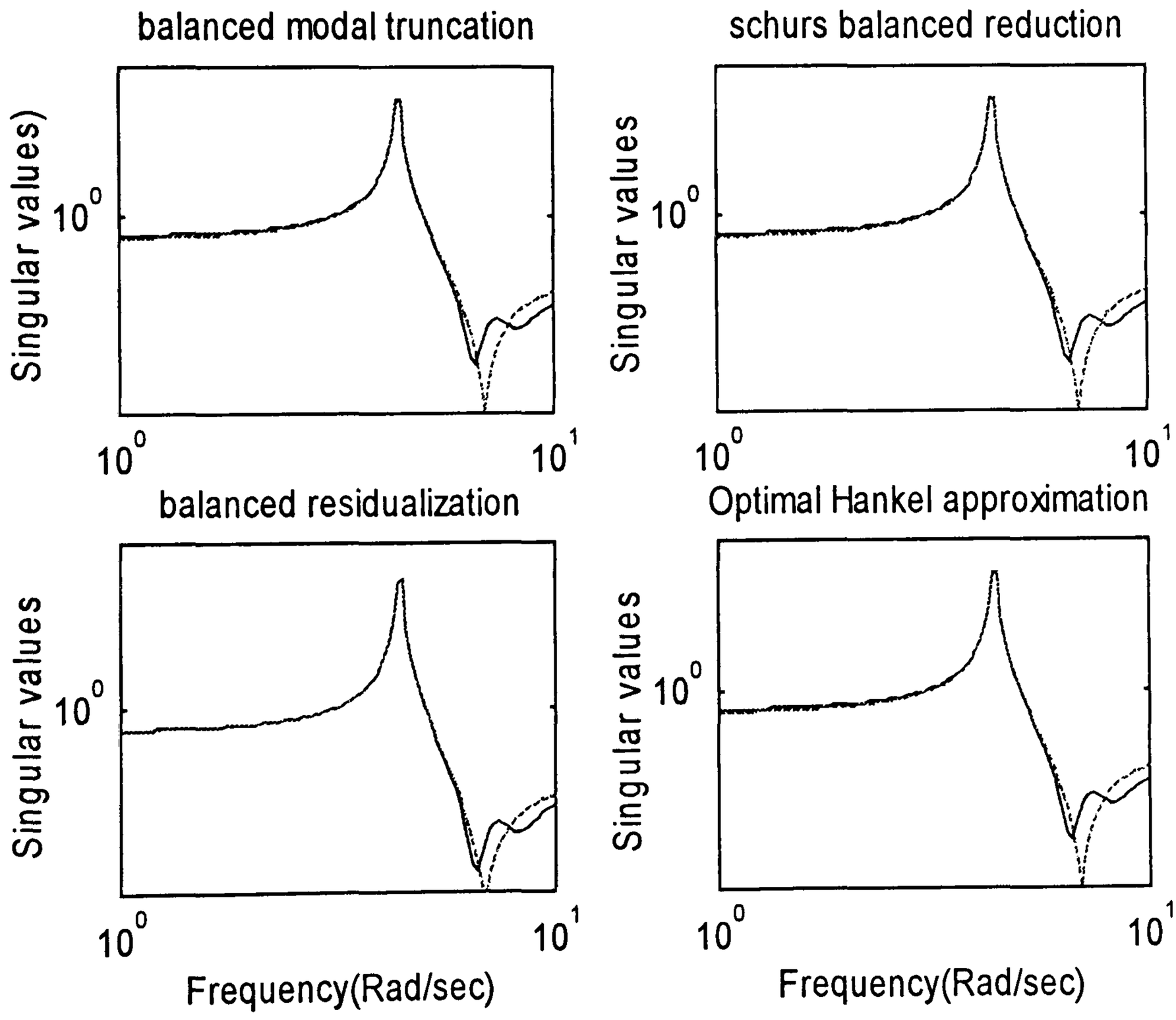

Fig. 7.2 Singular value response of plant
Solid: Full order plant; Dashed: Reduced order plant

From Fig 7.2, it can be seen that the frequency response of the reduced order plants in all of the methods are very close to the frequency response of the full order plant. The results obtained from the 4th order balanced truncation and the 4th order Schur's balanced truncation are nearly identical. Schur's technique, however, is more robust. For this particular plant, the computation of the necessary transformation matrices is well-conditioned and so the results are almost identical. The balanced residualisation technique shows better results in the low-frequency range (less than 10 rad/sec) but in the high frequency (beyond 10 rad/sec) range it exhibits its limitation. The 4th order optimal Hankel norm approximation is also nearly identical to that produced by the balanced truncation and Schur's truncation. For this particular system the reduced model obtained by the balanced residualisation technique should be used for controller design purposes. The frequency of an inter-area mode varies from system to system and from one operating condition to another in the same system. It is, at this stage, difficult to comment on the superiority of a particular technique over others in relation to the reduction in power system dynamic models for inter-area mode damping. The choice of model reduction technique in a particular power system model must be made after a comparative evaluation has been carried out.

7.2.2.3 SOLUTION TECHNIQUE

The optimisation problem in this research is solved by the Sequential Quadratic Programming (SQP) technique [111]. The SQP has three stages: **using the standard routine available in Matlab.**

(i) Updating of the Hessian matrix of the Lagrangian function

(ii) Quadratic programming problem solution

(iii) Line search and merit function calculation

In each iteration, a positive definite quasi-Newton approximation of the Hessian of the Lagrangian function is calculated using the Broyden-Fletcher-Goldfarb-Shano (BFGS) [112-115] method. In each iteration, a local quadratic approximation is made to compute an optimal search direction with the updated Hessian matrix. The optimal search direction is found as a solution to the local QP problem. The projection method suggested by Gill et. al. [116] is used. Once the optimal search direction is found, the optimum search length is found by another single variable optimisation

method that utilises a line search strategy with the objective to minimise a merit function. Of various merit functions, the one suggested by Han and Powell [117] seems to work very well when the original cost functions and constraints are highly non-linear in nature. This also ensures large contributions to the penalty parameter from constraints with smaller gradients, which would be the case for active constraints at the solution point.

7.3 DAMPING CONTROLLERS FOR THE STUDY SYSTEMS

Study system #1: The damping controller(s) was designed for the study systems. In Study system #1, SMES was located at bus #10. The transfer functions were evaluated in both operating conditions as defined in Chapter Four. This system had 32 states (7 for each generator and AVR and 4 for SMES in the open-loop). The model was reduced to 4^{th} order as already described in the last section. The plant parameter matrix P was formed. The desired set of eigenvalues in the closed-loop is specified as follows. The eigenvalues in the open-loop of the reduced system was first examined. The pre-fault operating case is considered as the normal operating point. The real part of the eigenvalues corresponding to the inter-area mode was moved further left. Two real poles were also introduced in the left half of the eigen-plane. This desired set was adequate to start the design process by optimisation. Table 7.2 displays the open-loop poles and the specified poles for the reduced system in the pre-fault operating case. The cost functions were formulated. The '*minimax*' routine available in the *Optimisation Toolbox* [118] that implements SQP was used. The '*minimax*' routine requires the '*foptions*' to be set. This is a vector with number of elements to be 18. The termination criteria for the cost function and the controller parameters (x) were relaxed to 0.01 and 0.05 respectively. This is acceptable in eigenvalue-distance minimisation. The rest of the inputs in '*foptions*' were set according to the number of cost functions. The detail of '*foptions*' is explained in [118]. The weights chosen were 1000, 100 and 50 for the poles in the right half, real poles with very slow decay rate and poles with poor damping. The ζ_{min} was selected as 0.20. The optimisation routine converged in less than 100 iterations. The actual pole locations are also listed in Table 7.2. The highlighted complex conjugate pole pair corresponds to the inter-area mode. It can be seen that it has moved substantially in the left half plane. This movement will guarantee adequate damping. The 2^{nd} order controller was obtained from the solution x and is given by:

$$K(s) = 1.86\frac{s^2 + 5.1774s + 0.0142}{s^2 + 4.3141s + 64.2839} \tag{7.11}$$

The frequency response of $K(s)$ is also shown in Fig. 7.3. It can be seen that the controller is very effective around the frequency of the inter-area mode. It does have very little gain in the other frequency ranges.

Table 7.2: Poles of the reduced plant (Study system #1)

Open-loop poles	Specified poles	Actual poles
-0.0421 ± j4.3835	**-0.6000 ± j4.2000**	**-0.9768 ± j4.0301**
-0.1099	-0.1500	-0.1100
-42.6761	-7.0000	-1.6008 ± j6.524
	-20.000	
	-65.000	-67.840

The results in Table 7.2 are related to the reduced model of the plant. The damping was checked before accepting this controller using the original full model of the plant. It was found in the original system that this controller provided adequate damping for the inter-area mode.

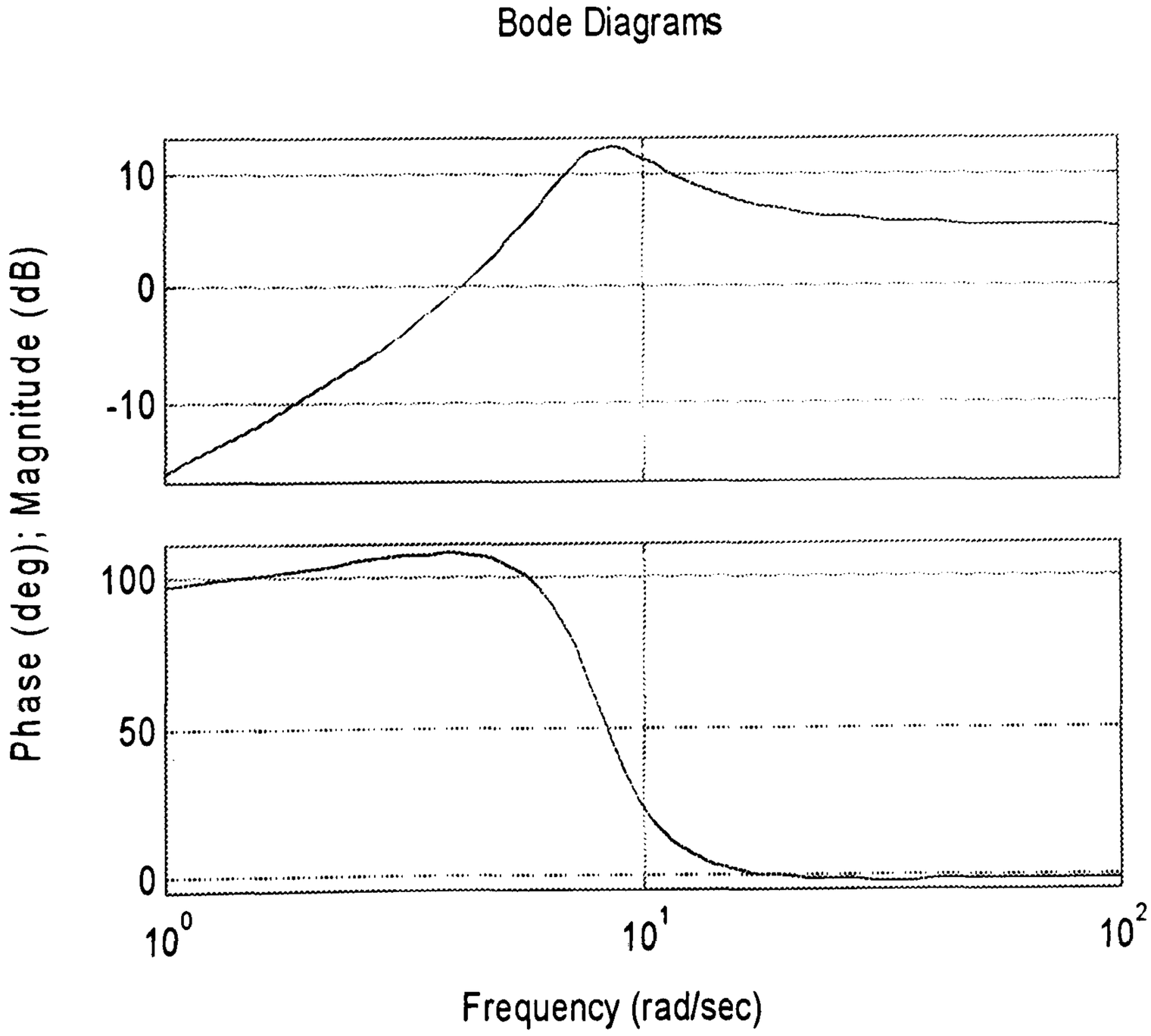

Fig. 7.3: Frequency response of $K(s)$

Study System #2: The Study system#2 has two inter-area modes (Ref. Table 4.17 in Chapter Four). The best locations to damp modes #1 and #2 are bus #15 and bus #8 respectively (Ref Table 6.2 in Chapter Four). Sequential design was again carried out. The system has 52 states including 4 states for a SMES located at bus #15. HSV analysis showed that as many as 44 states was ineffective in governing the dynamics of the system. The system was, therefore, reduced to 8^{th} order. The balanced modal truncation method provided the least errors in this system. The frequency response of the original and reduced system is shown in Fig. 7.4. It can be seen from Fig. 7.4 that the reduced system is a good approximation of the original system. It is also interesting to see that the input-output combination for a SMES located at bus #15 is very selective to inter-area mode #1 only. The choice of this location and the feedback signal will eliminate interactions with other modes as is evident from the frequency response.

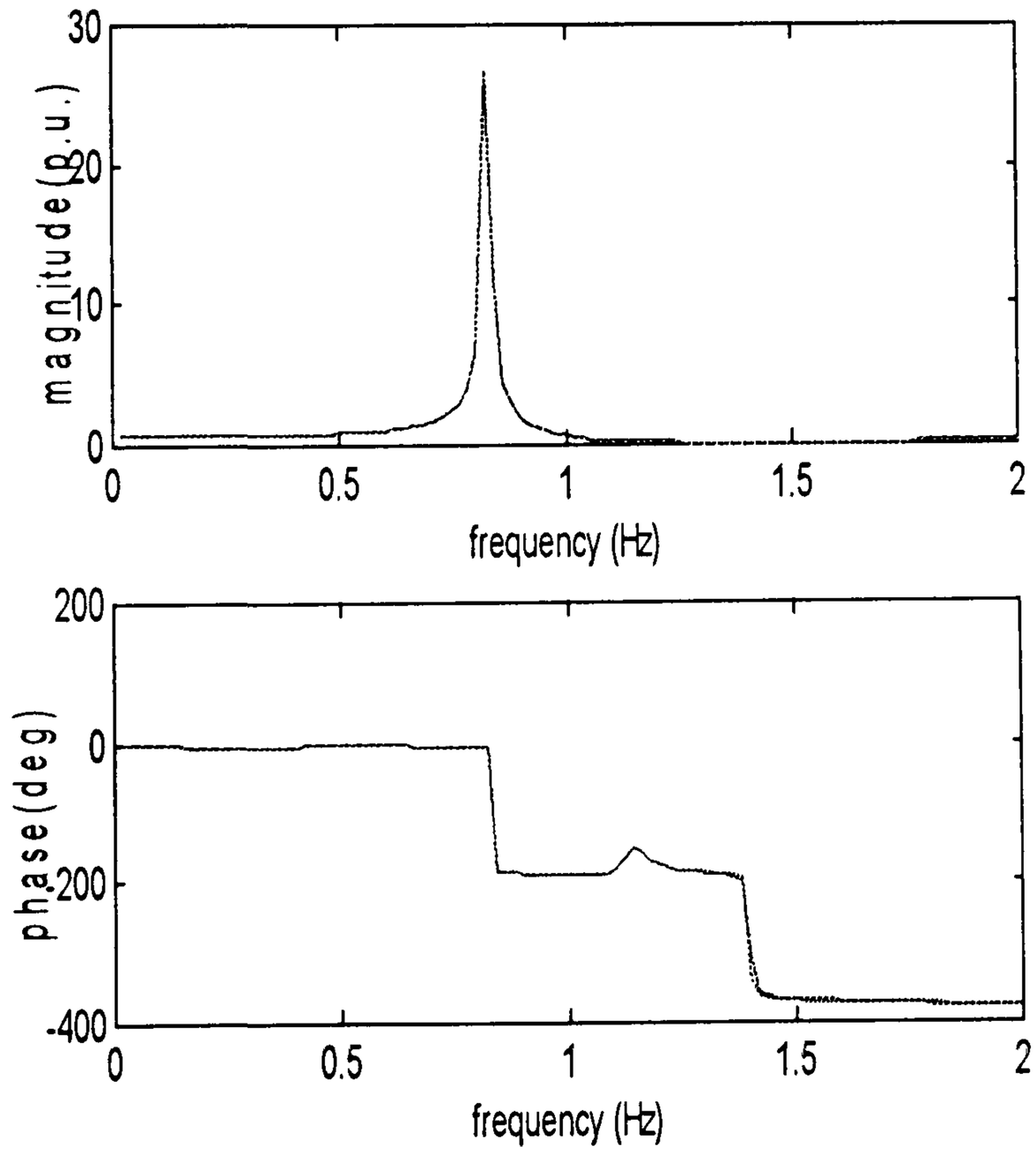

Fig 7.4: Frequency response of the original and the reduced system (Study system #2)
Solid line: Original system
Dashed line: Reduced system

The sequential design was performed. Mode #1 was considered the primary mode. Mode #2 (1.14 Hz) was the secondary mode. The plant parameter matrices were formed for the

reduced system in both operating cases. The eigenvalues were specified in the manner described for Study system #1. Cost functions were formulated. The weights were the same as that of Study system #1. The optimisation problem was solved by SQP. The controller was constructed from the solution of the optimisation problem. The damping ratios of the primary and secondary mode were examined. The procedure was repeated for all of the potential locations (busses #15, #11, #12 and #8). It was found that the controller obtained with SMES at busses #11 and #12 improved the damping of the primary mode but provided negative damping to the secondary mode (mode #2). The controllers on these SMES locations did not seem to have significant influence on the primary mode but provided maximum damping to the secondary inter-area mode. In view of this, it was decided that the controller for SMES location at bus #15 was considered best. The controller is given by:

$$K_1(s) = 0.28\frac{s^2 + 43.785s + 0.0687}{s^2 + 10.239s + 71.652} \tag{7.12}$$

The damping ratio of the secondary mode with the controller $K_1(s)$ was found insufficient. An increase in the gain of $K_1(s)$ slightly improved the damping of mode #2 but the natural frequency of mode #1 was changed appreciably. Such change was not acceptable as it might affect the transient stability performance of the system. It was decided that a second SMES and damping controller was needed. Bus #8 was the best location for damping mode #2. The SMES was located at bus #8 and the feedback signal $P_{8,7}$ as displayed in Table 6.3 of Chapter Six was selected. The controller ($K_1(s)$) was connected to the system. The input-output characteristic at bus #8 was computed. The original system had 60 states. The HSV analysis showed that the system could be reduced to 4th order. The frequency response of the original system and the reduced system is shown in Fig. 7.5. It can be seen from the frequency response that the reduced order system follows the original system very closely. The frequency response also provides other useful information: the input-output characteristic is sensitive to mode #2 only. The optimisation problem was formulated and solved. The 2nd order controller is given by:

$$K_2(s) = 0.63\frac{s^2}{s^2 + 10.239s + 71.652} \tag{7.13}$$

The controller provided adequate damping to mode #2. It was also found that this controller did not interfere with the damping of other modes.

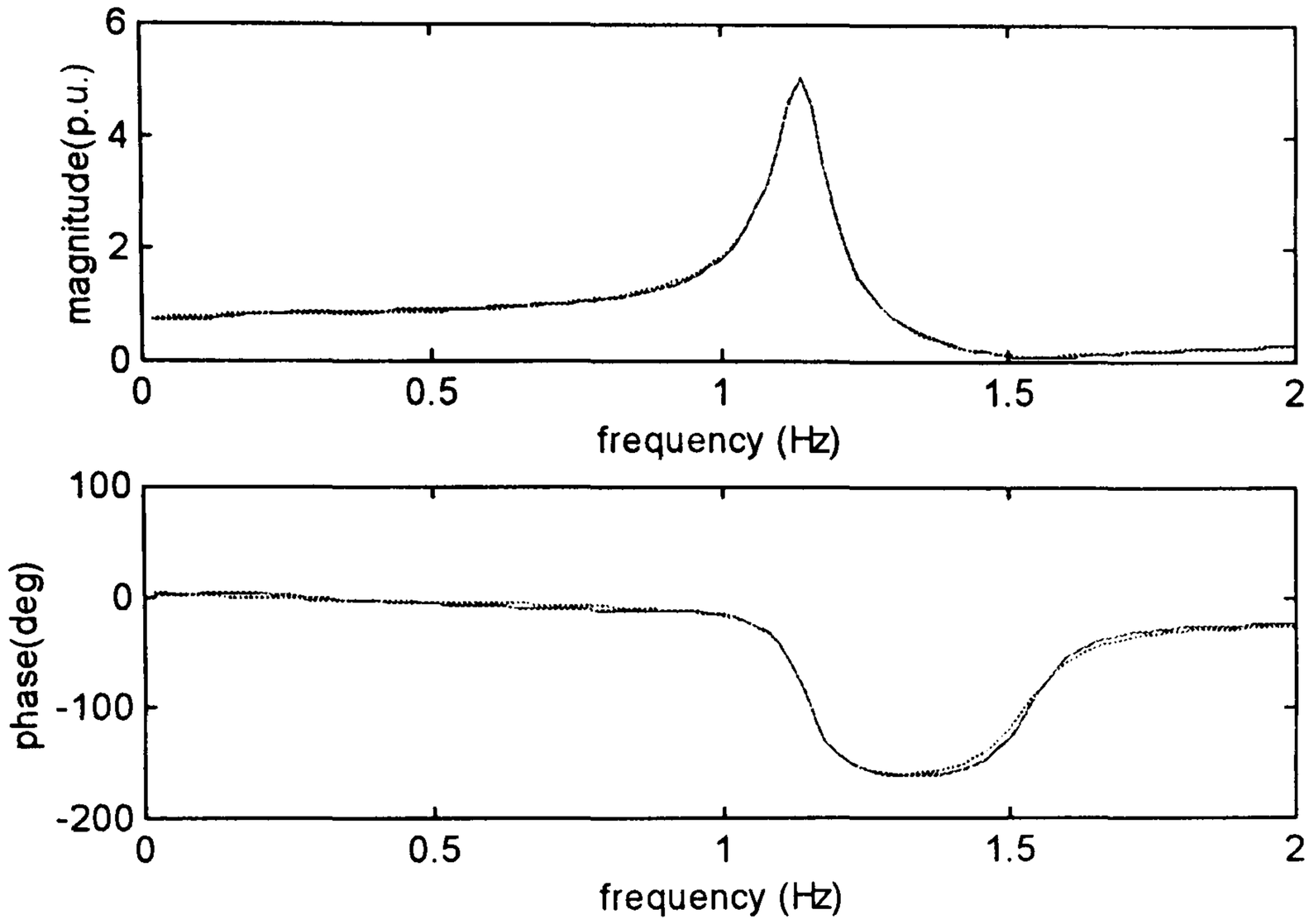

Fig 7.5: Frequency Response of the original and the reduced system (Study system #2)
Solid line: Original system
Dashed line: Reduced system

Study system #3: The controller design for this study system was similar to that for Study system #2. In Study system #3, there are four inter-area modes (ref. Table 4.18 of Chapter Four).

The improvement of mode #1 was first attempted. The system had 137 states including four states for a SMES at any particular location. From Table 6.3 in Chapter Six, it was found that the damping of mode #1 could be most influenced by a SMES at bus #54 with $P_{54,53}$ as the feedback signal. The controller design was, therefore, started with this location. The model reduction was performed best by balanced modal truncation. The system with 137 states was reduced to an equivalent one with 10 states. The frequency response of the reduced and the full system for the pre-fault operating case is displayed in Fig 7.6. Once again it can be inferred from Fig. 7.6 that as many as 127 states are ineffective in influencing the dynamics of the system. The controller design was carried out treating mode #1 as the primary mode and mode #2 to mode #4 as the secondary modes. The optimisation problem was formulated with the same weights. The 2^{nd} order controller was designed and connected to the original system to evaluate and

examine the damping ratios of all of the inter-area modes. All of the potential locations as listed in Table 6.3 of Chapter Six were attempted. It was found that a single SMES could not provide acceptable damping to all modes.

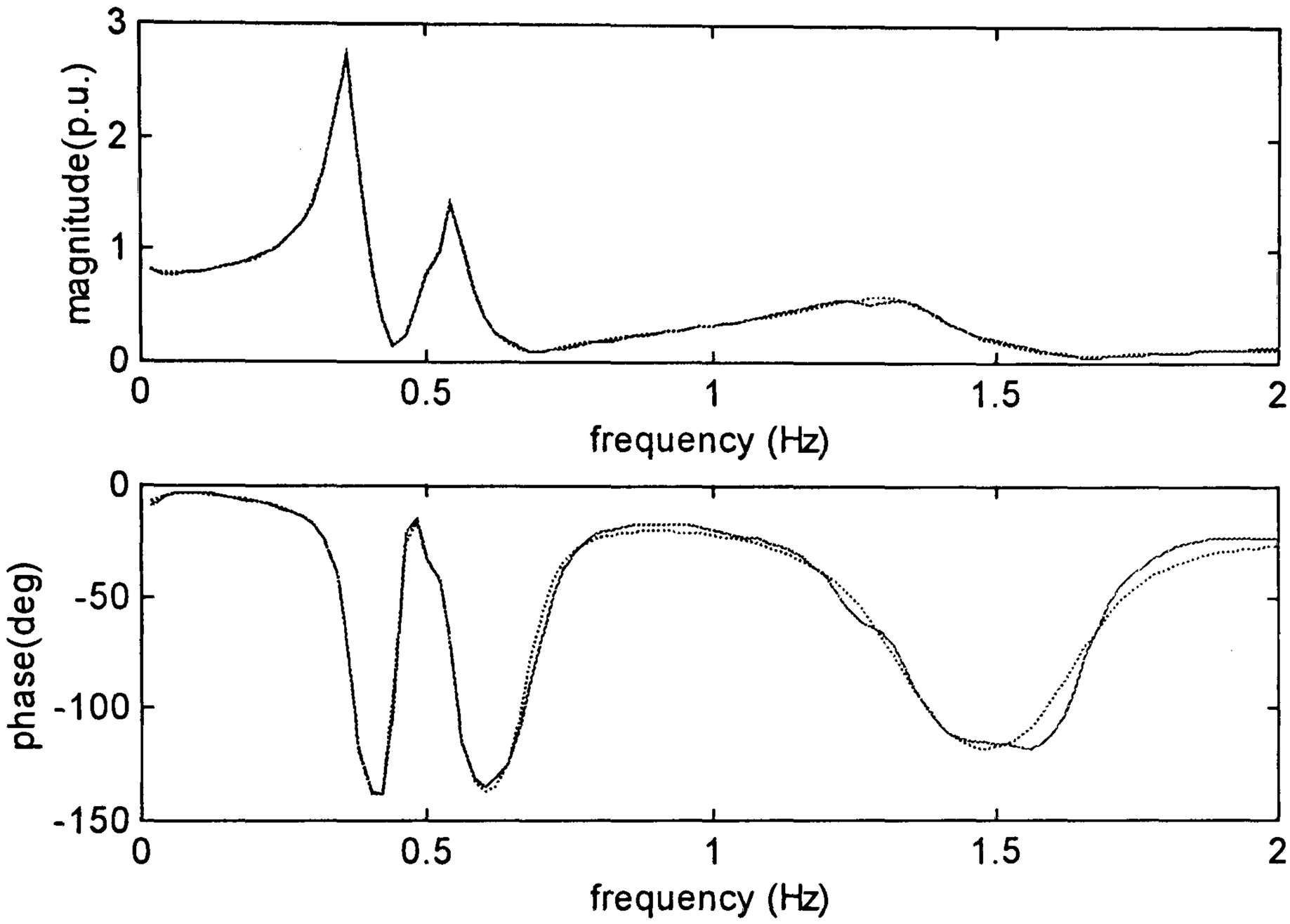

Fig 7.6: Frequency Response of the original and the reduced system (Study system #3)
Solid line: Original system
Dashed line: Reduced system

It was also found that bus #54 was the best location to damp mode #1 with maximum positive influence on the secondary modes (mode #2 to mode #4). The corresponding controller is given by:

$$K_1(s) = 2086.8\frac{s+0.0163}{s^2+422.83s+5004} \tag{7.14}$$

The controller $K_1(s)$ was then treated as an integral part of the system. The improvement of the damping of mode #2 was attempted. The input-output characteristics at different locations were computed for the pre-fault and post-fault operating cases. Model reduction was performed. The design was carried out at all of the locations except at bus #54. Mode #2 was treated as the primary mode. Modes #3 and #4 were treated as secondary modes. It was found that when the SMES was located at bus #16, the

improvement of the damping of the primary and secondary mode was most acceptable. The controller provided adequate damping to mode #2 and mode #4. It is given by:

$$K_2(s) = 14.433\frac{s^2 + 2.0714s + 0.11177}{s^2 + 54.156s + 53.26} \tag{7.15}$$

The damping of mode #3 was improved in the pre-fault case but not in the post-fault case. This meant that the damping contribution of this controller to mode #2 to #4 although acceptable for the pre-fault operating case, was not acceptable to the post-fault operating case. The increase in gain of the controller did not seem to help. It was decided that the third SMES is needed.

Two controllers in (7.14) and (7.15) were treated as an integral part of the system. The input-output characteristic with the third SMES was computed at different locations as indicated in Table 6.3 except in bus #54 and bus #16. It was found that bus #13 was best location to improve damping of mode #3 in both operating conditions. The controller is given by:

$$K_3(s) = 0.8027\frac{s^2 + 1.77e5s + 3.2755}{s^2 + 30329s + 5.23e5} \tag{7.16}$$

The controller $K_3(s)$ was also found to improve the damping of mode #4 in both operating cases. The damping ratios of all four modes with three controllers connected to the system were computed in both operating cases. It was found that the damping action provided by these three controllers was adequate.

The controller in all cases was appended with a washout circuit. The washout circuit has a transfer function of $\frac{sT_w}{1+sT_w}$ type. This prevents very low-frequency (less than 0.1 Hz) and/or steady-state deviation in the feedback signal that may appear in day to day operation. The time constant (T_w) can be in the range of 10 to 20 s. In a power system with a very low inter-area mode frequency, the time constant should be at the higher end of this range. The effect of the washout circuit is included in the performance analysis. Reference [92] discusses the detail of the washout filter in power-system-small-signal-analysis.

The performances of these controllers will be assessed in detail in the next section.

7.4 PERFORMANCE EVALUATIONS

The performance of the controller(s) was evaluated in the frequency and time domains. An eigenvalue analysis was carried out to evaluate the damping ratios for various operating conditions. The entries in Table 7.3 display the damping ratios and frequencies in the open-loop and closed-loop for Study system #1. It can be seen that the controller provides adequate damping for mode #1 in both the pre-fault and post-fault operating conditions.

Table 7.3: Damping ratios in both operating cases (Study system #1).

Mode No.	Open-loop (pre-fault)		Closed-loop (pre-fault)		Open-loop (post-fault)		Closed-loop (post-fault)	
	ζ	f (Hz)	ζ	f (Hz)	ζ	f (Hz)	ζ	f (Hz)
#1	**0.0096**	**0.6976**	**0.2312**	**0.6387**	**0.0031**	**0.5917**	**0.1966**	**0.5495**
#2	0.0852	1.1474	0.0856	1.1453	0.0856	1.1414	0.0857	1.1404
#3	0.1153	1.1545	0.1464	1.2266	0.1140	1.1497	0.1533	1.2132

The damping ratios of mode #2 and mode #3 are listed here to show the 'non-interfering' nature of the controller to local modes. The robustness of the controller was further verified at different values of power flow through the tie line. The load was considered as a constant impedance type. The pre-fault condition was assumed. The results are shown in Table 7.4. It can be seen that the damping controller ensures adequate damping when the direction of power flow reverses. The damping ratios in the post-fault conditions at various values of power flow were also computed and found to be adequate but are not displayed here.

Table 7.4: Damping ratios at various values of power flow (Study system#1)

Power Flow (Area #1→Area #2)	Open-loop		Closed-loop	
	ζ	f (Hz)	ζ	f (Hz)
00 MW	0.0263	0.7238	0.2300	0.6710
200 MW	0.0108	0.7142	0.2261	0.6583
400 MW	0.0096	0.6976	0.2312	0.6387
-400 MW	0.0090	0.6934	0.1782	0.6761

The effect of the variation in the load characteristics for the damping performance of the controller was evaluated in the pre-fault case. In addition to the CI type, four other types of loads were considered. They are CC, CP, an equal mix of CC

and CP and dynamic loads. The dynamic model of load as suggested in Chapter Three was considered. The results are displayed in Table 7.5. It can be seen from these results that the controller provides adequate damping even with different load characteristics. The damping ratios for the post-fault conditions were also found to be adequate. This indicates that the controller can maintain adequate damping in the face of variation in load characteristics.

Table 7.5: Damping ratios at different load characteristics (Study system #1)

Load Type	Closed-loop (pre-fault)	
	ζ	f (Hz)
CI	0.2312	0.6387
CC	0.2137	0.6486
CP	0.1890	0.6620
CC+CP	0.2025	0.6547
Dynamic	0.2180	0.6338

The same investigation was carried out for Study system #2. The effect of each of the controllers was evaluated first. Table 7.6 shows the damping contributed by $K_1(s)$ in (7.12). It can be seen that the damping of mode #1 is improved. This was also stated in the previous section. The nominal operating case of the 550 MW tie line power flow was considered along with CI type load for damping evaluation. The damping ratios were evaluated considering controller $K_2(s)$ in (7.13) in the system. The results are displayed in Table 7.7 for both operating cases. In Table 7.7, the open-loop refers to the presence of $K_1(s)$ only. The closed-loop refers to both $K_1(s)$ and $K_2(s)$ connected to the system. It can be seen from the results in Table 7.7 that $K_2(s)$ improves the damping of mode #2 in the pre-fault and post-fault operating cases. It can also be seen from the results in Table 7.7 that $K_2(s)$ does not have any adverse influence on the damping of mode # 1.

Table 7.6: Damping ratios in both operating cases with $K_1(s)$ only (Study system #2).

Mode No.	Open-loop (pre-fault)		Closed-loop (pre-fault)		Open-loop (post-fault)		Closed-loop (post-fault)	
	ζ	f (Hz)	ζ	f (Hz)	ζ	f (Hz)	ζ	f (Hz)
#1	**0.0001**	**0.8258**	**0.1943**	**0.8792**	**-0.0118**	**0.6918**	**0.1041**	**0.7102**
#2	0.0274	1.1466	0.0380	1.1439	0.0269	1.1359	0.0275	1.1352

Table 7.7: Damping ratios in both operating cases with $K_1(s)$ & $K_2(s)$ (Study system #2).

Mode No.	Open-loop (pre-fault)		Closed-loop (pre-fault)		Open-loop (post-fault)		Closed-loop (post-fault)	
	ζ	f (Hz)	ζ	f (Hz)	ζ	f (Hz)	ζ	f (Hz)
#1	0.1943	0.8792	0.2090	0.8870	0.1041	0.7102	0.1141	0.7051
#2	0.0380	1.1439	0.1451	1.1394	0.0275	1.1352	0.1159	1.1416

The results produced in Table 7.8 and 7.9 show the damping performance of the controller at different values of tie line power flows and for different types of load. Once again it can be seen that the controllers provide adequate damping at various tie line flows and against the widely varying nature of the loads. The pre-fault operating conditions were considered. The damping at post-fault operating conditions are not listed here but they were found adequate. It can be seen that without the controllers, the damping in the post-fault operating conditions (550 MW and 750 MW) are negative (ref. Table 4.14 and 4.16 in Chapter Four).

Table 7.8: Damping ratios at various values of power flow (Study system#2)

Power Flow (Area #3→Area #1& Area #2)	Mode #1 Closed-loop (pre-fault)		Mode #2 Closed-loop (pre-fault)	
	ζ	f (Hz)	ζ	f (Hz)
00 MW	0.3755	0.8466	0.1185	1.1261
550 MW	0.2090	0.8870	0.1451	1.1394
750 MW	0.1046	0.7490	0.1237	1.1391

Table 7.9: Damping ratios at different load characteristics (Study system #2)

Load Type	Mode #1 Closed-loop (pre-fault)		Mode #2 Closed-loop (pre-fault)	
	ζ	f (Hz)	ζ	f (Hz)
CI	0.2090	0.8870	0.1451	1.1394
CC	0.2550	0.9114	0.1456	1.0975
CP	0.3326	0.8862	0.1101	1.0340
CC+CP	0.2927	0.9092	0.1326	1.0686
Dynamic	0.2073	0.8966	0.1893	1.1403

The performances of the controllers were evaluated in Study system #3. The impact of each of the controllers on the damping of mode #1 to #4 was assessed. Table 7.10 - 7.12 display these results. It can be seen from these results that $K_1(s)$ in (7.14) mainly improves damping of mode #1. $K_2(s)$ in (7.15) improves the damping of modes #2 and #4. $K_3(s)$ in (7.16) improves the damping of mode #3 only.

Table 7.10: Damping ratios in both operating cases with $K_1(s)$ only (Study system #3).

Mode No.	Open-loop (pre-fault)		Closed-loop (pre-fault)		Open-loop (post-fault)		Closed-loop (post-fault)	
	ζ	f (Hz)	ζ	f (Hz)	ζ	f (Hz)	ζ	f (Hz)
#1	**0.061**	**0.36**	**0.157**	**0.40**	**0.044**	**0.33**	**0.18**	**0.35**
#2	0.039	0.49	0.052	0.49	0.025	0.48	0.047	0.48
#3	0.037	0.54	0.115	0.54	0.039	0.51	0.058	0.51
#4	0.049	0.79	0.049	0.79	0.049	0.79	0.049	0.79

Table 7.11:Damping ratios in both operating cases with $K_1(s)$ and $K_2(s)$ only (Study system #3)

Mode No.	Open-loop (pre-fault)		Closed-loop (pre-fault)		Open-loop (post-fault)		Closed-loop (post-fault)	
	ζ	f (Hz)	ζ	f (Hz)	ζ	f (Hz)	ζ	f (Hz)
#1	0.157	0.40	**0.161**	**0.41**	0.180	0.35	**0.197**	**0.35**
#2	0.115	0.54	**0.190**	**0.57**	0.058	0.51	**0.208**	**0.57**
#3	0.052	0.49	0.160	0.51	0.047	0.48	0.061	0.48
#4	0.049	0.79	**0.103**	**0.79**	0.049	0.79	**0.103**	**0.79**

Table 7.12: Damping ratios in both operating cases with $K_1(s)$, $K_2(s)$ and $K_3(s)$ (Study system #3).

Mode No.	Open-loop (pre-fault)		Closed-loop (pre-fault)		Open-loop (post-fault)		Closed-loop (post-fault)	
	ζ	f (Hz)	ζ	f (Hz)	ζ	f (Hz)	ζ	f (Hz)
#1	0.161	0.41	**0.212**	**0.39**	0.197	0.35	**0.203**	**0.35**
#2	0.190	0.57	**0.210**	**0.54**	0.208	0.57	**0.187**	**0.53**
#3	0.160	0.51	**0.217**	**0.67**	0.061	0.48	**0.256**	**0.63**
#4	0.103	0.79	**0.11**	**0.78**	0.103	0.79	**0.110**	**0.78**

The robustness of these controllers was further assessed for various levels of power transfer across NYPS and NETS. The robust damping performance of these controllers was evaluated in the face of different load characteristics. Table 7.13 and 7.14 list the damping ratios of all four inter-area modes. It can be inferred from these results that the controllers are very robust in ensuring adequate damping for various levels of tie line flows and types of load characteristics.

Table 7.13: Damping ratios at various values of power flow (Study system#3)

Power Flow (NETS→NYPS)	Mode #1 Closed-loop (pre-fault)		Mode #2 Closed-loop (pre-fault)		Mode #3 Closed-loop (pre-fault)		Mode #4 Closed-loop (pre-fault)	
	ζ	f (Hz)	ζ	f (Hz)	ζ	f (Hz)	ζ	f (Hz)
100 MW	0.212	0.39	0.210	0.54	0.217	0.67	0.110	0.78
500 MW	0.149	0.36	0.191	0.54	0.237	0.65	0.108	0.78
700 MW	0.102	0.35	0.182	0.54	0.249	0.63	0.107	0.78

Table 7.14: Damping ratios at different load characteristics (Study system#3)

Load Type	Mode #1 Closed-loop (pre-fault)		Mode #2 Closed-loop (pre-fault)		Mode #3 Closed-loop (pre-fault)		Mode #4 Closed-loop (pre-fault)	
	ζ	f (Hz)	ζ	f (Hz)	ζ	f (Hz)	ζ	f (Hz)
CI	0.212	0.39	0.210	0.54	0.217	0.67	0.110	0.78
CC	0.178	0.40	0.232	0.56	0.235	0.68	0.116	0.78
CP	0.180	0.39	0.236	0.61	0.240	0.68	0.120	0.77
CC+CP	0.172	0.40	0.238	0.58	0.241	0.68	0.119	0.77
Dynamic	0.216	0.39	0.211	0.54	0.232	0.67	0.109	0.78

Section 4.4 in Chapter Four suggested that the performance evaluations only in the frequency domain are not adequate. In eigenvalue analysis, the non-linearity associated with the dynamics of the system is not considered. It can be seen that the controllers designed by the WNEDM method for all of the study systems have robust performance against different operating points and different types of loads. In order to include the effect of non-linearity, device saturation etc. on the performance of the controller, simulations in the time domain were performed. The nature, location and duration of the disturbances are already described in Section 4.4. The behaviour of the same set of dynamic variables as plotted in Fig 4.4 to 4.6 is plotted here with the controllers connected to the systems. In addition to these variables the outputs of the SMES are also displayed. The pre-fault and post-fault conditions are as defined in Chapter Four. The displays in Fig.7.7 and 7.8 show the time domain behaviour of the dynamic variables of Study system #1.

From the plots in Fig 7.7, it can be seen that the inter-area oscillations observed in the dynamic variables are well damped with the controller connected to the system. The oscillation settles within 10 s after the fault is cleared. The outputs of the SMES, plotted in Fig 7.8, show that the real power output is heavily modulated. This is expected as the damping controller modulates the real power of the SMES. The reactive power output trace does not show much difference between the open-loop and closed-loop response. The reactive power block mainly provides dynamic voltage support after the fault. The main function of this is voltage control and not damping control. The real power output of the SMES is restricted to $\pm$ 10 MW. Following the disturbance, the real power output hits this limit. In about 5 to 10 s, linearity is regained and the controller damps the oscillation more effectively. The plots in Fig. 7.9 and 7.10 display the

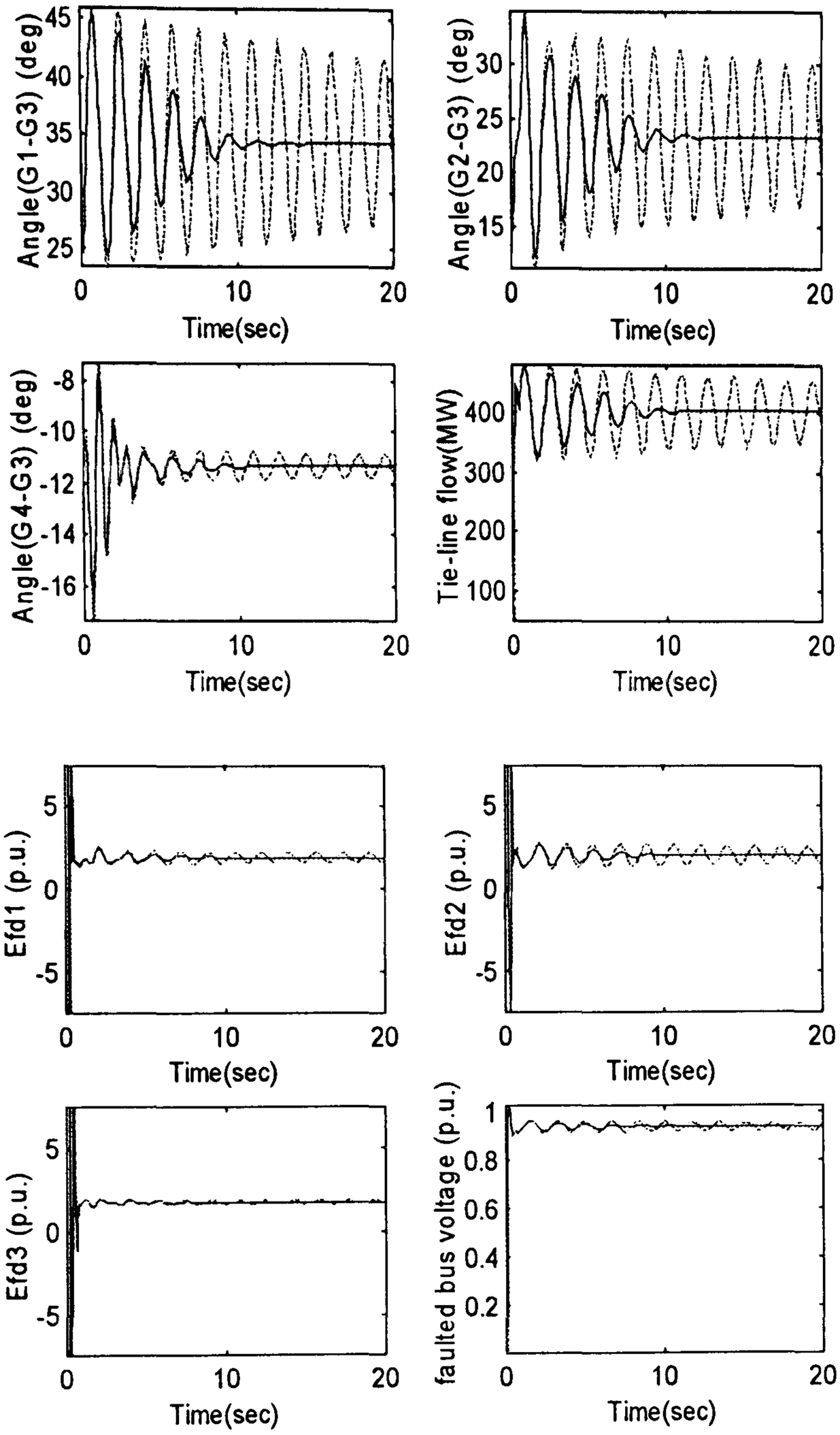

Fig 7.7: Response of Study system #1 under large disturbances
Solid line: with controller; Dashed line: without controller

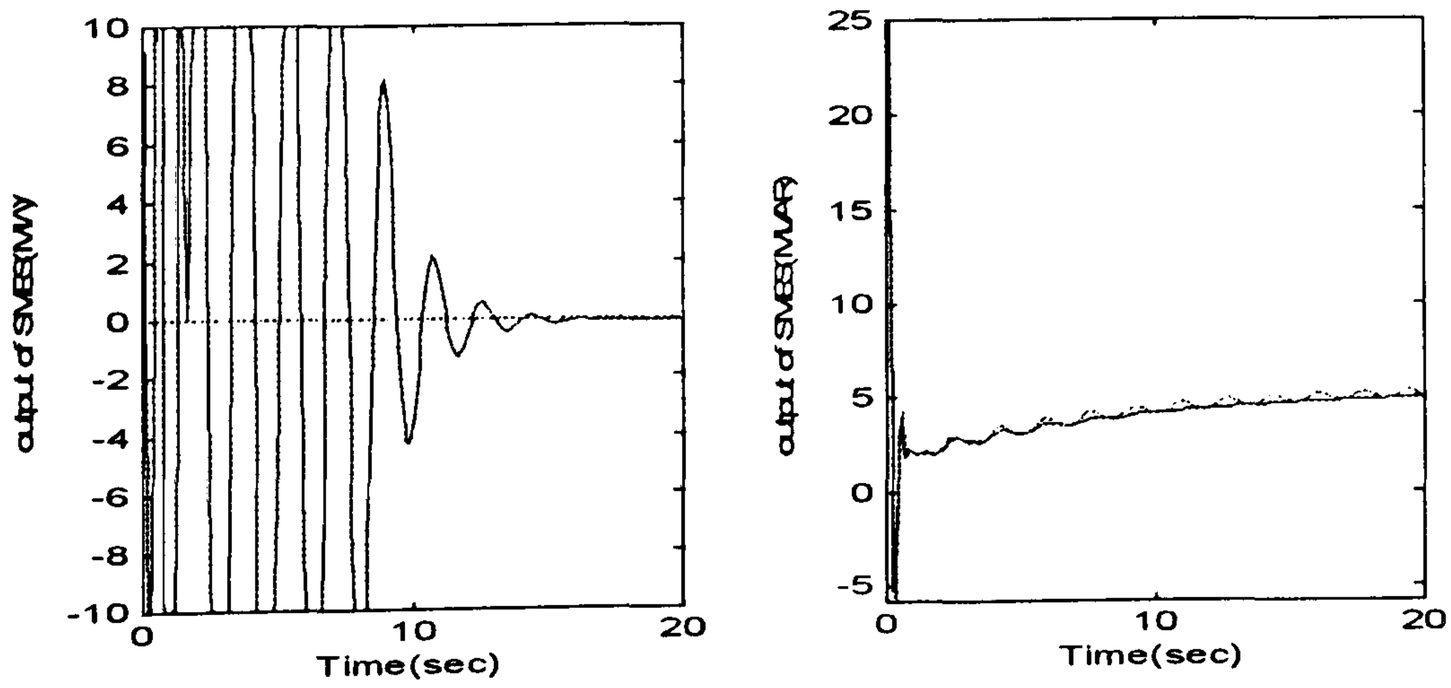

Fig 7.8: Response of SMES under large disturbance in Study system #1
Solid line: with controller; Dashed line: without controller

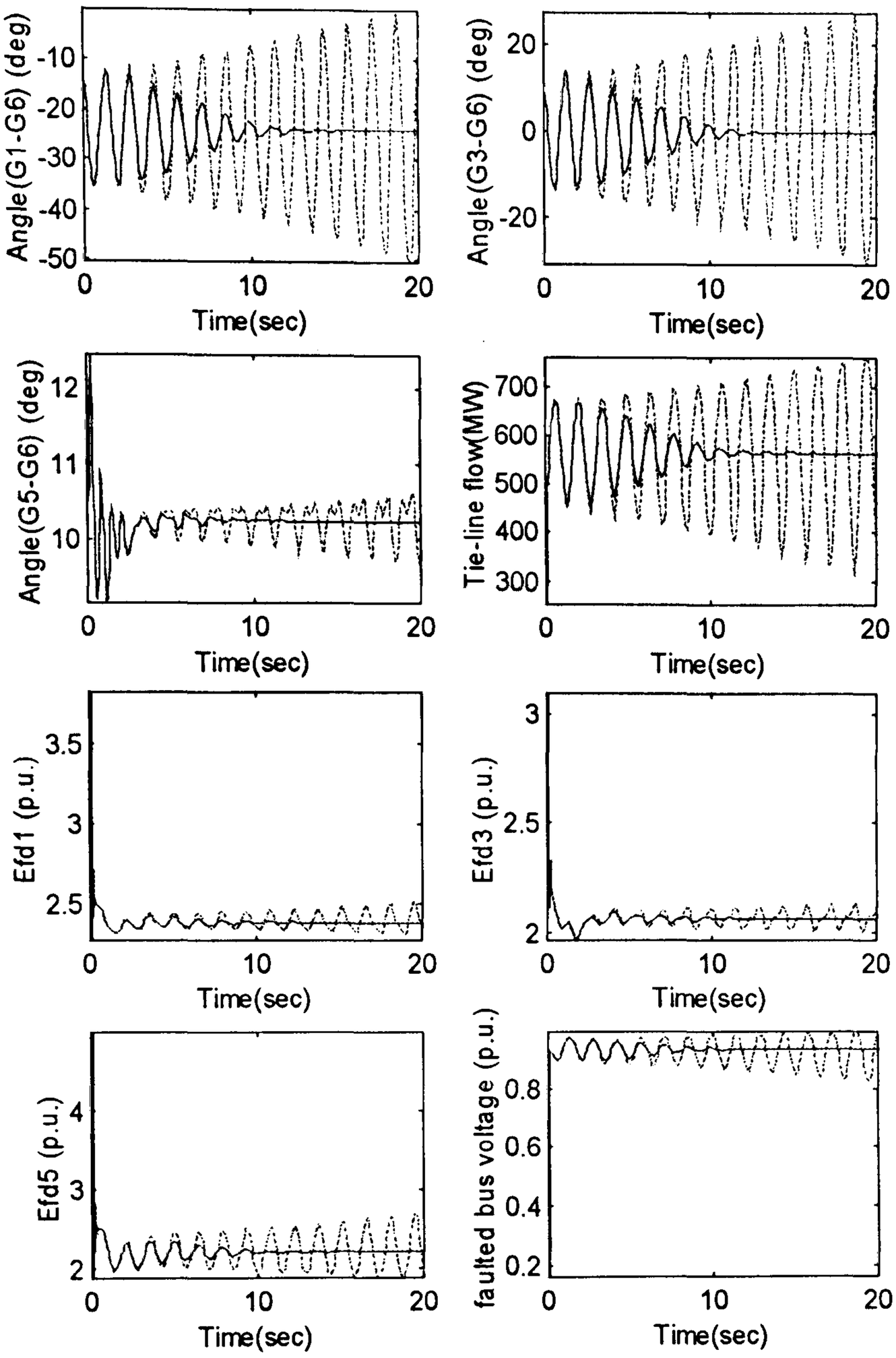

Fig 7.9: Response of Study system #2 under large disturbances
Solid line: with controller; Dashed line: without controller.

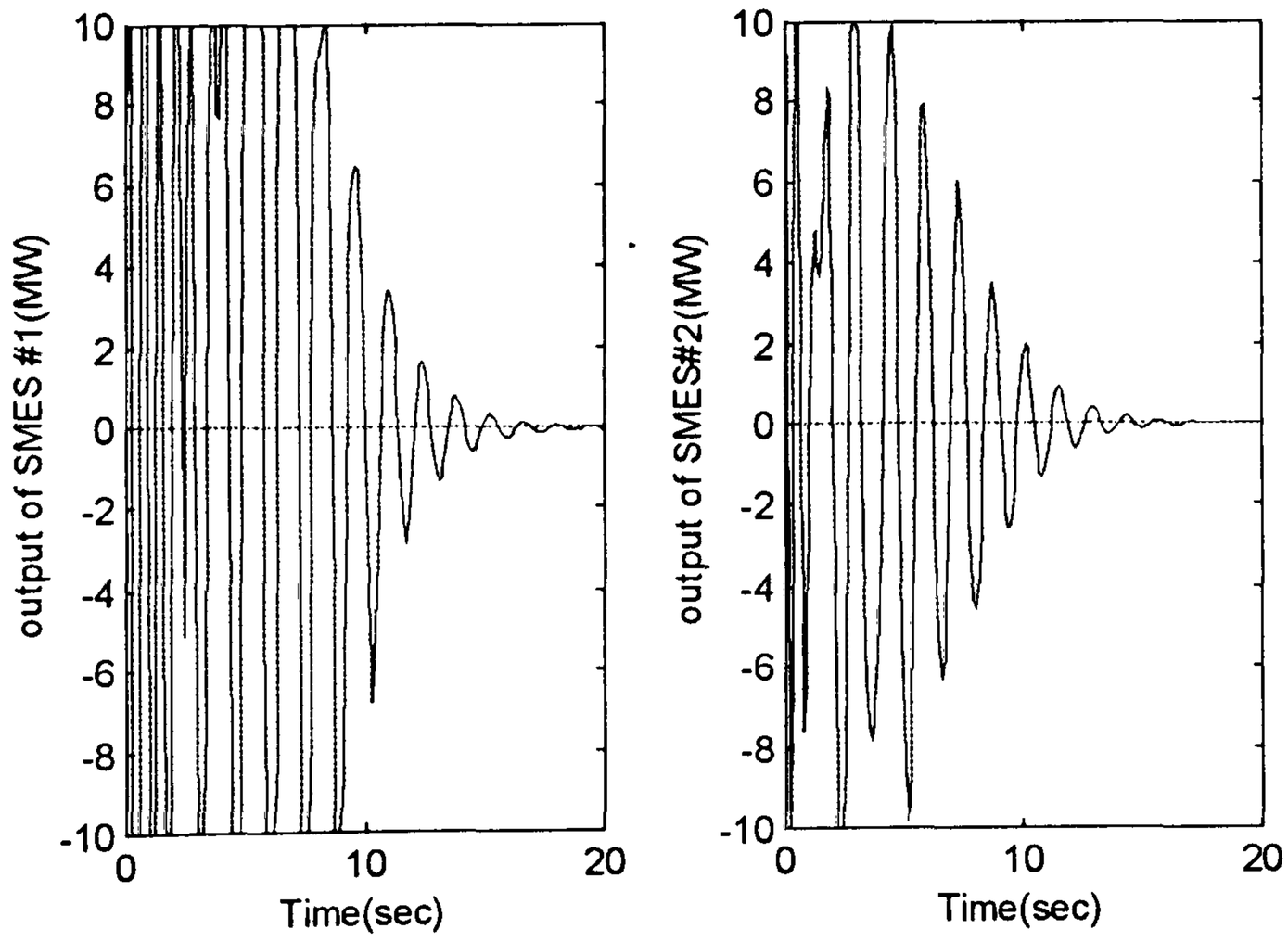

Fig 7.10: Response of SMES under large disturbance in Study system #2
Solid line: with controller; Dashed line: without controller

dynamic behaviour of Study system #2. The pre-fault and post-fault steady state operating conditions were described in Chapter Four.

It is shown that the system oscillations grow without controller action, as already investigated in Chapter Four. The actions of the controllers not only stabilise the system but ascertain damped behaviour also. The oscillations settle in this case in 10 to 12 s from the inception of the fault. The relative angular speed between G #5 and G #6 has initially higher frequency of oscillation. This is due to the effect of the local mode. The local mode oscillation settles in 2 to 3 s after which the dynamics are mainly governed by the inter-area modes. The real power outputs of the SMES units also show oscillatory response initially. The oscillations are eventually damped. In this case, it is also found that the outputs of the SMES units hit the limits.

The dynamic response of Study system #3 is plotted in Fig 7.11 and 7.12. The observation is similar to that in Study system #1 and #2. In this case, the response is very non-linear as there are four inter-area modes. The faulted bus voltage dropped to zero during fault period. The bus voltage recovered after the fault was cleared. The real power outputs of the SMES units oscillate initially within the limits. The oscillations settle down eventually in 10 to 15 s. The effect of device non-linearity and saturation, when included shows that the damping performances of the controllers in the three study systems are robust.

7.5 EVALUATION OF SMES RATINGS

The power and energy rating of the SMES units were evaluated based on the concepts described in Chapter Two. The power rating was restricted to ±10 MW. The energy rating was computed from the power trace as described in Chapter Two. It was found that the energy rating was 8.04 MJ for the SMES in Study system #1. The energy ratings of SMES #1 and #2 were 8.04 MJ and 4.77 MJ respectively in Study system #2. In Study system #3 the ratings were 10.52, 6.49 and 10.62 MJ respectively.

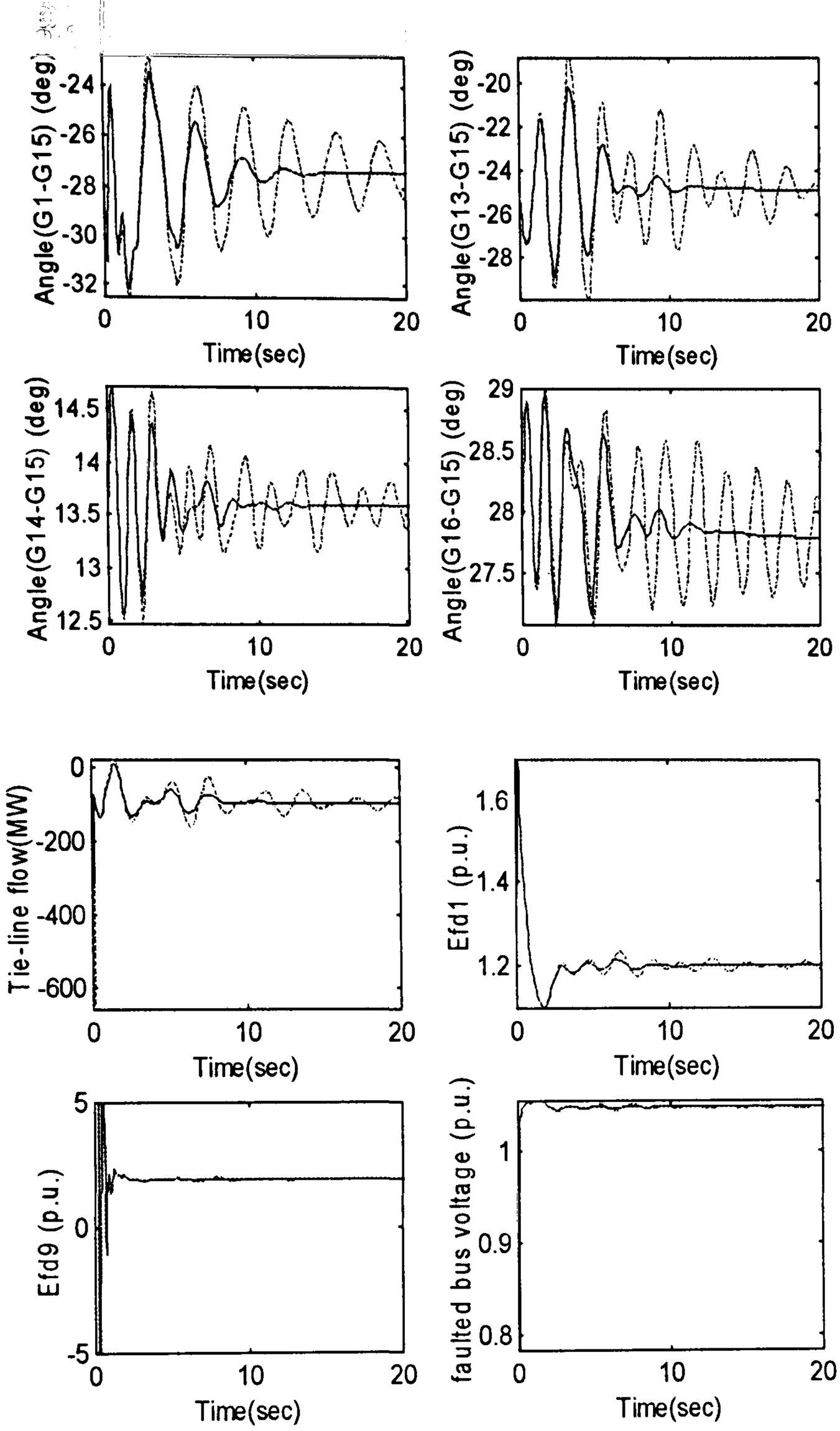

Fig 7.11: Response of Study system #3 under large disturbances
Solid line: with controller; Dashed line: without controller

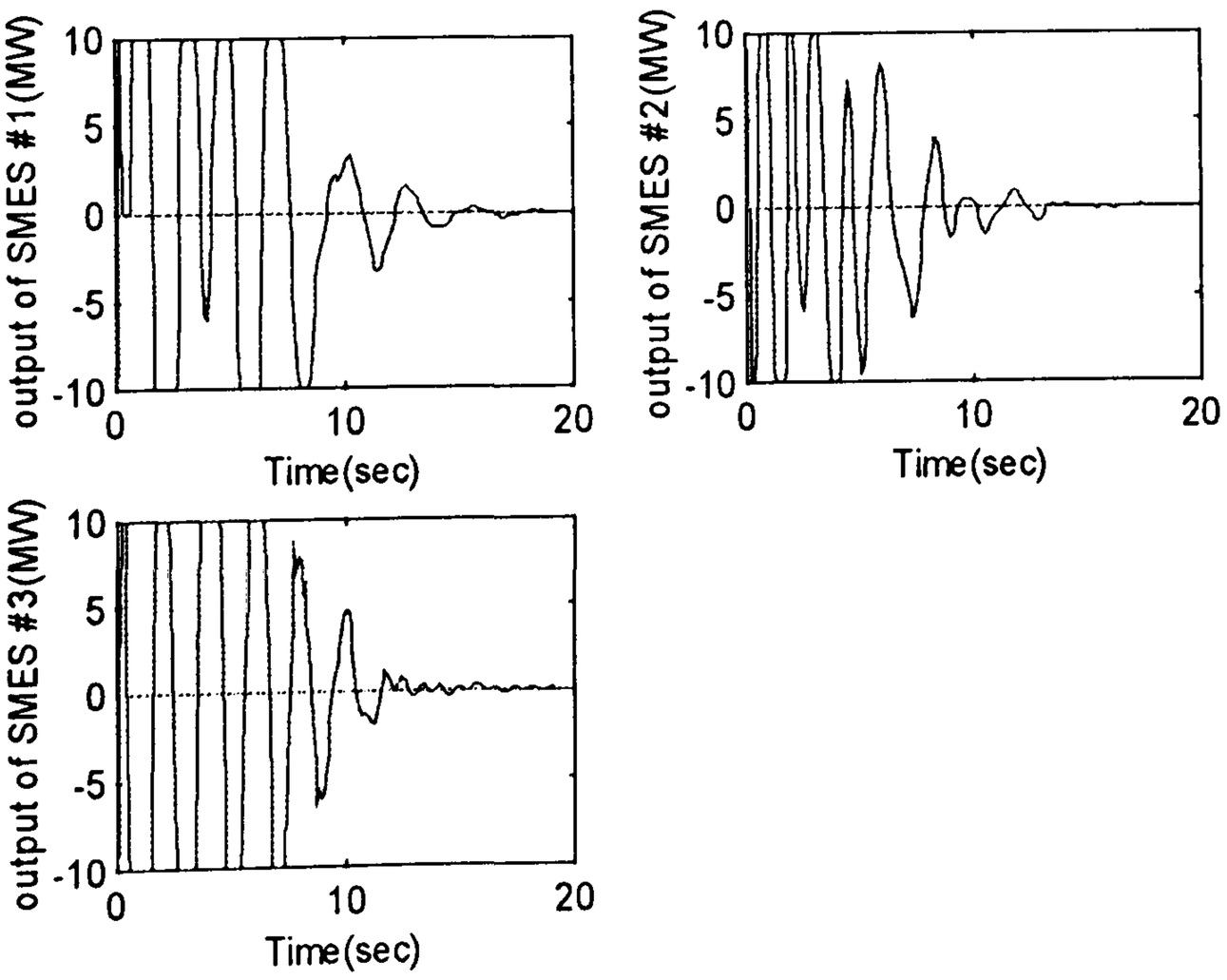

Fig 7.12: Response of SMES under large disturbance in study system #3
Solid line: with controller; Dashed line: without controller

The commercially available HTSC coils are in the range of 1-3 MJ [83]. Recent technology developments and demonstrations [83] for micro SMES (1-10 MJ) in the U.S.A. under the initiatives of the Department of Electronics (DOE), defence establishments and various other industrial houses are very encouraging. It is, therefore, highly likely that a 10 MJ SMES coil will be commercially available in the near future.

7.6 PERFORMANCE COMPARISONS

In power-system-damping-control-design, it is difficult to develop quantitative comparisons against which the performance of the controller can be tested. The reason is that the behaviour of the system during the fault is highly non-linear and it is very difficult, if not impossible, to construct the linear dynamical behaviour during the faulted period. Considering the pre-fault and post-fault steady state, the design was carried out. The comparison of the performance of a controller obtained by the WNEDM method with another controller obtained by a conventional method must be done carefully. The whole theory of controller design is based on the assumption of linear systems. So the comparison must be done for a class of disturbances that do not violate the linearised dynamical behaviour. The disturbance should be small in magnitude. In a power system, small disturbances appear very frequently. These disturbances are mainly triggered when a change in load demands takes place and they do not last beyond ten cycles (200 ms in 50 Hz. supply). The damping controller normally will respond to these small and temporary changes. The controller response should be small and smooth. A large spike on the controller outputs for small disturbances must always be avoided by careful design to prevent wear and tear of the SMES device. The controller obtained by a conventional technique does not always satisfy this property. Moreover, in a power system, a successful small-disturbance-performance simulation of the controller does not always guarantee success. The controller has to face large disturbances in reality. During the fault, the controller must not behave adversely to jeopardise the transient stability performance of the system. The output of the controller and several other devices during the fault are restricted within the limits. This is very evident from the time domain response of the system.

It has already been mentioned that a robust damping controller in a power system is one that can maintain an adequate damping ratio in the pre-fault and post-fault

steady state. If the maintenance of adequate damping against different operating cases is considered performance robustness of the controller in the frequency domain, an important question is asked: What cost is the performance robustness maintained at? In control system theory, it is a standard concept that better performance can be guaranteed with higher control effort. The amount of control effort implicitly relates to the cost of the controller. The control effort can be quantified as:

$$J = \sqrt{\int_0^\infty u(t)^2 dt} \tag{7.17}$$

where $u(t)$ is as shown in Fig. 7.1. In order to minimise J, the peak of the transfer function between 'r' and 'u' in Fig 7.1 should be minimised. This suggests a design scheme that minimises the H_∞ norm $\left\| K(1+GK)^{-1} \right\|_\infty$ [107]. It is known that the control cost can be more realistically captured through the H_2 norm [107] rather than the H_∞ norm; so in order to evaluate the control effort $\left\| K(1+GK)^{-1} \right\|_2$ should be computed.

Neither in the WNEDM method or in the root-locus based design, is the minimum control effort defined as criteria i.e. the design is not optimal so far as the cost is concerned but the cost of control can be evaluated to make a comparison between the performance and cost.

Study system #2 was considered. The controllers designed for this system are given in (7.12) and (7.13). The pre-fault and post-fault damping ratios are listed in Table 7.7. Two 2nd order controllers were designed by the root-locus method [103] for the same system for almost the same damping ratios as listed in Table 7.7. The controllers are given by:

$$K_{rl1} = 7.44\left(\frac{s^2 + 0.0085s}{s^2 + 36.30s + 51.82}\right) \tag{7.18}$$

$$K_{rl2} = 6.49\left(\frac{s^2 + 0.0067s}{s^2 + 43.27s + 0.002}\right) \tag{7.19}$$

The corresponding control efforts for these controllers were 28.34 and 28.26. The control efforts associated with the controllers in (7.12) and (7.13) were 4.83 and 1.80. The larger control effort indicates spiky response when subjected to a momentary

disturbance of small magnitude. The outputs of the controllers obtained by WNEDM and Root-locus method were evaluated for a small disturbance of 0.05 p.u. in magnitude. The duration of the disturbance was 200 ms. Disturbance was applied to the reference point of the closed-loop system (signal '*r*' in Fig. 7.1). The plots are shown in Fig. 7.13. It can be seen that the small disturbance performance of the controllers obtained by the WNEDM method are much better than those obtained by Root-locus technique in terms of system wear and tear. This indicates that in maintaining the same damping performance, the root-locus based control causes larger wear and tear of the SMES.

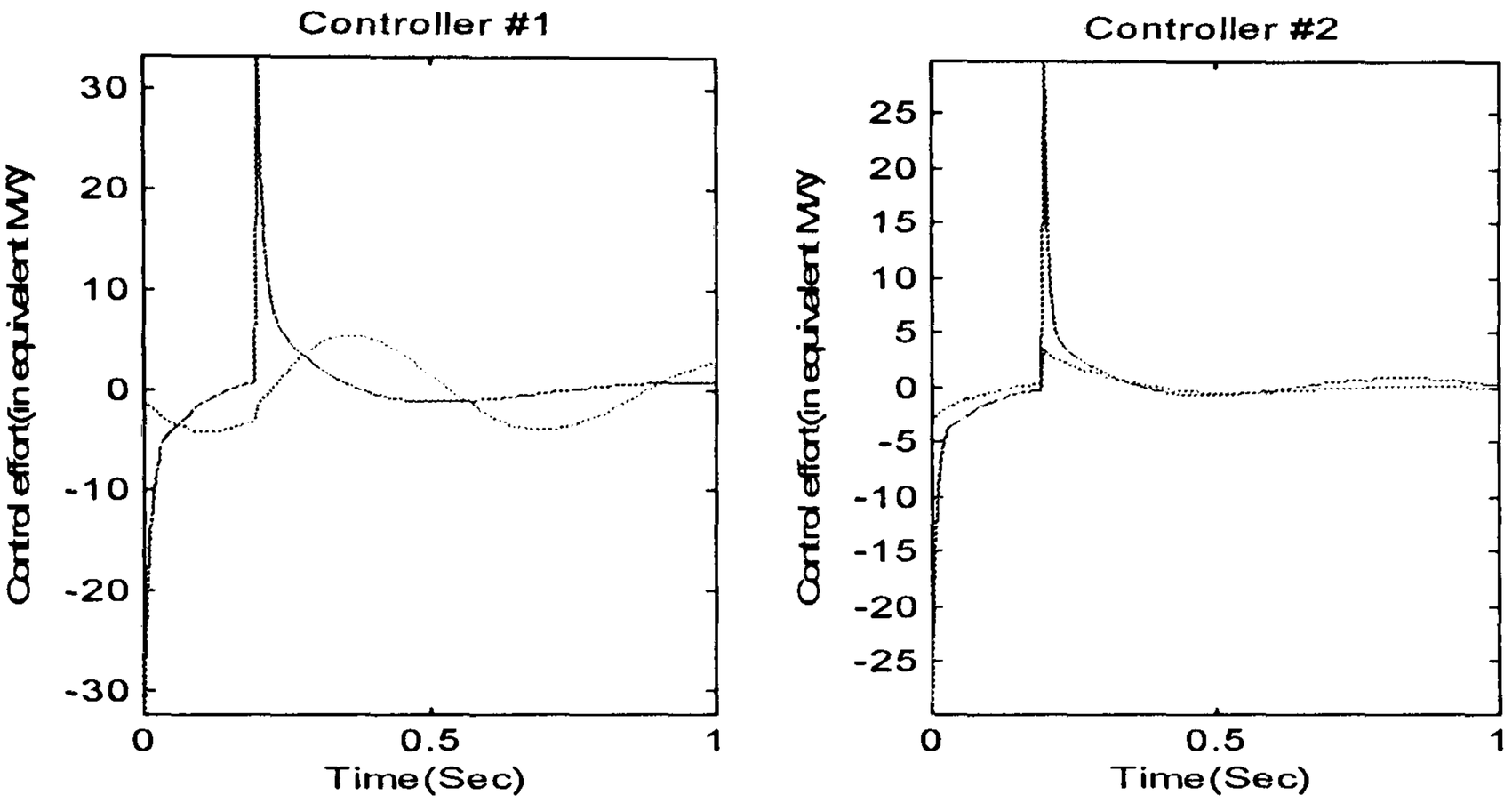

Fig 7.13: Controller response in the Study system #2 under small disturbance
(Same pre-fault damping but different control efforts).
Solid line: Response when Root-locus based controllers are connected
Dotted line: Response when WNEDM based controllers are connected

The damping performance of the controllers in (7.18) and (7.19) was investigated for the same control effort in both methods. This was done while the gain of the controllers in (7.18) and (7.19) was reduced to make the control effort equal to that of the controllers in (7.12) and (7.13). The new gains of the controllers in (7.18) and (7.19) were 1.04 and 0.37 respectively. The damping ratio in the pre-fault and post-fault conditions were computed and displayed in Table 7.15. The damping ratios obtained by the WNEDM based controllers are also listed on the Table 7.15 for comparison.

Table 7.15: Comparison of damping ratios obtained by two control design techniques

Mode No.	Open-loop (pre-fault)		closed-loop (pre-fault) WNEDM based control		closed-loop (pre-fault) Root-Locus based control		Open-loop (post-fault)		closed-loop (post-fault) WNEDM based control		closed-loop (post-fault) Root-Locus based control	
	ζ	f (Hz)	ζ	f (Hz)	ζ	f (Hz)	ζ	f (Hz)	ζ	f (Hz)	ζ	f (Hz)
#1	0.000	0.82	0.209	0.89	0.032	0.82	-0.01	0.69	0.114	0.70	0.010	0.69
#2	0.027	1.15	0.145	1.14	0.045	1.15	0.027	1.13	0.116	1.15	0.038	1.14

Table 7.15 shows that the WNEDM based controllers provide damping ratios of 0.209 and 0.145 in the pre-fault case for the control efforts of 4.83 and 1.80 respectively. The controllers obtained by the Root-locus design provide damping ratios of 0.032 and 0.045 in the pre-fault case for the same control efforts. This means that the WNEDM based controllers are better than that obtained by the root-locus method. The observation is similar for the post fault case also. The dynamic response of the system with two different sets of controllers were computed and plotted in Fig 7.14. The plots show that the WNEDM based controller provides better performance of the system than that by the controllers obtained by the Root-locus method.

The energy rating of the SMES units were computed. They were found 4.46 and 1.10 MJ respectively. The corresponding rating of the SMES units with WNEDM based controllers are 8.04 and 4.77 MJ respectively. Both sets of the controllers have the same control efforts but different ratings. This is due to the highly non-linear dynamical behaviour of the system. This means that the control effort defined as the H_2 norm is only realistic from the perspective of power system damping performance evaluations under small disturbance. In the large disturbance case, it is very important that the controller settles the oscillations in 10 to 15 s after the fault inception. The actual rating should be evaluated from the non-linear response of the system under worst contingency (disturbance) conditions.

The main objective of damping control design in the power system is that the controller must ensure adequate damping at different operating conditions. The adequacy of the damping is governed by the time to settle the oscillations following a large disturbance, including a short circuit, at the critical location of the system. In addition to this, the damping controllers must not interfere with the transient stability performance of the system during the fault. This objective can be achieved by conventional methods such as Root-locus, pole-placement, Bode design etc. These classical methods are also robust to some extent although the degree of robustness may be less than that by a controller obtained by a robust control method. The difference of these methods with the WNEDM is that the latter method considers all of the possible operating conditions during controller design but the classical methods do not. It can, in general, be said that the WNEDM method will always guarantee adequate robust damping performance whereas

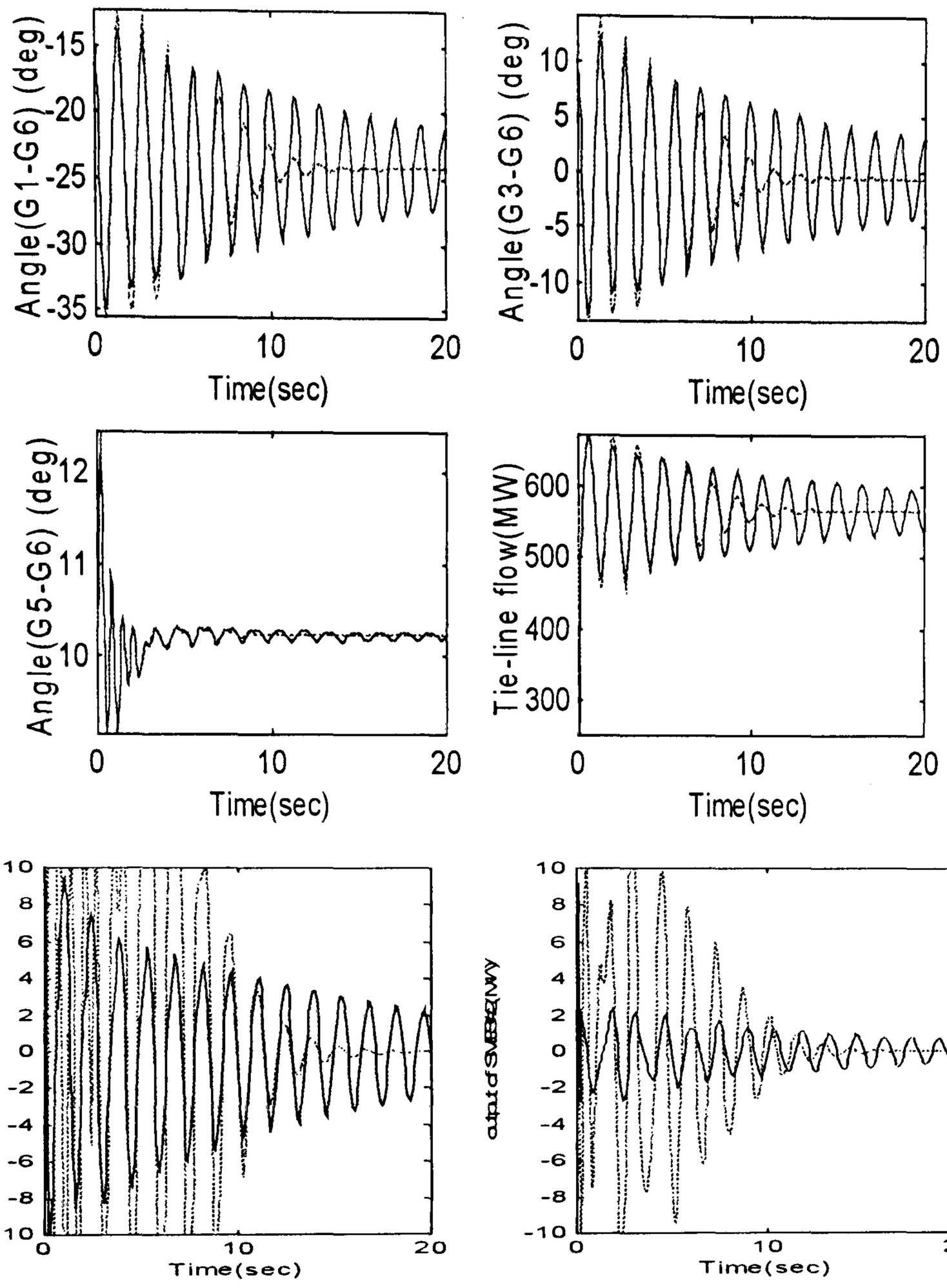

Fig 7.14: Dynamic response of the Study system #2 under large disturbances
(Same control efforts but different pre-fault damping).
Solid line: Response when Root-locus based controllers are connected
Dotted line: Response when WNEDM based controllers are connected

classical methods may fail to provide this at some operating condition. The control effort in the conventional method can be unusually high thus posing wear and tear problems for the SMES during small disturbances. This is a serious drawback with the Root-locus method. In general, the incidence of large disturbances in the system is not as frequent as the small disturbance. Although the damping controller has to withstand a large disturbance, the repeated occurrence of small disturbance will shorten the life cycle of the SMES if the controller has a large control effort such as the one obtained by the Root-locus method. It is always possible to design a robust controller with reduced

control effort using trial and error improvement strategies in classical techniques. The gain and phase margin concept in Bode design is an ideal example. The goal that can be achieved through a trial and error improvement strategy in classical control design can easily be achieved by the WNEDM method in a very systematic and methodical way. Robustness is guaranteed once the optimisation algorithm provides the solutions. In the light of the above discussion, it can be said that the WNEDM method is an alternative method to robust control design.

The control efforts were computed for the controllers in Study system #1 and #3. The observation is similar to that of Study system #2.

7.7 SUMMARY AND CONCLUSIONS

The WNEDM method is described in detail. The method is modified to provide stable damping controllers for power systems by including suitable constraints. The practical aspects of weight selections are also discussed. Some representative weights have been suggested. It is shown that these sets of weights works well for the three study systems under test. In view of this, it can be said that these weights are standard and not system specific as far as the power system damping design employing real power modulation of the SMES is concerned. The WNEDM method works very efficiently and successfully if the locations of the closed-loop poles are realistic. Once the best location and most effective feedback signals are decided, the order of the system is reduced drastically and then the method is applied for the controller design. Amongst the various model reduction techniques, the balanced residualisation technique provides the least model reduction error in Study system #1 and the balanced truncation system provides the least model reduction errors in Study system #2 and #3. It is observed that the superiority of a particular model reduction method is system specific; so no suggestions are made as to the use of a particular model reduction technique.

The damping control design problem is formulated as an optimisation problem. The SQP technique is adopted to solve the problem. The essential features of the SQP are also discussed.

The damping controller is designed for study systems #1, #2, #3. Study system #2 and #3 have multiple inter-area modes. More than one SMES devices have been used. The sequential decentralised design technique has been used to provide damping to all of the modes, one at a time.

The performance robustness of the controllers were evaluated at different operating conditions (pre-fault and post-fault), different levels of power flow through the tie lines and with different load characteristics. It is seen that the controllers are very robust. The controller designed for a particular inter-area mode does not interfere with the damping of other local, inter-area, exciter, controller mode etc. The controllers do not influence the transient stability performance of the system as are evidenced from the non-linear simulations of the systems under large disturbances. The controllers maintain adequate damping in the face of system non-linearity and device saturation.

Meaningful discussions are made when comparing the performances of the controllers with the performances provided by other controllers obtained by conventional techniques. To achieve the same damping performance, the control effort, required by the WNEDM based control, is generally less. It is shown, through simulations, that in the WNEDM based control, a small disturbance in the system can cause very little wear and tear of the SMES. This is not true with the root-locus control. However, it is possible to design a low order robust control employing classical techniques with a repeated trial and error improvement strategy. The WNEDM is introduced to power system damping control design practice as a methodical and systematic robust damping control design method.

CHAPTER EIGHT

DESIGN OF ROBUST DAMPING CONTROLLER- AN LMI APPROACH

8.1 INTRODUCTION

In this chapter, the design of a power system damping controller is proposed based on the Linear Matrix Inequalities (LMI) technique. The LMI based robust damping controller design methodology takes the transient response specifications into consideration in addition to the frequency domain specifications such as disturbance rejection, robust tracking, gain roll-off rate around the desired frequency band etc. The basic concept of robust controller design in an LMI framework with regional pole-placement objectives is discussed. The methodology is applied to the design of a damping controller for three study systems. The performance of the controller is verified through non-linear simulations under large disturbances.

8.2 LMIs – A BRIEF MATHEMATICAL OVERVIEW

A linear matrix inequality (LMI) is any constraint of the form [119].

$$A(x) := A_0 + x_1 A_1 + \ldots + x_N A_N < 0 \tag{8.1}$$

where, $\mathbf{x} = (x_1, x_2 \ldots x_N)$ is a vector of unknown scalars (the decision or optimisation variable), $A_0, \ldots A_N$ are given symmetric matrices, " < 0" stands for "negative definite", i.e. the largest eigenvalue of $A(x)$ is negative. The LMI in (8.1) is a convex constraint on $\mathbf{x}$ since $A(y) < 0$ and $A(z) < 0$ implies that $A[\varepsilon y + (1-\varepsilon)z] < 0, \ \forall \varepsilon \in [0,1]$

As a result,

- its solution set, called the *feasible set,* is a convex subset of $\mathbf{R}^N$
- finding a solution $\mathbf{x}$ to (8.1) ,if any, is a convex optimisation problem

Convexity has an important consequence: even though (8.1) has no analytical solution in general, it can be solved numerically with guarantees of finding a solution when one exists. Note that a system of LMI constraints can be regarded as a single LMI since $A_1(x) < 0, A_2(x) < 0, A_3(x) < 0 \ldots A_k(x) < 0$ is equivalent to $A(x) := diag(A_1(x), \ldots, A_k(x)) < 0$ where $diag(A_1(x), \ldots, A_k(x))$ denotes the block-

diagonal matrix with $A_1(x),\ldots,A_k(x)$ on its diagonal. Hence, multiple LMI constraints can be imposed on the vector of decision variables **x** without destroying convexity. In most control applications, LMI does not naturally arise in the canonical form (8.1), but rather in the form:

$$L(X_1,\ldots,X_n) < R(X_1,\ldots,X_n)$$

where, $L(.)$ and $R(.)$ are affine functions of some structured matrix variables $X_1,\ldots,X_n$. A simple example is the Lyapunov inequality:

$$A^T X + XA < 0 \tag{8.2}$$

where, the unknown X is a symmetric matrix. Defining $x_1,\ldots..x_N$ as the independent scalar entries of X, this LMI could be rewritten in the form (8.1). However it is more convenient and efficient to describe it in its natural form (8.2), which is the approach followed here.

Many control problems and design specifications have LMI formulations. This is especially true for Lyapunov based analysis and design and also for optimal LQG control, H-infinity control, robust pole-placement, covariance control, etc. Further applications of LMIs arise in estimation, identification, optimal design, structural design, matrix scaling problems, and so on. The main strength of the LMI formulation is the ability to combine various design constraints or objectives in a numerically tractable manner. Consider the dynamical system

$$\dot{\mathbf{x}} = A\mathbf{x} \tag{8.3}$$

The stability of the dynamical system (8.3) is equivalent to the feasibility of:

$$\text{Find } P = P^T \text{ such that } A^T P + PA < 0,\ P > 0.$$

This can be generalised to linear differential inclusions (LDI)

$$\dot{\mathbf{x}} = A(t)\mathbf{x} \tag{8.4}$$

where, $A(t)$ varies in the convex envelope of a set of LTI models:

$$A(t) \in Co\{A_1,\ldots A_n\} = \left\{\sum_{i=1}^{i=n} \alpha_i A_i : \alpha_i \geq 0, \sum_{i=1}^{i=n} \alpha_i = 1\right\} \tag{8.5}$$

A sufficient condition for the asymptotic stability of this LDI is the feasibility of:

$$\text{Find } P = P^T \text{ such that } A_i^T P + PA_i < 0,\ P > 0.$$

8.3 LMIs AND THEIR APPLICATION TO THE CONTROL DESIGN PROBLEM

The state-space approach to multivariable control design is a mature concept [107,108,120,121]. There have been various improvements and extensions to the state-space solution of the H_∞ central controller originally proposed by Doyle *et.al.* [122]. The basic task in H_∞ control centres on the solution of the relevant algebraic Riccati equation (ARE). The solvability of the ARE requires some assumptions as to the nature of the augmented plant. The plant should be 'regular', i.e. transfer functions from controls to controlled outputs and from disturbance to measured outputs have no invariant zeros at infinity or on the imaginary axis. Although some of these problems can be overcome in an extended version of the basic solution to the central controller, the case of the imaginary axis zeros remain problematic especially when reasonable closed-loop damping is required. Of particular concern is the pole-zero cancellation in a mixed sensitivity based problem formulation [123]. Pole-zero cancellations ensure the absence of the influence of the cancelled plant pole in the selected input-output pair. But it can manifest itself elsewhere in the system. If the cancelled pole is a poorly damped one, oscillations will be observed in the response of some other outputs when the time domain simulation is performed. A power system is a typical example where it is highly undesirable if the cancelled pole is a poorly damped electromechanical mode.

All of the above mentioned problems and restrictions encountered in a Riccati based design can be avoided if H_∞ constraints are translated into suitable LMIs and these LMIs are solved through any suitable convex optimisation techniques. In recent years LMIs have emerged as a powerful formulation and design technique for linear robust control problems [124-127]. As solving LMIs is a convex optimization problem, such formulations offer a numerically tractable means of solving problems that lack analytical solution.

Many classical control objectives in the frequency domain, such as, disturbance rejection, noise attenuation, gain roll-off rate in the desired frequency range can be addressed by a Riccati based H_∞ design. But some of the objectives in the time domain, such as, settling time, transient response may be best obtained by the LMI formulation. The placement of the closed-loop poles in a specific region of the left-half plane (LHP) for controlling the damping ratio is possible in LMI. Any convex region in the eigen-

plane can be analytically expressed as an LMI region. This is a great advantage with LMIs as it addresses the mixed objectives in the time and frequency domains. From the requirement of power-system-damping-control design this multi-objective feature of LMIs can be exploited to its full potential.

8.4 LMI FORMULATIONS OF THE MIXED-SENISITIVITY H_∞ DESIGN WITH ADDITIONAL POLE-PLACEMENT CONSTRANITS

Consider the standard mixed sensitivity set up as shown in Fig. 8.1.

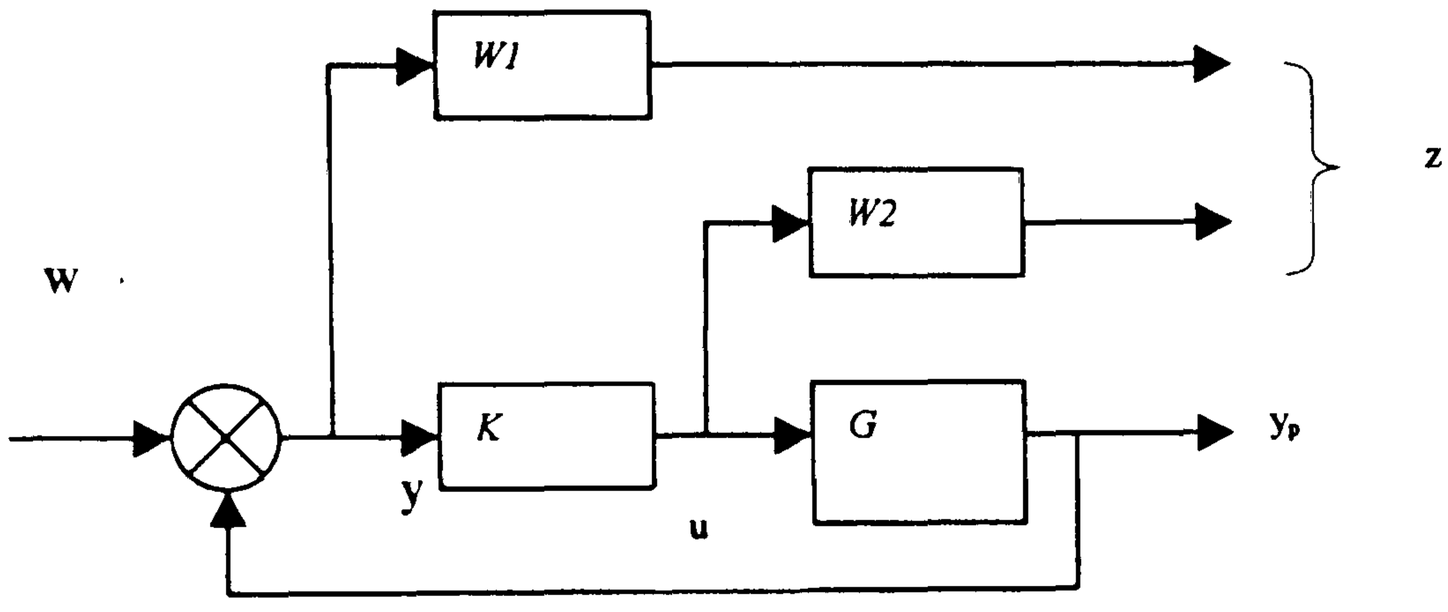

Fig. 8.1: Standard mixed sensitivity design set up.

G is the open-loop plant, K is the controller to be designed and W_1 and W_2 are weights. This design minimises a weighted mix of the transfer function $S = (I - GK)^{-1}$ that ensures disturbance attenuation and good tracking; $KS = K(I - GK)^{-1}$ that handles the robustness issues and constrains the controller effort. This mixed sensitivity (S/KS) design objective is represented as:

$$\left\| \begin{matrix} W_1 S \\ W_2 KS \end{matrix} \right\|_\infty \leq \gamma$$

where, 'γ' is the bound on H_∞ norm. Details of the mixed sensitivity control design can be found in [107]. The state-space description of the system above can be written as:

$$\dot{\mathbf{x}} = A\mathbf{x} + B_1\mathbf{w} + B_2\mathbf{u} \tag{8.6}$$

$$\mathbf{z} = C_1\mathbf{x} + D_{11}\mathbf{w} + D_{12}\mathbf{u} \tag{8.7}$$

$$\mathbf{y} = C_2\mathbf{x} + D_{21}\mathbf{w} + D_{22}\mathbf{u} \tag{8.8}$$

The controller K can also be described in state-space form:

$$\dot{\mathbf{x}}_k = A_k \mathbf{x}_k + B_k y \tag{8.9}$$

$$u = C_k \mathbf{x}_k + D_k y \tag{8.10}$$

D_{22} is dependent on the input-output relationship of the plant. For the small signal model of the SMES described in earlier chapters with line power as the stabilising feedback signal, the plant becomes strictly proper resulting in $D_{22} = 0$. Other FACTS devices with a specific choice of the stabilising feedback signal may result in a non-zero D_{22}. In those cases, the design can be carried out considering the plant as strictly proper (setting $D_{22} = 0$) and the resulting controller, K can be modified later to include the effect of D_{22} by $\hat{K} = K(I - D_{22}K)^{-1}$ [120]. So, without loss of generality, D_{22} can be set to zero making the derivation simpler.

The transfer function between *'w'* and *'z'* can be described as:

$$T_{zw} = \left\| \begin{matrix} W_1 S \\ W_2 KS \end{matrix} \right\| = C_{cl}(sI - A_{cl})^{-1} B_{cl} + D_{cl} \tag{8.11}$$

where,

$$A_{cl} = \begin{bmatrix} A + B_2 D_k C_2 & B_2 C_k \\ B_k C_2 & A_k \end{bmatrix};\ B_{cl} = \begin{bmatrix} B_1 + B_2 D_k D_{21} \\ B_k D_{21} \end{bmatrix}$$

$$C_{cl} = \begin{bmatrix} C_1 + D_{12} D_k C_2 & D_{12} C_k \end{bmatrix};\ D_{cl} = D_{11} + D_{12} D_k D_{21}$$

The objective of the mixed sensitivity minimisation is to find an internally stabilising controller that minimises $\left\| \begin{matrix} W_1 S \\ W_2 KS \end{matrix} \right\|_\infty$. In LMI formulation [124], the same objective is achieved in the sub-optimal sense if there exists an $X = X^T > 0$ such that:

$$\begin{pmatrix} A_{cl}^T X + X A_{cl} & B_{cl} & X C_{cl}^T \\ B_{cl}^T & -I & D_{cl}^T \\ C_{cl} X & D_{cl} & -\gamma^2 I \end{pmatrix} < 0 \tag{8.12}$$

with $\left\| C_{cl}(sI - A_{cl})^{-1} B_{cl} + D_{cl} \right\|_\infty < \gamma$; and the controller is said to be γ sub-optimal.

It is known that the transient response of a linear system is related to the location of its poles. For example, the step response of a second-order system with poles $\lambda = -\varsigma\omega_n \pm j\omega_d$ is fully characterised in terms of the undamped natural frequency $\omega_n = |\lambda|$, the damping ratio ς and the damped natural frequency ω_d. Acceptable transient response can be achieved by placing all of the closed-loop poles inside a conic sector as shown in Fig. 8.2.

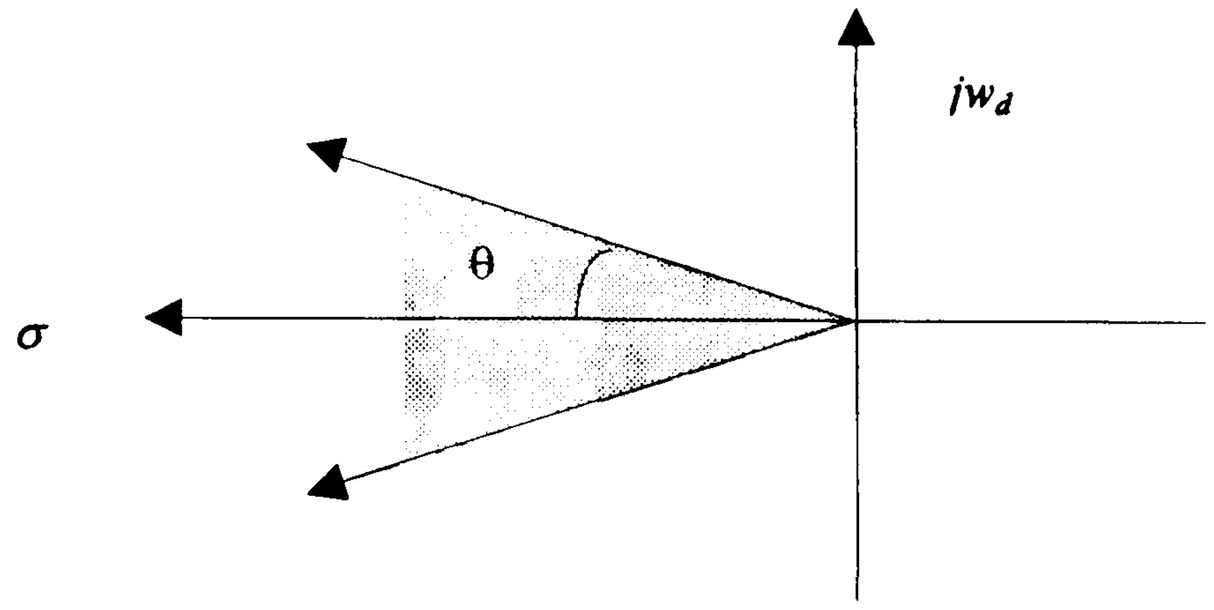

Fig 8.2: Region for the closed loop poles with minimum damping ratio $cos\theta$

The damping ratio of all the poles lying inside the sector is guaranteed to have minimum damping ratio $\varsigma = cos\,\theta$.

The LMI characterisation of the conical sector is straightforward. It is shown in [126] that the state matrix, A_{cl} of the closed loop system, has all of its poles inside this conical sector if and only if there exists $X_p = X_p^T > 0$ such that:

$$\begin{bmatrix} sin\theta\left(A_{cl}X_p + X_pA_{cl}^T\right) & cos\theta\left(A_{cl}X_p - X_pA_{cl}^T\right) \\ cos\theta\left(X_pA_{cl}^T - A_{cl}X_p\right) & sin\theta\left(A_{cl}X_p + X_pA_{cl}^T\right) \end{bmatrix} < 0. \qquad (8.13)$$

This can be expressed in Kronecker product form [120]:

$$\left[\eta \otimes A_{cl}X_p + \eta^T \otimes X_pA_{cl}^T\right] < 0 \qquad (8.14)$$

where, $\eta = \begin{pmatrix} sin\theta & cos\theta \\ -cos\theta & sin\theta \end{pmatrix}$

The two inequalities in (8.12) and (8.14) are not jointly convex as they can admit two different solutions ($X_\infty \neq X_p$). In order to enforce joint convexity, a common solution, $X_\infty = X_p = X$, can be sought with a certain degree of conservatism. The problem,

therefore, reduces to the minimisation of γ under H_∞ and the pole-placement constraints. Inequalities in (8.12) and (8.14) contain $A_\alpha X$, $C_\alpha X$ i.e. products of X and the controller variables. The resulting problem is therefore non-linear and so it cannot be handled by LMI optimisation directly. To make it linear, a change of controller variables is necessary. This is performed in [126,127] as follows:

Let X and X^{-1} be partitioned as:

$$X = \begin{pmatrix} R & M \\ M^T & * \end{pmatrix} \text{ and } X^{-1} = \begin{pmatrix} S & N \\ N^T & * \end{pmatrix}$$

where R and S are n x n symmetric matrices and '*' denotes an expression not relevant for the present purpose. From the identity $XX^{-1} = I$, it can be inferred that $X\begin{pmatrix} S \\ N^T \end{pmatrix} = \begin{pmatrix} I \\ 0 \end{pmatrix}$ which leads to $X\Pi_2 = \Pi_1$ with $\Pi_1 := \begin{pmatrix} R & I \\ M^T & 0 \end{pmatrix}$, $\Pi_2 := \begin{pmatrix} I & S \\ 0 & N^T \end{pmatrix}$. The new controller variables are defined as [127]:

$$\hat{A} = NA_kM^T + NB_kC_2R + SB_2C_kM^T + S(A + B_2D_kC_2)R \tag{8.15}$$

$$\hat{B} = NB_k + SB_2D_k \tag{8.16}$$

$$\hat{C} = C_kM^T + D_kC_2R \tag{8.17}$$

$$\hat{D} = D_k. \tag{8.18}$$

If M and N are of full row rank and if $\hat{A}, \hat{B}, \hat{C}, \hat{D}, R, S$ are given, the controller variable A_k, B_k, C_k, D_k can be computed from equations in (8.15)-(8.18). Moreover, if M and N are square (k=n) and invertible matrices, then A_k, B_k, C_k, D_k are unique. For full order controller design, one can always assume that M and N have full row rank. Hence, the variables A_k, B_k, C_k, D_k can always be replaced by $\hat{A}, \hat{B}, \hat{C}, \hat{D}$, without loss of generality.

Now pre-multiplying and post-multiplying the inequality $X > 0$ by $\Pi_2{}^T$ and Π_2, inequality (8.12) by diag (Π_2^T, I, I) and diag(Π_2, I, I), inequality (8.14) by $\Pi_2{}^T$ and Π_2, and performing the necessary change of controller variables as defined in (8.15)-(8.18), the following LMIs result:

$$\begin{pmatrix} R & I \\ I & S \end{pmatrix} > 0 \tag{8.19}$$

$$\begin{bmatrix} \Psi_{11} & \Psi_{21}^T \\ \Psi_{21} & \Psi_{22} \end{bmatrix} < 0 \tag{8.20}$$

$$\left[\eta \otimes \Phi + \eta^T \otimes \Phi^T\right] < 0 . \tag{8.21}$$

The variables in (8.19)-(8.21) are given by:

$$\Psi_{11} = \begin{bmatrix} \boldsymbol{AR} + \boldsymbol{RA}^T + \boldsymbol{B}_2\hat{\boldsymbol{C}} + \hat{\boldsymbol{C}}^T\boldsymbol{B}_2^T & \boldsymbol{B}_1 + \boldsymbol{B}_2\hat{\boldsymbol{D}}\boldsymbol{D}_{21} \\ \left(\boldsymbol{B}_1 + \boldsymbol{B}_2\hat{\boldsymbol{D}}\boldsymbol{D}_{21}\right)^T & -\gamma\boldsymbol{I} \end{bmatrix}$$

$$\Psi_{21} = \begin{bmatrix} \hat{\boldsymbol{A}} + \left(\boldsymbol{A} + \boldsymbol{B}_2\hat{\boldsymbol{D}}\boldsymbol{C}_2\right)^T & \boldsymbol{S}\boldsymbol{B}_1 + \hat{\boldsymbol{B}}\boldsymbol{D}_{21} \\ \boldsymbol{C}_1\boldsymbol{R} + \boldsymbol{D}_{12}\hat{\boldsymbol{C}} & \boldsymbol{D}_{11} + \boldsymbol{D}_{12}\hat{\boldsymbol{D}}\boldsymbol{D}_{21} \end{bmatrix}$$

$$\Psi_{22} = \begin{bmatrix} \boldsymbol{A}^T\boldsymbol{S} + \boldsymbol{S}\boldsymbol{A} + \hat{\boldsymbol{B}}\boldsymbol{C}_2 + \boldsymbol{C}_2^T\hat{\boldsymbol{B}}^T & \left(\boldsymbol{C}_1 + \boldsymbol{D}_{12}\hat{\boldsymbol{D}}\boldsymbol{C}_2\right)^T \\ \boldsymbol{C}_1 + \boldsymbol{D}_{12}\hat{\boldsymbol{D}}\boldsymbol{C}_2 & -\gamma\boldsymbol{I} \end{bmatrix}$$

where, $\Phi = \begin{pmatrix} \boldsymbol{AR} + \boldsymbol{B}_2\hat{\boldsymbol{C}} & \boldsymbol{A} + \boldsymbol{B}_2\hat{\boldsymbol{D}}\boldsymbol{C}_2 \\ \hat{\boldsymbol{A}} & \boldsymbol{S}\boldsymbol{A} + \hat{\boldsymbol{B}}\boldsymbol{C}_2 \end{pmatrix}$.

The LMI in (8.19 to 8.21) can be solved for $\hat{\boldsymbol{A}}, \hat{\boldsymbol{B}}, \hat{\boldsymbol{C}}, \hat{\boldsymbol{D}}, \boldsymbol{R}, \boldsymbol{S}, \Psi_{11}, \Psi_{21}, \Psi_{22}$. Once $\hat{\boldsymbol{A}}, \hat{\boldsymbol{B}}, \hat{\boldsymbol{C}}, \hat{\boldsymbol{D}}, \boldsymbol{R}, \boldsymbol{S}$ are known, $\boldsymbol{A}_k, \boldsymbol{B}_k, \boldsymbol{C}_k, \boldsymbol{D}_k$ can be evaluated from equations (8.15-8.18).

It is interesting to note that the LMI formulation of the mixed sensitivity based design objective along with the pole-placement objective in a desired region is appealing from a practical viewpoint. The H_∞ constraints, especially minimising $\left|\boldsymbol{W}_1(\boldsymbol{I} - \boldsymbol{GK})^{-1}\right|_\infty$ addresses the output disturbance rejection aspect and $\left|\boldsymbol{W}_2\boldsymbol{K}(\boldsymbol{I} - \boldsymbol{GK})^{-1}\right|_\infty$ addresses the minimum control effort and robust stability in the face of additive uncertainty in the plant [107]. The LMI in (8.21) guarantees a minimum damping ratio.

The numerical solution to the problem is always possible if the problem is feasible. Recently, many efficient specialised algorithms [128-133] have been reported in the literature to solve the control design problems via LMI formulations. In this research, the polynomial time projective algorithm is used to solve the LMIs in (8.19) to (8.21) as it is readily available in the *LMI Control Toolbox* [134] for use with Matlab [101].

8.5 FACTORS INFLUENCING LMI BASED DAMPING CONTROL DESIGN

The success of LMI based damping control design is heavily dependent on the shaping of the open-loop plant. The solution time is very much dependent on the order of the plant. These factors are discussed in brief before the design results for the Study systems are reported.

8.5.1 SELECTION OF WEIGHTS

Robust damping control design in electrical power systems is a problem of a very special nature. It is highly unsatisfactory if the damping controller modifies the natural frequencies of the electromechanical modes of the system drastically. This can have devastating consequences on the transient stability performance of the system. So the requirement is to shift the eigenvalues associated with electromechanical modes further left in the eigen-plane without significantly changing their imaginary components. In a Riccati based approach, it is very difficult to shape the open-loop transfer function of the system by the use of weighting functions to design the controller to achieve the desired shift in the eigen-plane. If the weights are not properly selected, the overall problem formulation fails to satisfy solvability conditions and the Riccati solver in MATLAB does not provide solutions. After repeated reformulation by way of adjusting the weights, it can be possible to obtain a solution, but the controller may not be successful in damping the electromechanical modes. This is due to the pole-zero cancellation already discussed in an earlier section. There have been several publications on H_∞ based damping control design for power systems in the last few years [100,110,135,136], but the methodologies of weight selections still lack clarity. The relationship between the open-loop electromechanical modes and the parameters of the weighting functions is still not clear. An attempt is made here to make the weight selection methodical and standard.

The standard design practice in H_∞ control design is to choose W_1, a high gain low-pass filter for output disturbance rejection. W_2 should be a high-pass filter in order to reduce the control effort in the high-frequency range. There should also be a low-pass filter to ensure robustness due to variation in plant model because of varying operating conditions. So there is a conflict in the nature of W_2 to ensure robustness and minimise control effort. The pole-placement objective can also be incorporated with the minimum

damping ratio. The typical frequency response of W_1 and W_2 is shown in Fig. 8.3. The 4th order reduced model of Study system #1 with SMES located at bus #10 was used before the augmentation with weights. The *'hinfmix'* function available in the *LMI toolbox* [134] was used. The pole-placement objective with minimum damping ratio of 0.10 was also incorporated as an additional LMI constraint. The controller obtained was of 12th order (order of the augmented plant). The controller was satisfactory for the reduced order plant but failed to maintain the stability for the original plant. Some of the small eigenvalues of the plant migrated to the right half of the eigen-plane. It was found that the controller had a high gain in the frequency range (0.001 to 0.1 Hz). The damping controller designed based on Root locus or WNEVDM method discussed earlier had a lower gain in that frequency range. So the weighting functions W_1 and W_2 were modified to ensure that controller had a low gain in that frequency range. The singular value response of W_1 and W_2 in modified form is shown in Fig. 8.4. W_1 was set to unity gain in the frequency range 1-100 rad /sec followed by a first order roll-off and W_2 was modified such that controller had some high-frequency gain. This did not pose any problem, as the open-loop frequency response of the plant shows very poor gain beyond 100 rad/sec, the controller action in that frequency range did not contribute to the closed-loop response significantly.

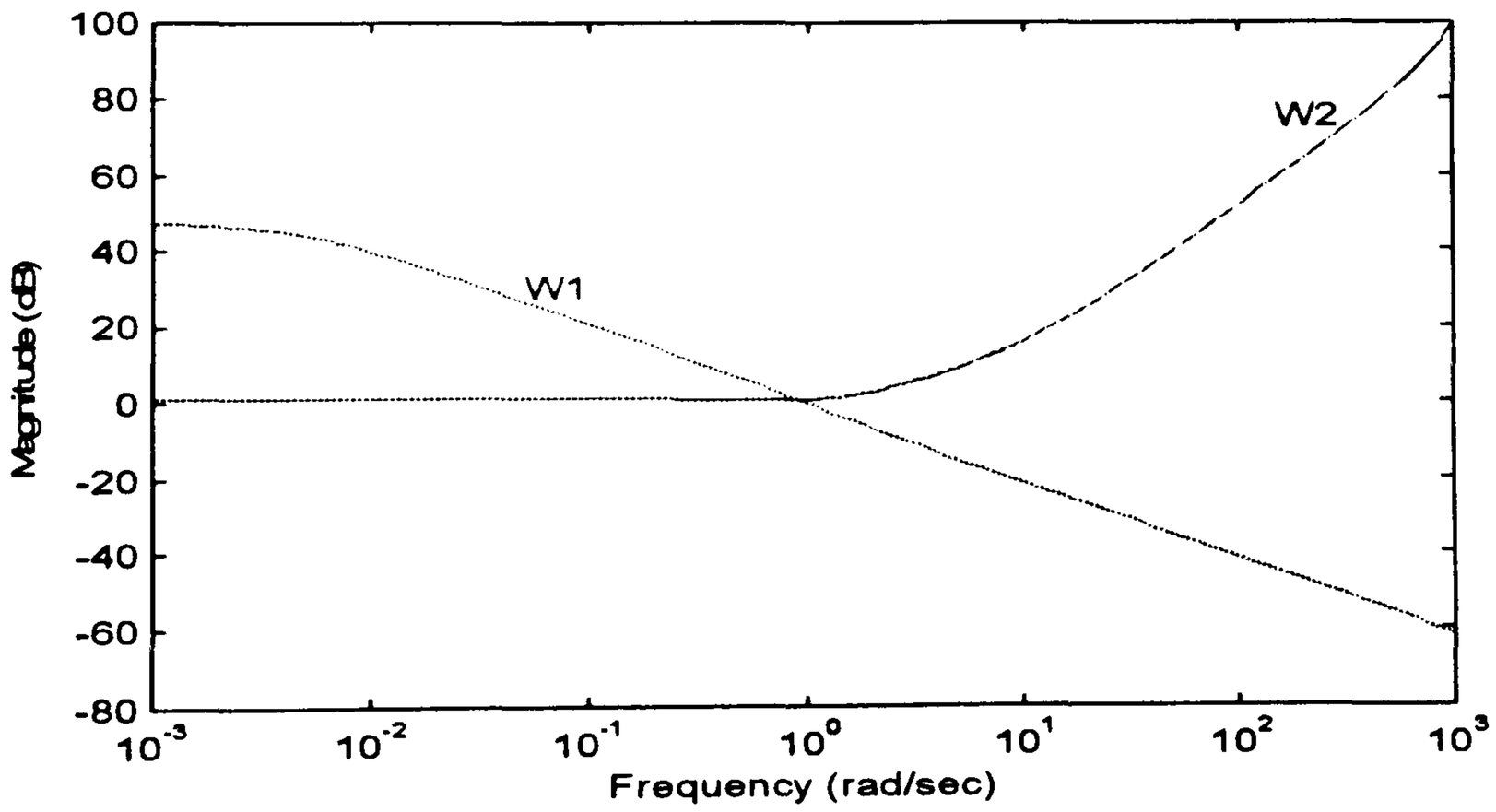

Fig. 8.3: Frequency response of W_1 and W_2

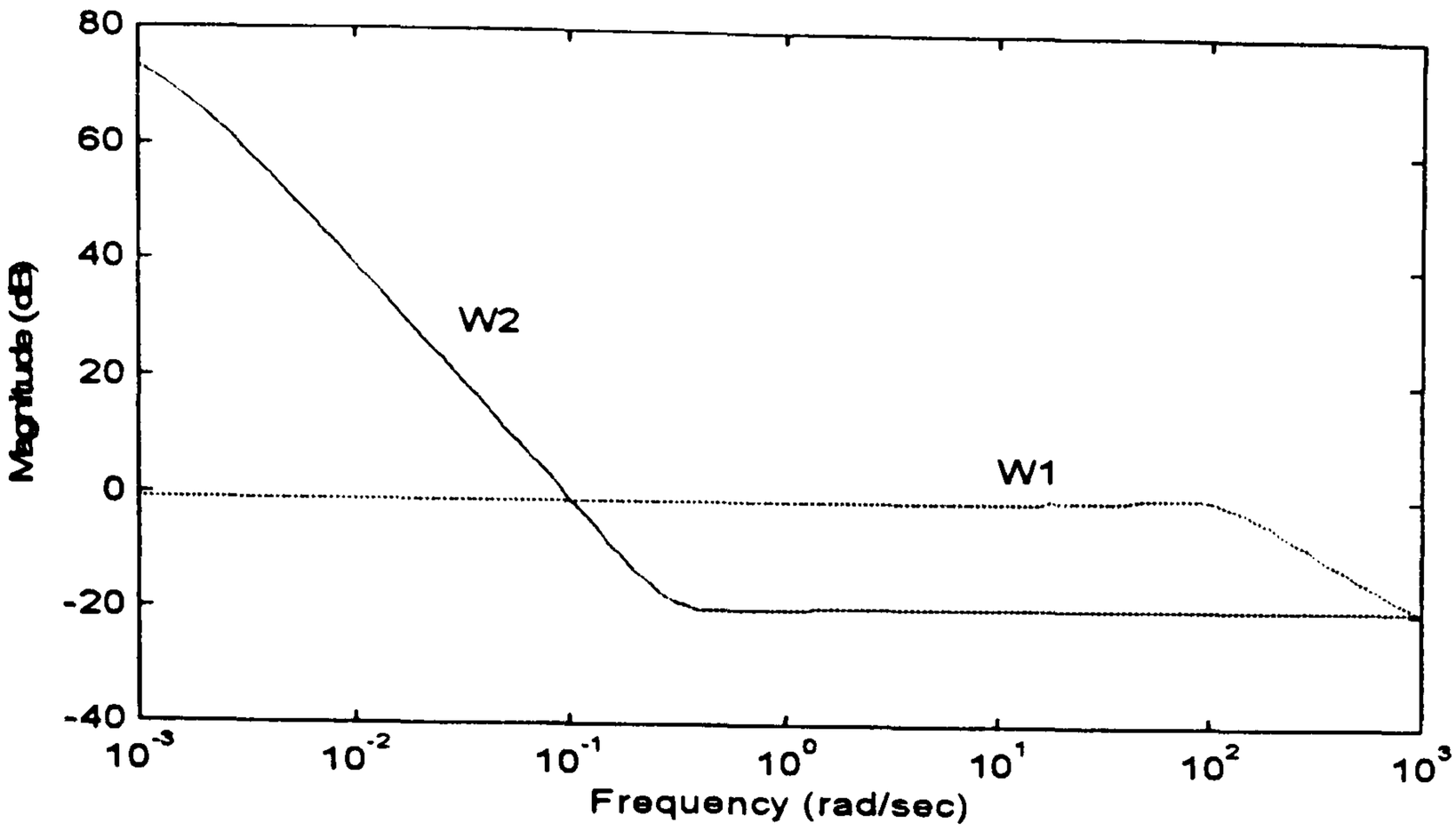

Fig. 8.4: Modified frequency response of W_1 and W_2

The transfer functions of the modified W_1 and W_2 are given by:

$$W_1 = \frac{1}{s+100} \tag{8.22}$$

$$W_2 = \frac{0.1055s^2 + 0.037s + 0.0094}{s^2 + 0.0020s} \tag{8.23}$$

This modified set of W_1 and W_2 have been found to shape the plants very well with three study systems to design the desired damping controllers.

8.5.2 MODEL REDUCTION

The convergence of the projection algorithm [128] implemented in the LMI toolbox [134] depends very much on the dimensions of the matrix X. For full order output feedback design, the order of the controller is the same as that of the order of the open-loop plant augmented by weights W_1 and W_2. It was found that the controller-design for a 15^{th} order plant took 1 to 2 minutes on a Pentium-II processor based computer. It took more than a day for a 50^{th} order plant in the same computer. In order to expedite the solution process in the LMI routine, the plant has to be reduced and then the controller design can be performed on the reduced plant. The different techniques of model reduction and the extent to which each individual open-loop plant of Study systems can be reduced were discussed in detail in the previous chapter. In view of this, they are not discussed here, rather the reduced model of the plants were used to augment with weights and the subsequent controller design.

8.6 DAMPING CONTROLLERS FOR THE STUDY SYSTEMS

The LMI based design of damping controllers was carried out for three study systems. The best locations and most effective feedback signals for SMES units have been identified already in the last chapter. They are bus #10 and $P_{10,6}$ in Study system #1, bus #15 and $P_{15,14}$ for mode #1, bus #8 and $P_{8,7}$ for mode #2 in Study system #2. The locations and signals in Study system #3 are bus #54 and $P_{54,53}$, bus #16 and $P_{16,18}$ and bus #13 and $P_{13,17}$ respectively. The sequential decentralised design as described earlier in Chapter Seven was followed for controller design in study systems #2 and #3. The primary and secondary modes were classified. The desired damping ratios were adopted in line with suggestions made in Chapter Five. The variation of the natural frequency was restricted between 10% to 20%. The open-loop plants were reduced by an appropriate model reduction method. The reduced plants are augmented by weights described in (8.22) and (8.23). The multi-objective feature of LMI was accessed through suitably defining the objective in the argument of the function *hinfmix* of the LMI toolbox [134]. The objective vector '*obj*' required four parameters to be set. The four parameter vector offered options of H_∞, H_2 norm minimisation within bounds those were also specified. The pole-placement option was passed through an argument *'region'*. The region was defined interactively by the command *'lmireg'*. As a good starting point, it was better to check the feasibility of the problem. Once the problem was found feasible, the optimal 'γ' was computed. The optimal 'γ' was obtained by setting four parameters of '*obj*' for the optimal H_∞ control problem. The pole-placement constraint was temporarily ignored during the optimal solution otherwise the problem in most of the case will be infeasible. Once the optimal gamma 'γ_{opt}' was found, the real design started putting the limit on 'γ' i.e. anything greater than 'γ_{opt}'. The objective of pole-placement was incorporated. The algorithm with 'γ' > 'γ_{opt}' provided a sub-optimal controller. Normally a large value of 'γ' was necessary to make the problem feasible with the pole-placement constraint. A Few iterations were necessary to adjust 'γ' to the required value. The codes were developed in Matlab to find the required 'γ'. For a system with multiple inter-area modes, pole-placement objective was used with caution. It was expected that damping controller for a particular SMES at a particular location would improve the damping of a particular mode. The damping of other modes would not be improved with

a single SMES. This was the limitation of a sequential design to incorporate additional pole-placement constraints simultaneously. The pole-placement objective put the constraint that each of the closed loop poles must lie inside the region specified. The LMI solver failed to find a single controller to improve damping to all modes. This was experienced in study systems #2 and #3. The LMI formulation with a pole-placement constraint is a multivariable design technique. It was possible to design multiple damping controllers employing multiple SMES devices simultaneously. The controller structure would have been centralised which was not possible to implement with local signals. In this research, controllers were designed based on the local signals. This was only possible through sequential design, while considering one SMES device at a time. In view of this, the pole-placement objective is only used in Study system #1. It was obvious that an optimal controller provided less damping than a sub-optimal controller. As the value of 'γ' was increased, larger control effort was allowed and it resulted in a controller that increased the damping ratio of the inter-area mode of interest. There is a limit on the 'γ' beyond which closed-loop damping could not improve further. From a power system viewpoint, the value 'γ' is very important. In all of the study systems, it was found that 'γ_{opt}' lied between 1.0 to 1.2. The iteration for 'γ' for the sub-optimal controller started with the optimal value and was allowed to increase in step to a value for which a damping ratio of the inter-area mode of interest ceased to improve. The step by which it was improved was taken as 5. It was found that in all of the study systems, a value of 'γ' in the range 95 to 110 provided satisfactory results. 'γ' was, therefore, selected as100.

The damping ratio evaluated and examined in the iterative process was for the reduced plant corresponding to one operating case (here pre-fault). The controller provided adequate damping in the full order plant. The controllers obtained were also of high order and were reduced to a lower order without greatly affecting the damping performance. The above exercise provided a 9th order controller for the 4th order reduced plant in Study system #1. The controller was reduced to 2nd order. The reduced controller provided adequate damping in the original full order plant. The controller is given by:

$$K(s) = -1.5417\left(\frac{s^2 + 18.95s + 0.0001}{s^2 + 9.07s + 128.7576}\right) \tag{8.24}$$

The sequential design for Study system #2 was carried out. The state-space model of the SMES at bus # 15 was considered first to design a damping controller for mode #1. The open-loop plant was reduced first. The same weights were used to augment the reduced plant. 'γ' = 100 worked very well to provide adequate damping of mode #1. The controller was reduced to a 2nd order one and was found to ensure adequate damping for the full order plant in both the pre-fault and post-fault operating cases. The state-space model of the SMES at bus #8 was derived with the controller connected to the SMES at bus #15. The SMES at bus #15, along with its damping controller, was then an integral part of the system. The pre-fault and post-fault steady-state models were derived. Model reduction was performed on the pre-fault plant. The reduced model was augmented with the same weights. The algorithm was run to provide the necessary controller. Once again, 'γ' = 100 provided a satisfactory controller. The controller was initially of high order and reduced to a 2nd order one. The damping of mode #2 in the original plant was checked with the reduced controller. It was found that the damping ratios in both operating conditions were adequate with the reduced order controllers given by:

$$K_1(s) = -1.2003\left(\frac{s^2 + 42.11s}{s^2 + 6.99s + 223.54}\right) \tag{8.25}$$

$$K_2(s) = -0.2312\left(\frac{s^2 + 11.08s}{s^2 + 3.5s + 97.49}\right) \tag{8.26}$$

The same exercise of sequential design was carried out in Study system #3. The damping controllers were designed for SMES devices at busses #54, #16 and #13 respectively. Three damping controllers were found to improve damping to all four modes. The same weights were found to work well. The same 'γ' = 100 was used. The controllers were reduced to the second order for ease of implementation. The reduced order controllers were tested in the original system. It was found that the damping of the original system was improved for both operating conditions. The controllers are given below:

$$K_1(s) = -1.6727\left(\frac{s^2 + 1247.6s + 0.008}{s^2 + 422.7s + 5018.32}\right) \tag{8.27}$$

$$K_2(s) = -1.1319\left(\frac{s^2 + 48293s + 0.10}{s^2 + 11068s + 166364}\right) \tag{8.28}$$

$$K_3(s) = -0.6820\left(\frac{s^2 + 4195763s + 77.37}{s^2 + 606464s + 10547530}\right) \tag{8.29}$$

8.7 PERFORMANCE EVALUATIONS

An eigenvalue analysis was carried out to evaluate the performance of the study systems at different operating conditions at various levels of power transfer. The variation of load model was also considered. The operating conditions that were used to evaluate the performance in the frequency domain were identical to that described in the last chapter. The washout filter as described earlier was also included in the system whilst carrying out eigenvalue analysis. The results for Study system #1 are displayed in Table 8.1 to 8.3.

Table 8.1: Damping ratios in both operating cases (Study system #1).

Mode No.	Open-loop (pre-fault)		Closed-loop (pre-fault)		Open-loop (post-fault)		Closed-loop (post-fault)	
	ζ	f (Hz)	ζ	f (Hz)	ζ	f (Hz)	ζ	f (Hz)
#1	**0.0096**	**0.6976**	**0.2018**	**0.7635**	**0.0031**	**0.5917**	**0.2226**	**0.6246**
#2	0.0852	1.1474	0.0852	1.1459	0.0856	1.1414	0.0856	1.1407
#3	0.1153	1.1545	0.1455	1.1630	0.1140	1.1497	0.1392	1.1526

Table 8.2: Damping ratios at various values of power flow (Study system#1)

Power Flow (Area #1→Area #2)	Open-loop		Closed-loop	
	ζ	f (Hz)	ζ	f (Hz)
00 MW	0.0263	0.7238	0.1875	0.7872
200 MW	0.0108	0.7142	0.1876	0.7791
400 MW	0.0096	0.6976	0.2018	0.7635
-400 MW	0.0090	0.6934	0.1321	0.7532

Table 8.3: Damping ratios at different load characteristics (Study system #1)

Load Type	Closed-loop (pre-fault)	
	ζ	f (Hz)
CI	0.2018	0.7635
CC	0.1932	0.7555
CP	0.1743	0.7475
CC+CP	0.1854	0.7513
Dynamic	0.2249	0.7373

Table 8.1 shows that the damping of inter-area mode (mode #1 in Table 8.1) is adequate in the pre-fault and post-fault closed-loop system. The damping of other two local modes are not changed much from their open-loop values. This indicates that the controller does not have any adverse influence on the modes for which it is not designed. This verifies that the adverse interaction of the controller with other electromechanical modes is virtually absent. The robustness of the damping controller was also tested at different values of power flow through tie lines. The results in Table 8.2 showes that even when 400 MW of power flows in the opposite direction (Area #2 to Area #1) the damping performance of the controller was adequate. The damping performance of the controller in the face of the variation in the nature of the loads are also very robust in nature as is evidenced from the results in Table 8.3.

The results in Table 8.4 to 8.7 correspond to the performance of the controllers in Study system #2. It is seen from Table 8.4 that $K_1(s)$ only improves the damping of mode #1. This is expected. The joint action of $K_1(s)$ and $K_2(s)$ shows that both the modes have adequate damping ratios in the pre-fault and post-fault operating condition. The effect of various power transfers and different types of loads on the damping ratios are displayed in Table 8.6 and 8.7 respectively. It is clear from the results in these tables that the controller provides robust damping for various power flows and different load characteristics.

Table 8.4: Damping ratios in both operating cases with $K_1(s)$ only (Study system #2).

Mode No.	Open-loop (pre-fault)		Closed-loop (pre-fault)		Open-loop (post-fault)		Closed-loop (post-fault)	
	ζ	f (Hz)	ζ	f (Hz)	ζ	f (Hz)	ζ	f (Hz)
#1	**0.0001**	**0.8258**	**0.2002**	**0.9153**	**-0.0118**	**0.6918**	**0.1354**	**0.7189**
#2	0.0274	1.1466	0.0356	1.1438	0.0269	1.1359	0.0273	1.1352

Table 8.5: Damping ratios in both operating cases with $K_1(s)$ & $K_2(s)$ (Study system#2)

Mode No.	Open-loop (pre-fault)		Closed-loop (pre-fault)		Open-loop (post-fault)		Closed-loop (post-fault)	
	ζ	f (Hz)	ζ	f (Hz)	ζ	f (Hz)	ζ	f (Hz)
#1	0.2002	0.9153	0.2001	0.9268	0.1354	0.7189	0.1451	0.7201
#2	0.0356	1.1438	0.1478	1.1417	0.0273	1.1352	0.1242	1.1423

Table 8.6: Damping ratios at various values of power flow (Study system#2)

Power Flow (Area #3→Area #1& Area #2)	Mode #1 Closed-loop (pre-fault)		Mode #2 Closed-loop (pre-fault)	
	ζ	f (Hz)	ζ	f (Hz)
00 MW	0.3740	0.9669	0.1282	1.1282
550 MW	0.2001	0.9262	0.1478	1.1417
750 MW	0.1268	0.7650	0.1300	1.1325

Table 8.7: Damping ratios at different load characteristics (Study system #2)

Load Type	Mode #1 Closed-loop (pre-fault)		Mode #2 Closed-loop (pre-fault)	
	ζ	f (Hz)	ζ	f (Hz)
CI	0.2001	0.9262	0.1478	1.1417
CC	0.2209	0.9714	0.1503	1.1085
CP	0.2853	1.0108	0.1157	1.0425
CC+CP	0.2442	0.9994	0.1408	1.0769
Dynamic	0.1946	0.9321	0.1801	1.1315

The same exercise on Study system #3 was carried out. The detailed results are displayed in Table 8.8 to 8.12. It can be seen that $K_1(s)$ improves the damping of mode #1 sufficiently. The action of $K_2(s)$ is reflected in the damping of mode #2 and #4. Controller $K_3(s)$ was necessary to ensure the adequate damping of mode #3 for both operating conditions. $K_3(s)$ was also seen to contribute to the damping of mode #4. The joint action of $K_2(s)$ and $K_3(s)$ was found to ensure the adequate damping of mode #4 thus eliminating the necessity of another damping controller. The actions of these three controllers were found to provide adequate damping for all of the four inter-area modes. The controllers were also robust in providing damping when power flow across NETS and NYPS varies as seen from the results in Table 8.11. The damping performances of the controllers were also found to be very good in the face of a variation in the load characteristics.

Table 8.8: Damping ratios in both operating cases with $K_1(s)$ only (Study system #3).

Mode No.	Open-loop (pre-fault)		Closed-loop (pre-fault)		Open-loop (post-fault)		Closed-loop (post-fault)	
	ζ	f (Hz)	ζ	f (Hz)	ζ	f (Hz)	ζ	f (Hz)
#1	**0.061**	**0.36**	**0.159**	**0.40**	**0.044**	**0.33**	**0.18**	**0.35**
#2	0.039	0.49	0.052	0.49	0.025	0.48	0.047	0.48
#3	0.037	0.54	0.115	0.54	0.039	0.51	0.058	0.52
#4	0.049	0.79	0.049	0.79	0.049	0.79	0.049	0.79

Table 8.9:Damping ratios in both operating cases with $K_1(s)$ and $K_2(s)$ only (Study system #3)

Mode No.	Open-loop (pre-fault)		Closed-loop (pre-fault)		Open-loop (post-fault)		Closed-loop (post-fault)	
	ζ	f (Hz)	ζ	f (Hz)	ζ	f (Hz)	ζ	f (Hz)
#1	0.159	0.40	**0.164**	**0.42**	0.18	0.35	**0.204**	**0.35**
#2	0.052	0.49	**0.245**	**0.57**	0.047	0.48	**0.255**	**0.57**
#3	0.115	0.54	0.163	0.52	0.058	0.52	0.061	0.48
#4	0.049	0.79	**0.114**	**0.79**	0.049	0.79	**0.114**	**0.79**

Table 8.10: Damping ratios in both operating cases with $K_1(s)$, $K_2(s)$ and $K_3(s)$ (Study system #3).

Mode No.	Open-loop (pre-fault)		Closed-loop (pre-fault)		Open-loop (post-fault)		Closed-loop (post-fault)	
	ζ	f (Hz)	ζ	f (Hz)	ζ	f (Hz)	ζ	f (Hz)
#1	0.164	0.42	**0.217**	**0.40**	0.204	0.35	**0.210**	**0.35**
#2	0.245	0.57	**0.255**	**0.55**	0.255	0.57	**0.211**	**0.53**
#3	0.163	0.52	**0.229**	**0.68**	0.061	0.48	**0.276**	**0.65**
#4	0.114	0.79	**0.122**	**0.78**	0.114	0.79	**0.122**	**0.78**

Table 8.11: Damping ratios at various values of power flow (Study system#3)

Power Flow (NETS→NYPS)	Mode #1 Closed-loop (pre-fault)		Mode #2 Closed-loop (pre-fault)		Mode #3 Closed-loop (pre-fault)		Mode #4 Closed-loop (pre-fault)	
	ζ	f (Hz)	ζ	f (Hz)	ζ	f (Hz)	ζ	f (Hz)
100 MW	0.217	0.40	0.255	0.54	0.228	0.68	0.122	0.78
500 MW	0.154	0.37	0.226	0.54	0.253	0.66	0.119	0.78
700 MW	0.110	0.36	0.211	0.54	0.269	0.64	0.118	0.78

Table 8.12: Damping ratios at different load characteristics (Study system#3)

Load Type	Mode #1 Closed-loop (pre-fault)		Mode #2 Closed-loop (pre-fault)		Mode #3 Closed-loop (pre-fault)		Mode #4 Closed-loop (pre-fault)	
	ζ	f (Hz)	ζ	f (Hz)	ζ	f (Hz)	ζ	f (Hz)
CI	0.217	0.40	0.255	0.54	0.228	0.68	0.122	0.78
CC	0.180	0.40	0.270	0.57	0.260	0.69	0.129	0.77
CP	0.180	0.39	0.238	0.63	0.307	0.70	0.127	0.76
CC+CP	0.173	0.40	0.264	0.60	0.280	0.70	0.129	0.77
Dynamic	0.220	0.40	0.257	0.54	0.243	0.68	0.121	0.78

Robustness performance has been verified in the frequency domain for small disturbances. A non-linear simulation was necessary to evaluate the performance of the controllers under large disturbances especially during and after a system fault. This gave

an opportunity to excite the non-linearity, saturation and limits on the output of the controllers and other dynamic components in the power system.

The non-linear simulation was performed for the three study systems. The nature of the fault, duration of the fault and post-fault operating conditions have all been described in Section 4.4. The time domain behaviour of the dynamic variables as shown in Section 4.4, is now shown with the action of the controllers. Fig. 8.5 and 8.6 show the dynamic behaviour of Study system #1. It is clear from Fig. 8.5 that the controller settles the oscillation despite system non-linearity and device output limits.

The response of the SMES is shown in Fig. 8.6. The real power output of the SMES initially oscillates between the limits of ± 0.10 and following this period, linearity is regained and the oscillations eventually settle in 10 to 12 seconds.

The time domain responses in Fig. 8.7 and 8.8 correspond to Study system #2. It can be seen from these plots that the oscillations settle in 10 to 12 s. The controller outputs also oscillate between the limits. The observations can be made from the response of the Study system #3 shown in Fig. 8.9 and 8.10.

The time domain simulation shows that the controllers perform very well even under large disturbances. The robust damping performance is also verified in the time domain.

8.8 EVALUATION OF SMES RATINGS

The power rating of all the SMES units in the three study systems was restricted to ± 10 MW as described in Chapter Two and Chapter Seven. The energy rating associated with each SMES unit was evaluated using the method described in Chapter Two. It was found that the energy rating of the SMES in Study system #1 was 9.54 MJ. The energy rating of the SMES units in Study system #2 are 6.53 MJ and 5.19 MJ respectively. The Study system #3 requires three SMES devices having energy rating of 10.53 MJ, 5.93 MJ and 10.70 MJ. The SMES of size in the range of 1-10 MJ is expected to be available in the market commercially in the near future [83].

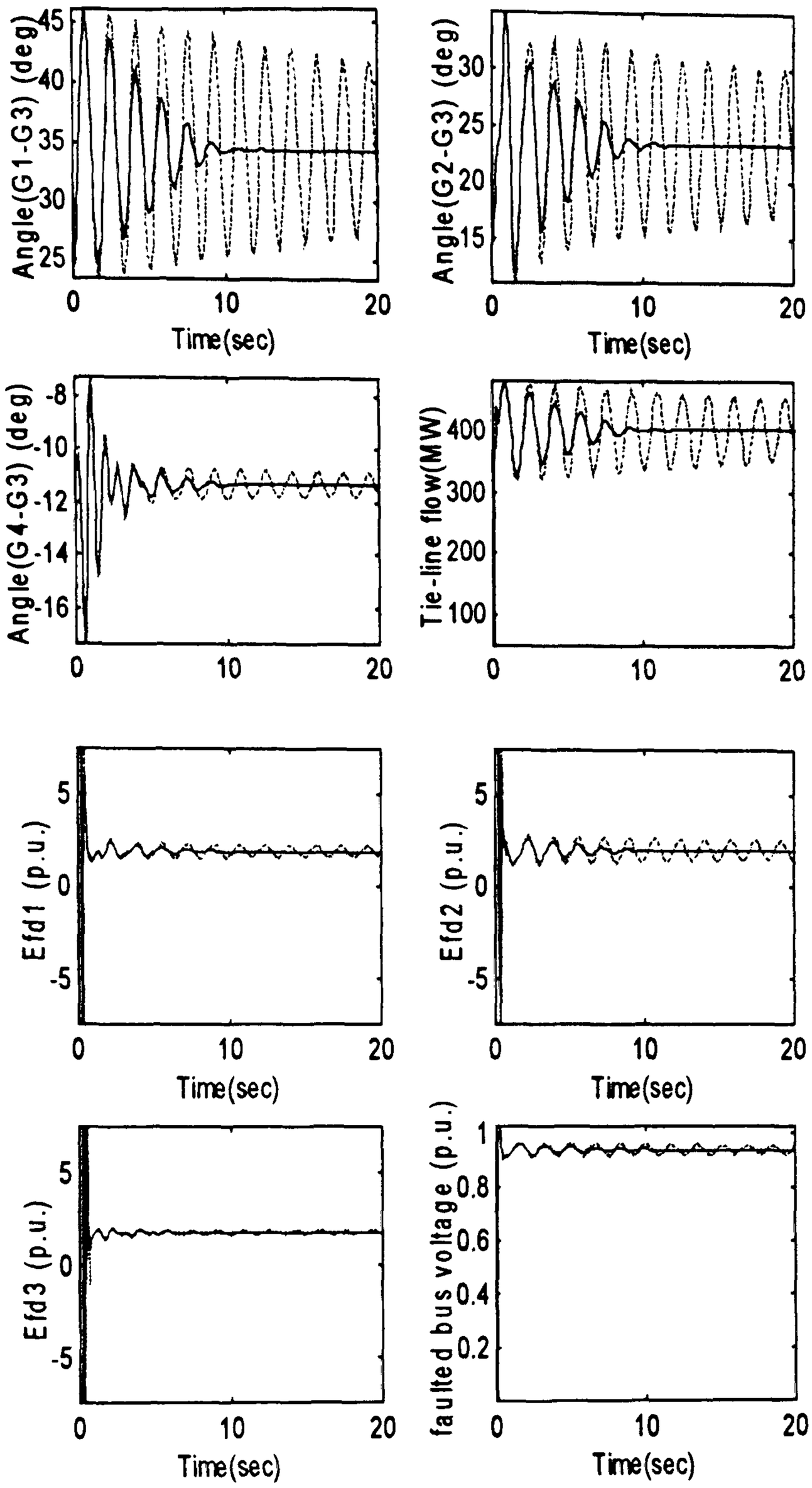

Fig 8.5: Response of Study system #1 under large disturbances
Solid line: with controller; Dashed line: without controller

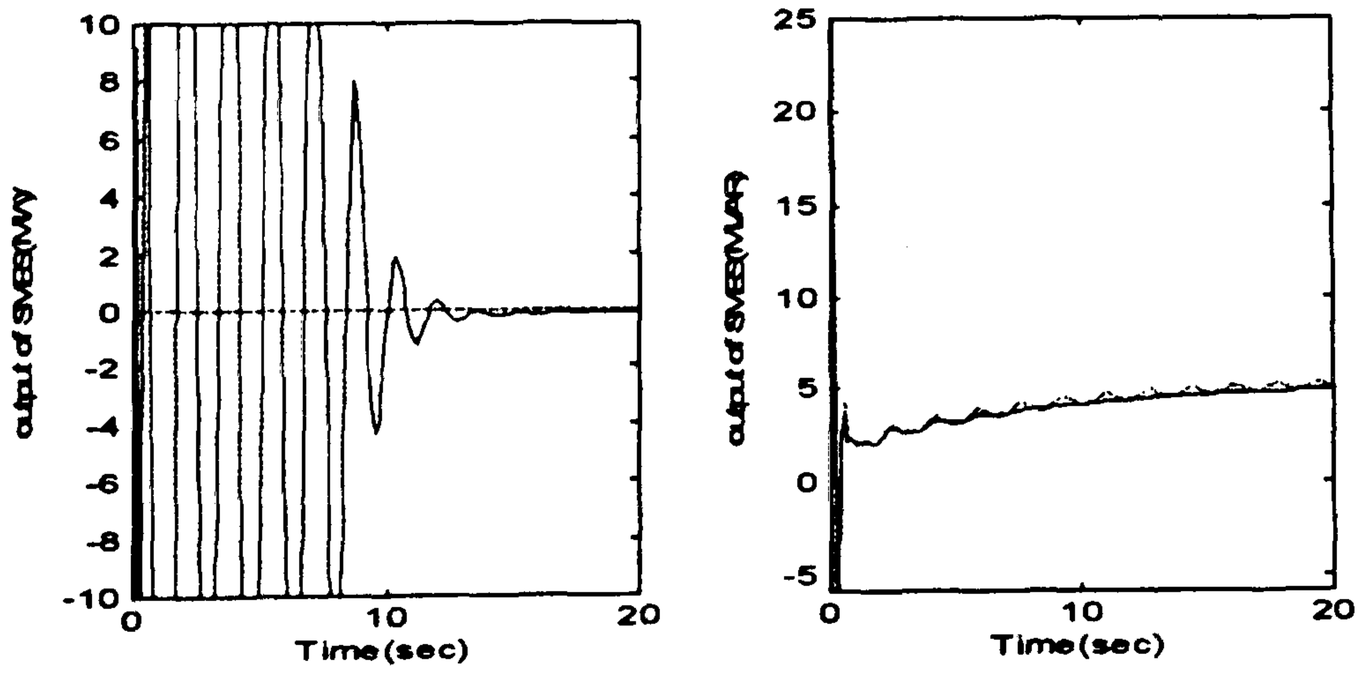

Fig 8.6: Response of SMES under large disturbance in Study system #1
Solid line: with controller; Dashed line: without controller

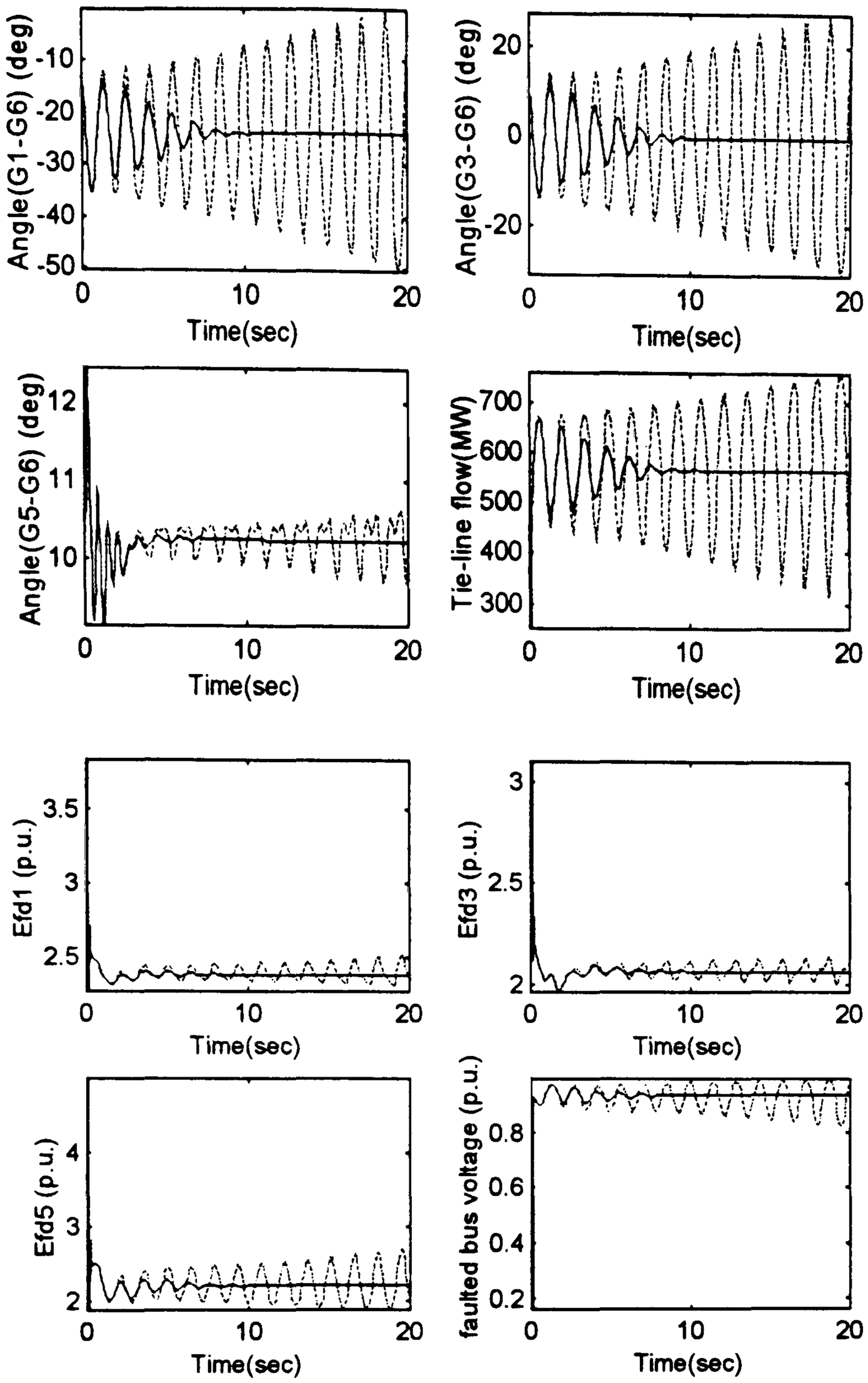

Fig 8.7: Response of Study system #2 under large disturbances
Solid line: with controller; Dashed line: without controller

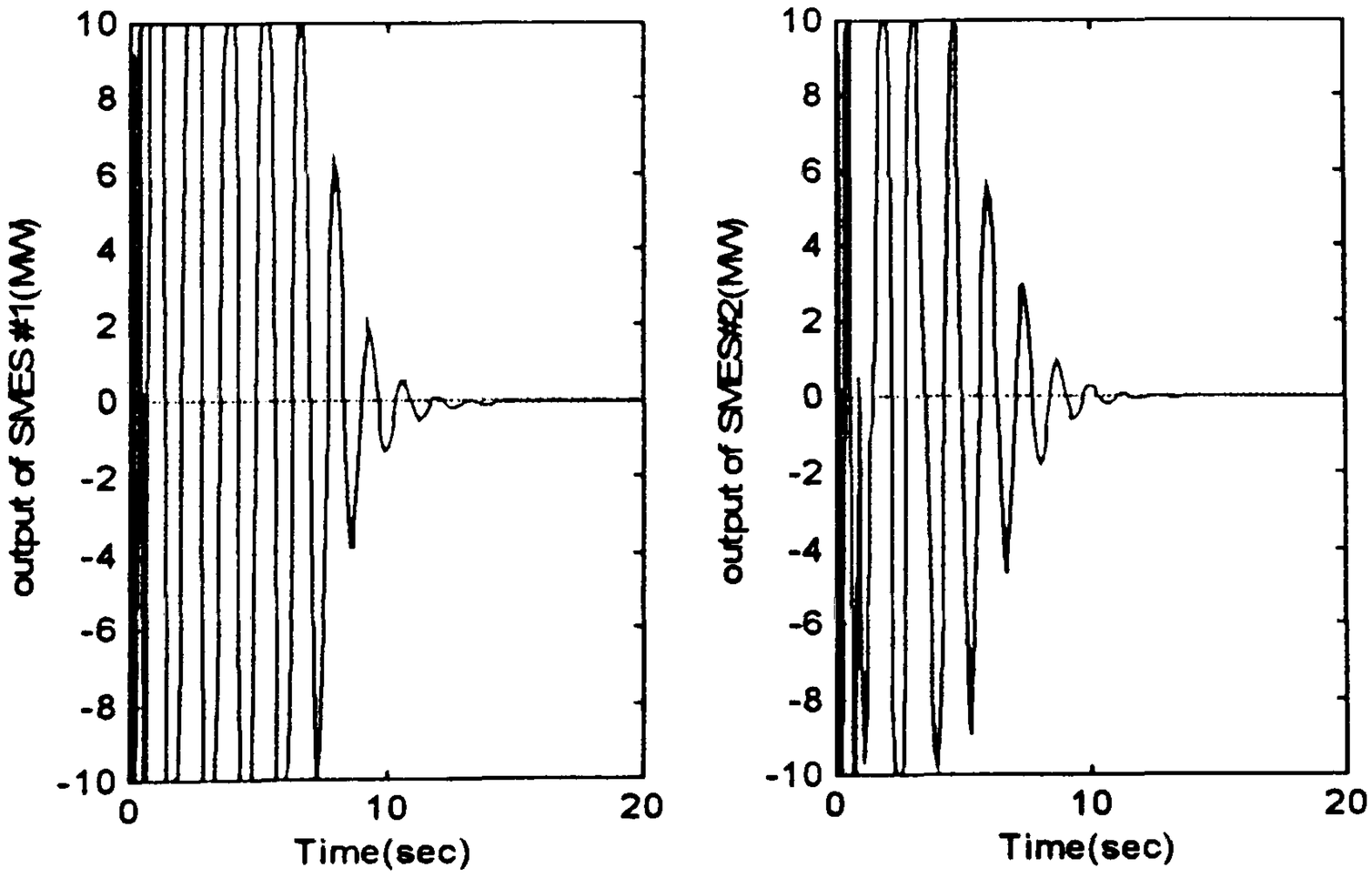

Fig 8.8: Response of SMES under large disturbance in Study system #2
Solid line: with controller; Dashed line: without controller

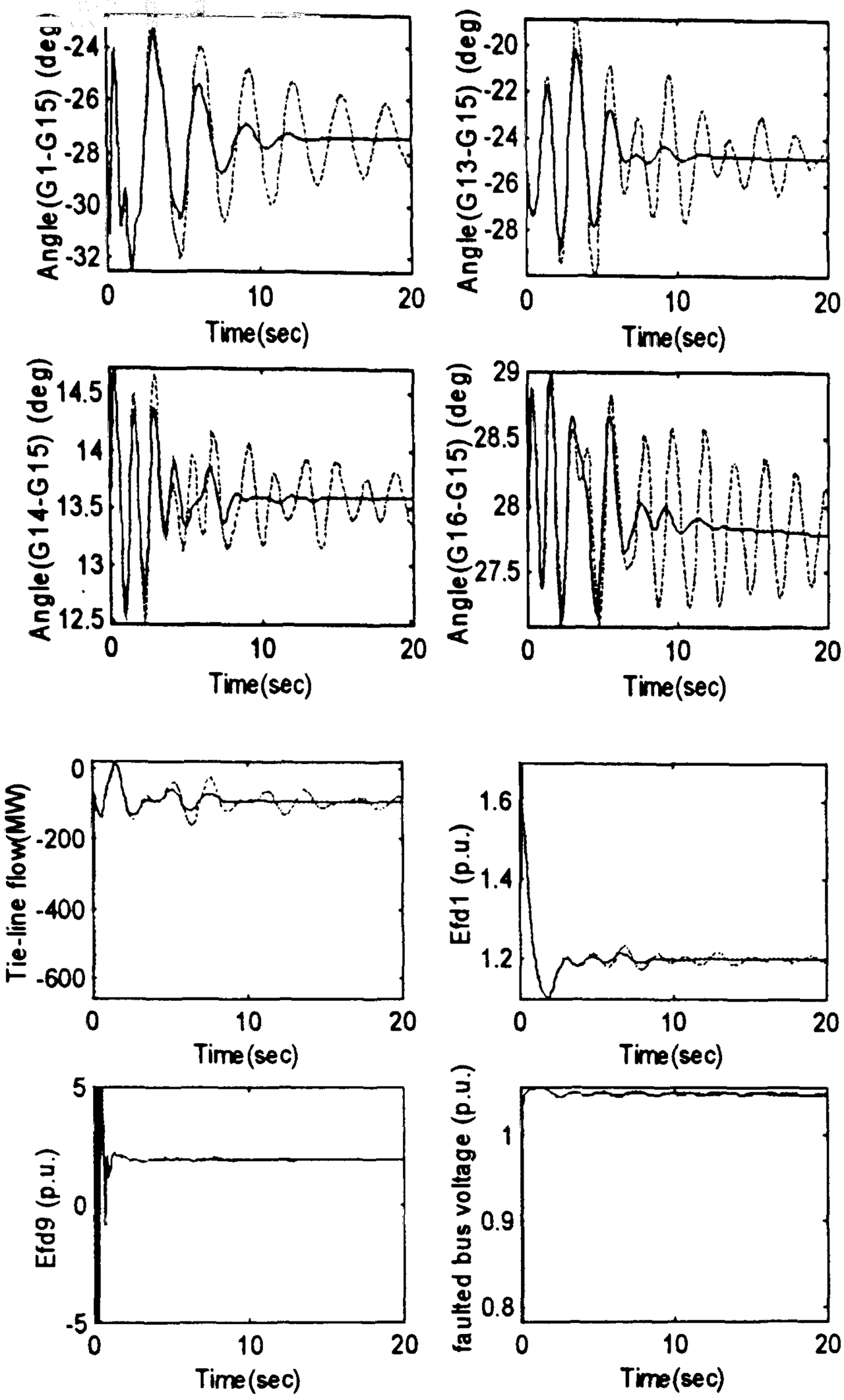

Fig 8.9: Response of Study system #3 under large disturbances
Solid line: with controller; Dashed line: without controller

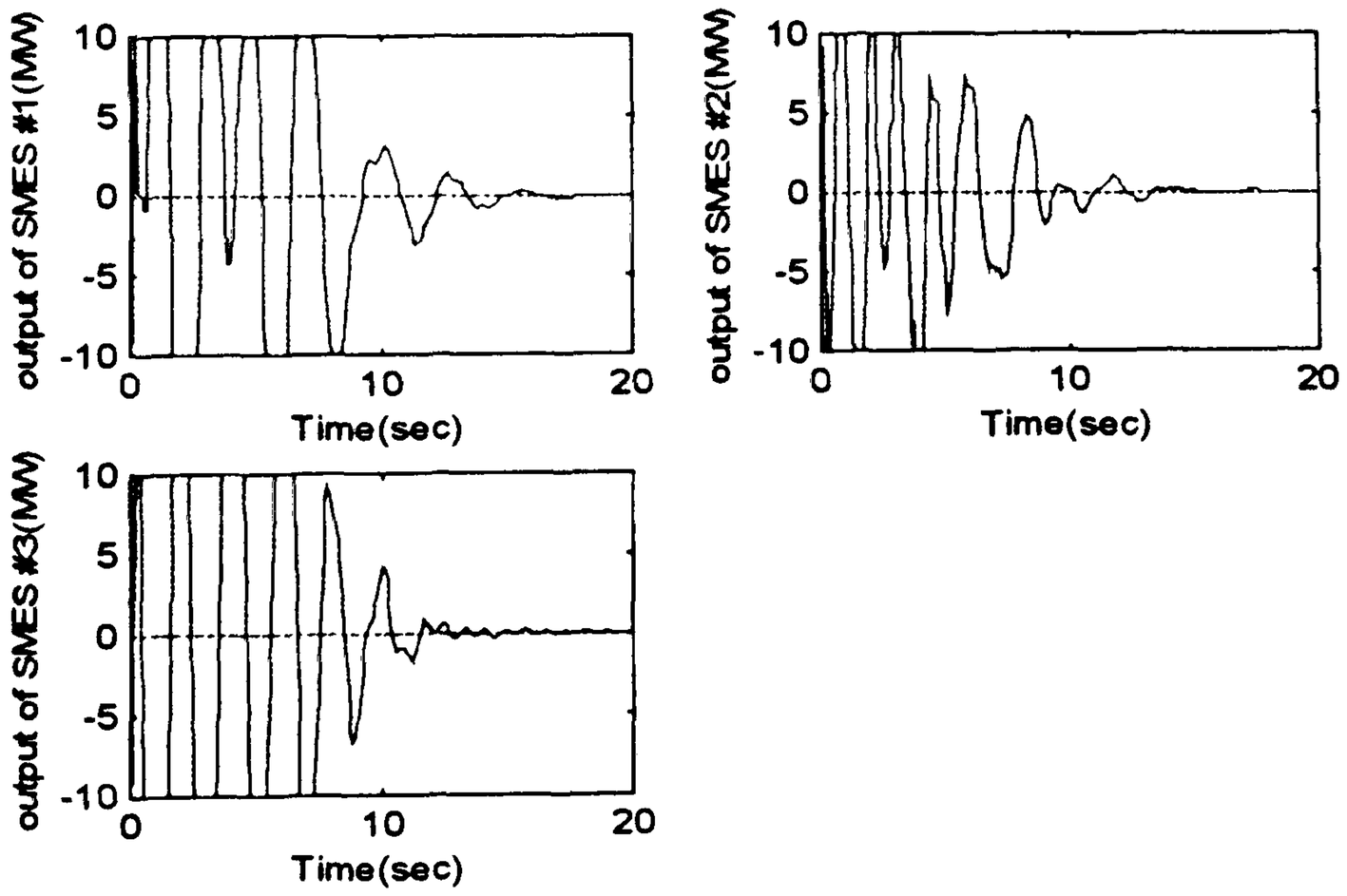

Fig 8.10: Response of SMES under large disturbance in Study system #3
Solid line: with controller; Dashed line: without controller

8.9 PERFORMANCE COMPARISONS

A comparison of the two approaches of H_∞ control was initially carried out. Study system #3 was considered. The damping controller for the SMES at bus #54 was designed in an attempt to improve the damping of mode #1. The 10^{th} order reduced plant in the pre-fault case was augmented with the weights already described. The command '*hinfric*' and '*hinflmi*' in LMI Toolbox [134] were used for the Riccati and LMI based solutions respectively. Both of the Riccati and LMI approaches provided optimal design with 'γ_{opt}' equal to 1.18. The damping ratios were very poor with the optimal controller. The bound on 'γ' was increased beyond the optimal value to get a controller with better damping performance. 'γ' = 100 was decided. The same γ and weights were used to get sub-optimal controllers by both of the methods. The controllers in both methods were of 14^{th} order. The poles and zeros of the controllers are listed in Table 8.13. The damping ratios provided by these controllers in the closed-loop were also evaluated. Both of the pre-fault and post-fault operating cases were considered. The inter-area and controller modes are abbreviated as IA #1-#4 and C #1-#3 respectively. The damping ratios and frequencies are displayed in Table 8.14. It can be seen from the results that the controller obtained by the LMI approach provides higher damping ratios than that provided by the controller obtained by the Riccati approach. It can also be seen that the controller obtained by Riccati approach introduces poorly damped controller modes into the vicinity of inter-area modes. Similar observations were made in study systems #1 and #2 and so are not described in detail. This justifies the superiority of the numerical approach over the analytical approach for the solution of a mixed sensitivity-H_∞ problem.

Table8.13: Poles and zeros of the 14^{th} order controllers.

LMI approach		Riccati approach	
poles	zeros	poles	zeros
-11959	-870.4	-78.005 ± j80.119	-40.224
-1588	-140.41	-94.704	-36.141
-138.03	-39.798	-0.9645 ± j9.9983	-0.7517 ± j8.3855
-16.068 ± j14.062	-2.7031 ± j7.0412	-0.3173 ± j4.1792	-0.1448 ± j3.4158
-0.3390 ± j3.1232	-0.3206 ± j3.1534	-0.0745 ± j3.1239	-0.0596 ± j3.1139
-0.8221 ± j2.9510	-0.8551 ± j2.9942	-0.0781 ± j2.7752	-0.1419 ± j2.2897
-0.3337 ± j0.12734	-0.2670 ± j0.2694	-0.0845 ± j0.0615	-0.06
-0.25097	-0.0009 ± j4.68e-6	-0.0609	-0.001
			-0.0009

Table 8.14: Closed-loop damping by two control approaches.

IA/ Cont. Mode	Pre-fault				Post-fault			
	LMI Controller		Riccati Controller		LMI Controller		Riccati Controller	
	ς	f(Hz)	ς	f(Hz)	ς	f(Hz)	ς	f(Hz)
IA#1	**0.15**	**0.42**	**0.06**	**0.36**	**0.23**	**0.36**	**0.04**	**0.34**
IA#2	0.05	0.50	0.04	0.50	0.05	0.49	0.03	0.50
IA#3	0.13	0.55	0.03	0.54	0.06	0.52	0.04	0.52
IA#4	0.05	0.79	0.05	0.79	0.05	0.79	0.05	0.79
C #1			0.02	0.44			0.02	0.44
C #2			0.02	0.50			0.02	0.50
C #3			0.07	0.67			0.07	0.67

The performance of LMI based controllers were compared with that of the root-locus based controllers. Study system #2 was considered. The exercise of H_2 norm computation as an estimate of the control efforts in the pre-fault case was carried out. The control efforts of $K_1(s)$ and $K_2(s)$ in (8.25) and (8.26) were 9.93 and 1.29. This corresponded to the pre-fault damping ratios of 0.2001 and 0.1478 for mode #1 and #2 respectively. The pre-fault damping ratios, very close to these values, were achieved with the root-locus controllers in (7.18) and (7.19). The control efforts were 28.34 and 28.26. This meant that the controllers obtained by the LMI technique had better small disturbance performances. This is further verified from the plots of the control efforts in Fig. 8.11. The nature and duration of the small disturbance to obtain these plots were the same as that in Chapter Seven i.e. the disturbance was 0.05 p.u. in magnitude and its duration was for 200 ms.

The controller gains in (7.18) and (7.19) were adjusted to reduce the control effort from 28.34 to 9.93 and 28.26 to 1.29. This resulted in the same control effort in both methods. It was necessary to see the pre-fault and post-fault damping of the system. The results are displayed in Table 8.15. It can be seen that the root-locus controllers provide a damping of 0.0578 and 0.0338 for mode #1 and #2 respectively. The post-fault values are 0.0248 and 0.0304 respectively. These values are much less than those provided by the LMI based controllers with the same control effort. Damping performance was further verified through non-linear simulation under a large disturbance. The dynamic responses are plotted in Fig. 8.12. It is clear from the plots in Fig. 8.12 that the damping performance of the LMI-controllers are much better than that obtained by the root-locus-controller with the same control effort.

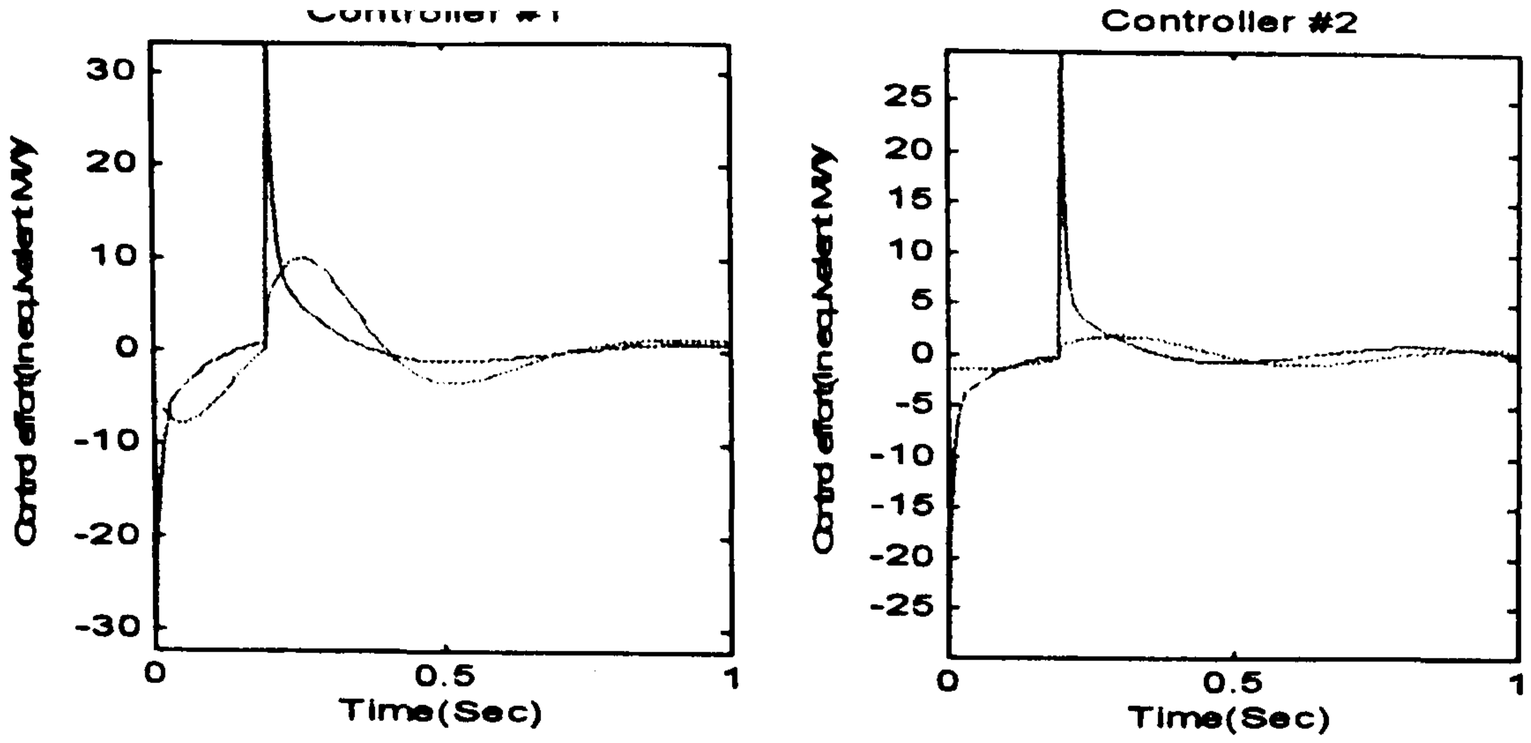

Fig 8.11: Controller response in the Study system #2 under small disturbance
(Same pre-fault damping but different control efforts).
Solid line: Response when Root-locus based controllers are connected
Dotted line: Response when LMI based controllers are connected

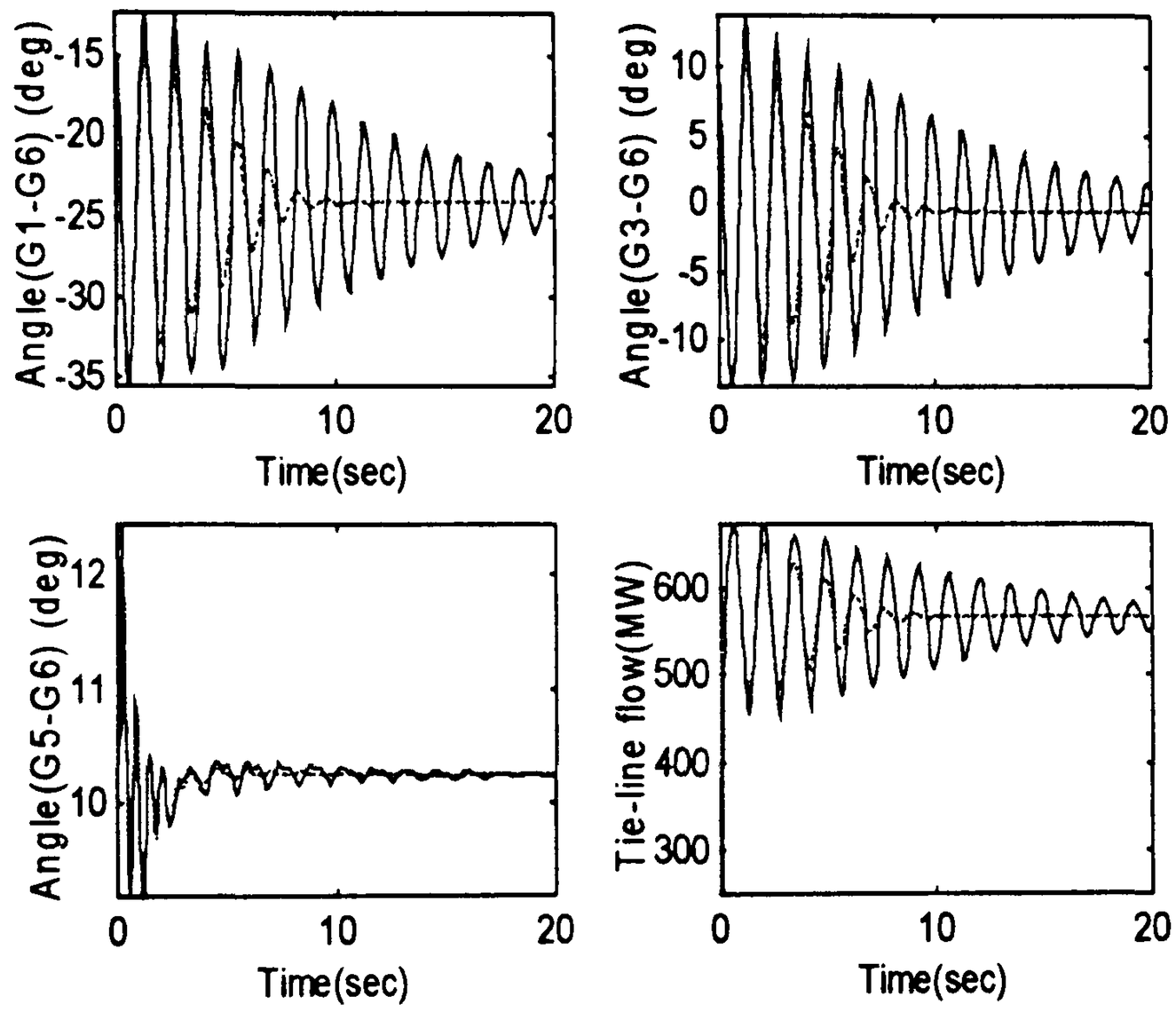

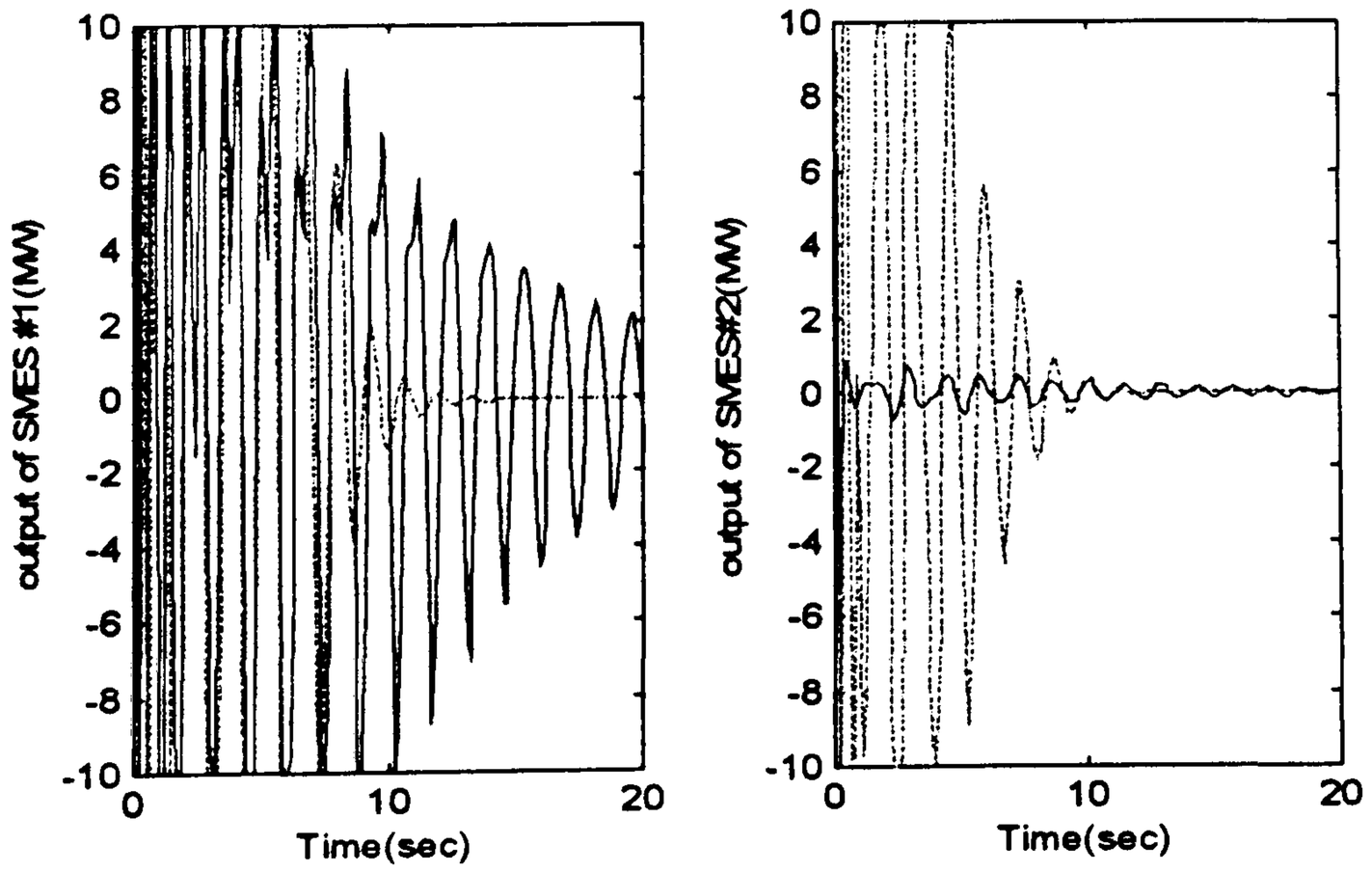

Fig 8.12: Dynamic response of Study system #2 under large disturbances
(Same control efforts but different pre-fault damping).
Solid line: Response when Root-locus based controllers are connected
Dotted line: Response when LMI based controllers are connected

Table 8.15: Comparison of damping ratios obtained by two different control techniques

Mode No.	Open-loop (pre-fault)		closed-loop (pre-fault) LMI based control		closed-loop (pre-fault) Root-Locus based control		Open-loop (post-fault)		closed-loop (post-fault) LMI based control		closed-loop (post-fault) Root-Locus based control	
	ζ	f (Hz)	ζ	f (Hz)	ζ	f (Hz)	ζ	f (Hz)	ζ	f (Hz)	ζ	f (Hz)
#1	0.000	0.82	0.200	0.92	0.057	0.84	-0.01	0.69	0.145	0.72	0.024	0.69
#2	0.027	1.15	0.147	1.14	0.033	1.14	0.027	1.13	0.124	1.14	0.030	1.13

The observation in study systems #1 and #3 were similar and hence are not discussed here. In general, it can be said that the LMI based design is robust and the control effort required, to maintain it, is less. The numerical approach to solve the control problem provides a better damping ratio than the analytical approach. One of the design objectives is to minimise the control effort and hence always provides a cost effective and robust controller. The drawback associated with root-locus based design is absent in the case of LMI based control.

8.10 SUMMARY AND CONCLUSIONS

The concept of LMI based damping control design is introduced to power systems. A mathematical overview of the LMIs is described. The formulations of linear control design problems as LMIs are discussed. The LMI formulation of mixed sensitivity H_∞ design is described. The pole-placement constraints as an essential objective in the time domain are incorporated as additional LMIs. The derivation of LMI based controller is put forward systematically. The relative discussion on the solvability conditions of the LMI and Riccati approaches to H_∞ mixed-sensitivity-control-design is made. Unlike in the Riccati approach, the regularity assumption of the plant is absent on an LMI approach to satisfy the solvability conditions. A successful attempt is made to standardise the weights in a mixed sensitivity design from a power system damping control viewpoint. It is shown that the same sets of weights work very well with the three study systems.

The controllers designed for the three study systems are reduced to 2^{nd} order for ease of implementation. The damping performances of the reduced controllers are tested in the frequency domain at different operating conditions. It was shown that the damping in the pre-fault and post-fault conditions is adequate. The performance of the

controllers is further tested for various levels of tie line flows. The controllers can also maintain adequate damping even when the tie line flows vary significantly. The controllers can even maintain robust damping when the characteristics of load change. It is also very interesting to see that the controllers do not interfere with the damping of other modes, especially local modes and other inter-area modes.

Non-linear simulations were performed to verify the robustness performance of the controller in the presence of non-linearities and device saturation in the systems. The dynamic responses in the time domain clearly prove that the controllers can withstand the effect of large disturbances and do not affect the transient stability performance of the systems.

The damping performance of the LMI based controller is compared with that of Riccati based controller in the same augmented plants with identical bounds on γ. It was proved that the numerical nature of the solution in LMI always provides a damping controller with better damping ratios in the closed-loop. The poorly damped controller modes in the inter-area frequency range are absent in the numerical solution. The Riccati approach of the analytical solution for the controller structure provides a controller that cannot provide adequate damping for the inter-area modes of interest. Moreover, several lightly damped controller modes are introduced because of the nature of the solution. These controller modes always interfere with the transient stability performance of the system. They also adversely interact with the other modes in the post-fault dynamic period.

Less control effort is needed to maintain adequate damping ratios. This is expected as the design optimises the control efforts. This also ensures much less wear and tear of the system during repeated small disturbances. The root-locus based control for the same damping performance is seen to require a large control effort.

CHAPTER NINE

CONCLUSIONS AND FURTHER WORK

9.1 INTRODUCTION

In this chapter, general conclusions are drawn on the work that has been carried out. Some of the results lead to observations/conclusions that are claimed as original contributions to the knowledge of the inter-area mode damping control problem. A brief outline of future work is also given.

9.2 OVERALL CONCLUSIONS

The work that has been reported in the previous chapters is summarised in the following subsections.

9.2.1 ANALYSING THE INTER-AREA MODE DAMPING PROBLEM

The overview of the low-frequency inter-area oscillations is discussed in detail. The oscillations experienced by major interconnected utilities over the last few decades have been described. This aids in an appreciation of the importance of the problem even in efficient, economic and reliable power systems. The various existing practices adopted by these utilities are also discussed to develop a clear understanding of the damping control strategy.

A detailed model of an interconnected system comprising of many machine groups and several other dynamic devices is synthesised taking several standard models of various subsystems. Standard models of synchronous machine and its control systems, models of networks and loads are described. The small signal model of the SMES is also described. The overall system model is linearised around possible operating conditions to extract the system state matrix. Three study systems are described. The pre-fault and post-fault steady state conditions are defined. The potential electromechanical modes are identified through eigenvalue analysis. The "direction cosine" approach is applied to identify coherent machine and bus groups. The influences of various factors, such as machine model, excitation system characteristics, level of power flows through tie lines, the strength of the tie lines and different types of loads on the damping ratios and the natural frequency of the inter-area modes are explored. The results of the three study

systems revealed that the two damper windings on the q-axis and one damper winding on the d-axis are sufficient to represent rotor-damping contribution to inter-area modes. The faster and high gain excitation systems always contribute negative damping thus reducing the overall damping of the systems. The variation of power flow through tie lines also influences the inter-area mode damping. Higher power flows always reduces damping as it indirectly forces the AVR to act. Stronger tie lines (many tie-circuits) always improve the damping of the inter-area modes as a result of maintaining better voltage profiles. The relationship between the nature of the loads and the inter-area mode damping is very complex and is often not straightforward. Damping is very dependent on the distribution of the loads throughout the system, voltage characteristics of the load, relative electrical distances amongst the loads, generation and tie lines. The dynamic (induction motor type) loads generally improve damping as a result of sharing some of the oscillating energy within coherent areas. These factors are well investigated and well documented. The non-linear simulations were also used to examine the effect of large disturbances on the dynamical behaviour of the system in the presence of device non-linearity and saturation. The inter-area modes are also found from the system response as further validation of the eigenvalue analysis results.

9.2.2 SMES AS A POSSIBLE SOLUTION

It is found that the modulation of the injected real power by a shunt device can control real power oscillations very quickly and effectively. In view of this, the application of SMES is found very suitable to damp the oscillations. The basic principle of operation of a SMES unit is described. A brief historical overview of SMES in power system applications is given. The benefits of SMES in power systems are discussed. The current status of the technology development across the world is also elaborated. The guidelines to compute the rating of the SMES are also discussed.

The practices adopted by various utilities on setting damping design specifications are discussed. It is found that the design specification varies from utility to utility. A new approach is introduced to set damping design specifications in an attempt to standardise design guidelines. The safety margin is also discussed in view of non-linear nature of the system dynamics triggered by large disturbances.

The modal controllability, observability and residue approach are applied to select the most effective locations of the SMES and also the most effective feedback

signals. The choice of signals is restricted to local ones for better reliability. The real power in the adjacent line is most effective considering their self-limiting action during fault. The potential locations and effective feedback signals are suggested for the study systems.

9.2.3 ROBUST DAMPING CONTROL DESIGN BY THE WNEDM APPROACH

The strategy of a low-order robust damping controller based on the WNEDM method is introduced in power systems. The method is modified to provide a stable damping controller for power systems by including suitable constraints. For systems with more than one critical inter-area mode, sequential design is carried out to damp one mode at a time. The practical aspects of weight selections are also discussed. Some suggested weights are seen to work for three study systems. It is concluded that these weights are standard and not system specific as far as the power system damping design employing real power modulation of the SMES is concerned. The WNEDM method works very efficiently and successfully in power system damping control design. The design algorithm works very well if the system model is reduced drastically and then the method is applied for controller design. In Study system #1, the balanced residualisation technique provides least model reduction error. The balanced truncation system provides least model reduction errors in Study system #2 and #3. It is observed that the superiority of a particular model reduction method is system specific, so no suggestions are made for using a particular model reduction technique in a power system.

9.2.4 ROBUST DAMPING CONTROL DESIGN BY LMI APPROACH

The concept of LMI approach to H_∞ damping control design is introduced in power systems. The preliminary mathematics of the LMI is described. The formulation of a mixed-sensitivity H_∞ design in the LMI framework is discussed. The pole-placement constraints as an essential objective in the time domain are incorporated as additional LMIs. The derivation of an LMI based controller is carried out very methodically through the substitution of new controller variables. Sequential decentralised design is performed for a system with multiple inter-area modes thus requiring multiple SMES controllers. The discussion on the solvability conditions of the LMI and Riccati based approach to H_∞ mixed-sensitivity-control-design is made. Unlike a Riccati based

approach, the regularity assumption of the plant is absent in an LMI approach, in order to satisfy the solvability conditions. A successful attempt is made to standardise the weights in a mixed sensitivity design from a power system damping control viewpoint. It is shown that the same sets of weights work very well with three study systems.

9.2.5 CONTROLLER PERFORMANCE

The performance of the controllers obtained by the WNEDM and LMI approaches are discussed in detail. The performance is initially evaluated in the frequency domain using an eigenvalue technique. The damping ratio of the pre-fault and post-fault steady state conditions are first checked with the controllers connected. The effect of the variation of the power flow through tie lines and the different types of loads are evaluated. It is found that the controllers are robust in all of these cases. The controllers do not degrade the damping of the other modes, especially the local and other inter-area modes.

Non-linear simulations are performed to validate the robustness performance of the controller in the presence of non-linearities and device saturation in the systems. The dynamic response in the time domain clearly proves that the controllers can withstand the effect of large disturbances and are not affected by the transient stability performance of the systems.

The damping performances of the controllers obtained by these methods are compared with the performances by the controllers obtained by the root-locus technique. It is found that the controller obtained by the root locus approach provides costly controller action for the same pre-fault damping performance. The H_2 norm of the controller output to a reference input is unusually high in the root-locus approach. As a result of this, the small disturbance performance of the root-locus design is unacceptable as it causes greater wear and tear of the SMES. The small disturbance performance of the WNEDM and LMI based control methods are very good. For the same H_2 norm of the controller output to the reference input, the damping provided by WNEDM and LMI based design is much better.

The damping performance of the LMI based controller is compared with that of a Riccati based controller in the same augmented plants with identical bounds on γ. It is shown that the numerical nature of solution in the LMI method always provides a

damping controller with better damping ratios in the closed loop. The poorly damped controller modes in the inter-area frequency range are absent in the numerical solution. The Riccati approach of an analytical solution for the controller structure provides a controller that cannot provide adequate damping for the inter-area mode of interest. Moreover, several lightly damped controller modes are introduced because of the nature of the solution. These controller modes always interfere with the transient stability performance of the system. They also interact adversely with the other modes in the post-fault dynamic period.

A non-linear simulation is carried out to evaluate the large disturbance performance of the controllers obtained by both approaches. It is found that the controllers initially hit the limits of their outputs. Following the clearances of the fault, the oscillations effectively settle in 10 to 12 seconds by the action of the controllers.

9.3 FURTHER WORK

The work that can be carried out as a further extension to this thesis is described in the following sections.

9.3.1 APPLICATION OF THESE APPROACHES TO INCLUDE OTHER FACTS DEVICES

The whole of the conclusions in this thesis is based on the results obtained by the real power modulation of the SMES device. These methods can be extended to include other FACTS devices listed in Chapter One. The weights that have been claimed as standard for real power modulation of the system through SMES devices may not be so with other FACTS devices. There is scope to further explore the possibility of standardising the weights in other FACTS devices. A feedback signal other than line real power for other FACTS devices can be chosen. The interactions amongst various modes (control and electromechanical) must be studied in other devices.

9.3.2 APPLICATION OF THESE APPROACHES TO DAMP TORSIONAL OSCILLATIONS

This thesis does not consider the torsional oscillation problem triggered by subsynchronous resonance in a series compensated system. It is assumed that they, if exist, are well damped by some other means. In an inter-area mode damping design this assumption is fair particularly with a FACTS device which is other than controllable

series capacitor. These techniques can be extended to include torsional modes (10 to 45 Hz). A suitable input-output can be chosen to derive an effective model of the system to the damping control design of the torsional modes. There is much scope in looking for suitable model reduction and weight selection techniques for designing a successful controller.

9.3.3 APPLICATION TO MID-TERM AND LONG-TERM STABILITY PROBLEMS

The concept of mid-term and long-term stability are introduced to the area of the power system dynamics to deal with the problems associated with severe system upsets in the longer time frame. Severe system upsets result in large excursions of voltage, frequency and power flows thereby invoking the actions of slow processes, controls and protections not modelled in small signal and transient stability studies. The characteristic time of the processes and devices activated by the large voltage and frequency shifts will range from a matter of seconds to several minutes. The long-term stability analysis assumes that the inter-machine synchronising power oscillations have settled; the results being the uniform system frequency. The phenomena that accompany large scale and longer duration system upsets are boiler dynamics of thermal units, pen stock and conduit dynamics of hydro units, automatic generation control, power plant and transmission system protection/control, transformer saturation, and off-nominal frequency effects on loads and the network.

These slower devices should first be modelled. The robust control design problem needed to ensure minimum loss of the service in the island system, can be formulated. The WNEDM and LMI approach can be used to design the control associated with such slower devices.

9.3.4 EXPLORING THE POSSIBILITIES OF OTHER DECENTRALISED CONTROL TECHNIQUES

The WNEDM method is applicable for a single-input-single-output (SISO), multi-input-single-output (MISO) and single-input-multi-output (SIMO) problem. The extension to multi-input-multi-output (MIMO) should be explored further in a decentralised manner. The LMI approach is a multivariable approach, i.e all of the controllers can be designed in a single step. This will result in a centralised controller.

Centralised control has several drawbacks. The signals have to be transmitted to all of the devices located at different physical locations and thereby lowering the reliability margin. Secondly the interactions amongst the cross-coupled term of the controller has to be minimised. The iterative-LMI approach suggested in [137] can be further pursued.

9.3.5 INCLUSION OF REACTIVE POWER MODULATION OPTION TO MINIMISE THE RATINGS OF THE SMES

The inclusion of the reactive power channel into the LMI formulation to damp the same mode can be attempted in order to reduce the rating requirement of the device. This should be done with caution in order to avoid any interactions between the control channels. The risk of interaction is very high in this case and the control design problem should be carefully formulated and solved.

APPENDIX A

LINEARIZATION OF DAE IN (3.53) TO (3.77) OF CHAPTER THREE

The linearization of the nonlinear differential algebraic equations (3.53) – (3.77) gives rise to the following set of linear differential algebraic equations. The three-damper-winding model case is considered here for linearisation. Linearisation of other machine models are carried out in similar manner and so are not shown here.

Equations describing dynamics of the i^{th} machine:

$$\frac{d\Delta\delta_i}{dt} = C_{\omega i}\Delta\omega_i \tag{A.1}$$

$$\frac{d\Delta\omega_i}{dt} = \frac{1}{M_i}\left[\begin{array}{l} C_{m1i}\Delta T_{mi} + C_{m2i}\Delta E_{qi}' + C_{m3i}\Delta E_{di}' + C_{m4i}\Delta\Psi_{1di} + C_{m5i}\Delta\Psi_{2qi} + \\ C_{m6i}\Delta I_{qi} + C_{m7i}\Delta I_{di} + C_{m8i}\Delta\omega_i \end{array}\right] \tag{A.2}$$

$$\frac{d\Delta E_{qi}'}{dt} = +\frac{1}{T_{doi}'}\left[C_{q1i}\Delta E_{qi}' + C_{q2i}\Delta\Psi_{1di} + C_{q3i}\Delta E_{fdi} + C_{q4i}\Delta I_{di}\right] \tag{A.3}$$

$$\frac{d\Delta E_{di}'}{dt} = -\frac{1}{T_{qoi}'}\left[C_{d1i}\Delta E_{di}' + C_{d2i}\Delta\Psi_{2qi} + C_{d3i}\Delta I_{qi}\right] \tag{A.4}$$

$$\frac{d\Delta\Psi_{1di}}{dt} = \frac{1}{T_{doi}''}\left[C_{sd1i}\Delta E_{qi}' + C_{sd2i}\Delta\Psi_{1di} + C_{sd3i}\Delta I_{di}\right] \tag{A.5}$$

$$\frac{d\Delta\Psi_{2qi}}{dt} = -\frac{1}{T_{qoi}''}\left[C_{sq1i}\Delta E_{di}' + C_{sq2i}\Delta\Psi_{2qi} + C_{sq3i}\Delta I_{qi}\right] \tag{A.6}$$

where, the coefficients are:

$$C_{\omega i} = 1.0\,;\; M_i = \frac{2H_i}{\omega_i}$$

$$C_{m1i} = 0.0;$$

$$C_{m2i} = -\frac{\left(X_{di}'' - X_{lsi}\right)}{\left(X_{di}' - X_{lsi}\right)} I_{qio}; C_{m3i} = -\frac{\left(X_{qi}'' - X_{lsi}\right)}{\left(X_{qi}' - X_{lsi}\right)} I_{dio}; C_{m4i} = -\frac{\left(X_{di}' - X_{di}''\right)}{\left(X_{di}' - X_{lsi}\right)} I_{qio}$$

$$C_{m5i} = \frac{\left(X_{qi}' - X_{qi}''\right)}{\left(X_{qi}' - X_{lsi}\right)} I_{dio};$$

$$C_{m6i} = -\frac{\left(X_{di}'' - X_{lsi}\right)}{\left(X_{di}' - X_{lsi}\right)} E_{qio}' - \frac{\left(X_{di}' - X_{di}''\right)}{\left(X_{di}' - X_{lsi}\right)} \Psi_{1dio} + \left(X_{qi}'' - X_{di}''\right) I_{dio}$$

$$C_{m7i} = -\frac{\left(X_{qi}'' - X_{lsi}\right)}{\left(X_{qi}' - X_{lsi}\right)} E_{dio}' + \frac{\left(X_{qi}' - X_{qi}''\right)}{\left(X_{qi}' - X_{lsi}\right)} \Psi_{2qi} + \left(X_{qi}'' - X_{di}''\right) I_{qio}$$

$$C_{m8i} = -D_i;$$

$$C_{q1i} = -\frac{(X_{di} - X_{di}')(X_{di}' - X_{di}'')}{(X_{di}' - X_{lsi})^2} - 1;$$

$$C_{q2i} = +\frac{(X_{di} - X_{di}')(X_{di}' - X_{di}'')}{(X_{di}' - X_{lsi})^2};$$

$$C_{q3i} = 1.0; \; C_{q4i} = (X_{di} - X_{di}') - \frac{(X_{di} - X_{di}')(X_{di}' - X_{di}'')}{(X_{di}' - X_{lsi})};$$

$$C_{d1i} = +\frac{(X_{qi} - X_{qi}')(X_{qi}' - X_{qi}'')}{(X_{qi}' - X_{lsi})^2} + 1;$$

$$C_{d2i} = +\frac{(X_{qi} - X_{qi}')(X_{qi}' - X_{qi}'')}{(X_{qi}' - X_{lsi})^2};$$

$$C_{d3i} = (X_{qi} - X_{qi}') - \frac{(X_{qi} - X_{qi}')(X_{qi}' - X_{qi}'')}{(X_{qi}' - X_{lsi})};$$

$$C_{sd1i} = 1; C_{sd2i} = -1; C_{sd3i} = \left(X_{di}' - X_{lsi}\right)$$

$$C_{sq1i} = 1; C_{sq2i} = 1; C_{sq3i} = -\left(X_{qi}' - X_{lsi}\right)$$

Equations describing exciter of type DC1A [93] dynamics:

$$\frac{d\Delta V_{tri}}{dt} = \frac{1}{T_{ri}}\left[C_{tr1}\Delta V_{tri} + C_{tr2}\Delta V_t\right] \tag{A.7}$$

$$\frac{d\Delta E_{fdi}}{dt} = \frac{1}{T_{Ei}}\left[C_{fd1i}\Delta E_{fdi} + C_{fd2i}\Delta V_{ri}\right] \tag{A.8}$$

$$\frac{d\Delta V_{ri}}{dt} = \frac{1}{T_{Ai}}\left[C_{r1i}\Delta E_{fdi} + C_{r2i}\Delta V_{ri} + C_{r3i}\Delta R_{fi} + C_{r4i}\Delta V_{tri}\right] \tag{A.9}$$

$$\frac{d\Delta R_{fi}}{dt} = \frac{1}{T_{fi}}\left[C_{rf1i}\Delta E_{fdi} + C_{rf2i}\Delta R_{fi}\right] \tag{A.10}$$

$$\frac{d\Delta V_{tri}}{dt} = \frac{1}{T_{ri}}\left[C_{tr1i}\Delta V_{tri} + C_{tr2i}\Delta V_{ti}\right] \tag{A.11}$$

$$C_{tr1} = 1.0; C_{tr2} = -1.0$$

$$C_{fd1i} = \left(-K_{ei} - ABe^{BE_{fdio}}\right); C_{fd2i} = 1.0;$$

$$C_{r1i} = -\frac{K_{ai}K_{fi}}{T_{fi}}; C_{r2i} = -1.0; C_{r3i} = K_{ai}; C_{r4i} = -K_{ai};$$

$$C_{rf1i} = \frac{K_{fi}}{T_{fi}}; C_{rf2i} = -1.0; C_{tr1i} = -1.0; C_{tr2i} = 1.0;$$

Load dynamics:

$$\frac{d\Delta\theta_{Li}}{dt} = -\frac{1}{K_{qwi}}\left[-\Delta Q_{SMi} + \Delta S_{qi} + \Delta Q_{Li}\right] \tag{A.12}$$

$$\frac{d\Delta V_{Li}}{dt} = -\frac{1}{K_{pwi}T_i}\left[-\Delta P_{SMi} + \Delta S_{pi} + \Delta P_{Li} - \frac{K_{pwi}}{K_{qwi}}\left(-\Delta Q_{SMi} + \Delta S_{qi} + \Delta Q_{Li}\right)\right] \tag{A.13}$$

when,

$$\Delta P_{Li} = n_{pi}\frac{P_{Li0}}{V_{Li0}}\left(\frac{V_{Li}}{V_{Li0}}\right)^{(n_{pi}-1)} \tag{A.13.1}$$

$$\Delta Q_{Li} = n_{qi}\frac{Q_{Li0}}{V_{Li0}}\left(\frac{V_{Li}}{V_{Li0}}\right)^{(n_{qi}-1)} \tag{A.13.2}$$

$$\begin{aligned}
\Delta S_{pi} = &\Big(\sum_{k=1}^{k=n} V_{i0}V_{k0}\left[-G_{ik}Sin(\theta_{i0}-\theta_{k0}) + B_{ik}Cos(\theta_{i0}-\theta_{k0})\right] - V_{i0}{}^2B_{ii}\Big)\Delta\theta_i \\
&+V_{i0}V_{k0}\left[G_{ik}Sin(\theta_{i0}-\theta_{k0}) - B_{ik}Cos(\theta_{i0}-\theta_{k0})\right]\Delta\theta_k + \\
&\Big(\sum_{k=1}^{k=n} V_{k0}\left[-G_{ik}Cos(\theta_{i0}-\theta_{k0}) + B_{ik}Sin(\theta_{i0}-\theta_{k0})\right] + V_{i0}G_{ii}\Big)\Delta V_i \\
&+V_{i0}\left[G_{ik}Cos(\theta_{i0}-\theta_{k0}) + B_{ik}Sin(\theta_{i0}-\theta_{k0})\right]\Delta V_k
\end{aligned} \tag{A.13.3}$$

$$\begin{aligned}
\Delta S_{qi} = &\Big(\sum_{k=1}^{k=n} V_{i0}V_{k0}\left[G_{ik}Cos(\theta_{i0}-\theta_{k0}) + B_{ik}Sin(\theta_{i0}-\theta_{k0})\right] - V_{i0}{}^2G_{ii}\Big)\Delta\theta_i \\
&+V_{i0}V_{k0}\left[-G_{ik}Cos(\theta_{i0}-\theta_{k0}) - B_{ik}Sin(\theta_{i0}-\theta_{k0})\right]\Delta\theta_k + \\
&\Big(\sum_{k=1}^{k=n} V_{k0}\left[G_{ik}Sin(\theta_{i0}-\theta_{k0}) - B_{ik}Cos(\theta_{i0}-\theta_{k0})\right] - V_{i0}B_{ii}\Big)\Delta V_i \\
&+V_{i0}\left[G_{ik}Sin(\theta_{i0}-\theta_{k0}) - B_{ik}Cos(\theta_{i0}-\theta_{k0})\right]\Delta V_k
\end{aligned} \tag{A.13.4}$$

SMES system:

$$\frac{d\Delta P_{SMi}}{dt} = +\frac{1}{T_{cpi}}\left(-\Delta P_{SMi} + \Delta P_{smsi}\right) \tag{A.14}$$

$$\frac{d\Delta Q_{smci}}{dt} = \frac{1}{T_{v2i}}\left[-\Delta Q_{smci} + K_{vi}\left(\frac{T_{v1i} - T_{vmi}}{T_{vmi}}\right)\Delta V_{smti} + K_{vi}\left(\Delta V_{smsi} - \frac{T_{v1i}}{T_{vmi}}\Delta V_{ti}\right)\right]$$

(A.15)

$$\frac{d\Delta Q_{SMi}}{dt} = \frac{1}{T_{cqi}}\left(-\Delta Q_{SMi} + \Delta Q_{smci}\right) \tag{A.16}$$

$$\frac{d\Delta V_{smti}}{dt} = \frac{1}{T_{vmi}}\left(-\Delta V_{smti} + \Delta V_{ti}\right) \tag{A.17}$$

Linearising non-linear algebraic equations associated with each of the machines, one obtains the following linear algebraic equations:

$$C_{sa1i}\Delta\delta_i + C_{sa2i}\Delta E_{qi}' + C_{sa3i}\Delta\Psi_{1di} + C_{sa4i}\Delta I_{qi} + C_{sa5i}\Delta I_{di} + C_{sa6i}\Delta\theta_i + C_{sa7i}\Delta V_i = 0$$

(A.18)

$$C_{sa8i}\Delta\delta_i + C_{sa9i}\Delta E_{di}' + C_{sa10i}\Delta\Psi_{2qi} + C_{sa11i}\Delta I_{qi} + C_{sa12i}\Delta I_{di} + C_{sa13i}\Delta\theta_i + C_{sa14i}\Delta V_i = 0$$

(A.19)

$$C_{sa1i} = -V_{io}Sin(\delta_{io} - \theta_{io}); C_{sa2i} = -\frac{\left(X_{di}'' - X_{lsi}\right)}{\left(X_{di}' - X_{ls}\right)}; C_{sa3i} = -\frac{\left(X_{di}' - X_{di}''\right)}{\left(X_{di}' - X_{lsi}\right)}$$

$$C_{sa4i} = R_{si};\ C_{sa5i} = -X_{di}'';\ C_{sa6i} = V_{io}Sin(\delta_i - \theta_i); C_{sa7i} = Cos(\delta_i - \theta_i);$$

$$C_{sa8i} = V_{io}Cos(\delta_{io} - \theta_{io}); C_{sa9i} = \frac{\left(X_{qi}'' - X_{lsi}\right)}{\left(X_{qi}' - X_{ls}\right)}; C_{sa10i} = -\frac{\left(X_{qi}' - X_{qi}''\right)}{\left(X_{qi}' - X_{lsi}\right)}$$

$$C_{sa11i} = -X_{qi}''\,;$$

$$C_{sa12i} = -R_{si}\,; C_{sa13i} = -V_{io}Cos(\delta_i - \theta_i)\,; C_{sa14i} = Sin(\delta_i - \theta_i)\,;$$

$$\begin{aligned}
&(-V_{i0}I_{qi0}Sin(\delta_{i0} - \theta_{i0}) - V_{i0}I_{di0}Cos(\delta_{i0} - \theta_{i0}))\Delta\delta_i + \\
&(V_{i0}I_{qi0}Sin(\delta_{i0} - \theta_{i0}) + V_{i0}I_{di0}Cos(\delta_{i0} - \theta_{i0}))\Delta\theta_i + \\
&V_{i0}Cos(\delta_{i0} - \theta_{i0})\Delta I_{qi} - V_{i0}Sin(\delta_{i0} - \theta_{i0})\Delta I_{di} + \\
&(I_{qi0}Cos(\delta_{i0} - \theta_{i0}) - I_{di0}Sin(\delta_{i0} - \theta_{i0}))\Delta V_i - \Delta S_{pi} = 0
\end{aligned} \tag{A.20}$$

$$\begin{aligned}
&(-V_{i0}I_{qi0}Cos(\delta_{i0} - \theta_{i0}) + V_{i0}I_{di0}Sin(\delta_{i0} - \theta_{i0}))\Delta\delta_i - \\
&(V_{i0}I_{qi0}Cos(\delta_{i0} - \theta_{i0}) + V_{i0}I_{di0}Sin(\delta_{i0} - \theta_{i0}))\Delta\theta_i + \\
&-V_{i0}Sin(\delta_{i0} - \theta_{i0})\Delta I_{qi} - V_{i0}Cos(\delta_{i0} - \theta_{i0})\Delta I_{di} - \\
&(I_{qi0}Sin(\delta_{i0} - \theta_{i0}) + I_{di0}Cos(\delta_{i0} - \theta_{i0}))\Delta V_i - \Delta S_{qi} = 0
\end{aligned} \tag{A.21}$$

APPENDIX B

PARAMETRS OF THE STUDY SYSTEMS

B.1 STUDY SYSTEM #1

Load flow solutions when 400 MW flows from Area #1 to Area #2

			GENERATION		LOAD	
BUS	**VOLTS**	**ANGLE**	**REAL**	**REACTIVE**	**REAL**	**REACTIVE**
1.0000	1.0300	21.6291	7.2000	1.8144	0	0
2.0000	1.0100	11.5945	7.2000	2.1701	0	0
3.0000	1.0300	00.000	6.3253	1.5522	0	0
4.0000	1.0100	-9.0625	6.0000	1.8708	0	0
5.0000	0.9681	-3.9397	0	0	10.0000	1.0000
6.0000	0.9677	-22.1413	0	0	16.0000	1.0000
7.0000	1.0074	14.9880	0	0	0.0000	-0.0000
8.0000	0.9659	-13.1003	0	0	0.0000	-0.0000
9.0000	0.9814	4.6411	0	0	0	0
10.0000	0.9841	-14.8367	0	0	-0.0000	-0.0000
11.0000	1.0101	-5.8157	0	0	0.0000	0.0000

For other power flow pattern, the loads and the generations are adjusted to result in desirable tie line flow.

LINE DATAS

From Bus	**To Bus**	**R (p.u.)**	**X (p.u.)**	**B (p.u)**	**Tap ratio**	**Phase**
1	7	0	0.0167	0	0.0	0.0
2	9	0	0.0167	0	0.0	0.0
3	11	0	0.0167	0	0.0	0.0
4	10	0	0.0167	0	0.0	0.0
5	8	0.0110	0.1100	0.1925	0.0	0.0
5	8	0.0110	0.1100	0.1925	0.0	0.0
5	8	0.0110	0.1100	0.1925	0.0	0.0
6	10	0.0010	0.0100	0.0175	0.0	0.0
7	9	0.0025	0.0250	0.0437	0.0	0.0

8	6	0.0110	0.1100	0.1925	0.0	0.0
8	6	0.0110	0.1100	0.1925	0.0	0.0
8	6	0.0110	0.1100	0.1925	0.0	0.0
9	5	0.0010	0.0100	0.0175	0.0	0.0
10	11	0.0025	0.0250	0.0437	0.0	0.0

MACHINE DATAS (Identical for all machines except for *H*-constants)

Datas are expressed in per unit with respective machine base.

Base MVA= 900; X_{ls} =0.2; R_s = 0.0025; X_d = 1.8; $X_d^{'}$ = 0.3; $X_d^{''}$= 0.25; $T_{d0}^{'}$ = 8.0; $T_{d0}^{''}$= 0.03;

X_q= 1.7; $X_q^{'}$=0.55; $X_q^{''}$= 0.25; $T_{q0}^{'}$= 0.40; $T_{q0}^{''}$=0.05; H_1 =H_2=6.50 s.; H_3=H_4=6.175 s. D=0.0;

EXCITER DATAS (Identical for all units)

Type: ST1A

T_r= 0.01 s; K_a= 200; T_a=0.055 s; T_b = 1.0 s; T_c = 10.0 s V_{Rmax} = 7.5 (p.u.); V_{Rmin}= -7.5 (p.u.)

Type DC1A

T_r= 0.05 s; K_a= 20; T_a=0.055 s; V_{Rmax} = 4.5 (p.u.) V_{Rmin}= -4.5 (p.u.); T_e= 0.36 s; S_{e1}= 0.0056; S_{e2}= 1.075; K_f= 0.125; T_f=1.8 s

DYNAMIC LOAD DATAS

K_{pw}=0.40; K_{qw}= -0.03; K_{pv}= 0.3; K_{qv}=-2.8; K_{qv2}=2.1; T= 8.5 s

SMES DATAS

T_{cp}=T_{cq} = 0.026 s; K_v=10.0; T_{v1} = 1.0 s; T_{v2}=10.0 s; T_{vm} = 0.02 s.

B.2 STUDY SYSTEM #2

Load flow solution when 550 MW flows in the tie lines between Area #3 and Area #1 and Area #2.

			GENERATION		LOAD	
BUS	**VOLTS**	**ANGLE**	**REAL**	**REACTIVE**	**REAL**	**REACTIVE**
1.0000	1.0300	-18.4226	8.0000	3.8684	0	0
2.0000	1.0300	-18.4226	8.0000	3.8684	0	0
3.0000	1.0300	-1.6040	8.0000	1.7679	0	0

4.0000	1.0300	-1.6040	8.0000	1.7679	0	0
5.0000	1.0300	2.0496	8.0000	2.5624	0	0
6.0000	1.0300	0.0000	5.8145	2.3153	0	0
7.0000	0.9442	-30.8770	0	0	20.0000	6.0000
8.0000	0.9759	-26.0602	0	0	-0.0000	0.0000
9.0000	0.9732	-28.4287	0	0	3.0000	-1.0000
10.0000	0.9899	-26.2211	0	0	-0.0000	-0.0000
11.0000	0.9978	-13.4985	0	0	8.0000	2.0000
12.0000	1.0097	-8.9848	0	0	-0.0000	-0.0000
13.0000	0.9638	-28.6707	0	0	6.0000	-0.0000
14.0000	0.9766	-9.4019	0	0	8.0000	2.0000
15.0000	0.9969	-5.4263	0	0	-0.0000	0.0000
16.0000	0.9629	-19.0120	0	0	0.0000	-0.0000

For other power flow pattern, the loads and generations are adjusted to result in desirable tie line flow.

LINE DATAS

From Bus	To Bus	R (p.u.)	X (p.u.)	B (p.u)	Tap ratio	Phase
1	8	0	0.0167	0	0.0	0.0
2	8	0	0.0167	0	0.0	0.0
3	12	0	0.0167	0	0.0	0.0
4	12	0	0.0167	0	0.0	0.0
5	15	0	0.0167	0	0.0	0.0
6	15	0	0.0167	0	0.0	0.0
7	8	0.0005	0.0050	0	0.0	0.0
7	9	0.0010	0.0100	0	0.0	0.0
9	10	0.0005	0.0050	0	0.0	0.0
9	13	0.0010	0.0100	0	0.0	0.0
10	11	0.0088	0.0833	1.4516	0.0	0.0
10	11	0.0088	0.0833	1.4516	0.0	0.0
10	11	0.0088	0.0833	1.4516	0.0	0.0

11	12	0.0005	0.0050	0	0.0	0.0
13	16	0.0086	0.0830	0.1606	0.0	0.0
13	16	0.0086	0.0830	0.1606	0.0	0.0
13	16	0.0086	0.0830	0.1606	0.0	0.0
14	16	0.0086	0.0830	0.1606	0.0	0.0
14	16	0.0086	0.0830	0.1606	0.0	0.0
14	16	0.0086	0.0830	0.1606	0.0	0.0
15	14	0.0005	0.0050	0	0.0	0.0

MACHINE DATAS (Identical in all of the six machines)

The value of all the parameters are identical to those listed in Study system #1. The inertia constant H is 3.5 s for all of the units.

EXCITER DATAS (Identical in all of the six machines)

The values are same as in study system #1.

DYNAMIC LOAD DATAS

Same as in Study system #1

SMES DATAS (Identical for both of the SMES devices)

The parameters are as listed in Study system #1.

B.3 STUDY SYSTEM #3

Load flow solution when 100 MW flows in the tie lines between NETS and NYPS.

			GENERATION		LOAD	
BUS	**VOLTS**	**ANGLE**	**REAL**	**REACTIVE**	**REAL**	**REACTIVE**
1.0000	1.0450	10.8528	2.5000	1.1548	0	0
2.0000	0.9800	14.4107	5.4500	1.8428	0	0
3.0000	0.9830	16.4403	6.5000	1.9875	0	0
4.0000	0.9970	17.4924	6.3200	1.0709	0	0
5.0000	1.0110	16.0139	5.0520	1.6234	0	0
6.0000	1.0500	20.3357	7.0000	2.1975	0	0
7.0000	1.0630	22.5644	5.6000	0.9851	0	0
8.0000	1.0300	16.4532	5.4000	0.0030	0	0

9.0000	1.0250	20.7882	8.0000	0.0492	0	0
10.0000	1.0100	15.9039	5.0000	0.0605	0	0
11.0000	1.0000	18.3469	10.0000	-0.1728	0	0
12.0000	1.0156	4.8617	13.5000	2.4914	0	0
13.0000	1.0110	0	35.9142	8.7543	0	0
14.0000	1.0000	46.0243	17.8500	0.6218	0	0
15.0000	1.0000	39.7848	10.0000	0.6718	0	0
16.0000	1.0000	45.5297	40.0000	4.6003	0	0
17.0000	1.0290	-6.8046	0	0	60.0000	3.0000
18.0000	0.9935	38.5921	0	0	24.7000	1.2300
19.0000	1.0501	12.2738	0	0	0.0000	0.0000
20.0000	0.9904	10.8411	0	0	6.8000	1.0300
21.0000	1.0325	10.3137	0	0	2.7400	1.1500
22.0000	1.0501	14.9965	0	0	0	0
23.0000	1.0450	14.7084	0	0	2.4800	0.8500
24.0000	1.0386	7.8521	0	0	3.0900	-0.9200
25.0000	1.0598	9.6977	0	0	2.2400	0.4700
26.0000	1.0561	8.1988	0	0	1.3900	0.1700
27.0000	1.0434	6.3142	0	0	2.8100	0.7600
28.0000	1.0520	11.3328	0	0	2.0600	0.2800
29.0000	1.0509	13.9700	0	0	2.8400	0.2700
30.0000	1.0536	6.0686	0	0	-0.0000	-0.0000
31.0000	1.0573	8.6303	0	0	-0.0000	0.0000
32.0000	1.0511	10.9564	0	0	0.0000	0.0000
33.0000	1.0563	7.4727	0	0	1.1200	-0.0000
34.0000	1.0652	2.5372	0	0	-0.0000	-0.0000
35.0000	1.0139	2.5329	0	0	-0.0000	0.0000
36.0000	1.0423	-0.8475	0	0	1.0200	-0.1946
37.0000	1.0365	6.5853	0	0	0.0000	-0.0000
38.0000	1.0558	8.6771	0	0	0.0000	-0.0000
39.0000	1.0057	-8.4423	0	0	2.6700	0.1260
40.0000	1.0677	15.2164	0	0	0.6563	0.2353
41.0000	0.9994	44.4892	0	0	10.0000	2.5000

42.0000	0.9991	38.9245	0	0	11.5000	2.5000
43.0000	1.0147	-7.6065	0	0	0.0000	0.0000
44.0000	1.0140	-7.6366	0	0	2.6755	0.0484
45.0000	1.0178	2.5251	0	0	2.0800	0.2100
46.0000	1.0324	9.6462	0	0	1.5070	0.2850
47.0000	1.0738	7.3628	0	0	2.0312	0.3259
48.0000	1.0765	9.2792	0	0	2.4120	0.0220
49.0000	1.0117	12.8815	0	0	1.6400	0.2900
50.0000	1.0119	19.3313	0	0	1.0000	-1.4700
51.0000	1.0221	6.5226	0	0	3.3700	-1.2200
52.0000	1.0338	5.7198	0	0	1.5800	0.3000
53.0000	1.0591	6.6150	0	0	2.5270	1.1856
54.0000	1.0516	8.4338	0	0	-0.0000	-0.0000
55.0000	1.0328	5.4317	0	0	3.2200	0.0200
56.0000	1.0059	4.3141	0	0	5.0000	1.8400
57.0000	1.0072	5.2538	0	0	0.0000	-0.0000
58.0000	1.0093	5.9351	0	0	0.0000	0.0000
59.0000	0.9995	3.6644	0	0	2.3400	0.8400
60.0000	0.9990	3.1221	0	0	5.2200	1.7700
61.0000	1.0391	2.5792	0	0	1.0400	1.2500
62.0000	1.0184	8.4534	0	0	-0.0000	-0.0000
63.0000	1.0141	7.5963	0	0	-0.0000	-0.0000
64.0000	1.0553	7.6199	0	0	0.0900	0.8800
65.0000	1.0157	7.7854	0	0	-0.0000	0.0000
66.0000	1.0134	6.2381	0	0	0	0
67.0000	1.0171	6.1423	0	0	3.2000	1.5300
68.0000	1.0334	7.6789	0	0	3.2900	0.3200

The other values of tie line flows are created by adjusting generations and loads in some of the key busses in NETS and NYPS areas.

LINE DATAS

From Bus	To Bus	R (p.u.)	X (p.u.)	B (p.u)	Tap ratio	Phase
17	13	0	0.0033	0	1.0400	0
17	43	0.0005	0.0276	0	0	0
18	16	0	0.0030	0	1.0000	0
18	42	0.0040	0.0600	2.2500	0	0
19	4	0.0007	0.0142	0	1.0700	0
19	20	0.0007	0.0138	0	1.0600	0
20	5	0.0009	0.0180	0	1.0090	0
21	22	0.0008	0.0140	0.2565	0	0
22	6	0	0.0143	0	1.0250	0
22	23	0.0006	0.0096	0.1846	0	0
23	7	0.0005	0.0272	0	0	0
23	24	0.0022	0.0350	0.3610	0	0
25	8	0.0006	0.0232	0	1.0250	0
25	26	0.0032	0.0323	0.5310	0	0
26	27	0.0014	0.0147	0.2396	0	0
26	28	0.0043	0.0474	0.7802	0	0
26	29	0.0057	0.0625	1.0290	0	0
28	29	0.0014	0.0151	0.2490	0	0
29	9	0.0008	0.0156	0	1.0250	0
30	31	0.0013	0.0187	0.3330	0	0
30	32	0.0024	0.0288	0.4880	0	0
31	10	0	0.0260	0	1.0400	0
31	38	0.0011	0.0147	0.2470	0	0
32	11	0	0.0130	0	1.0400	0
32	33	0.0008	0.0099	0.1680	0	0
33	34	0.0011	0.0157	0.2020	0	0
33	38	0.0036	0.0444	0.6930	0	0
34	36	0.0033	0.0111	1.4500	0	0
35	34	0.0001	0.0074	0	0.9460	0

35	45	0.0007	0.0175	1.3900	0	0
36	12	0	0.0075	0	1.0400	0
36	17	0.0005	0.0045	0.3200	0	0
37	27	0.0013	0.0173	0.3216	0	0
37	52	0.0007	0.0082	0.1319	0	0
38	46	0.0022	0.0284	0.4300	0	0
39	44	0	0.0411	0	0	0
39	45	0	0.0839	0	0	0
41	14	0	0.0015	0	1.0000	0
41	40	0.0060	0.0840	3.1500	0	0
42	15	0	0.0015	0	1.0000	0
42	41	0.0040	0.0600	2.2500	0	0
43	44	0.0001	0.0011	0	0	0
44	45	0.0025	0.0730	0	0	0
45	51	0.0004	0.0105	0.7200	0	0
46	49	0.0018	0.0274	0.2700	0	0
47	48	0.0025	0.0268	0.4000	0	0
48	40	0.0020	0.0220	1.2800	0	0
49	18	0.0076	0.1141	1.1600	0	0
50	18	0.0012	0.0288	2.0600	0	0
50	51	0.0009	0.0221	1.6200	0	0
53	27	0.0320	0.3200	0.4100	1.0000	0
53	30	0.0008	0.0074	0.4800	0	0
53	31	0.0016	0.0163	0.2500	0	0
53	47	0.0013	0.0188	1.3100	0	0
53	54	0.0035	0.0411	0.6987	0	0
54	1	0	0.0181	0	1.0250	0
54	25	0.0070	0.0086	0.1460	0	0
54	55	0.0013	0.0151	0.2572	0	0
55	52	0.0011	0.0133	0.2138	0	0
55	56	0.0013	0.0213	0.2214	0	0

56	57	0.0008	0.0128	0.1342	0	0
56	66	0.0008	0.0129	0.1382	0	0
57	58	0.0002	0.0026	0.0434	0	0
57	60	0.0008	0.0112	0.1476	0	0
58	2	0	0.0250	0	1.0700	0
58	59	0.0006	0.0092	0.1130	0	0
58	63	0.0007	0.0082	0.1389	0	0
59	60	0.0004	0.0046	0.0780	0	0
60	61	0.0023	0.0363	0.3804	0	0
61	30	0.0019	0.0183	0.2900	0	0
61	30	0.0019	0.0183	0.2900	0	0
61	36	0.0022	0.0196	0.3400	0	0
61	36	0.0022	0.0196	0.3400	0	0
62	3	0	0.0200	0	1.0700	0
62	63	0.0004	0.0043	0.0729	0	0
62	65	0.0004	0.0043	0.0729	0	0
64	63	0.0016	0.0435	0	1.0600	0
64	65	0.0016	0.0435	0	1.0600	0
65	66	0.0009	0.0101	0.1723	0	0
66	67	0.0018	0.0217	0.3660	0	0
67	68	0.0009	0.0094	0.1710	0	0
68	19	0.0016	0.0195	0.3040	0	0
68	21	0.0008	0.0135	0.2548	0	0
68	24	0.0003	0.0059	0.0680	0	0
68	37	0.0007	0.0089	0.1342	0	0

MACHINE DATAS (in p.u. on respective machine base)

Mach. No	Bus No.	Base MVA	X_{ls}	R_s	X_d	X_d'	X_d''	T_{d0}'	T_{d0}''
1	1	100	0.0125	0	0.1000	0.0310	0.0250	10.200	0.0500
2	2	100	0.0350	0	0.2950	0.0697	0.0500	6.5600	0.0500
3	3	100	0.0304	0	0.2495	0.0531	0.0450	5.7000	0.0500
4	4	100	0.0295	0	0.2620	0.0436	0.0350	5.6900	0.0500
5	5	100	0.0270	0	0.3300	0.0660	0.0500	5.4000	0.0500
6	6	100	0.0224	0	0.2540	0.0500	0.0400	7.3000	0.0500
7	7	100	0.0322	0	0.2950	0.0490	0.0400	5.6600	0.0500
8	8	100	0.0280	0	0.2900	0.0570	0.0450	6.7000	0.0500
9	9	100	0.0298	0	0.2106	0.0570	0.0450	4.7900	0.0500
10	10	100	0.0199	0	0.1690	0.0457	0.0400	9.3700	0.0500
11	11	100	0.0103	0	0.1280	0.0180	0.0120	4.1000	0.0500
12	12	100	0.0220	0	0.1010	0.0310	0.0250	7.4000	0.0500
13	13	200	0.0015	0	0.0148	0.0027	0.0020	5.9000	0.0500
14	14	100	0.0017	0	0.0180	0.0029	0.0023	4.1000	0.0500
15	15	100	0.0017	0	0.0180	0.0029	0.0023	4.1000	0.0500
16	16	200	0.0021	0	0.0178	0.0036	0.0027	7.8000	0.0500

Mach. No	X_q	X_q'	X_q''	T_{q0}'	T_{q0}''	D	$H(s)$
1	0.0690	0.0280	0.0250	1.5000	0.0350	4.0000	42.000
2	0.2820	0.0600	0.0500	1.5000	0.0350	9.7500	30.200
3	0.2370	0.0500	0.0450	1.5000	0.0350	10.000	35.800
4	0.2580	0.0400	0.0350	1.5000	0.0350	10.000	28.600
5	0.3100	0.0600	0.0500	0.4400	0.0350	3.0000	26.000
6	0.2410	0.0450	0.0400	0.4000	0.0350	10.000	34.800
7	0.2920	0.0450	0.0400	1.5000	0.0350	8.0000	26.400
8	0.2800	0.0500	0.0450	0.4100	0.0350	9.0000	24.300

9	0.2050	0.0500	0.0450	1.9600	0.0350	14.000	34.500
10	0.1150	0.0450	0.0400	1.5000	0.0350	5.5600	31.000
11	0.1230	0.0150	0.0120	1.5000	0.0350	13.600	28.200
12	0.0950	0.0280	0.0250	1.5000	0.0350	13.500	92.300
13	0.0143	0.0025	0.0020	1.5000	0.0350	66.000	496.00
14	0.0173	0.0025	0.0023	1.5000	0.0350	100.00	300.00
15	0.0173	0.0025	0.0023	1.5000	0.0350	100.00	300.00
16	0.0167	0.0030	0.0027	1.5000	0.0350	100.00	450.00

EXCITER DATAS

Machine #1 to #8 has DC1A type excitation. The exciter parameters are identical in all of these eight machines. The machine # 9 is equipped with ST1A type excitation systems. The rest of the machines are assumed on manual excitation control. The parameters are listed as follows:

Type ST1A

T_r= 0.01 s; K_a= 200; T_a=0.00; T_b= 0.0 s; T_c = 0.0 s V_{Rmax} = 5.0 (p.u.); V_{Rmin}= -5.0 (p.u.)

Type DC1A

T_r= 0.01 s; K_a= 40; T_a=0.02; V_{Rmax} = 10 (p.u.) V_{Rmin}= -10 (p.u.); K_e = 1.0; Te= 0.785 s; S_{e1}= 0.070; S_{e2}= 0.91; K_f= 0.03; T_f=1.0 s

PSS DATAS

The machine #9 is also equipped with a speed-input power system stabiliser. The parameters are as follows:

K_{pss} = 0.0318; T_m = 0.01 s; T_w = 10.0 s.; T_1=T_3= 0.2 s; T_2=T_4= 0.1 s.

DYNAMIC LOAD DATAS

The parameters are same as in Study system #1.

SMES DATAS

The parameters of three SMES devices are identical. The parameters of each of these are same as in Study system #1.

REFERENCES

[1] P. L. Dandeno, "General Overview of Steady-state (Small Signal) Stability in Bulk Electricity Systems," *International Journal of Electric Power and Energy Systems*, Vol. 4, No. 4, October 1982.

[2] O.W. Hanson, C. J. Goodwin, and P. L. Dandeno, " Influence of Excitation and Speed Control Parameters in Stabilizing Intersystem Oscillations," *IEEE Trans. on Power Apparatus and Systems*, Vol. 87, No. 5, May 1968, pp. 1306-1313.

[3] CIGRE Publication, "Analysis and Control of Power System Oscillation", *CIGRE Special Publication 38.01.07*, Technical Brochure 111, 1996.

[4] F. R. Schleif, G.E. Martin, and R. R. Angell, " Damping of System Oscillations with a Hydro-Generating Unit," *IEEE Trans. on Power Apparatus and Systems*, Vol. 86, No. 4, April 1967, pp. 438-442.

[5] F. R. Schleif and J.H. White, "Damping for Northwest-Southwest Tie Line Oscillations – An Analogue Study," *IEEE Trans. on Power Apparatus and Systems*, Vol. 85, No. 12, December 1966, pp. 1234-1247.

[6] R. L. Cresap, D.N. Scott, W.A. Mittelstadt, and C.W. Taylor, "Damping of Pacific AC Intertie Oscillations via Modulation of the Parallel Pacific HVDC Intertie," *CIGRE paper* 14-05, Paris, 1978.

[7] R.L.Lee, M.J. Beshir, A.T. Finely, D.R. Hayes, J. C. Hsu, H. R. Peterson, C.L. Deshazo, and D.W. Gerlach, "Application of Static Var Compensator for the Dynamic Performance of the Mead-Adelanto and Mead-Phoenix Transmission Projects," *IEEE PES T&D Conference and Exposition*, Chicago, IL, 1994.

[8] D.L. Bauer, W.D. Buhr, S.S. Cogswell, D.B. Cory, G.B. Ostroski, and D.A. Swarsson, "Simulation of Low Frequency Undamped Oscillations in Large Power Systems," *IEEE Trans. on Power Apparatus and Systems*, Vol. 94, No. 2, March/April 1975, pp. 207-212.

[9] R. L. Bolden, P. J. Wallace, and Q. W. Grainger, "Considerations in the Improvement of System Damping on the Southeast Australian Interconnected System," *CIGRE paper* 31-05, Paris 1982.

[10] W. Fairney, A. Myles, T. M. Whitelegg, and N.S. Murray, "Low Frequency Oscillations on the 275 kV Interconnectors between Scotland and England," *CIGRE Paper* 31-08, Paris, September 1982.

[11] K. M. Trantor, "Installation of Power System Stabilisers and the Evaluation of Settings," *IEE Proc. C*, Vol.135, No. 3, May 1988, pp. 244-250.

[12] T. Anderson, J. L. Dallachy, and J.A. Toal, "Model Identification Tests and Tests to Prove the Damping Performance of a Digitally Controlled Static Excitation Systems," *CIGRE Paper* 11-305, Paris, 1996.

[13] Y.Y. Hsu, S. W. Shyue, and C.C. Su, "Low Frequency Oscillations in Longitudinal Power System: Experience with Dynamic Stability of Taiwan Power System," *IEEE Transactions on power systems*, Vol. 2, No. 1, February 1987, pp. 92-100.

[14] P. Kundur, M.Klein, G. J. Rogers, and M. S. Zywno, "Application of Power System Stabilizers for Enhancement of Overall System Stability," *IEEE Trans. on Power Systems*, Vol. 4, No. 2, May 1989, pp. 614-626.

[15] P. Gomes, A. L. B. Bomfim, A.S.A. Pedroso, and N. Martins, "Application of Eigenvalue Technique in Power System Dynamics," *Symposium on Specialists in Eectrical Operational Planning*, August 1987.

[16] P. Gomes, J. B. Nazareno, H. Valgas, N. Zeni, and J. F.M. Carvalho, "Application of Power System Stabilizers on the Brazilian Interconnected Power System," *CIGRE Paper* 37-303, Paris, 1992.

[17] A. E. Hammad, "Analysis of Power System Stability Enhancement By Static Var Compensators," *IEEE Trans. on Power Systems*, Vol.1, November 1986, pp. 222-227.

[18] E.V. Larsen, J.J. Sanchez-Gasca, and J.H. Chow, "Concepts for Design of FACTS Controllers to Damp Power Swings," *IEEE Trans. on Power Systems*, Vol. 10, No. 2, May 1995, pp. 692-697.

[19] E. V. Larsen and J.H. Chow, "SVC Control Design Concepts for System Dynamic Performance," *IEEE Tutorial Course: Application of static VAR systems for system dynamic performance*, paper 87 TH01875-5-PWR, pp. 36-53,1987.

[20] M. Noroozian and G. Andersson, "Damping of Power System Oscillations by Use of Controllable Components," *IEEE Trans. on Power Delivery*, Vol. 9, No. 4, October 1994, pp. 2046-2054.

[21] M. Noroozian and G. Andersson, "Damping of Inter-area and Local Modes by Use of Controllable Components," *IEEE Trans. on Power Delivery*, Vol. 10, No. 4, October 1995, pp. 2007-2012.

[22] N. Yang, Q. Liu, and J.D. Mccalley, "TCSC Controller Design for Damping Inter-area Oscillations," *IEEE Trans. on Power Systems*, Vol. 13, No. 4, November1998, pp. 1304-1310.

[23] L. Gyugi, N.G. Hingorani, P.R. Nannery, and N. Tai, "Advanced Static Var Compensator Using Gate Turn-off Thyristors for Utility Applications," *CIGRE Paper* 23-203, Paris, August 1990.

[24] E. Larsen, N. Miller, S. Nilsson, and S. Lindgren, "Benefits of GTO Based Compensation Systems for Electric Utility Applications," *IEEE Trans. on Power Delivery*, Vol. 7, October 1992, pp. 2056-2063.

[25] R. J. Koessler, B. Fardanesh, M.I. Henderson, and R. Adapa, "Energy Storage Applications in New York State'', *FACTS Applications, IEEE Power Engineering Society,* 96TP 116-0, pp. 8.46-8.51.

[26] H.M. Ellis, J.E. Harddy, A.L. Blythe, and J.W. Skooglund, "Dynamic Stability of the Peace River Transmission System," *IEEE Trans. on Power Apparatus and Systems,* Vol. 85, No. 6, June 1966, pp. 586-600.

[27] IEEE Task Force Report, "A Description of Discrete Supplementary Controls for Stability," *IEEE Trans. on Power Apparatus and Systems*, Vol. 97, No. 1, January 1978, pp. 149-165.

[28] D. L. Carson and D.S. Maki, "Feasibility Study for Application of a Thyristor Controlled Braking Resistor (TCBR) on the Northern MAPP Transmission System," *FACTS Applications, IEEE Power Engineering Society*, 96TP 116-0, pp. 8.19-8.21.

[29] H. A. Peterson and P.C. Krause, "Damping of Power Swings in a Parallel AC and DC System," *IEEE Trans. on Power Apparatus and Systems*, Vol. 85, No. 12, December 1966, pp. 1231-1239.

[30] T. Smed and G. Andersson, "Utilizing HVDC to Damp Power Oscillations," *IEEE Trans. on Power Delivery,* Vol. 8, No. 2, October 1993, pp. 2007-2012.

[31] A. M. Sharaf and R. Doraiswami, "Stabilizing an AC Link by Using Static Phase Shifter," *IEEE Trans. on Power Apparatus and System*, Vol.102, No. 4, April 1983, pp. 788-796.

[32] P. Wood, "Study of Improved Load-Tap-Changing for Transformers and Phase Angle Regulators," *EPRI Reports* EL-6079, EPRI, November 1988.

[33] M. La Scala, R. Sbrizzai, F. Torelli, and M. Trovato, "Enhancement of Interconnected Power System Stability Using a Control Strategy Involving Static Phase Shifters," *International Journal of Electrical Power and Energy Systems*, Vol. 15, No. 6, 1993, pp. 387-396.

[34] C. F. Lu, C.C. Liu, and C. J. Wu, "Dynamic Modelling of Battery Energy Storage System and Application to Power System Stability," IEE Proc. C, Vol. 142, No. 4, July 1995, pp. 429-435.

[35] H. Clark, "Chino Battery Stabilizer Project: Battery Application to System Damping," *FACTS Applications, IEEE Power Engineering Society*, 96TP 116-0, pp. 8.88-8.90

[36] H. A. Peterson, N. Mohan, and R.W. Boom, "Superconductive Energy Storage Inductor-converter Units for Power Systems," *IEEE Trans. on Power Apparatus and Systems*, Vol. 94, No. 4, April 1975, pp. 1337-1348.

[37] Y. Mitani, K. Tsuji, and Y. Murakami, "Application of SMES to Improve Power System Dynamic Performance," *IEEE Trans. on Power Systems*, Vol. 3, No. 4, November 1988, pp. 1418-1425.

[38] C. J. Wu and Y. S. Lee, "Application of Superconducting Magnetic Energy Storage to Improve the Damping of Synchronous Generator," *IEEE Trans. on Energy Conversion*, Vol. 6, No. 4, December1991, pp. 573-578.

[39] J.B. Simo and I. Kamwa, "Exploratory Assesment of the Dynamic Behaviour of Multimachine Stabilized by a SMES Unit," *IEEE Trans. on Power Systems*, Vol. 10, No. 3, August 1995, pp. 1566-1571.

[40] R. I. Schermer, H. J. Boeing, and J. Dean, "30 MJ Superconducting Magnetic Energy Storage for BPA Transmission Line Stabiliser," *IEEE Trans. on Magnetics*, Vol.17, No. 5, September 1981, pp. 1950-1953.

[41] J. D. Rogers, R. I. Schermer, B. L. Miller, and J.F. Hauer, "30 MJ Superconducting Magnetic Energy Storage System for Utility Transmission Line Stabilisation," *Proc. of the IEEE*, Vol. 71, No. 9, September 1983, pp. 1099-1107.

[42] H. J. Boeing and J. F. Hauer, "Commissioning Test of the Bonneville Power Administration 30 MJ Superconducting Magnetic Storage Unit," *IEEE Trans. on Power Apparatus and System*, Vol.104, No. 2, February 1985, pp. 302-312.

[43] J.F. Hauer and H.J. Boeing, "Control Aspects of the Tacoma Superconducting Magnetic Energy Storage Project," *IEEE Trans. on Power Systems*, Vol. 2, No. 2, May 1987, pp. 443-450.

[44] L. Gyugi, "A Unified Power Flow Control Concept for Flexible AC Transmission Systems," *IEE Proc. C*, Vol. 139, No. 4, July 1992, pp. 323-331

[45] L. Gyugi, C.D. schauder, S. L. Williams, T.R. Rietman, D.R. Torgerson, and A.Edris, "The Unified Power Flow Controller: A New Approach to Power Transmission Control," *IEEE Trans. on Power Delivery*, Vol. 10, No. 2, April 1995, pp. 1085-1095.

[46] K. K. Sen and E. J. Stacey, "UPFC-Unified Power Flow Controller: Theory, Modelling and Application," *IEEE Trans. on Power Delivery*, Vol. 13, No. 4, October 1998, pp. 1453 –1460.

[47] N. G. Hingorani, "Flexible AC Transmission Systems (FACTS): An Overview," presented at the panel session of *FACTS, IEEE Winter Power Meeting*, 1990, Atlanta, Georgia.

[48] M. Ferrier, "Stockage d'energie dans un enroulement supraconducteur", *Journal of the International Institute of Refrigeration, Low Temperature and Electric Power*, 1969, pp. 150.

[49] R.W. Boom and H. A. Peterson, "Superconducting Energy Storage for Power Systems," *IEEE Trans. on Magnetics*, Vol. 8, No. 3, September 1972, pp. 701-703.

[50] N. Mohan, "Superconducting Energy storage Inductors for Power Systems," Ph.D dissertation, Electrical and Computer Engineering Dept., Univ. of Wisconsin, Madison, May 1973.

[51] R. J. Loyd, G.F. Moyer, J.R. Purcell, and J. Alcorn, *Conceptual Design and Cost of Superconducting Magnetic Energy Storage Plant,* EPRI Report EM-3457, April 1984.

[52] R. J. Loyd, S.M. Schoenung, T. Nakamura, W. Hassenzahl, J.D. Rogers, J.R. Purcell, D.W. Lieurance, and M.A. Hilal, "Design Advances in Superconducting Magnetic Energy Storage for Electric Utility Load Leveling," *IEEE Trans. on Magnetics*, Vol. 23, No.2, March 1987, pp. 1323-1330.

[53] M. Masuda and T Shintomi, "The conceptual design of a utility-scale SMES," *IEEE Trans. on Magnetics,* Vol. 23, No.2, March 1987, pp. 549-552.

[54] J. D. Rogers, R. I. Schermer, B. L. Miller and J.F. Hauer, "30 MJ superconducting magnetic energy storage system for utility transmission line stabilisation", *Proc. of the IEEE,* Vol. 71, No. 9, September 1983, pp. 1099-1107.

[55] O.R. Christianson, Y. M. Eyssa, X. Huang, S. K. Singh and R. W. Boom, "Conductor selection for SMES applications," *Advanced Cryogenics Engg.*, Vol. 39, 1994, pp. 821-828.

[56] R. W. Boom, "The UW-SMES design," *IEEE Trans. on Applied Superconductivity*, Vol.3, No. 1, March 1993, pp. 320-327.

[57] J. M. Pfotenhauer, "Test results from the SMES proof of principle experiment," *IEEE Trans. on Magnetics,* Vol. 27, No. 2, March 1991, pp. 1704-1707.

[58] C. A. Luongo, R.J. Lyod, and S.D. Peck, "SMES Conductor Selection: An Engineering Perspective," *IEEE Trans. on Applied Superconductivity*, Vol. 3, No.1, March 1993, pp. 332-336.

[59] R. J. Loyd, T. E. Walsh, and E.R. Kimmy, "Key Design Selection of the 20.4 MWh SMES/ETM," *IEEE Trans. on Magnetics*, Vol. 27, No.2, March 1991, pp. 1710-1715.

[60] R. J. Loyd, T. E. Walsh, E.R. Kimmy, and B.E. Dick, "An Overview of the SMES ETM Program: The Bechtel Team's Perspective," *IEEE Trans. on Magnetics*, Vol. 25, No. 2, March 1989, pp. 1569-1575.

[61] G. W. Ullrich, "Summary of the DNA SMES Development Program," *IEEE Trans. on Applied Superconductivity*, Vol. 5, No. 2, June 1995, pp. 416-419.

[62] C. Rix, C. A. Luongo, W.G. Bingham, A. M. Bulc, K.M. Cooke, D. Lieurance, K.D. Partain, and S.D. Peck, "A self-supporting SMES concept," *Cryogenics*, Vol. 34, 1994, pp. 737-740

[63] C. A. Luongo, "Review of the Bechtel Team's SMES design and future plan for a technology demonstration unit," *IEEE Trans. on Applied Superconductivity*, Vol. 5, No. 2, June 1995, pp. 416-419.

[64] S.D. Peck, J. Zeigler, and C. A. Luongo, "Tests on a 200 kA cable-in-conduit-conductor for SMES application," *IEEE Trans. on Applied Superconductivity*, Vol. 4, No. 4, December 1994, pp. 199-204.

[65] C. DeWinkel and J. D. Lamoree, "Storing power for critical loads," *IEEE Spectrum*, June 1993, pp. 38-42.

[66] M. Parizh, A. Kamal Kalafal, and R. Wilcox, "Superconducting Magnetic Energy Storage for Substation Applications," *IEEE Trans. on Applied Superconductivity*, Vol. 7, No. 2, June 1997, pp. 849-852.

[67] D. W. Lieurance, "Global cost optimization of 1-10 MWh toroidal SMES," *IEEE Trans. on Applied Superconductivity*, Vol. 7, No. 1, March 1997, pp. 14-17.

[68] D.W. Sarbarth, D.T. Heckworth, T.D. Hordubay, O.R. Christianson, and W.V. Hassenzahl, "Design and Construction of the 4 Tesla Background Coil for the Navy SMES Cable Test Apparatus," *IEEE Trans. on Applied Superconductivity*, Vol. 7, No. 2, June 1997, pp. 840-843.

[69] S. Jeong, V.S. Vysotosky, M. Takayasu, and J.V. Minervini, "Superconducting Pulse Coil Set for Stability Test of Superconducting Cables," *IEEE Trans. on Applied Superconductivity*, Vol. 7, No. 2, June 1997, pp. 211-214.

[70] Y. Lvovsky and C.M. Rey, "Quench Protection and Stragnant Normal Zones in a Large Cryostable SMES," *IEEE Trans. on Applied Superconductivity*, Vol. 7, No. 2, June 1997, pp. 857-860.

[71] A. Bautista et al., "Design, manufacturing and cold test of a superconducting coil and its cryostat for SMES applications," *IEEE Trans. on Applied Superconductivity*, Vol. 7, No. 2, June 1997, pp. 853-856.

[72] I. J. Iglesius, A Bautista, and M. Visiers, "Experimental and Simulated Results of a SMES Fed by a Current Source Inverter," *IEEE Trans. on Applied Superconductivity*, Vol. 7, No. 2, June 1997, pp. 861-864.

[73] H. Makinen, R. Mikkonen, and J. T. Erikson, "The availability analysis of a 100 kWh SMES," *IEEE Trans. on Magnetics*, Vol. 30, No. 4, July 1994, pp. 2604-2607.

[74] D.G. Akopyan et al, "Magnetic Energy Storage," *IEEE Trans. on Magnetics*, Vol. 28 No. 1, January 1992, pp. 398-401.

[75] C. Marinucci and J. Vecsey, "Discharge performance analysis of the Swiss Superconducting Magnetic Energy Storage Model," *IEEE Trans. on Magnetics*, Vol. 28 No. 1, January 1992, pp. 402-403.

[76] N. I. Doinikov et al. "900 MJ toroidal transformer type inductive energy storage," *IEEE Trans. on Magnetics*, Vol. 28 No. 1, January 1992, pp. 414-417.

[77] V. V. Andrianov et al., "Conceptual design of a 100 MJ SMES," *IEEE Trans. on Magnetics*, Vol. 27 No. 2, March 1991, pp. 2329-2332.

[78] H. Spath, H. Steinhart, P. Komarek, K.P. Jungst, W. Maurer, H.J. Haubrich, and T. Tischbein, "100 kJ/100 kW SMES for compensation of first pulsing loads," *Proc. of the IEA Syposium on the Use of Superconductivity in Energy Storage*, Karlshrue, Germany, October 25-27, 1994.

[79] Y. Masada, H. Miohi, K. Ogiso, and F. Nonaka, "Development of elementary technologies for 100 kWh/40 MW toroidal SMES," *Proc. of the IEA Syposium on the Use of Superconductivity in Energy Storage*, Karlshrue, Germany, October 25-27, 1994.

[80] T. Imayoshi et al., "Development of a 1 kWh-class Module-type SMES Design Study," *IEEE Trans. on Applied Superconductivity*, Vol. 7, No. 2, June 1997, pp. 844-848.

[81] S. Banerjee, J. K. Chatterjee, and S.C. Tripathy, "Application of SMES as load frequency stabilizer," *IEEE Trans. on Energy Conversion*, Vol. 5, No. 1, March 1990, pp. 46-51.

[82] S.C. Tripathy, R. Balsubramanian, and P.S.C Nair, "Adaptive automatic generation control with superconducting magnetic energy storage in power systems," *IEEE Trans. on Energy Conversion*, Vol. 7, No. 3, September 1992, pp. 434-441.

[83] C. A. Luongo, "Superconducting storage systems: an overview," *IEEE Trans. on Magnetics*, Vol. 32, No. 4, July 1996, pp. 2214-2223.

[84] S. Bartos and G.T. Heydt, "Increased operating flexibility for superconducting magnetic energy storage systems through the use of self commutation," *IEEE Trans. on Power Systems*, Vol 3, No. 3, August 1988, pp. 1132-1142.

[85] S. Banerjee, J. K. Chatterjee, and S.C. Tripathy, "Application of magnetic storage unit as continuous VAR controller," *IEEE Trans. on Energy Conversion*, Vol. 5, No. 1, March 1990, pp. 39-46.

[86] K.S Tam and P. Kumar, "Impact of superconducting magnetic energy storage on electric power transmission," *IEEE Trans. on Energy Conversion*, Vol. 5, No. 3, September 1990, pp. 501-511.

[87] P. M. Anderson, B. L. Agarwal, and J.E. Van Ness, *Subsynchronous Resonance in Power Systems*, IEEE Press, 1990.

[88] C.J. Wu and Y.S. Lee, "Application of simultaneous active and reactive power modulation of superconducting magnetic energy storage unit to damp turbine generator subsynchronous oscillation", *IEEE Trans. on Energy Conversion*, Vol.8, No. 1, March 1993, pp. 63-70.

[89] O. Wasynczuk, "Damping subsynchronous resonance using energy storage," *IEEE Trans. on Power Apparatus and Systems*, Vol. 101, No. 4, April 1982, pp. 905-914.

[90] R. J. Koessler, B. Fardanesh, M.I. Henderson, and R. Adapa, "Energy storage applications in New York State," *IEEE Power Engineering Society*, FACTS Applications, 96TP 116-0, pp. 8.46-8.51.

[91] P.W. Sauer and M.A. Pai, *Power System Dynamics and Stability*, Prentice Hall, N.J. 1998

[92] P. Kundur, *Power system stability and control*, Mc.Graw Hill, U.S.A. 1994.

[93] *IEEE Recommended Practice for Excitation System Models for Power System Stability Studies*, IEEE Standard 421.5-1992.

[94] K. Walve, "Modelling of power system components under severe disturbances," *CIGRE paper 38-18*, August 1986.

[95] B. C. Pal, "Hopf Bifurcations as Affected by Exciter and Load Dynamics in Power Systems," *Journal of the Instituition of Engineers*, India, pp. 166-169, 1996.

[96] L. Rouco, F.L. Pagola, A. Garcia-Cerrada, J.M. Rodriguez and R.M. Sanz, "Damping of Electromechanical Oscillations in Power Systems with Superconducting Magnetic Energy Storage Systems- Location and Controller Design", *Proc. of 12th Power System Computation Conference, Dresden*, Aug 19-23,1996, pp.1097-1104.

[97] S.B. Yusof, G.J. Rogers, and R.T.H. Alden, "Slow Coherency Based Network Partitioning Including Load Buses," *IEEE Trans. on Power Systems*, Vol. 8, No. 3, August 1993, pp.1375-1382.

[98] M. Klein, G.J. Rogers, and P. Kundur, "A Fundamental Study of Inter-area Oscillations in Power Systems," *IEEE Trans. on Power Systems*, Vol. 6, No. 3, August 1991 pp.914-921.

[99] G. N. Taranto, *Robust control design for power system damping controllers with applications to FACTS devices*, Ph.D thesis, Rensselaer Polytechnique Institute, December, 1994

[100] G. N. Taranto, J. K Shiau, J.H. Chow, and H.A. Othman, "Robust decentralised design of multiple FACTS damping controllers," IEE. Proc. Generation, Transmission and Distribution, Vol. 144, No.1, Jan. 1997, pp.61-67.

[101] *Matlab Users Guide*, The Math Works Inc. U.S.A, 1998

[102] G. Rogers, *Power System Toolbox*, Cherry Tree Inc., Canada, 1998.

[103] C. L. Philips and R. D. Harbor, *Feedback control synthesis*, 3rd edition, Prentice Hall, 1996.

[104] N. Martins and L.T.G Lima, "Determination of suitable locations for power system stabilizer and static var compensators for damping electromechanical oscillations in large power systems," IEEE Trans. on Power Systems, Vol. 5, No. 4, November 1990, pp.1455-1469.

[105] W. E. Schmitendorf and C. Wilmers, "Simultaneous stabilization via low order controllers," Control and Dynamic Systems, Vol. 35, Academic Press Inc. San Diego CA, 1991, pp. 165-184.

[106] C. T. Chen, *Linear System Theory and Design,* Holt, Rinehart and Winston, New York 1984.

[107] S. Skogestad and I. Postlethwaite, *Multivariable feedback control analysis and design* John Willey and Sons, 1996.

[108] D. J Limebeer and M. Green, *Linear Robust Control,* Prentice Hall, 1995.

[109] R. Y. Chiang and M. G. Sofonov, *Robust Control Toolbox for use with Matlab,* The Math Works Inc., 1996.

[110] M. Klein, L. X. Lee, G. J. Rogers, S. Farrokhpay and N. J. Balu, "H_∞ damping controller design in large power systems," *IEEE Trans. on Power Systems*, Vol. PWRS-10, No. 1, February 1995, pp. 158-166.

[111] R. Fletcher, *Practical methods of Optimization*, Vol. 2, John Wiley and Sons., 1980.

[112] C.G. Broyden, "The Convergence of a class of Double -rank Minimization Algorithms," *Journal of Institute of Maths Applications*, Vol. 6, pp. 76-90, 1970.

[113] R. Fletcher, "A new Approach to Variable Metric Algorithms," *Computer Journal*, Vol. 13, pp. 317-322, 1970.

[114] D. Goldfarb, "A Family of Variable Metric Updates Derived by Variational Means," *Mathematics of Computing*, Vol. 24, pp. 23-26, 1970.

[115] D.F. Shanno, "Conditioning of Quasi-Newton Methods for Function Minimization," *Mathematics of Computing*, Vol. 24, pp. 647-656, 1970.

[116] P.E. Gill, W. Murray and M.H. Wright, *Numerical linear Algebra and Optimization,* Vol. 1, Addison Wesley, 1991.

[117] G. Dantzig, *Linear Programming and Extensions,* Princeton University Press, Princeton, 1963.

[118] M.A. Branch and Andrew Grace, *" Optimization Toolbox for use with Matlab"*, The Math Works Inc., 1996.

[119] S.P Boyd, L El Ghaoui, E. Feron, and V. Balakrishnan, *Linear Matrix Inequalities in Systems and Control Theory.* Philadelphia, PA: SIAM 1994.

[120] K. Zhou , J. Doyle and K. Glover, *Robust and Optimal Control*, Prentice Hall, 1995.

[121] R. E. Skelton, T Iwasaki and K. Grigoriadis, *A Unified Algebraic Approach to Linear Control Design,* Taylor and Francis, 1998.

[122] J. C. Doyle, K. Glover, P. P. Khargonekar and B. A. Francis, "State-space solutions to standard H_2 and H_∞ control problems," *IEEE Trans. on Automat. Control.* Vol. 34, No. 8, pp. 831-847, August 1989.

[123] J.Sefton, and K. Glover, "Pole/zero cancellations in the general H_∞ problem with reference to a two block design," *Systems & Control Letters* 14(1990) pp. 295-306.

[124] P. Gahinet and P. Apkarian, "A linear matrix inequality approach to H_∞ control," *Intl. Journal. of Robust and Non-linear Control*, Vol. 4, 421- 448(1994).

[125] T. Iwasaki and R.E. Skelton, "All controllers for the general H_∞ control problem: LMI existence conditions and state-space formulas," *Automatica*, Vol. 30, No. 8, pp. 1307-1317.

[126] M. Chilali and Pascal Gahinet, "H_∞ Design with Pole Placement Constraints: An LMI Approach." *IEEE Trans. on Automatic Control*, Vol. 41, No. 3, pp. 358-367, March 1996.

[127] C. Scherer, P.Gahinet and M. Chilali, "Multiobjective Output-Feedback Control via LMI Optimization," *IEEE Trans. on Automatic Control*, Vol. 42, No. 7, pp. 896-911, July 1997.

[128] A. Nemirovskii and Pascal Gahinet, "The Projective Method for Solving Linear Matrix Inequalities," *Proc. of the American Control Conference*, 1994, pp. 840-844.

[129] Pascal Gahinet and A. Nemirovskii, "The Projective Method for Solving Linear Matrix Inequalities," *Mathematical Programming*, Vol. 77, No.2, pp. 163-190, 1997.

[130] X. Xin, L. Guo and C. B. Feng, "Reduced order controllers for continuous and discrete-time singular H-infinity control problems based on LMI," Automatica, Vol. 32, No. 11, pp. 1581-1585

[131] L. Elghaoui, F. Oustry and M. Aitrami, "A cone complementarity linearization algorithm for static output-feedback and related problems," *IEEE Trans. on Automatic Control*, Vol. 42, No.8, pp. 1171-1176, 1997.

[132] R.E. Benton and D. Smith, "Static output feedback stabilisation with prescribed degree of stability," *IEEE Trans. on Automatic Control*, Vol. 43, No.10, pp. 1493-1496, 1998.

[133] T. Iwasaki and R. E. Skelton, "The XY-centering algorithm for the dual LMI problem: A new approach to fixed-order control design," *International Journal of Control*, Vol. 62, No. 6, pp. 1257-1272, 1995.

[134] P. Gahinet, A. Nemirovski, A.J. Laub, M.Chilali , *"LMI Control Toolbox for use with Matlab"*, The Math Works Inc., 1995.

[135] G.N. Taranto and Joe. H. Chow, "A robust frequency domain optimization Technique for tuning series compensation damping controllers", *IEEE Trans. on Power Systems*, Vol. 10, No. 3, August 1995, pp. 1219-1225.

[136] Q. Zhao and J. Jiang, "A TCSC damping controller design using robust control theory," *Intl. Journal of Electrical Power and Energy Systems*, Vol. 20, No. 1, pp. 25-33, 1998.

[137] Y. Y. Cao, Y. X. Sun and W.J. Mao, "Output feedback decentralized stabilization: ILMI approach," Systems and Control Letters Vol. 35, pp. 183-194, 1998.

PUBLICATIONS

The following list of publication supports the work reported in this thesis.

Journal:

1. B. C. Pal, A. H. Coonick, I. M. Jaimoukha, and H. El-Zobaidi, "A Linear Matrix Inequality Approach to Robust Damping Control Design in Power Systems with Superconducting Magnetic Energy Storage Device," PE-439-PWRS-0-01-1999, in press

2. B. C. Pal, A. H. Coonick, D.C. Macdonald, "Robust Damping Controller Design in Power Systems with Superconducting Magnetic Energy Storage Device," accepted for publication in *IEEE Trans. on Power Systems*.

3. B. C. Pal, A. H. Coonick, and B. J. Cory, "Robust Damping of Inter-area Oscillations in Power Systems with Superconducting Magnetic Energy Storage Devices," accepted for publication in *IEE Proceedings: Generation, Transmission and Distribution*, London, U. K.